

**ADDITIVE TISSUE MANUFACTURING FOR
BREAST RECONSTRUCTION; COMBINING
CAD/CAM WITH ADIPOSE TISSUE
ENGINEERING**

Mohit Prashant Chhaya
Bachelor of Biotechnology Innovation (Hons)

Submitted in fulfilment of the requirements for the degree of
Doctor of Philosophy

School of Chemistry, Physics and Mechanical Engineering
Science and Engineering Faculty
Queensland University of Technology

2015

Keywords

Additive manufacturing, melt extrusion, breast tissue engineering, composite scaffold, polycaprolactone, anatomically-shaped scaffolds, patient-specific scaffolds, large volume tissue engineering, animal models, finite element analysis, computer modelling.

Abstract

Breast tissue engineering is an interdisciplinary field which combines expertise from engineering, cell biology, material science and plastic surgery primarily aiming to reconstruct breasts following a post-tumour mastectomy. Since breast implants also have a cosmetic function, there are a variety of factors that need to be considered in order to achieve an ideal surgical and cosmetic outcome. An off-the-shelf 3D printed macroporous scaffold therefore may be unnatural-looking and problematic for a large number of patients with unusual body shapes. This thesis is therefore focused on fabricating scaffolds that can be tailored and customised for each individual patient.

As part of this PhD project, an integrated strategy was developed whereby image is first taken of the breast region of a mastectomy patient using medical imaging techniques such as 3D laser scanning, CT or MRI scans. Software packages were then developed to process the captured images into a patient-specific 3D computer-aided design (CAD) model which is then sent to a bioprinter to be fabricated in the form of a scaffold suitable for tissue engineering. Concurrently, on the tissue culture side, 2 tissue engineering strategies – precursor cell induction vs body-as-a-bioreactor approach were explored. In the precursor cell induction strategy, patient-specific scaffolds were seeded with human umbilical cord perivascular cells and cultured under static conditions for 4 weeks and subsequently 2 weeks in a biaxial rotating bioreactor. These tissue-engineered constructs were then seeded with Human Umbilical Vein Endothelial Cells and implanted subcutaneously into athymic nude rats for 24 weeks. Angiogenesis and adipose tissue formation were observed throughout all constructs at all timepoints. The percentage of adipose tissue compared to overall tissue area increased from 37.17% to 62.30% between week 5

and week 15 ($p < 0.01$), and increased to 81.2% at week 24 ($p < 0.01$). In case of the body-as-a-bioreactor approach, we devised a concept of delayed fat injection combined with an empty biodegradable scaffold. 3 study groups were included in this study:

- 1) Empty scaffold.
- 2) Scaffold containing 4 cm³ lipoaspirated adipose tissue.
- 3) Empty scaffold + 2 week prevascularisation period. After 2 weeks of prevascularisation, 4 cm³ of lipoaspirated adipose tissue was injected into scaffolds.

The implants were placed in immunocompetent minipigs and the animals were sacrificed after 24 weeks. Histological evaluation showed that multiple areas of well vascularised adipose tissue were found in all groups. The negative control empty scaffold group had the lowest relative area of adipose tissue (8.31% \pm 8.94) which was significantly lower than both lipoaspirate-only (39.67% \pm 2.04) and prevascularisation + lipoaspirate group (47.32% \pm 4.12) and also compared to native breast tissue (44.97% \pm 14.12) ($p < 0.05$, $p < 0.01$ and $p < 0.01$ respectively).

During the course of this PhD project, a clinically viable route to design and fabricate biodegradable patient-specific scaffolds directly from 3D imaging data sets has been demonstrated. To our knowledge we are the first group showing a sustained regeneration of high volume adipose tissue over a long period of time using patient-specific biodegradable scaffolds.

List of Publications

The following is a list of published, accepted or submitted manuscripts that are relevant to the work performed in this PhD project.

1. **Mohit Prashant Chhaya**, Ferry Petrus Wilhelmus Melchels, Paul Severin Wigggenhauser, Jan-Thorsten Schantz, Dietmar Werner Hutmacher. 2013. *Breast Reconstruction Using Biofabrication-Based Tissue Engineering Strategies*. Biofabrication: Micro- and Nano-fabrication, Printing, Patterning and Assemblies. Atlanta: Elsevier Publishing.
2. Boris Michael Holzapfel, **Mohit Prashant Chhaya**, Ferry Petrus Wilhelmus Melchels, Nina Pauline Holzapfel, Peter Michael Prodingler, Ruediger von Eisenhart-Rothe, Martijn van Griensven, Jan-Thorsten Schantz, Maximilian Rudert, and Dietmar Werner Hutmacher. “Can Bone Tissue Engineering Contribute to Therapy Concepts after Resection of Musculoskeletal Sarcoma?,” *Sarcoma*, vol. 2013, Article ID 153640, 10 pages, 2013. doi:10.1155/2013/153640
3. **Chhaya, MP**, Melchels, FPW, Holzapfel, BM, Baldwin, JG, Hutmacher, DW. 2014. Sustained Regeneration of High-volume Adipose Tissue for Breast Reconstruction using Computer Aided Design and Biomanufacturing. *Biomaterials*. Accepted.
4. **Mohit P. Chhaya**, Inesa Sukhova, Dietmar W. Hutmacher, Daniel Mueller, Hans-Guenther Machens, Arndt F. Schilling and Jan-Thorsten Schantz. 2014. Evaluation of modified breast implant surfaces in a Minipig-Model. *Plastic and Reconstructive Surgery*. Submitted.
5. **Chhaya, MP**, Rosado-Balmayor, E, Schantz, JT, Hutmacher, DW. 2015. Breast Reconstruction using Computer Aided Design and Biomanufacturing – towards engineering clinically relevant volumes of adipose tissue. Manuscript in Preparation.

The following is a list of publications that are not relevant to the work performed in this PhD project but published during the PhD candidature:

1. Pedro F Costa, Cédryck Vaquette, Jeremy Baldwin, **Mohit Prashant Chhaya**, Manuela E Gomes, Rui L Reis, Christina Theodoropoulos and Dietmar W Hutmacher. 2014. *Biofabrication of customized bone grafts by combination of additive manufacturing and bioreactor knowhow*. Biofabrication: 6(3).

PRESENTATIONS AND PAPERS IN REFERRED CONFERENCE PROCEEDINGS

1. Inesa Sukhova, **Mohit Prashant Chhaya**, Dietmar Hutmacher, Daniel Mueller, Hans-Günther Machens, Jan-Thorsten Schantz. 2014. *In vivo evaluation of newly modified breast implant surfaces in a Minipig-Model*. In: Jahrestagung der Deutsche Gesellschaft der Plastischen, Rekonstruktiven und Aesthetischen Chirurgen, Munich 2014.
2. **Mohit P. Chhaya**, Ferry P.W. Melchels, Boris Michael Holzapfel, Jeremy G. Baldwin and Dietmar W. Hutmacher. 2014. Sustained Regeneration of High-volume Adipose Tissue for Breast Reconstruction using Computer Aided Design and Biomanufacturing. In: Australasian Society of Biomaterials and Tissue Engineering, Lorne, Victoria 2014.
3. **Mohit P. Chhaya**, Ferry P.W. Melchels, Boris Michael Holzapfel, Jeremy G. Baldwin and Dietmar W. Hutmacher. 2013. CAD/CAM-assisted breast reconstruction. In: Australasian Society of Biomaterials and Tissue Engineering, Barossa Valley, South Australia 2014.

4. **Mohit P. Chhaya**, Ferry P.W. Melchels, Boris Michael Holzapfel and Dietmar W. Hutmacher. 2013. Breast reconstruction using CAD/CAM and adipose tissue engineering. In: European Society of Biomaterials, Madrid 2013.
5. Ferry P.W. Melchels, **Mohit P. Chhaya**, Paul S. Wiggemhauser, Jan T. Schantz and Dietmar W. Hutmacher. 2012. Breast reconstruction using CAD/CAM and adipose tissue engineering. In: World Biomaterials Conference 2012; Chengdu, China.
6. **Chhaya, Mohit P.**, Melchels, Ferry P.W., Wiggemhauser, Paul S. Schantz, Jan-Thorsten and Hutmacher, Dietmar W. 2012. Patient-specific scaffolds for breast reconstruction. RACI Queensland Student Polymer Symposium. 13 September 2012.

Table of Contents

KEYWORDS I	
ABSTRACT II	
LIST OF PUBLICATIONS.....	IV
TABLE OF CONTENTS.....	VII
LIST OF FIGURES.....	IX
LIST OF TABLES.....	XII
LIST OF ABBREVIATIONS.....	XIII
STATEMENT OF ORIGINAL AUTHORSHIP.....	XIV
PROLOGUE XV	
CHAPTER 1: INTRODUCTION.....	17
1.1 Introduction.....	17
1.2 Breast tissue engineering.....	18
1.3 Main purposes of the PhD project.....	20
1.4 Possible outcomes and significance.....	21
CHAPTER 2: LITERATURE REVIEW.....	24
2.1 Current approaches aimed at breast reconstruction.....	24
2.1.1 Prosthetic implant-based reconstruction.....	25
2.1.2 Cellular breast reconstruction.....	26
2.2 Engineering challenges.....	30
2.2.1 Imaging.....	31
2.2.2 Triangulated surface model.....	32
2.2.3 Scaffold design and porosity.....	33
2.2.4 Scaffold Manufacturing.....	34
2.3 Formation of tissue constructs.....	39
2.3.1 Scaffold Biomaterial.....	41
2.3.2 Microenvironment.....	50
2.3.3 Vascularisation.....	50
2.4 Decellularisation-based scaffolds.....	51
2.5 Angiogenic growth factors.....	53
2.6 <i>In vivo</i> prevascularization.....	55
2.7 Cells.....	55
2.8 Animal models.....	61
2.9 Concluding remarks.....	65
CHAPTER 3: RESEARCH DESIGN.....	67
3.1 Investigate whether surface modifications of breast implants on a microscopic level have a major influence on the cellular behaviour and foreign body response leading to capsular contracture.....	68
3.2 Development of a methodology to design and fabricate highly customised patient-specific biodegradable scaffolds.....	70
3.2.1 Conversion a medical imaging data set into a CAD format suitable for additive manufacturing.....	70
3.2.2 Generation of computer numerical code (CNC) from CAD models.....	71
3.2.3 Development of automated algorithms to rapidly generate finite element models of a set of scaffolds varying in porosity, pore geometry, filament thickness, and pore interconnectivity directly from the CNC machining code.....	72
3.3 Breast tissue engineering and <i>in vivo</i> assessment.....	74
3.3.1 <i>In vivo</i> test for subcutaneous adipogenesis and vascularisation in a nude rat model.....	74
3.3.2 <i>In vivo</i> test for subglandular adipogenesis and vascularisation in minipig model.....	74
CHAPTER 4: RESEARCH REPORTS.....	77
4.1 STUDY ONE: Evaluation of modified breast implant surfaces in a Minipig-Model.....	77
4.1.1 Introduction.....	78
4.1.2 Materials and Methods.....	80
4.1.3 Results.....	85
4.1.4 Discussion.....	96
4.1.5 Conclusion.....	100
4.1.6 Supplementary Figures and Tables:.....	100

4.2	STUDY TWO: Development of a methodology to design and fabricate highly customised patient-specific biodegradable scaffolds	102
4.2.1	Development of a methodology to design and fabricate highly customised patient-specific biodegradable scaffolds	102
4.2.2	Establishment of a methodology to fabricate porous patient-specific scaffolds from solid 3D computer-aided-design (CAD) models obtained through medical imaging scans.....	106
4.2.3	Development of a software package for rapid generation of finite element models from numerical-code programming languages.....	115
4.2.4	Overall Discussion	126
4.2.5	Conclusion.....	129
4.3	STUDY THREE: Sustained Regeneration of High-volume Adipose Tissue for Breast Reconstruction using Computer Aided Design and Biomanufacturing.....	131
4.3.1	Introduction.....	132
4.3.2	Methods and Materials	134
4.3.3	Results	143
4.3.4	Discussion.....	152
4.3.5	Conclusion	157
4.3.6	Acknowledgements	158
4.3.7	Supplementary Tables and Figures.....	158
4.4	STUDY FOUR Breast Reconstruction using Computer Aided Design and Biomanufacturing – towards engineering clinically relevant volumes of adipose tissue	161
4.4.1	Introduction.....	161
4.4.2	Materials and Methods	164
4.4.3	Results	168
4.4.4	Discussion.....	184
4.4.5	Conclusion	189
	CHAPTER 5: DISCUSSION, CONCLUSIONS AND FUTURE DIRECTIONS	191
5.1	Summary of Study 1.....	192
5.2	Summary of Study 2.....	194
5.3	Summary of Study 3.....	195
5.4	Summary of Study 4.....	197
5.5	Limitations and recommendations for future work	199
5.5.1	Biopolymer characteristics and degradation models were simplified for the FE analysis	199
5.5.2	Scaffold mechanical properties	200
5.5.3	Scaffold <i>in vivo</i> degradation behaviour	204
5.5.4	Characterisation of tissue morphology and make-up.....	206
5.5.5	Scaffold form in study 4 was not adequate for delayed fat injections.....	206
5.5.6	Drug Delivery using biodegradable scaffolds	207
5.6	Overall discussion and conclusion	208
	EPILOGUE 212	
	REFERENCES	216
	CHAPTER 6: APPENDIX	238

List of Figures

Figure 2.1.1 Examples of capsular contracture around breast implants.	26
Figure 2.1.2 The BRAVA System and Lipofilling for Augmentation of a tuberous breast deformity.....	28
Figure 2.1.3 Breast reconstruction using the DIEP flap	29
Figure 2.2.1 CAD model of a healthy breast obtained using a laser scanner.....	33
Figure 2.2.2 Generation of porosity on a solid model.....	34
Figure 2.2.3 Generation of porous structures from a solid breast model.....	34
Figure 2.2.4 Intra-operative use of the mould to shape the breast in flap transplantation-reconstruction.....	39
Figure 2.3.1 Tissue Engineering strategy for breast reconstruction..	40
Figure 2.3.2 Conceptual diagram of a bioprinting system adapted for breast tissue reconstruction.....	48
Figure 2.3.3 Graph showing the degradation of the scaffold over time interlayed with different cellular events taking place during tissue regeneration.....	49
Figure 2.9.1 Visualisation of thesis flow.....	68
Figure 4.1.1 Gross morphology of S, SP and LP implants prior to implantation.....	86
Figure 4.1.2 SEM images of the surface of the implants at 20 week time point.....	87
Figure 4.1.3 Bar graph showing the Young's moduli of unused silicone implants and used implants after 20 weeks of <i>in vivo</i> implantation.....	89
Figure 4.1.4 Masson's Trichrome staining showing representative images of tissue morphology of fibrous capsules from implants removed at 10 week time point.....	93
Figure 4.1.5 Representative immunological staining images of protein expressions in capsules extracted at 10 week time point.....	95
Figure 4.1.6 Representative immunological staining images of protein expressions in capsules extracted at 20 week time point.....	96
Figure 4.2.1 The effect of threshold levels on the quality of the 3D model.	105
Figure 4.2.2 Rendering of the 3D model before (A) and after (B) of the re-meshing process using quadratic edge collapse method.....	106
Figure 4.2.3 Flow diagram of the algorithm used to slice the 3D STL file into an array of 2D slices	108
Figure 4.2.4 Mathematical equation used to derive the coordinates of the points in the 3D model intersecting the slicing line	109
Figure 4.2.5 Visualisation of layer contours of all layers generated from a breast scaffold	110
Figure 4.2.6 Matlab plot of all points derived from a randomly selected layer	109
Figure 4.2.7 Matlab-based visualisation of naïve algorithm for adding raster lines.....	111
Figure 4.2.8 Matlab output of naïve algorithm showing irregularly spaced raster lines.....	111
Figure 4.2.9. Results of sweep line algorithm to generate raster lines plotted in Matlab.	113
Figure 4.2.10 (LEFT) Algorithm governing rotational matrices. (RIGHT) Results from implementing the algorithm on a randomly selected layer (plotted using Matlab).	114
Figure 4.2.11 Results showing fabrication of different types of scaffolds using the STL-Gcode conversion algorithm as a proof-of-concept	114

Figure 4.2.12 Algorithmic steps designed to parse the nodes from a CNC tool-path file.....	118
Figure 4.2.13 Matlab visualization of the node-split algorithm to increase result accuracy. Top left shows the original set of nodes parsed from the CNC output.....	119
Figure 4.2.14 Geometry, node locations and the coordinate system for BEAM188 3-D Finite Strain Beam. Image adapted from [308].	120
Figure 4.2.15 Intelligent travel path sensing algorithm to detect layers having multiple closed loops	121
Figure 4.2.16 Matlab plot of a randomly selected layer containing two closed loops connected by a non extruding raster line	122
Figure 4.2.17 (TOP) FE nodes and elements of a breast scaffold with travelling paths not separated. (BOTTOM) FE nodes and elements of a breast scaffold with travelling paths separated using the intelligent travel path sensing algorithm.	122
Figure 4.2.18 Differences in distribution of bending moments in FE meshes of scaffolds with different architectures.	123
Figure 4.2.19 TOP: Schematic diagram of the test setup used for compression testing of scaffolds.	124
Figure 4.2.20 Mesh optimization study performed to test the accuracy of the meshes and the FEA method.	125
Figure 4.2.21 Distribution of bending moments (units N.mm) in breast scaffolds with different filament thicknesses. Left: 0.2mm Filament thickness, Centre: 0.4mm, Right, 0.8mm filament diameter.....	Error! Bookmark not defined.
Figure 4.3.1 Scaffold fabrication and characterisation.....	143
Figure 4.3.2 Fluorescence signal from the GFP-labelled HUVECs detected using an IVIS bioluminescence scanner.....	145
Figure 4.3.3 Scaffolds explanted after 24 weeks showed good integration with the host tissue with no observable signs of inflammation and fibrotic encapsulation.	146
Figure 4.3.4 Hematoxylin and Eosin (H&E) staining of tissue samples explanted at week 5 and 15 and 24.....	148
Figure 4.3.5 Box and whiskers plot showing the adipose tissue area relative to total tissue area over 24 weeks.....	149
Figure 4.3.6 Histological staining of scaffolds explanted on week 24.	151
Figure 4.3.7 Cell morphology on day 1 post seeding suspended in fibrin glue.	159
Figure 4.3.8 Images depicting the workflow of the automated algorithm to count the number of adipose cells on a histology section and also their cell surface areas.....	159
Figure 4.3.9 Schematic diagram of the test setup used for compression testing of scaffolds.	159
Figure 4.3.10 Graph showing comparison of volumes of scaffolds used for adipose tissue engineering research.	160
Figure 4.3.11 Illustration showing the position of the samples collected using biopsy punch outs at weeks 5 and 15.	160
Figure 4.4.1 Overall concept of the prevascularisation and delayed fat injection concept..	164
Figure 4.4.2 Rendering of the CAD model used to fabricate the scaffold.....	169
Figure 4.4.3 Implantation process of the scaffolds	171
Figure 4.4.4 Explantation images showing the integration of TECs with the host tissue.....	172
Figure 4.4.5 Representative images showing H&E staining of tissue explanted from the empty scaffold group (superficial layers).	173
Figure 4.4.6 Representative images showing H&E staining of tissue explanted from the empty scaffold group (deep layers).	174

Figure 4.4.7 Representative images showing H&E staining of tissue explanted from native breast tissue.	175
Figure 4.4.8 H&E stained sections of lipoaspirate-only group (superficial layers).....	176
Figure 4.4.9 H&E stained sections of lipoaspirate-only group (deep layers).	177
Figure 4.4.10 H&E stained sections of prevascularisation + lipoaspirate group (superficial layers).	178
Figure 4.4.11 H&E stained sections of prevascularisation + lipoaspirate group (deep layers)..	179
Figure 4.4.12 Representative H&E-stained micrographs of regions around the scaffold strands showing non-specific minor granulomatose reactions.	180
Figure 4.4.13 Representative images of Masson’s Trichrome stained tissue sections.	181
Figure 4.4.14 (a) Clustered column graph showing tissue composition at week 24 in various groups..	183
Figure 5.1 Illustration of the relationship between porosity, pore sizes, cellular response and mechanical strength. Adapted from Holzapfel et al [317].	201
Figure 5.2 Graphic showing subglandular vs submuscular placement of implants. Figure adapted from Myckatyn [386].....	202
Figure 5.6.1: Rendering of a breast-shaped scaffold containing a collapsible network of interconnected tubes filled with a fluid (blue) or hydrogel (red)	239
Figure 5.6.2. Prototype of a breast-shaped porous tissue engineering scaffold (white) containing templates for spacers (black). Photos with blue background show a convergent design of spacers, while photos with off-white backgrounds show a non-convergent design.	239
Figure 5.6.3: Rendering of a breast shaped scaffold containing regions of low porosity and low mechanical integrity (regions are shown in red).....	240
Figure 5.6.4: A specialised surgical cutting tool will be designed to remove such regions.....	240
Figure 5.6.5: The void left behind by removal of the low porosity regions will be used for lipofilling (fat tissue shown in yellow)	240
Figure 5.6.6. Fabricated breast shaped scaffold (white) containing regions of low porosity and low mechanical integrity (black).	241
Figure 5.6.7. A cutting tool used to punch out the regions of low porosity and mechanical integrity.....	241
Figure 5.6.8. The void left behind by removal of the low porosity regions (highlighted with red circle) can be used for lipofilling.....	241
Figure 5.6.9 (TOP) Gross morphological images of scaffold containing void structures with and without the fat injected into the voids.....	242
Figure 5.6.10: Left: Conventional laydown pattern consisting of continuous struts. Centre, Right: Our novel laydown patterns consisting of discontinuous struts	245
Figure 5.6.11: On the left, conventional laydown pattern. On the right: Modified laydown pattern consisting of offset struts. Note that the struts in Y axis are not laid directly on top of each other. We not only can lay down the struts differently in every second layer but also create a repetition after every nth layer.....	246
Figure 5.6.12: Left: Conventional laydown pattern. Right: Modified laydown pattern	246
Figure 5.6.13: Other examples of novel laydown patterns.	246
Figure 5.6.14. Left: Control polycaprolactone scaffold containing straight struts. Centre: Scaffold with zigzag laydown pattern. Right: Scaffold with zigzag laydown pattern AND offset between layers.	247
Figure 5.6.15. Stress vs Strain curves of scaffolds with either straight struts or a zigzag pattern of struts.	248

Figure 5.6.16. Timeline showing the evolution of the overall scaffold shape throughout the PhD project.....	249
---	-----

List of Tables

Table 3.2.1. Description of four common commercially available AM techniques. All figures taken from Melchels <i>et al</i> [4]. Reproduced with permission	36
Table 2.2.2. Mechanical properties of elastomeric biomaterials. Adapted from Shi <i>et al</i> [125]. Reproduced with permission	44
Table 4.1 Scaffold properties.....	126
Table 4.2 List of primary antibodies	158
Table 4.3 Comparison of breast/body volumes of humans and rodents	159

List of Abbreviations

<i>Full name</i>	<i>Abbreviation</i>
Additive manufacturing	AM
Adipose-derived Mesenchymal Stem Cells	AMSC
Computer Numerical Control	CNC
Computer-Aided Design	CAD
Computer-Aided Manufacturing	CAM
Computer Tomography	CT
Extracellular matrix	ECM
Fetal Bovine Serum	FBS
Finite Element Analysis	FEA
Fused Deposition Modelling	FDM
Gcode	G Programming language code
Growth Factors	GF
Hounsfield Units	HU
Human Umbilical Cord Perivascular Cells	HUCPVC
Human Umbilical Vein Endothelial Cells	HUVEC
Magnetic Resonance Imaging	MRI
Mega Pascal	MPa
Melt extrusion	ME
Mesenchymal stem cell	MSC
Micro-computer tomography	μ CT
Phosphate buffer solution	PBS
Poly(caprolactone-co-DL_lactide)	P(CL-DLLA)
Poly(glycolic acid)	PGA
Poly(lactic acid)	PLA
Poly(L-lactic-co-glycolic acid)	PLGA
Poly(L-lactide)	PLLA
Poly(trimethylene carbonate)	TMC
Polycaprolactone	PCL
Power of hydrogen	pH
Rapid prototyping	RP
Regenerative Medicine	RM
Scanning electron microscopy	SEM
Sodium hydroxide	NaOH
Specific Pathogen Free	SPF
Three dimensional	3D
Tissue Engineered Construct	TEC
Tissue Engineering	TE
Vascular endothelial growth factor	VEGF

Statement of Original Authorship

The work contained in this thesis has not been previously submitted to meet requirements for an award at this or any other higher education institution. To the best of my knowledge and belief, the thesis contains no material previously published or written by another person except where due reference is made.

Signature: [QUT Verified Signature](#)

Date: 04 June 2015

Prologue

I remember vividly how the start of this project came to be. In October of 2011, I was working as a research assistant in the labs of Dr. Mia Woodruff at the Institute of Health and Biomedical Innovation (IHBI). At the time I never thought IHBI would continue to remain my “2nd home” for the next 3 years. Late one night, one of the other RAs, Edward Ren, and I were examining some microscope images when Edward told me that he was applying for a PhD position. I’d never considered staying on for a PhD. I’d always wanted to go out to the real world, run a business, become an entrepreneur etc. But over the next 2 hours, Ed told me how I could never manage researchers without ever being into the shoes of a scientist. At the end of the discussion and after mulling the notion a bit more, I had pretty much set my mind onto doing a PhD.

Thus I began searching for researchers whose interests were similar to mine. There are many high calibre researchers at QUT which made my decision very difficult. I also emailed a Professor at the Karolinska Institute and another at the Australian Institute of Bioengineering and Nanotechnology to see if they had any positions available. Fortunately, I recalled that one of the Professors at IHBI, whom I’d previously helped build a business plan for the first-ever melt electrospinning machine, is involved in additive manufacturing and tissue reconstruction research. I immediately went to the website of Professor Dietmar Hutmacher and looked up his research interests and, having found an instant match, shot him an email at around midnight. Dietmar emailed me back at around 1.30am asking me to come in for an interview the following morning. So here I was, 7 days before the scholarship round deadline, meeting my future boss about a PhD project. At the interview, we mostly

talked about the German football league, the Bundesliga, and towards the end we started discussing about a potential project. He showed me a few proposals he had. One of them was about designing a perfusion-flow bioreactor, another was about melt electrospinning and a 3rd one about periosteum tissue engineering. While all these projects were really fascinating, they did not match my interests. It was in this moment, when all hope was slowly fading, that Dietmar said “We have one more project. It’s really new and not much work has been done on it”. He passed a 3-page proposal into my hands. I looked at the cover. It was titled ... “Breast Tissue Engineering”.....

Chapter 1: Introduction

1.1 Introduction

The fundamental concept underlying tissue engineering (TE) is the use of a combination of cells, biomaterials and physico-chemical factors to improve or replace a biological organ. Langer and Vacanti [2] describe tissue engineering as “an interdisciplinary field that applies the principles of engineering and life sciences towards the development of biological substitutes that restore, maintain or improve tissue function” and as such it reflects the congruence of seemingly disparate domains: clinical medicine, engineering and biology. The scaffold is expected to perform various functions, including the support of cell colonization, migration, growth and differentiation. Furthermore, the design physicochemical properties, morphology and degradation kinetics of Tissue Engineered Constructs (TEC) must also be considered [3, 4]. Owing to such complex design, complex regulatory pathways and an intellectual challenge of enormous magnitude, the progress of the TE field with respects to its headline goal – to create living replacement parts for the human body – has been slow[5]. However, the work of the past twenty years by leading scientists and research laboratories in the area have served to clarify our understanding of the underlying factors important to achieve the full extent of TE’s therapeutic vision. Particular shortcomings of the current TE paradigm involving large volume prefabricated scaffolds include the inability to: i) mimic the cellular organization of natural tissues; ii) upscale fabrication methods to the economically viable scale necessary for clinical application; and iii) address the issue of vascularization of the TEC.

1.2 Breast tissue engineering

Since the turn of the 21st century, impetus has been gradually growing towards TE-based regeneration of adipose tissue for breast reconstruction post-mastectomy. Breast cancer is the most frequent cancer among women with an estimation of 1.67 million of new cases diagnosed worldwide in 2012 resulting in 522,000 deaths.[6] Owing to the large number of clinical occurrences, breast reconstruction following lumpectomy (partial removal of breast tissue) or radical mastectomy (total removal of the breast) has become the sixth most common reconstructive procedure performed in America [7]. Lumpectomy defects of less than 25% of the total breast volume can typically be corrected by rearranging the local breast tissue. Larger lumpectomies and mastectomies require more comprehensive reconstruction modalities [8]. Studies show that many women who have had a mastectomy tend to suffer from a syndrome “marked by anxiety, insomnia, depressive attitudes, occasional ideas of suicide, and feelings of shame and worthlessness”[9]. Reconstruction of the breast mound following a mastectomy has proven to alleviate the sense of mutilation and suffering that women experience post-surgery. As a result, breast reconstruction is offered as a valuable option to any woman undergoing surgery for breast cancer.

Currently, a majority of breast reconstructions are performed with the use of non-degradable prosthetic implants or by transplantation of autologous free or pedicled tissue flaps consisting of skin, muscle and connected vasculature [8]. It is known that reconstruction using silicone-based implants leads to formation of a rigid fibrous tissue surrounding the implant on an average 5-10 years post surgery - giving a spherical and unnatural appearance to the breast [8, 10]. Reconstruction using autologous tissue is also associated with tissue resorption and necrosis [11, 12].

Since the publication of the highly cited research paper by Patrick [13] who used preadipocyte-seeded polyglycolic acid (PLGA) scaffolds for regenerating small volumes of adipose tissue, although many research groups around the world [14-22] have made progress towards the regeneration of small volumes of adipose tissue, significant breakthroughs towards regenerating clinically relevant volumes of fat remain elusive. An avid reader will notice that these research groups are ultimately targeting perhaps the most critical challenge facing large volume adipose tissue regeneration – vascularisation. Within the human body, a majority of the cells lie within a distance of 100-200 μm from the nearest capillary, with this spacing providing an adequate environment for nutrient diffusion, oxygen supply and waste removal [23]. Consistent with this discovery, researchers aiming to regenerate tissue using biodegradable scaffolds discovered that this limitation only allowed cells within a distance of 200 μm from the nearest nutrient source to survive and participate in the regeneration process [24, 25]. As most such scaffolds rely on the principle of diffusion for transporting nutrients and oxygen to the cells, a diffusion gradient is formed within the construct where the cells at the periphery of the constructs have greater accessibility to nutrients and are therefore most viable. The viability and cell number decreases with the thickness of the construct owing to differences in nutrient concentration [26]. It has been speculated that this is the cause for the unpredictability in the engineering of adipose tissue with a thickness greater than a few hundred microns in the laboratory [26].

Furthermore, the body and breast shape and size of each woman are different [27-29]. Since breast implants also have a cosmetic function, there are a variety of factors that need to be considered in order to achieve an ideal surgical and cosmetic outcome. An off-the-shelf 3D printed macroporous scaffold therefore may be

unnatural-looking and problematic for a large number of patients with unusual body shapes. Our research is therefore focused on generating scaffolds that can be tailored and customised for each individual patient.

In order to overcome these key barriers and engineering challenges, we envisage an integrated strategy where images are first taken of the breast region of a mastectomy patient using medical imaging techniques such as 3D laser scanning, CT or MRI scans. The images captured can then be processed into a patient-specific 3D computer-aided design (CAD) model which is then sent to a bioprinter to be fabricated in the form of a scaffold appropriate for tissue engineering. Concurrently, on the tissue culture side, fat tissue is harvested from the patient. Pre-adipocytes or adipose-derived mesenchymal stem cells (AMSCs) and endothelial cells are then separated from it and co-cultured onto the fabricated scaffold. Finally, after sufficient vascularisation and adipose cell growth is achieved *in vitro*, the TEC is implanted back into the patient to regenerate the breast shape.

1.3 Main purposes of the PhD project

The purpose of this research project was three-fold:

- 1) Investigate whether surface morphology of silicone implants on a microscopic level has a major influence on the cellular behaviour and foreign body response.
- 2) Develop a methodology to design highly customised patient-specific biodegradable scaffolds using a combination of medical imaging and additive manufacturing technologies.

- a. Developing a streamlined methodology to convert a medical imaging data set into a CAD format suitable for additive manufacturing.
 - b. Developing computer algorithms allowing researchers to design internal architecture of scaffolds directly from CAD files.
 - c. Development of automated algorithms allowing researchers to rapidly generate finite element models of a set of scaffold and pore architectures directly from computer-numerical-control (CNC) machining codes.
- 3) Assess the adipose tissue regeneration capabilities of patient-specific biodegradable scaffolds *in vivo*.

1.4 Possible outcomes and significance

As a direct outcome of this PhD project, we are the first group demonstrating a clinically viable route to achieve sustained regeneration of high volume adipose tissue over a long period of time. From a translational research point of view, this research will enable the development of world's first regenerative medicine-based therapy for breast reconstruction. Requiring only one surgical procedure, this technology demonstrates an adequate cost effectiveness ratio and is therefore expected to be driven forward to broad clinical use within a short span of time.

Key outcomes of this project include the development of innovative new strategies for additive tissue manufacturing for soft tissue interfaces and advancement of the translation of novel Tissue Engineering/Regenerative Medicine (TE/RM) technologies into clinical application. More specifically, direct outcomes of this PhD project would:

- 1) Deliver a modular, user friendly software allowing researchers to design complex pore architectures within solid CAD models with a level of sophistication and control over extrusion parameters not available with current computer-aided-manufacturing (CAM) software.
- 2) Streamline the process of designing and fabricating patient-specific scaffolds by incorporating *in silico* FEA-based pre-testing methods into the design process – allowing a significant shift from the currently popular heuristic methods of scaffold design.
- 3) Provide a reproducible subglandular large animal model which makes it possible to test non degradable (silicone) implants as well as degradable scaffolds in an *in vivo* environment that is very close to the human equivalent. This will allow researchers to iteratively improve the surface microstructures designs of both implants and scaffolds for tissue engineering leading to novel approaches that can limit the incidences of capsular contracture and can enhance regeneration of native adipose tissue.

Perhaps the biggest economic significance of this project can be realised through the development of an integrated scaffold design and manufacturing system which can be used in a clinical setting. Demographic data reveals that due to the ageing population, breast cancer incidences will increase over the coming years [30, 31]. The drive, to develop implant design and surgical planning tools allowing an efficient communication of a desired cosmetic outcome between the surgeon and the patient, is an important cosmetic as well as therapeutic issue - especially considering that 15-30% of all surgeries require subsequent corrective surgeries to achieve the desired cosmetic outcome [7]. The additional burden on the healthcare system per patient per follow-on surgery is approximately AUD 5000 [32]. Since 70% of all

patients undergo an average of 2 follow-on surgeries [33], the total healthcare burden on the Australian healthcare system alone amounts to AUD 273 million per year. By giving the surgeons access to a sophisticated regenerative-medicine based personalised scaffold system which effectively communicates the desired shape and contours of the breast prior to and during the surgery our proposed technology demonstrates an adequate cost effectiveness ratio and is therefore expected to be driven forward to broad clinical use within a short span of time. Using a sophisticated simulation model of the adoption rate of our technology, we estimate that at a mere 50% adoption rate, the potential efficacy savings for both inpatient and outpatient care in Australia alone could average in the range of \$75 million to \$100 million per year.

Chapter 2: Literature Review


PAPER ONE (Published as a Book chapter)

Breast reconstruction using biofabrication-based tissue engineering strategies

Chhaya, MP, Melchels, FPW, Wiggemhauser, PS, Schantz, JT and Hutmacher, DW.

The authors listed below have certified* that:

1. they meet the criteria for authorship in that they have participated in the conception, execution, or interpretation, of at least that part of the publication in their field of expertise;
2. they take public responsibility for their part of the publication, except for the responsible author who accepts overall responsibility for the publication;
3. there are no other authors of the publication according to these criteria;
4. potential conflicts of interest have been disclosed to (a) granting bodies, (b) the editor or publisher of journals or other publications, and (c) the head of the responsible academic unit, and
5. they agree to the use of the publication in the student's thesis and its publication on the QUT ePrints database consistent with any limitations set by publisher requirements.

Contributor	Statement of contribution
Mohit P. Chhaya	Conceptualised the publication, performed background and literature search. Wrote the manuscript.
 Signature	
Date 30 Jan 2015	
Ferry PW Melchels	Involved in the conception and design of the project. Assisted in reviewing the manuscript.
Paul Severin Wiggemhauser	Assisted in reviewing the manuscript.
Jan-Thorsten Schantz	Provided clinical images and images. Reviewed manuscript.
Dietmar W. Hutmacher	Involved in the conception and design of the project. Provided technical guidance and assisted in reviewing the manuscript.

Principal Supervisor Confirmation

I have sighted email or other correspondence from all Co-authors confirming their certifying authorship.

Dietmar W. Hutmacher  30.01.2015
Name Signature Date

2.1 Current approaches aimed at breast reconstruction

Currently, there are 3 main surgical approaches for reconstructive surgery following lumpectomy or mastectomy: reconstruction with autologous tissue (reconstruction with silicone implants, free/pedicled flaps and lipofilling).

Due to copyright restrictions, this published book chapter is not available here. For further information, please view the publisher's website at:

<http://store.elsevier.com/Biofabrication/isbn-9781455730049/>

Chapter 3: Research Design

The overall aim of this PhD project was to develop a novel additive manufacturing technology platform enabling fabrication of patient-specific breast scaffolds and test their adipogenic potential within an *in vivo* environment. The overall aim was then further sub-divided into 4 smaller sub-aims:

- 1) Investigate whether surface modifications of breast implants on a microscopic level influence cellular behaviour, foreign body response and capsular contracture.
- 2) Development of a methodology to reproducibly fabricate highly customised patient-specific biodegradable scaffolds.
- 3) Assessment of adipogenic potential of small volume TECs within a subcutaneous nude-rat small animal model.
- 4) Assessment of adipogenic potential of scaled-up large volume TECs within a subglandular minipig large animal model.

Fig 3.1 shows the flow of activities undertaken and methodologies developed as part of this PhD project.

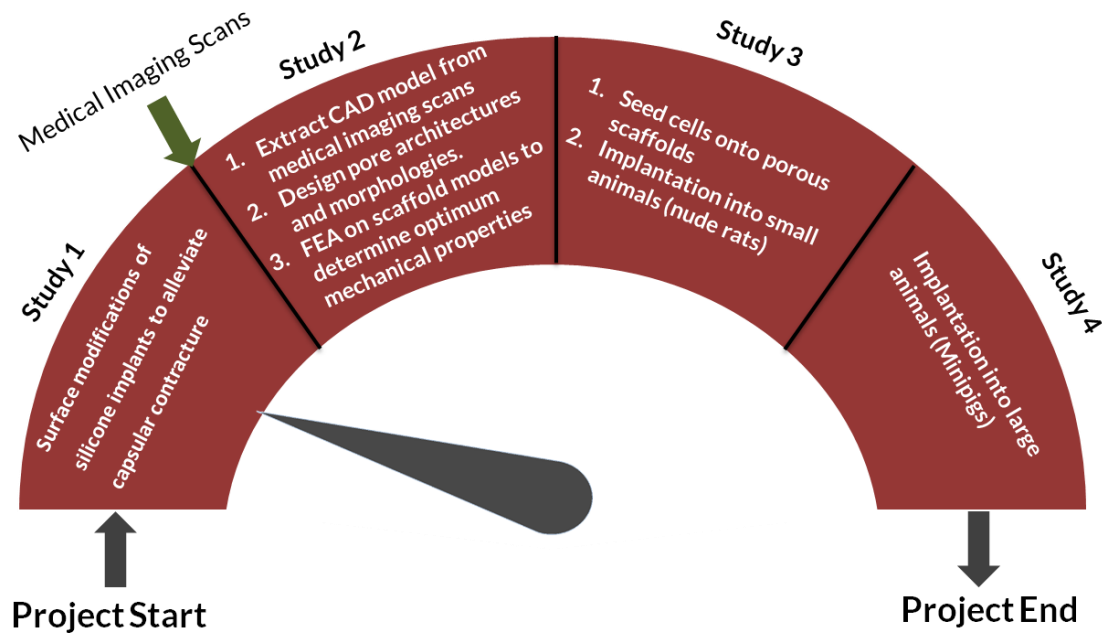


Figure 2.9.1 Visualisation of project flow

3.1 Investigate whether surface modifications of breast implants on a microscopic level have a major influence on the cellular behaviour and foreign body response leading to capsular contracture

After a thorough literature review, minipigs were found as appropriate model animals to study breast TE due to their tissue makeup being comparable to humans. Along with the aim of establishing a large animal model, a sub-aim of this project was to study the interactions between the implant surface and surrounding tissue in order to minimise the chances of an adverse fibrosis reaction. The study evaluated the impact of three different surface structures on the development of fibrosis and subsequent capsular contracture. These three surface morphologies consisted of a smooth surface, a textured surface with large pores and a textured surface with small pores. It was hypothesised that the data obtained in terms of surface roughness and its impact on tissue adhesion and fibrosis would provide unique insights which would influence the design of porous biodegradable scaffolds from a completely different point of view.

For the purposes of establishment of the animal model, commercially available 40cc silicone implants (kindly provided by Mentor LLC) were used. The implants were manufactured with 3 different surfaces: one surface with 100 pores per inch, having an average surface pore diameter of 57.71 microns (Small pores – SP); one surface with 65 pores per inch, having an average surface pore diameter of 95.52 microns (Large pores – LP) and one with a smooth surface (S). Six female adult Ellegaard Göttingen Minipigs were randomly allocated to two groups: a 10-weeks and a 20-weeks group. N=6 implants were placed in separate subglandular pockets in each animal.

The operation was well tolerated by all animals. No clinical signs of infection were noticed and the blood level of leucocytes was not elevated at any time of the study. At the end of the 20 week implantation period, it was observed that capsules derived from LP implants had the highest stiffness, followed by SP while S implants showed the lowest stiffness. Corresponding with capsule stiffness, LP implants also had a significantly higher stiffness compared to both SP and S implants ($p < 0.01$). In terms of tissue makeup, S group showed the least amount of collagen at 10-week time point while SP group were found to have the highest concentration. At 20-week time point, the collagen expression in S and LP group increased while it decreased in case of SP implants. Immunohistological staining performed on the tissue sections showed that at 10-week time point, S group had the highest concentration of alpha smooth muscle actin (SMA) while SP had the lowest; whereas at 20-week time point LP implants had the highest expression of alpha SMA and SP still showing the lowest expression. At 10-week time point, SP group showed the highest expression of Integrin B1 while S implant had the least expression. None of the groups showed any major expression of osteopontin at any of the time points.

Using the newly developed minipig model, we showed that there exists a correlation between the surface microtopology of a breast implant and the tissue response. However, this effect, at least within the experimental time period, did not improve the outcome of capsular contracture significantly when compared to smooth implants, suggesting that it may be challenging to guide the cellular response on the surface of the implants by modifications in surface design.

Therefore, based on our observations and those made by previous research studies, whereby it was shown that porous polyurethane foams are effective at significantly reducing the onset the capsular contracture[243-246], it was concluded that a porous biodegradable implant based on tissue engineering principles would provide an effective solution to many of the challenges posed by current generation of silicone implants. The following sections describe, in a step-by-step way, the novel methodologies developed within this PhD project to design and fabricate such porous highly customised scaffolds for breast reconstruction.

3.2 Development of a methodology to design and fabricate highly customised patient-specific biodegradable scaffolds

3.2.1 Conversion a medical imaging data set into a CAD format suitable for additive manufacturing

3D data can be obtained from a variety of medical imaging options including MRI scans, CT scans and laser digitiser scans. A methodology needed to be established to convert this data into CAD models in a format suitable for additive manufacturing. Beyond breast tissue engineering, it is evident that such a methodology will be appropriate for generating 3D models for potentially any defect in the human body. It was therefore decided to test the versatility of the method on medical imaging scans of a different region of the human body. High resolution CT scans (segment thickness of 1mm) of the breast region of a female patient and of a patient having a

skeletal tumour in the hip region were kindly provided by collaborators at the Department of Plastic Surgery and Department of Orthopaedic Surgery, Klinikum Rechts der Isar (Technical University Munich). In order to differentiate the soft tissue from bone within the imaging data, thresholding technique was employed [247]. Using the thresholding technique, a preliminary surface model of the region of interest (ROI) was generated using GNU 3D reconstruction software Invesalius 3.0 (Brazilian Public Software Portal). In order to create a 3D model suitable for additive manufacturing purposes, the model size needed to be reduced from approximately 1GB to 10MB or less. Re-meshing of the model, to reduce the number of triangles in the model without causing a loss to the overall structure of the object, was undertaken using the method of quadric error metrics [248].

Automatic functionality of open source software, Meshlab, was then employed to perform repairs on the CAD model. Such repairs included closing of holes on the surface, removal of duplicate faces, unifying normals for all triangles and removal of degenerate faces. The resultant file was deemed appropriate for additive manufacturing.

3.2.2 Generation of computer numerical code (CNC) from CAD models

Computer numerical code (CNC) is a programming language which controls the movements of most additive manufacturing systems. Therefore in order to fabricate a scaffold using a 3D printer, it becomes important to convert the 3D CAD model into a series of 2D cross-sectional slices and to program the movements of the 3D printer using these 2D slices as a guiding template – a process called slicing. A custom software/algorithm was therefore developed to slice the CAD models into CNC codes.

The developed software works in 3 successive steps. In the first step, the algorithm slices the CAD model saved in the Standard Tessellation Language (STL) format into 2D slices separated in the Z-axis by a distance defined by the user. The X/Y/Z coordinates of the outlines of these slices is saved in Scalable Vector Graphics (SVG) format. Once the layer contours are obtained, the next step would be to fill these outlines with an infill pattern. The current version of this slicing software can only implement line-based rasters. The spacing between these lines is defined by the user. Once the raster line generation process is complete, the raster lines of every layer are still aligned parallel to each other – compromising fluid flow and mechanical properties within the scaffolds. In order to generate the criss-cross rastering-based pattern commonly used in scaffolds, a rotational matrix has been implemented. Finally, the X/Y/Z coordinates of the rotated and aligned raster line segments are connected into a continuous line and saved in the CNC machining code format.

3.2.3 Development of automated algorithms to rapidly generate finite element models of a set of scaffolds varying in porosity, pore geometry, filament thickness, and pore interconnectivity directly from the CNC machining code

Using the scaffold design software described in the previous section, the porosity and pore sizes of the scaffolds can be tailored independently by changing the laydown pattern. The optimal porosity is always determined by a trade-off between mechanical properties and pore volume available for tissue ingrowth, as increasing porosity inevitably leads to reduction in mechanical stiffness[249]. Stiffness and strength should be sufficient in the context of breast tissue engineering, as the scaffold should be sufficiently robust to not only resist changes in shape *in vitro* as a result of cell contraction forces *yet also* the wound contraction forces which will be invoked during tissue regeneration. Furthermore, the breast region is also subjected

to high biomechanical loads during sleeping and sports activities, and the TECs must be able to withstand those forces over a long period of time.

Current methods of optimally designing a scaffold to balance mechanical strength and porosity depend largely on heuristic-based approaches, whereby scientists fabricate a large number of scaffold design candidates in the hope that one candidate will display suitable mechanical and physical properties when subjected to compression/tensile/torsional testing. However, this approach is inherently inefficient as the time needed to fabricate a single scaffold can range from 30 minutes to >5 hours depending on the size of the scaffold and print resolution. Moreover, the current approach also lends itself to increased cost of expensive biomaterials and waste (if proper biopolymer recycling systems are not in place).

Therefore, we developed automated algorithms to integrate *in silico* FEA-based pre-testing methods into the scaffold design process.

Parameters such as laydown pattern, filament spacing and filament thickness, which primarily control the mechanical properties of the scaffold are controlled by the software controlling the Fused Deposition Modelling (FDM) machine and are described within the CNC machining code. The movement of the FDM head, and consequently the final architecture, entirely depends on the CNC code. Therefore, generation of a finite element mesh directly from the CNC has the potential to recapitulate the final architectural properties of the scaffold.

A custom algorithm was therefore developed to generate finite element models (FEM) of scaffolds directly from the CNC code. Output from the software was directly fed into commercial finite element analysis (FEA) software Abaqus v12.0 (Dassault Systemes) to perform *in silico* compression testing of n=15 breast scaffold candidates with variations in laydown pattern, filament spacing and filament

thickness. Scaffold designs whose mechanical properties were deemed to be appropriate for breast tissue engineering were fabricated using a commercial 3D printer (Replicator, Makerbot industries, New York, USA). These fabricated scaffolds underwent compression testing using an Instron 5848 microtester fitted with a 500N load cell (Instron, Norwood, USA) to validate their mechanical properties. From the data obtained from the compression testing, one was chosen for further *in vitro* and *in vivo* testing.

3.3 Breast tissue engineering and *in vivo* assessment

3.3.1 *In vivo* test for subcutaneous adipogenesis and vascularisation in a nude rat model

Here we investigated patient-specific breast scaffolds fabricated from poly(D,L)-lactide polymer with pore sizes >1 mm for their potential use in long-term sustained regeneration of high volume adipose tissue.

The scaffold geometry was obtained via laser scanning from a mastectomy patient. All scaffolds (n=5), fabricated using Fused Deposition Modelling and, observing the tissue response towards textured surfaces described in Section 2.2, were etched with 0.5M NaOH for 5 minutes to introduce surface roughness and texture. Scaffolds were seeded with human umbilical cord perivascular cells and cultured under static conditions for 4 weeks and subsequently 2 weeks in a biaxial rotating bioreactor. These tissue-engineered constructs were then seeded with Human Umbilical Vein Endothelial Cells and implanted subcutaneously into athymic nude rats for 24 weeks. Angiogenesis and adipose tissue formation were observed throughout all constructs at all timepoints. The percentage of adipose tissue compared to overall tissue area increased from 37.17% to 62.30% between week 5 and week 15 ($p < 0.01$), and increased to 81.2% at week 24 ($p < 0.01$). The stiffness of the constructs decreased by

66% over 24 weeks, while the seeded endothelial cells self organised to form a functional capillary network.

3.3.2 De novo adipose tissue generation using a scaffold-based body-as-a-bioreactor approach

In our previous study, we undertook a progenitor-cell based approach towards adipose tissue regeneration. However, these cell-based approaches also lead to several disadvantages – ranging from problems with scaling up of tissue culture to requiring complex GMP-certified laboratories for tissue culturing [250-256]. Therefore, in this study we devised a concept of delayed fat injection combined with an empty biodegradable scaffold. 3 study groups were included in this study:

- 1) Empty scaffold.
- 2) Scaffold containing 4 cm³ lipoaspirated adipose tissue.
- 3) Empty scaffold + 2 week prevascularisation period. After 2 weeks of prevascularisation, 4 cm³ of lipoaspirated adipose tissue was injected into scaffolds.

6 implants were placed in each animal (n = 2 per group) and the animals were sacrificed after 24 weeks. Histological evaluation showed that multiple areas of well vascularised adipose tissue were found in all groups. The negative control empty scaffold group had the lowest relative area of adipose tissue (8.31% ± 8.94) which was significantly lower than both lipoaspirate-only (39.67% ± 2.04) and prevascularisation + lipoaspirate group (47.32% ± 4.12) and also compared to native breast tissue (44.97% ± 14.12) (p<0.05, p<0.01 and p<0.01 respectively). However, there was no statistically significant difference in relative adipose tissue area between the native breast tissue, lipoaspirate-only and prevascularisation + lipoaspirate group.

In this study, we have shown regeneration of *de novo* autologous adipose tissue by injecting a small volume of lipoaspirated tissue with no additional growth factors, cell transplantation or ligated vascular pedicles by introducing a completely novel prevascularisation technique that uses the patient's own body as a bioreactor and a source of blood vessels.


Chapter 4: Research Reports

4.1 STUDY ONE (PAPER TWO)

Mohit P. Chhaya, Inesa Sukhova, Dietmar W. Hutmacher, Daniel Mueller, Hans-Guenther Machens, Arndt F. Schilling and Jan-Thorsten Schantz.

The authors listed below have certified* that:

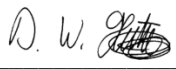
1. they meet the criteria for authorship in that they have participated in the conception, execution, or interpretation, of at least that part of the publication in their field of expertise;
2. they take public responsibility for their part of the publication, except for the responsible author who accepts overall responsibility for the publication;
3. there are no other authors of the publication according to these criteria;
4. potential conflicts of interest have been disclosed to (a) granting bodies, (b) the editor or publisher of journals or other publications, and (c) the head of the responsible academic unit, and
5. they agree to the use of the publication in the student's thesis and its publication on the QUT ePrints database consistent with any limitations set by publisher requirements.

Contributor	Statement of contribution
Mohit P. Chhaya	Performed laboratory experiments, data analysis and interpretation. Wrote the manuscript.
	
Signature	
Date 30 Jan 2015	
Inesa Sukhova	Performed animal surgeries, animal monitoring and microbiological data collection. Aided experimental design, data analysis and Manuscript preparation.
Dietmar W. Hutmacher	Provided technical guidance, aided data analysis and manuscript preparation.
Daniel Mueller	Aided manuscript preparation
Hans-Guenther Machens	Aided manuscript preparation
Arndt F. Schilling	Aided manuscript preparation
Jan-Thorsten Schantz	Involved in the conception and design of the project. Provided technical guidance and assisted in reviewing the manuscript.

Principal Supervisor Confirmation

I have sighted email or other correspondence from all Co-authors confirming their certifying authorship.

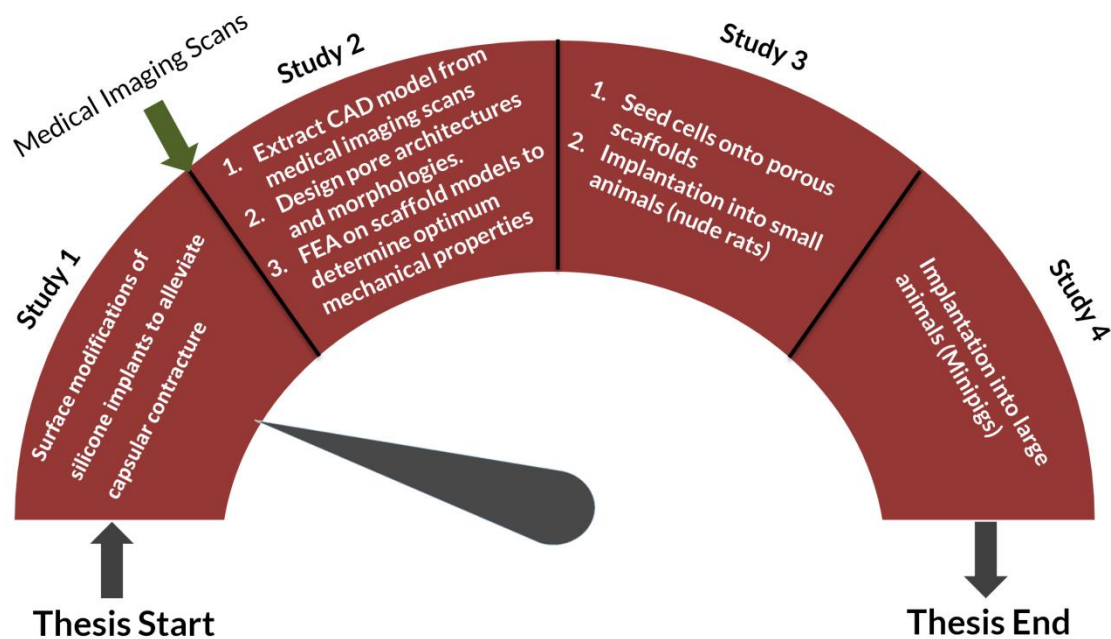
Dietmar W. Hutmacher
Name


Signature

30.01.2015
Date

Thesis Progress:

The following figure shows the flow of activities undertaken and methodologies developed as part of this PhD project. This study will aim to investigate whether surface modifications of breast implants on a microscopic level have a major influence on the cellular behaviour and foreign body response leading to capsular contracture



4.1.1 Introduction

Breast cancer is a major cause of illness for women, being responsible for more than 230,000 cases in 2011 in the US alone [257]. The most common surgical procedures to remove the tumor are lumpectomy, which is a partial removal of breast tissue, and total mastectomy, which is a total removal of the breast. Such procedures have a negative psychological effect on the well-being of the patient. They induce a psychological syndrome marked by “anxiety, insomnia, depressive attitudes, occasional ideas of suicide, and feelings of shame and worthlessness” [9]. There are several surgical approaches undertaken to reconstruct the aesthetic form of the

breast, of which the use of silicone breast implants continues to remain the reconstructive method of choice [258]. Among local complications experienced by women who have undergone reconstruction with silicone breast implants in the ensuing years, capsular contracture is the most common problem [259]. Capsular contracture refers to a foreign body reaction resulting into the formation of a capsule of rigid fibrous tissue around the implant [37-40]. Cell mediated contracture of this capsule ultimately leads to a spherical appearance of the breast and restricted shoulder or arm movement [41]. The frequency of occurrence of capsular contracture ranges from 15-45% depending on the study and the patient cohort that is investigated [10, 42-44]. The risk rises significantly when the breasts are irradiated following the implantation [45-48].

Capsular contracture is classified according to the Baker classification system [260], as follows: grade I, breast absolutely natural; grade II, minimum contracture; grade III, moderate contracture; and grade IV, severe contracture.

The pathophysiologic sequence of events leading to capsular contracture is still open to debate. A number of factors, including foreign body reaction, hematoma, and peri-implant infection, have been suggested to be the important in the pathologic process [261, 262]. Several lines of evidence suggest a role of subclinical peri prosthetic infection in capsular contracture pathogenesis [262-265]. In this process, local skin flora (e.g., coagulase-negative staphylococci, *Propionibacterium acnes*, and *Corynebacterium* species) may gain access to breast implants during or following placement. Bacterial biofilms on the implant then stimulate fibrosis around the implant, ultimately leading to capsular contracture [266, 267].

Ever since it was revealed that polyurethane-coated implants have lower rates of capsular contracture [243-246, 268, 269], research and industrial efforts have been

directed towards determining new ways of surface modifications to improve the outcome of silicone implants. Several studies have attempted subcutaneous and submuscular implantation of textured implants into animal models and evaluated the histology of the subsequently formed capsules. While some studies reported evidence of tighter and thicker capsules around textured implants compared with smooth implants [243, 270, 271], others showed a reduced occurrence of contracture with textured surface implants [272, 273].

To investigate these issues further, we designed an experimental model in the Göttingen Minipig using a bilateral subglandular pocket, with the only experimental variable being surface morphology. The surface morphologies consisted of a smooth surface, a textured surface with large pores and a textured surface with small pores.

The aims of the study were to (1) establish a Göttingen Minipig model that developed capsular contracture and was reproducible, (2) biomechanically analyse the elastic modulus of the capsules and the implants to assess the degree of overlying soft-tissue contracture, and (3) assess the effect of surface texturing in this model histologically.

4.1.2 Materials and Methods

Silicone Implants

All implants were kindly provided by Mentor LLC (Santa Barbara, USA), each having a volume of 40cc and a filling with Mentor Memory Gel™ Cohesive I™. The implants were manufactured with 3 different surfaces: one surface with 100 pores per inch, having an average surface pore diameter of 57.71 μm , another surface with 65 pores per inch, having an average surface pore diameter of 95.52 microns, and one with a smooth surface (data supplied by the manufacturer – see Supplementary Table 1). Hereon, the implants with an average pore diameter of 57.71 μm will be referred

to as Textured Small Pores (or SP abbreviated), implants with an average pore diameter of 95.52 μm will be referred to as Textured Large Pores (or LP abbreviated), while non-textured smooth implants will be referred to as Smooth (or S abbreviated).

Surgical procedure

The animal experiments were approved by the Animal Ethics Committee of the State of Bavaria, Germany. Eight female adult specific-pathogen-free (SPF) Ellegaard Göttingen Minipigs were used in this study. The minipigs were randomly allocated to two groups: a 10-weeks and a 20-weeks group. The operation was performed under general anesthesia, following the standard protocol of sterility requirements for breast augmentation procedures. During the implantation procedure of the first two minipigs just one big separate pocket was created on each side through a 20 cm incision in the middle of the abdomen. With this approach, the implants came into contact with each other in the middle of the pocket and formed a combined capsule. Therefore a separate evaluation of the capsules was not possible and the two minipigs were excluded from the study. Consequently, we modified the procedure in the remaining 6 minipigs by dissecting three separate subglandular pockets per side, one for each implant (Supplementary Fig. 1). 6 implants were placed in each animal (2 SP, 2 LP, 2 smooth). After the placement of the implants each pocket was closed up, so that the implants were fixed inside their separate pockets and had no contact to each other. Afterwards the tissue was closed in layers, the skin with a continuous subcuticular suture and three additional simple interrupted stitches.

Clinical evaluation of capsular contracture

The animals were monitored daily until the 14th postoperative day and subsequently weekly for postoperative complications and incidence of capsular contracture

according to the Baker score. At time of explantation the scoring was performed by a second surgeon.

Explantation

The explantation operation was performed under sterile conditions. Before washing the operation area, a microbiological swab from this skin area was taken. Through a lateral incision on both sides, each implant was removed *en bloc* along with its surrounding capsule (Supplementary Fig. 2). Directly after dissociating the implant from the capsule, a microbiological swab was taken from one half of the implant. The capsule from this half was sent for histological examination. From the remaining half, a capsule sample was taken for microbiological culturing and SEM scanning.

Mechanical Testing and Scanning Electron Microscopy

Compression testing was performed on the explanted scaffolds using an Instron 5848 microtester fitted with a 500N load cell (Instron, Norwood, USA). In order to minimise mechanical damage to the samples, the testing protocol comprised of a 50% compression in the case of silicone implants and 15% compression in the case of fibrotic capsules – both at a rate of 1mm/min.

The surface morphology of the implants and the fibrous capsules was examined using scanning electron microscopy (SEM) (Quanta SEM/FIB) at 10 kV. The samples were prepared according to our standard operating protocol for scanning electron microscopy (SEM) sample preparation: After collection the samples were fixed in 3% Glutaraldehyde at 4°C for at least 2d, subsequently washed with PBS, dehydrated in graded ethanol series and sputtered with gold.

Histological stainings

Hematoxylin & Eosin (H & E)

Implants were harvested from the pigs after 10 and 20 weeks. After explantation, tissue samples were fixed with 4% PFA, dehydrated and embedded in paraffin wax using a tissue processor (Excelsior ES, Thermo Scientific, Waltham, USA). Constructs were horizontally sliced to 7µm thickness, deparaffinised with Rotihistol, rehydrated with a decreasing series of ethanol and stained with H & E. Stained slides were scanned with the SCN400 slide scanner (Leica, Solms, Germany) at 20x magnification.

Massons Trichrome

The slides were deparaffinised with Xylene, rehydrated with a decreasing series of ethanol and re-fixed in Bouin's solution at room temperature overnight. After rinsing in tap water for 10 minutes, the slides were stained in Weigert's iron haematoxylin for 10 minutes, rinsed in running warm tap water, stained in Biebrich scarlet-acid fuchsin solution for 10 minutes and transferred directly into aniline blue solution and stained for 10 minutes. The slides were rinsed briefly in distilled water and differentiated into 1% acetic acid solution for 5 minutes.

Immunohistochemical staining

Endogenous peroxidase activity was blocked by incubating the slides with 3% H₂O₂ at room temperature. Slides were washed thrice with Tris-HCL (pH 7.4) for 2 minutes and placed in tri-sodium citrate buffer for 20 min at 95 °C in a decloaking chamber. The slides were incubated with 2% bovine serum albumin (BSA) for 60 minutes at room temperature and incubated with pre-diluted corresponding primary antibody overnight at 4°C. All primary antibodies used are listed in Supplementary Table 2. The slides were then incubated with immunoglobulin as secondary antibody as part of the DAKO Envision Dual Link System-HRP (Ref: K4061, Dako, Glostrup, Denmark) for 30-45 min at room temperature. The slides were washed 3 times with

Tris-HCl and colour was developed by incubating the slides with 3,3'-Diaminobenzidine (DAB) solution (1:50) [DAKO liquid DAB+ substrate Chromagen System, Ref: K3468, Dako, Glostrup, Denmark]. Finally, the slides were washed once with Tris-HCl for 2 minutes and counter-stained with Haematoxylin for 2 minutes followed by 30 second immersion in 0.1% Ammonium Hydroxide.

All histological evaluations were performed blinded.

Histomorphometry

Histomorphometrical analysis to determine capsule thickness was undertaken using a semi-automated approach. The measurements were performed blinded on 10 consecutive sections from each sample at each timepoint. The slides were relabelled by a co-worker who kept the ID key throughout the measurement period. Tiled images representing the entire section were imported as a batch in ImageJ (National Institute of Health, Bethesda, USA) and measurement lines, approximately 50µm apart, were defined on the fibrotic capsule. Thickness of the fibrotic capsule was derived from the average lengths of these measurement lines.

Microbiology

For the capsule tissue dissociation test, 1 cm² biopsy from each fibrous capsule was dissociated in 1ml Phosphate-buffered saline (PBS) with gentle MACS™ Dissociator (Miltenyi Biotec GmbH, Bergisch Gladbach, Germany) under sterile conditions. From the dissociated capsule tissue as well as from the swabs mentioned in the explantation section a microbiological differentiation was performed.

Statistics

All data are represented as mean ± SD and are subjected to one-way analyses of variance (one-way ANOVA) and Tukey's post-hoc test (Sigmaplot 12.5). Significance levels were set at $p < 0.05$.

4.1.3 Results

Microbiological Analysis

No clinical signs of infection were noticed and the blood level of leucocytes was not elevated at any time of the study. The bacteria found on the implants and capsules corresponded to the bacterial skin flora of the minipigs. In the 10-weeks group no microbiological swabs from the textured small implant surfaces showed any bacterial growth. However, in 3 of 4 (75%) capsules prepared by dissociation technique a moderate growth of *Staphylococcus lugdunensis* was detected. In 2 of 4 (50%) large textured surfaces a moderate growth of bacteria was found, *Staphylococcus xylosus* with both methods and *Staphylococcus lugdunensis* only by dissociation. Bacteria (*Staphylococcus hyicus*) in the smooth surface group were found in 1 of 4 (25%) fibrous capsules biopsies. The swabs were negative. In the 20-weeks group in 1 of 8 (12.5 %) textured small surfaces an isolated growth of *Staphylococcus hyicus* in the swabs was observed. The same bacteria were found in the collagen capsule of this implant after dissociation. In addition a growth of *Staphylococcus xylosus* was detected only by dissociation technique. In 3 of 8 (37.5 %) fibrous capsules from large textured surfaces a bacterial growth (*Staphylococcus hyicus*, *Streptococcus viridans*, *Staphylococcus epidermidis*) was detected. All the microbiological swabs were negative. 2 of 8 (25%) fibrous capsules from smooth implants showed positive bacterial growth (*Staphylococcus capitis*, *Staphylococcus warneri*) in the biopsy. In this group all the microbiological swabs were negative as well. Overall more bacteria were detected with the dissociation technique than with the conventional swab method.

Clinical Observations

The operation was well tolerated by all animals, the wound healing process had no complications and no clinical signs of infection were apparent. The first palpable

capsular contracture occurred 6 weeks post implantation. After 10 weeks most of the implants developed a Baker II capsular contracture, only 25% of the SP implants showed a Baker III capsular contracture. Corresponding to the macroscopic observations the number of severe capsular contracture (Baker III/IV) increased in all groups after 20 weeks. The smooth surface implants showed with 37% the lowest occurrence of severe capsular contracture (Baker III/IV), followed by implants with small pores with 50%. Most frequently we could observe severe capsular contracture around implants with large pores (62.5%). However, the differences between the three groups were not significant.

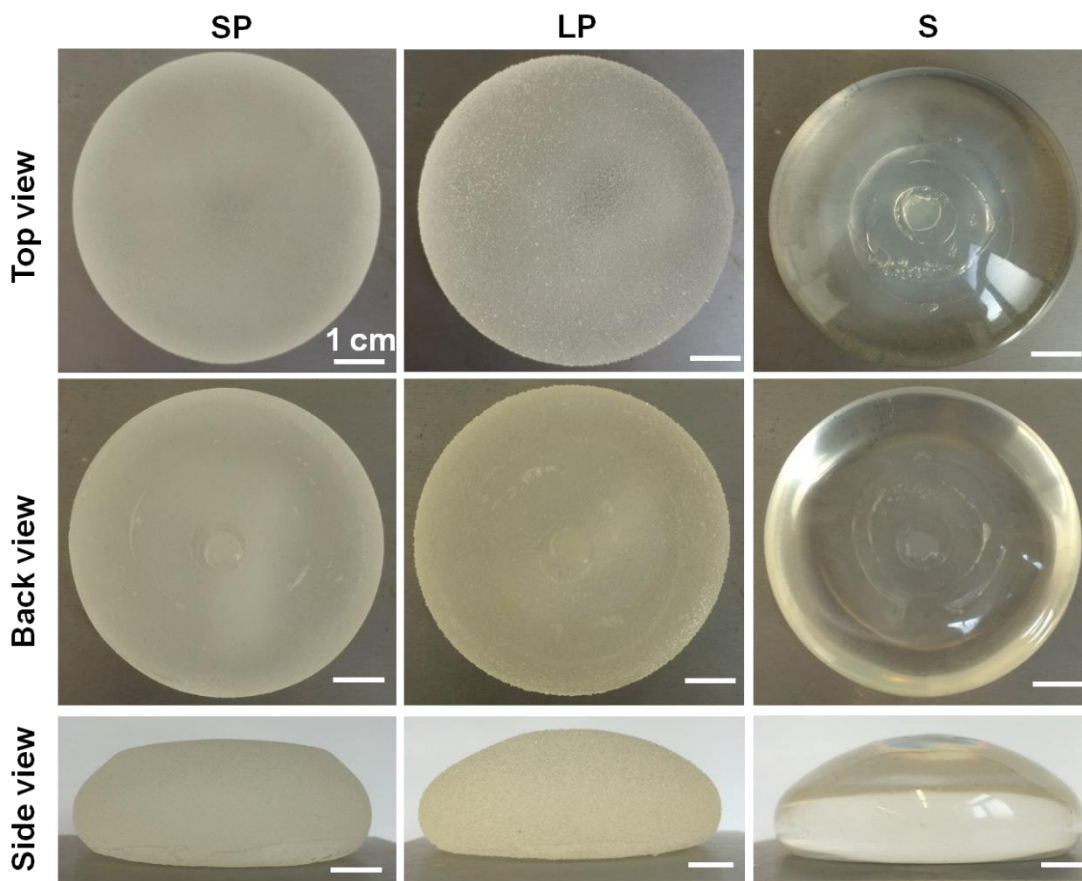


Figure 4.1.1 Gross morphology of S, SP and LP implants prior to implantation

SEM

The scanning electron microscopy illustrates the different surface architecture of the three different surface types (Fig. 4.1.1). The surface of the LP implants consists of

irregularly arranged peaks and valleys building the pore structure. The SP implants show very similar pore architecture, albeit smaller sized pores. The corresponding capsules reveal a complementary imprint of the pores indicating tissue ingrowth inside these pores (Fig. 4.1.2).

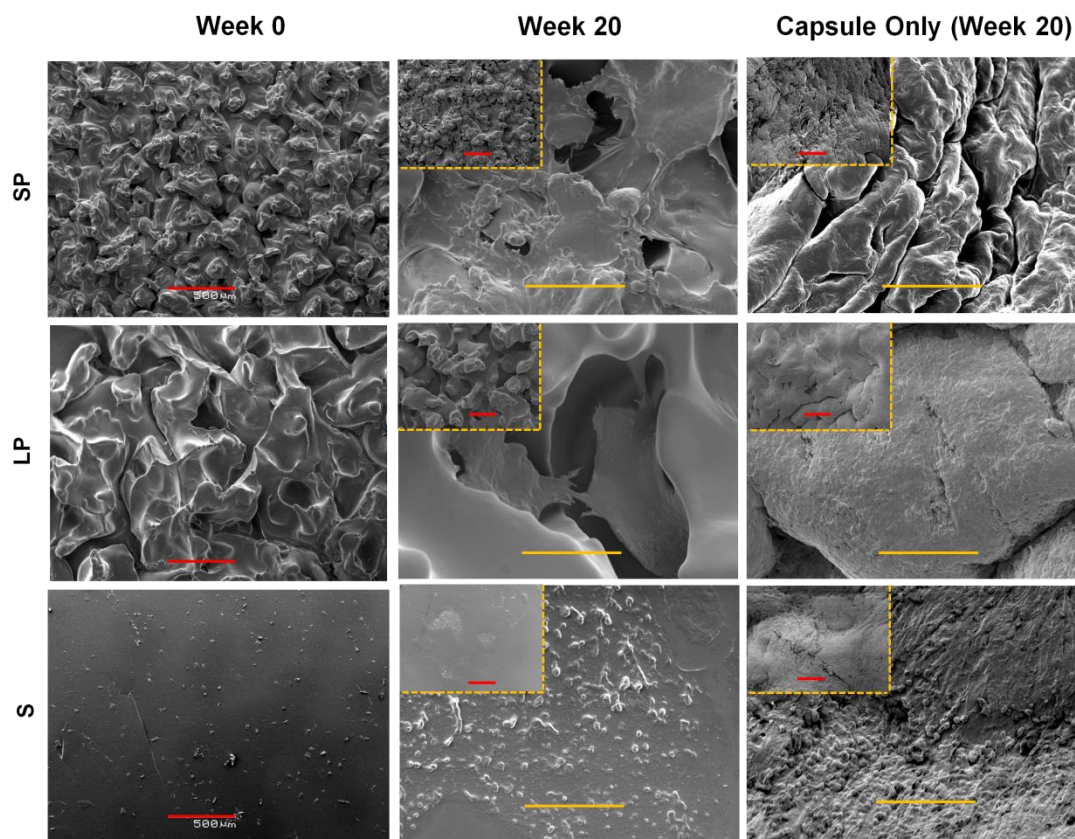


Figure 4.1.2 SEM images of the surface of the LP implants consisting of irregularly arranged peaks and valleys building the pore structure at 20 week time point. The SP implants show very similar pore architecture, however, smaller sized. The corresponding capsules reveal a complementary imprint of the pores indicating tissue ingrowth inside these pores. Red scale bars represent 500 μ m. Yellow scale bars represent 100 μ m

Biomechanical testing

Biomechanical analysis of intact implants revealed that all devices remained intact and compliant throughout the experimental period. 20 weeks post-implantation, the increase in stiffness of the S and SP implants was not statistically significant, while we observed a statistically significant increase in stiffness in the LP implants (Fig 4.1.3a; $p < 0.05$). At the end of the experimental period, SP implants had the highest stiffness, followed by LP implants, while the S implants had the lowest stiffness. The

intra-group differences in stiffness at week 20 were all statistically significant ($p < 0.05$ between S-LP; $p < 0.01$ between LP-SP and S-SP).

In case of capsules, the specimens had both geometrical as well as structural non-linearities, therefore a stiffness modulus cannot be defined. However, a plot of Reaction Force vs Strain shown in Fig 4.1.3b provides an idea of the inherent stiffness of the capsules (data averaged for $n=15$ samples – 2000 data points per sample). Only average values have been shown. Standard deviations for individual data points have not been shown to preserve legibility). Concurring with the stiffness data of intact implants, capsules extracted from the S implants had the lowest stiffness, followed by SP. Contrary to the observation in the intact implants, capsules extracted from the LP implants showed the highest stiffness.

Capsule Thickness

Within the 10-week time point, no significant differences were observed in the mean capsule thicknesses (Fig 4.1.3c). The thickness was determined to be around $2000\mu\text{m}$. However, significant inter-group differences were observed in the thickness of the capsule samples extracted at the 20-week time point. Overall, capsules extracted from 20-week time point were significantly thicker compared to those extracted from 10-week time point. The thickest capsule was observed in case of LP implants – corresponding well with the biomechanical testing data. Large variability was observed in the specimen capsule thickness from the SP implants and the difference in the capsule thickness between S and SP implants was not statistically significant.

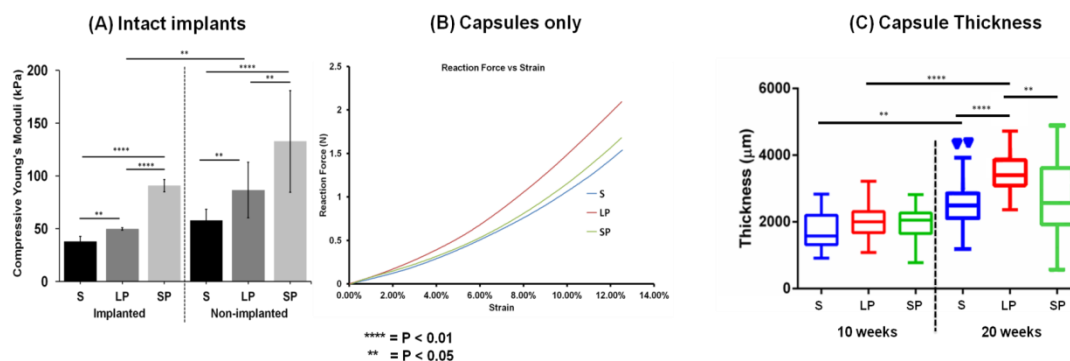


Figure 4.1.3 (A) Bar graph showing the Young's moduli of unused silicone implants and used implants after 20 weeks of *in vivo* implantation. Prior to implantation, SP implants had the highest overall stiffness, while S and LP implants had similar stiffnesses. However, after 20 weeks implantation, the stiffness value of SP implants grew significantly while those of S and LP implants remained relatively constant. (B) Line graph showing Force vs Displacement plots from the compression testing of extracted capsules surrounding the implant. LP capsules showed the highest stiffness, while the stiffnesses of S and SP implants were similar. (C) Box and Whiskers plot of capsular thicknesses at 10 week and 20 week time points. At the 10 week time point, the capsular thicknesses of all implants was the same; however, after 20 weeks, the thickness of capsules from all groups was seen to increase. LP capsules were found to be the thickest, whereas there was no statistically difference between the thicknesses of S and SP capsules.

Tissue Morphology

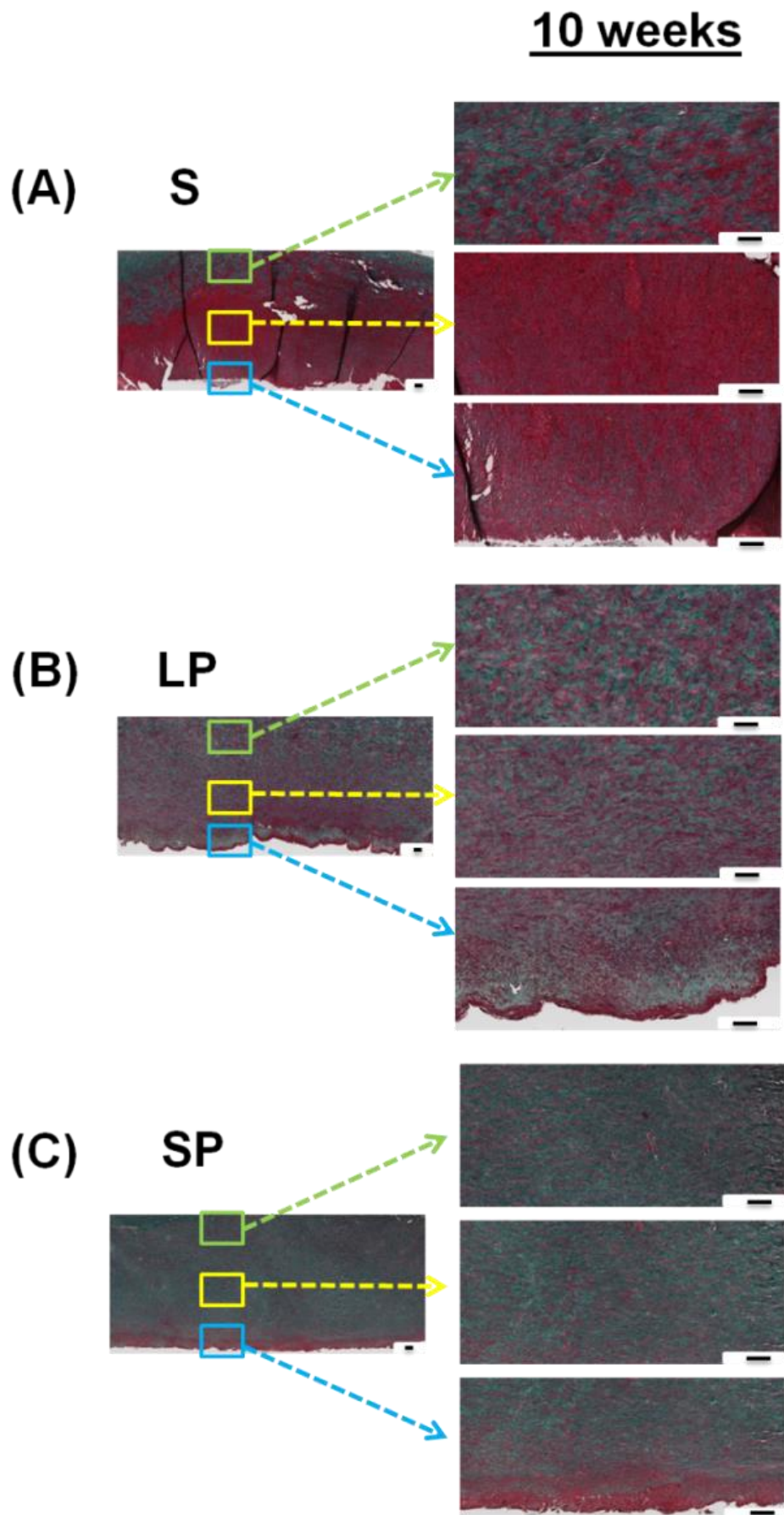
10 weeks time point:

Masson's Trichrome Staining showed that at the 10-week time point (Fig 4.1.4 a-c) S implants had the lowest accumulation of collagen throughout the thickness of the capsule (Fig 4.1.4a). SP implants had the highest overall accumulation (Fig 4.1.4c). Also, the collagen fibres seemed to align continuously parallel to the implant surface. Interestingly, the capsule-implant interface area did not show any collagen fibres. Capsules from LP implant showed an intermediate distribution of randomly aligned collagen fibres (Fig 4.1.4b). Similar to the capsules from SP implants, the capsule-implant interface was devoid of collagen.

20 weeks time point:

Overall, capsules derived at the 20-week time point (Fig 4.1.4 d-f) showed a higher accumulation of collagen in all specimens. A trend reversal was also observed where S capsules showed the highest accumulation of well-aligned collagen fibres throughout the thickness of the capsule (Fig 4.1.4d). SP and LP capsules displayed a

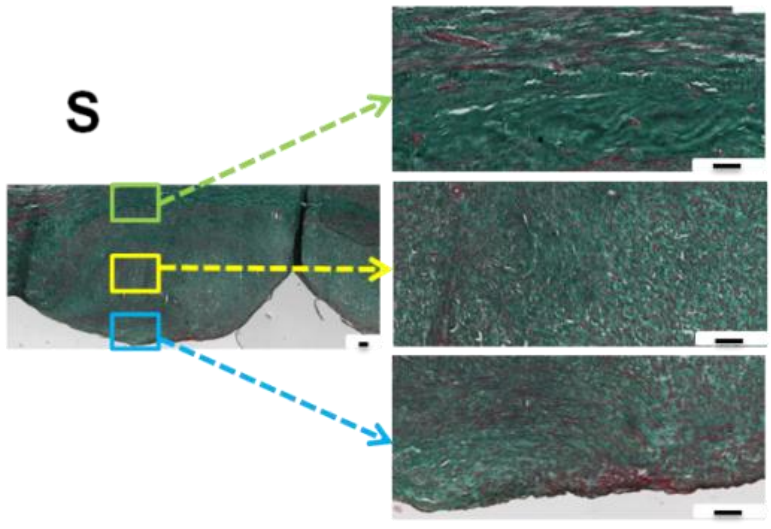
non-aligned and discontinuous collagen fibre network at the tissue-implant interface (Fig 4.1.4 e-f). The density and the alignment of these fibres increased with increasing distance from the interface.



20 weeks

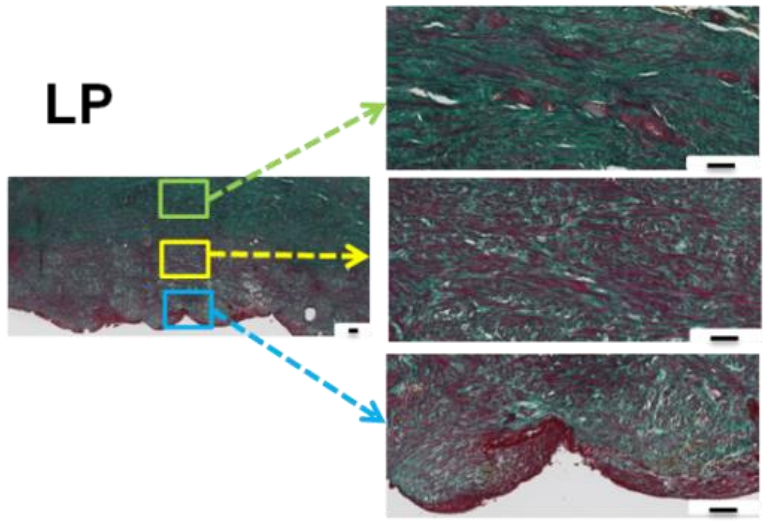
(D)

S



(E)

LP



(F)

SP

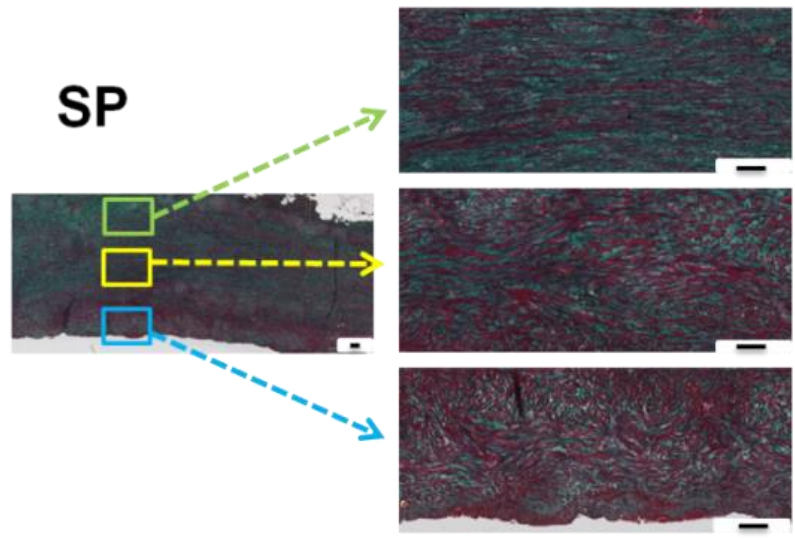


Figure 4.1.4 (A-C) Masson's Trichrome staining showing representative images of tissue morphology of fibrous capsules from implants removed at 10 week time point. Blue boxes and arrows show the regions at the tissue-implant interface and green boxes show capsular regions distal to the implant. S implants had the lowest accumulation of collagen throughout the thickness of the capsule (A). On the other hand, SP implants had the highest overall accumulation (C). Also, the collagen fibres seemed to align continuously parallel to the implant surface. The capsule-implant interface area did not show any collagen fibers. Capsules from LP implant showed an intermediate distribution of randomly aligned collagen fibres (B). Similar to the capsules from SP implants, the capsule-implant interface did not contain collagen. All error bars represent 100µm.

(D-F) Masson's Trichrome staining showing representative images of tissue morphology of fibrous capsules from implants removed at 20-week time point.

Overall, capsules derived at the 20 week time point showed a higher accumulation of collagen in all specimens. A trend reversal was also observed where S capsules showed the highest accumulation of well-aligned collagen fibers throughout the thickness of the capsule (D). SP and LP capsules displayed a non-aligned and discontinuous collagen fiber network at the tissue-implant interface (E, F). The density and the alignment of these fibers increased as the distance from the interface increased. All error bars represent 100µm.

Immunohistology

10 weeks time point:

As observed with Trichrome staining, S capsules showed the least amount of Collagen 1 through the thickness of the capsule, while SP capsules the highest amount (Fig 4.1.5 d-f).

On the other hand, staining for Alpha SMA showed an opposite trend, with S capsules showing the highest concentration throughout the thickness, followed by LP and with SP capsules having the least concentration of Alpha SMA (Fig 4.1.5 g-i).

Integrin B1, which plays an essential role in cell adhesion [274-277], was present all across the thickness of the SP capsules – including the tissue-implant interface. On the other hand, S capsules only showed an Integrin B1 expression at the tissue-

implant interface. Finally, the expression in LP capsules was limited to areas considerably further away from the tissue-implant interface (Fig 4.1.5 j-l).

Expression of Osteopontin, which has been shown to be involved in the regulation of pathological mineralisation [278], was also tested (Fig 4.1.5 m-o). Only SP capsules showed isolated patches of Osteopontin expression. S and LP capsules did not show any evidence of Osteopontin expression.

20 weeks time point:

As described previously, the collagen expression in all samples increased between 10- and 20-week time points (Fig 4.1.6 d-f).

As the collagen 1 levels increased, the expression of Alpha SMA decreased concomitantly (Fig 4.1.6 g-i). LP showed the largest spread of Alpha SMA however the regions which did show its expression were small and scattered. On the contrary, SP capsules showed smaller regions of Alpha SMA which were concentrated near the tissue-implant interface.

Integrin B1 expression pattern remained the same in case of S and LP capsules (Fig 4.1.5 j-l); however, it was seen to increase considerably in case of SP capsules. While the highest concentration of Integrin B1 expression was seen at the tissue-implant interface of SP capsules, less intense expression was also noted throughout the thickness of the capsule.

No sample at the 20-week time-point showed a significant expression of Osteopontin (Fig 4.1.5 m-o).

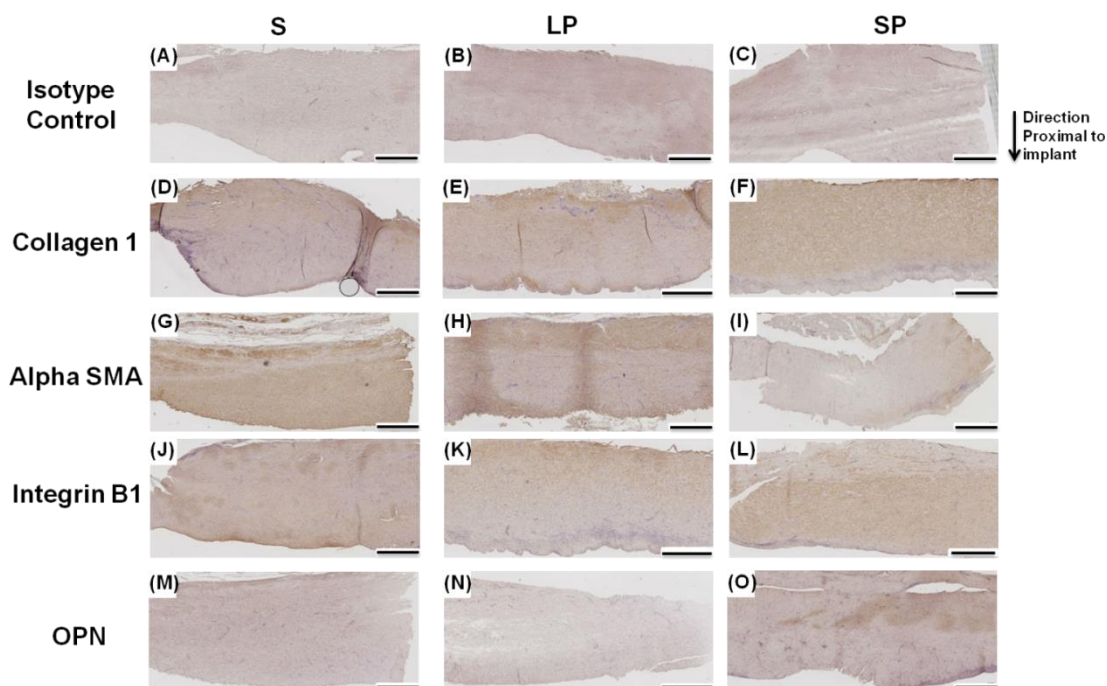


Figure 4.1.5 Representative immunological staining images of protein expressions in capsules extracted at 10 week time point. S capsules showed the least amount of Collagen 1 through the thickness of the capsule (D), while SP capsules the highest amount (F). Staining for Alpha SMA showed an opposite trend, with S capsules showing the highest concentration throughout the thickness (G), followed by LP (H) and with SP (I) capsules having the least concentration of Alpha SMA. Integrin B1 was present all across the thickness of the SP capsules – including the tissue-implant interface (j-l). On the other hand, S capsules only showed an Integrin B1 expression at the tissue-implant interface (J). Finally, the expression in LP capsules was limited to areas considerably further away from the tissue-implant interface. Only SP capsules showed isolated patches of Osteopontin expression. S and LP capsules did not show any evidence of Osteopontin expression. All error bars represent 1mm.

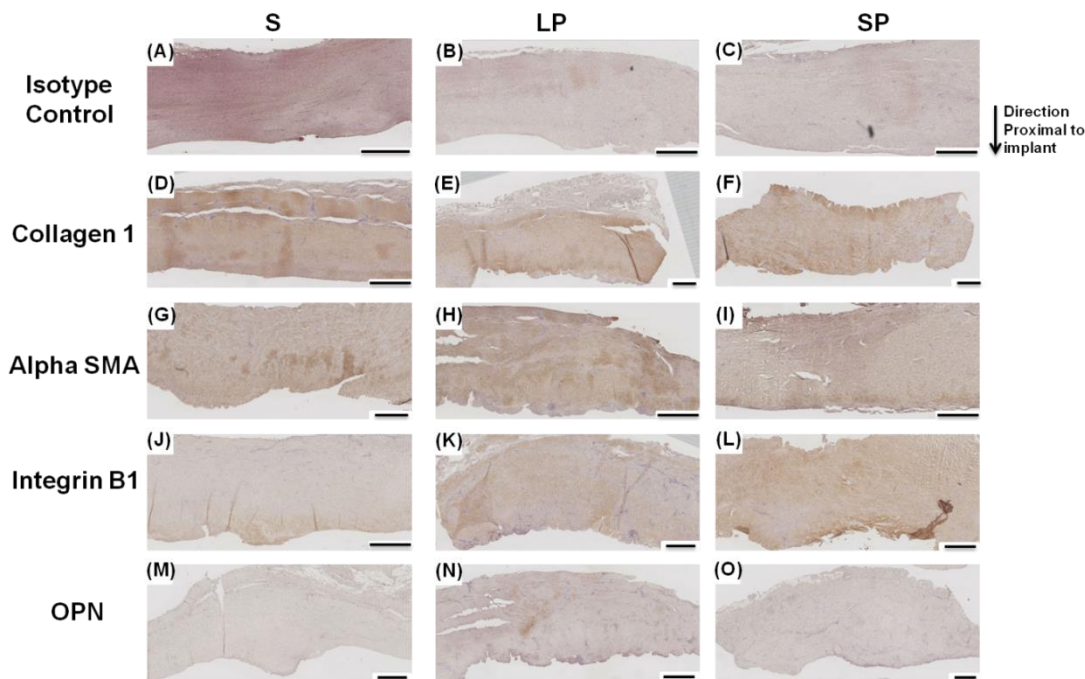


Figure 4.1.6 Representative immunological staining images of protein expressions in capsules extracted at 20 week time point. It is noteworthy to observe that Collagen 1 was detected near the tissue-implant interface in all groups (D-F). The levels of Alpha SMA decreased in all groups (G-I). LP showed the largest spread of Alpha SMA however the regions which did show its expression were small and scattered (H). On the contrary, SP capsules showed smaller regions of Alpha SMA which were concentrated near the tissue-implant interface (I). Integrin B1 expression pattern remained relatively unchanged from Week 10 in case of S and LP capsules (J, L); however, it was seen to increase considerably in case of SP capsules (L). While the highest concentration of Integrin B1 expression was seen at the tissue-implant interface of SP capsules, less intense expression was also noted throughout the thickness of the capsule. No samples at the 20 week time-point showed a significant expression of Osteopontin (M-O).

4.1.4 Discussion

Tissue interaction with implant surfaces is of critical importance for the biocompatibility of biomaterials and prosthetic implants. The foci of this study were on establishing a minipig model to study capsular contracture and determining the effect of implant surface topology on fibrosis around the silicone implant. When silicone implants are placed in the human body, they elicit a chronic inflammatory response characterised by a fibrotic capsule that eventually contracts. Studies have shown that this capsule does not adhere to the implant surface itself, allowing for relative sliding and friction between tissue and implant [279]. It has been speculated that this friction, in turn, promotes the accumulation of inflammatory cells at the

implant-tissue interface and thereby causes significant clinical problems. In their topical review on implant surfaces, Recum and van Kooten [279] propose that, if connective tissue adhesion can be achieved, it would anchor the implant in its tissue bed, eliminate the dead space surrounding it and alleviate the problems associated with the formation of a chronic inflammatory tissue capsule. Ratner further reviewed various surface modifications which could lead to a better adhesion between the implant and tissue and concluded that surface roughness on a micrometer scale has a significant effect on the cellular response and behaviour [280].

In this study, we have created a reproducible porcine subglandular model of capsule formation which allows a comparison of histology with biomechanics. According to Clugston *et al.*, [273] some characteristics of the skin of small animals such as rats and rabbits differ greatly from those of humans due to the ample mobility of the panniculus carnosus area. Pigs on the other hand have a well-differentiated epidermal structure, with a thick dermis that is rich in elastic fibres and more strongly attached to deeper tissues. In other words, they have certain similarities with humans, but structural differences persist that are inherent to the species [281, 282]. In addition, the study was directed towards evaluating whether or not implantation of smooth and textured implants could generate different tissue responses and lead to different capsule stiffness. Using this model, our results indicate that implant surface topology has a significant impact on the stiffness and composition of the fibrous capsules surrounding the implant. Capsules extracted from SP implants had stiffness values very close to that of those extracted from smooth implants. Capsules extracted from LP implants had the highest thickness and also the highest stiffness. Brohim *et al* [283] showed that pores smaller than 150 μ m in height or depth lead to formation of a continuous capsule which increases capsule thickness and the risk of capsular

contracture. Since the average pore-height in the SP and LP implants used in this study ranged from 63-75 μm , it seems likely that the pores were not sufficiently deep to have a major influence on capsular thickness and consequently capsular contracture. Future studies using SP and LP implants with pore depths ranging from 50-200 μm are therefore required to provide further insights into the relationship between pore depth and capsular thickness.

It has long been known that a major cause of capsular contracture is the presence of myofibroblasts characterized by abundant stress fibres and increased ECM production [284, 285]. Previous research has established that the most prominent marker of fibroblast to myofibroblast transition is αSMA and the high contractile behaviour generated by αSMA in stress fibers plays a fundamental role in remodelling injured tissue in wound healing [286, 287]. Results from our study indicate that alpha SMA expression levels significantly rose in case of capsules extracted from textured implants containing large pores. Based on the above cited research, it can be concluded that fibroblasts in these capsules are undergoing transformation into myofibroblasts, eventually leading to capsular contracture. This effect is clearly reflected in the biomechanical data, where capsules extracted from these implants also showed the highest stiffness. Although the capsules extracted from textured implants containing small pores show a high expression of alpha SMA at the 10 week time point, the expression levels decreased dramatically over the following 10 weeks – to the point where the regions expressing alpha SMA were localised near the tissue-implant interface which could perhaps be an indication of a stronger bond between the tissue and the implant. As described previously, a stronger tissue-implant bond is hypothesized to play a crucial role in alleviating the effects of capsular contracture. However, further research is needed to determine whether this

localized expression of alpha SMA does lead to better bonding at the tissue-implant interface.

Perhaps Integrin B1 is a better indicator of a stronger bond at the tissue-implant interface. As mentioned previously, Integrins are a family of heterodimeric transmembrane glycoproteins that mediate cell attachment and adhesion [274-277]. While this protein has been studied extensively, there is a lack of studies specifically targeting its role in capsular contracture. Our results, however, give a strong indication that different implant surface morphologies lead to distinct expression patterns of Integrin B1 which correlate with the capsule stiffness measurements.

Interestingly, there was less collagen 1 detected using immunohistochemistry in LP samples compared to what was observed in the Trichrome staining. It is possible that other collagens (especially collagen III) play a role that are detected by Trichrome staining but not by the specific collagen I antibody [243].

Histomorphological analysis of the capsules in this study demonstrated a direct relationship between the thickness of the capsule and its stiffness, which corroborates previous studies [288, 289]. As expected, a reduction in alpha-smooth muscle actin and an increase in collagen also correlated with capsule stiffness. A review of the literature demonstrates studies that support [290, 291] and contradict [292, 293] these findings.

The presented study can be classified as a simplified experimental model of a complex biological phenomenon seen in human tissue interactions with silicone implants; hence, while meaningful, the data may not be completely translatable. However, since all implants tested were composed of the same synthetic material, their inflammatory responses should be comparable. For future studies, it would be

interesting to test textured implants with a range of different pore sizes and also perhaps to run the experiment for a longer time period.

4.1.5 Conclusion

There exists a correlation between the surface microtopology of a breast implant and the tissue response. However, this effect, at least within the experimental time period, did not improve the outcome of capsular contracture significantly when compared to smooth implants.

The reported *in vivo* model now makes it possible to test implants in an environment that is very close to the human equivalent. This will allow researchers to iteratively improve the surface microstructures designs and hopefully lead to novel approaches that can limit the incidences of capsular contracture.

4.1.6 Supplementary Figures and Tables:

Implant Surface	Average diameter of the surface pore (micron)	Average length of the peaks (micron)	Average length of the valleys (micron)
100ppi texture (SP)	57.71	63.30	56.15
65ppi texture (LP)	95.52	70.02	74.36
Smooth (S)	no pores	no pores	no pores

Supplementary Table 1: Implant surface characteristics of the three tested implant-types; ppi: pores per inch; SP: Small Pores; LP: Large Pores; S: Smooth

Primary Antibodies	Description
Collagen 1	Polyclonal Mouse Anti-Collagen: Ref ab90395 (Abcam, Cambridge, England)
Smooth Muscle Actin	Rabbit Polyclonal Anti-Alpha Smooth

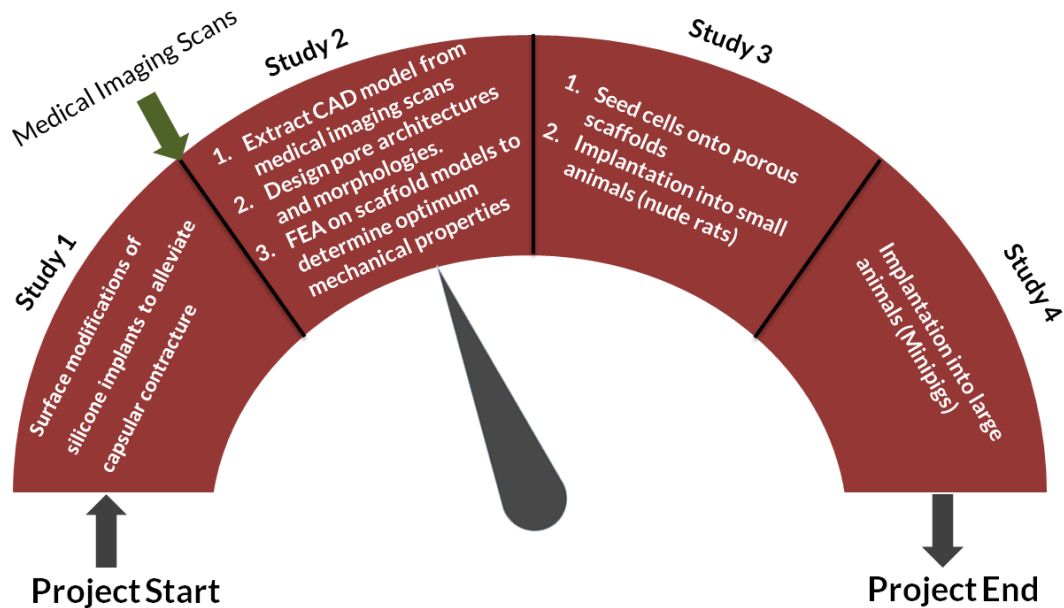
	Muscle Actin antibody: Ref ab5694 (Abcam, Cambridge, England)
Integrin B1	Rabbit Polyclonal Anti-Integrin B1 antibody: Ref 4706P (Cell Signalling Technologies, Denver, USA)
Osteopontin	Rabbit Polyclonal Anti-Osteopontin antibody: Ref ab8448 (Abcam, Cambridge, England)

Supplementary Table 2. List of primary antibodies.

4.2 STUDY TWO

Thesis Progress:

The following figure shows the flow of activities undertaken and methodologies developed as part of this PhD project. The previous study showed that textured implants did not improve the outcome of capsular contracture significantly when compared to smooth implants. It was concluded that a porous biodegradable implant based on tissue engineering principles would provide an effective solution to many of the challenges posed by current generation of silicone implants. This chapter details the methodologies developed as part of this PhD project to fabricate patient-specific scaffolds using medical imaging scans.



4.2.1 Development of a methodology to design and fabricate highly customised patient-specific biodegradable scaffolds

4.2.1.1 Introduction

For reconstructing a 3D model of a patient's body region using medical imaging methods, 2 approaches are commonly used: generating 3-dimensional volume from a

surface scan (eg laser scanning) and generating a 3D surface out of a 3D volume scan (eg MRI/CT/Ultrasound). The methodology developed in this study is primarily related to merging the volume with the surface to yield a solid CAD model suitable for additive manufacturing purposes. In order to validate this novel methodology, two proof-of-concept trials were undertaken:

1. Generating 3D volume of a breast from surface scans using a laser digitiser (described in detail by Melchels *et al* [91]) . Briefly, a Vivid 910 dot-laser scanner with built-in high precision camera (Konica Minolta, Marinouchi, Japan) was used to perform a 3D scan of the patient from three angles (0° frontal, and -30° and $+30^{\circ}$ oblique anterior). The images were imported in Rapidform2006 (Inus Technology, Seoul, South Korea) and merged into a single-shell object [81]. A custom surfacing algorithm was generated to model a virtual chest wall which was merged with the breast surface shell to obtain a watertight model of the solid breast. This watertight model was then meshed and exported as a Standard-Tessellation-Language (STL) file.
2. Generating a high-fidelity 2D surface from a volume scanned using MRI/CT scans. Commercial software is then used to generate a 3D volume of the region of interest from a stack of 2D scan slices.
 - a. Beyond breast tissue engineering, it is evident that such a methodology will be appropriate for generating 3D models for potentially any defect in the human body. It was therefore decided to test the versatility of the method also on medical imaging scans of a different region of the human body (the hip).
 - b. Clinical high resolution CT scans (segment thickness of 1mm) of a patient having a skeletal tumour in the hip region were kindly

provided by collaborators at the Department of Orthopaedic Surgery, Klinikum Rechts der Isar (Technical University Munich, Germany). Approximately 3000 slices of the region were taken and saved in the DICOM format.

4.2.1.2 Materials and Methods

Software

To render the surface of the scan region in 3D, free (GNU GPL 2) 3D reconstruction software Invesalius 3.0 (Brazilian Public Software Portal) was utilised.

Region of Interest (ROI)

A free-form region of interest (ROI) was sketched manually along the boundary of the hip bone.

Thresholding

In order to differentiate the soft tissue from the bone, thresholding technique was employed [247]. Bone was identified in the threshold range of -17 to 1802 Hounsfield units (HU), while soft tissue was identified in the range of -590 to -370 HU which is consistent with previously published studies [294, 295]. This distinction is important because the same technique can also be used to isolate the soft tissue in the breast region and reconstruct the surface of the breast.

The quality of the 3D model changes with threshold level being used. Holes are generally seen in the model where the threshold levels have been too high to detect the sparser bone areas. While small-sized holes can be filled with a hole-filling algorithm, large sized holes can cause severe problems during the additive manufacturing process. Moreover, scan artefacts arising due to imperfections in the scan, metallic implants within the patient or patient movements during the scan are

more likely to be included in the 3D model when the threshold level is too low. Such artefacts are also problematic for the additive manufacturing process. Because the bone density in various bone-types is different, the threshold levels will vary from scan to scan. Therefore, the optimum threshold level will need to be determined by finding the right balance between the number of holes within the model and scan artefacts every time a model needs to be generated (see Fig 4.2.1).



Figure 4.2.1 The effect of threshold levels on the quality of the 3D model. A - Threshold level at 1900 Hounsfield units (HU) which is too high resulting in holes within the 3D model. B – Thresholding level at 100 HU resulting into artefacts arising out of imperfections in the CT scan. C – Optimum threshold level resulting into completely formed bone with minimum artefacts.

Model re-meshing and repairing:

The CAD model generated using Invesalius was approximately 1GB in file-size. Most currently available computer systems, due to memory and RAM limitations, are unable to process such large CAD files for purposes of additive manufacturing. Therefore, the file size needed to be reduced to 10MB or less. Therefore, the number of triangles within the STL file needs to be reduced without causing a loss to the overall structure of the object. Re-meshing of the model was undertaken using the method of quadric error metrics, explained in detail by Garland *et al* [248] with the aid of a MeshLab software (ISTI-CNR research centre, Rome, Italy). Briefly, the algorithm aims to merge edges shared between adjacent groups of triangles into one. When this operation is complete, all edges and faces connected to the removed vertices are connected to the newly formed vertex. In order to undertake the

simplification, the boundary preserving weight parameter of the algorithm was chosen to be 1.0 meaning that the boundary of the model has the same importance as the rest; whereas values higher than 1 raise the boundary importance and produce the effect of removing fewer vertices on the border. Using these settings, the CAD model was re-meshed down to a file-size of ~3MB.

Automatic functionality of Meshlab was then employed to perform repairs on the CAD model. Such repairs included closing of holes on the surface, removal of duplicate faces, unifying normals for all triangles and removal of degenerate faces (Fig 4.2.2 shows the results of the re-meshing operation). The resultant CAD file was saved in the Standard Tessellation Language (STL) format to be used for further processing.

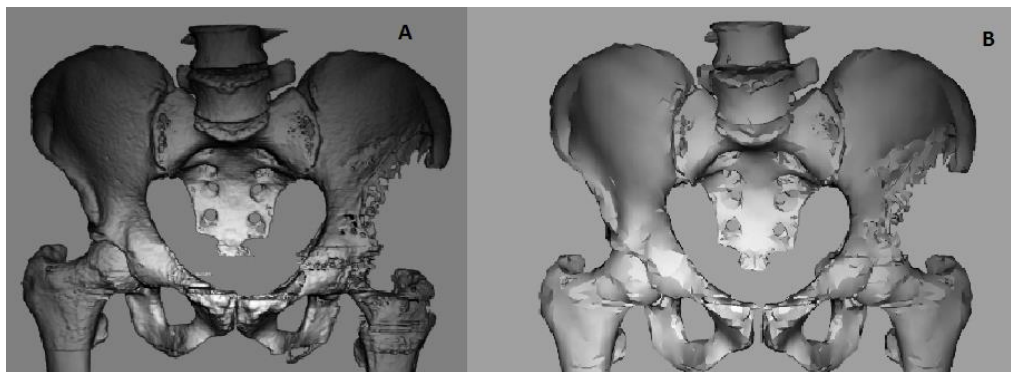


Figure 4.2.2 Rendering of the 3D model before (A) and after (B) of the re-meshing process using quadratic edge collapse method. As evident from the images, the shape fidelity of the models was maintained despite the reduction in the number of triangles defining the model. In other words, the morphology of the final processed 3D model did not change during the re-meshing process.

4.2.2 Establishment of a methodology to fabricate porous patient-specific scaffolds from solid 3D computer-aided-design (CAD) models obtained through medical imaging scans

CAD models generated from medical imaging datasets are solid, water-tight structures with no porosity. Such models are inappropriate for use in tissue engineering because the host tissue cannot infiltrate the interior regions of the scaffolds. Therefore, a custom software was designed which takes a solid, non

porous CAD file as an input and introduces porosity in the model to make it suitable for tissue engineering purposes.

As mentioned in Chapter 2, the size and shape of every human body is different. Therefore, the shape and size of every scaffold needs to be customised. Also, different tissues of the body have different requirements in terms of mechanical properties, porosity requirements etc. Additive manufacturing (AM) represents one of the few manufacturing platforms which can produce such highly customised products in an automated manner.

Every AM machine fabricates the product in a layer by layer fashion (see Chapter 3 for more details). Therefore, the software developed to fabricate porous models from solid CAD files using AM technologies works by slicing a solid 3D model into a number of 2D sections, generating an outline of every such 2D section and generate architectural patterns within these outlines. These outlines and generated patterns can be converted into a number of different file formats to suit different types of AM machines.

The following sections describe the workings of the software developed to fabricate porous models from solid CAD files using AM technologies in more detail.

1) Slicing CAD files to generate an array of 2D layer contours:

In the first step, the algorithm slices the CAD file (in the Standard Tessellation Language – STL format) into 2D slices separated by a distance defined by the user. The X,Y,Z coordinates of the outlines of these slices is saved in Scalable Vector Graphics (SVG) format. The algorithm and process used to slice the STL files is given in Fig 4.2.3 and 4.2.4. Fig 4.2.5 shows a set of points defining a randomly

selected 2D slice. Fig 4.2.6 shows all 2D slices stacked on top of each other to form the complete 3D scaffold geometry.

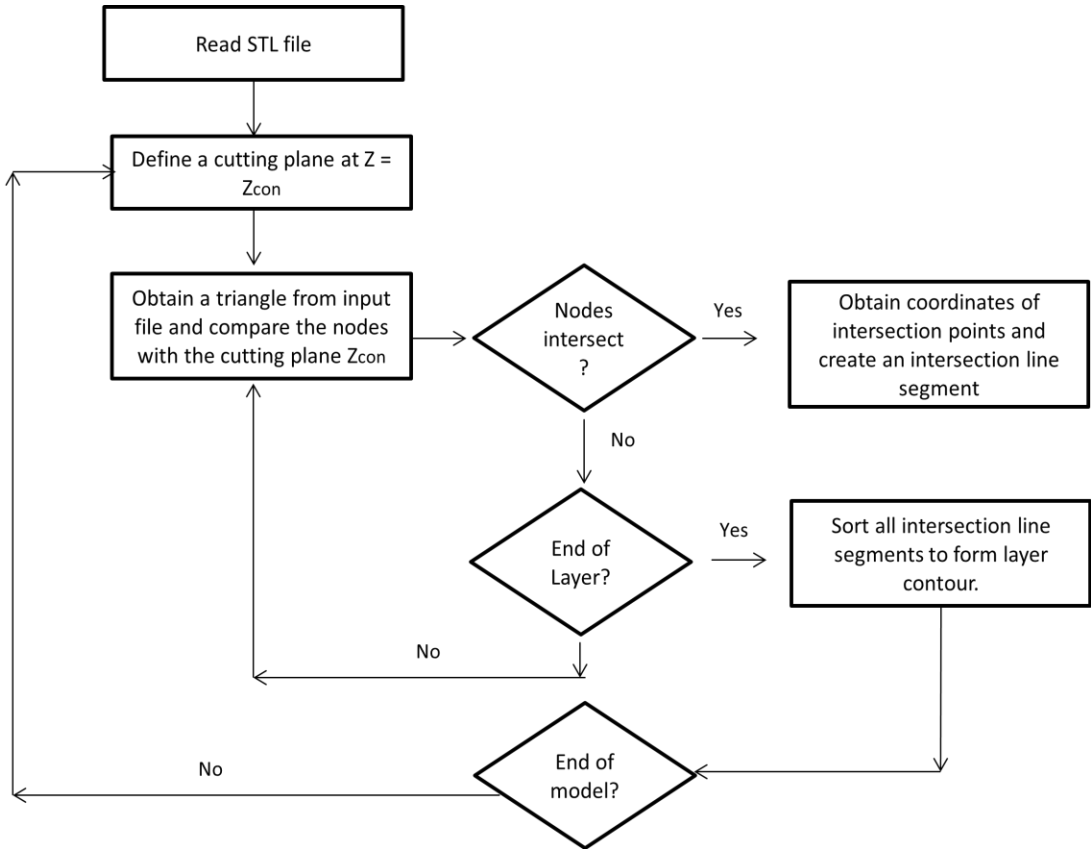
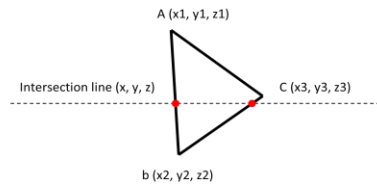


Figure 4.2.3 Flow diagram of the algorithm used to slice the 3D STL file into an array of 2D slices

Intersection points Detection



Checking condition to see which lines intersect

$z1 \leq z \leq z2$ **OR** $z1 \leq z \leq z3$ **OR** $z2 \leq z \leq z3$

Once intersecting lines are found, equation to find (X, Y) coordinate of the points where triangle edge is intersected by slicing plane:

$$\frac{X-X1}{X2-X1} = \frac{Y-Y1}{Y2-Y1} = \frac{Z-Z1}{Z2-Z1}$$

Figure 4.2.4 Mathematical equation used to derive the coordinates of the points in the 3D model intersecting the slicing line

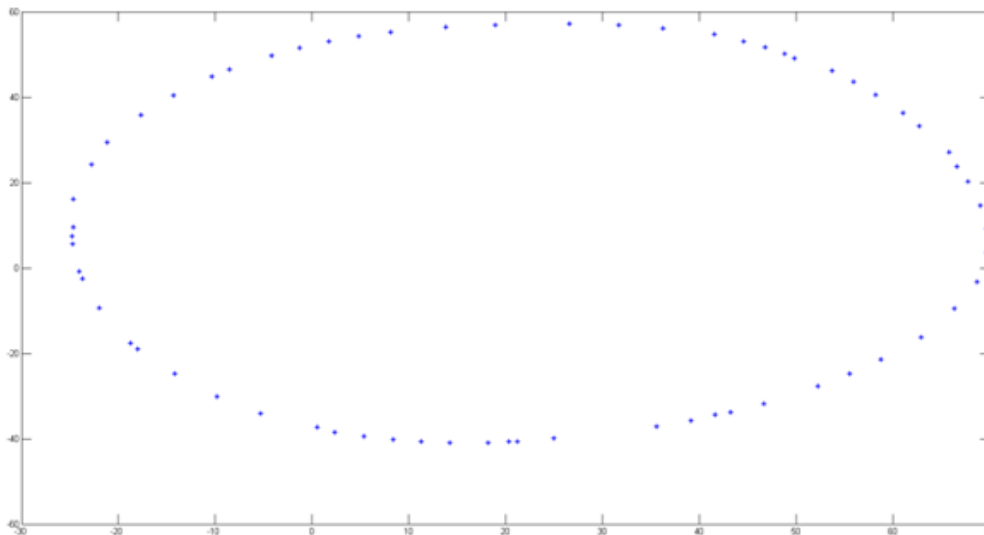


Figure 4.2.5 Matlab plot of all points derived from a randomly selected layer

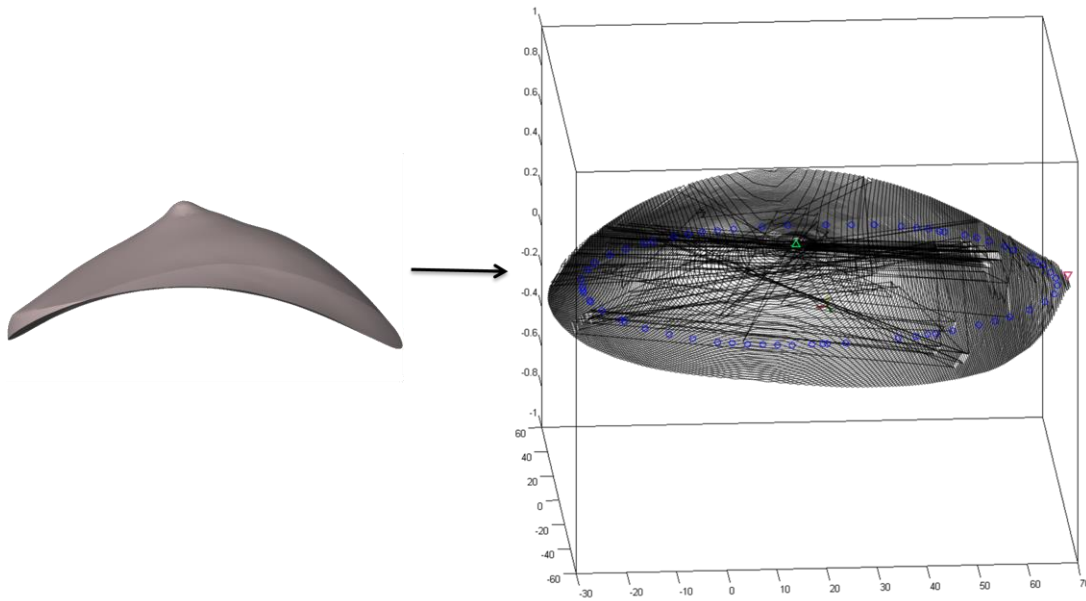


Figure 4.2.6 Visualisation of layer contours of all layers generated from a breast scaffold

2) Adding rastering lines by plane sweep algorithm.

As a second step, the algorithm produces n equally spaced imaginary lines intersecting the boundary of each layer. As shown in Fig 4.2.5, each boundary is defined by a set of unequally-spaced points. The spacing between these lines controls the porosity of the final structure.

A naïve raster lines-adding algorithm would divide the layer into 2 segments by using a contour dividing line and then simply connect a point on the $-X/-Y$ side of the symmetry plane to its corresponding point in the $+X/+Y$ side of the plane (Fig 4.2.7). Such a naïve implementation would work if all the points along the boundary of the layer are equally spaced. However, as mentioned previously, in most cases each layer is represented by a set of irregularly spaced points. Therefore, the naïve algorithm would output a set of lines whose spacing cannot be controlled (4.2.8).

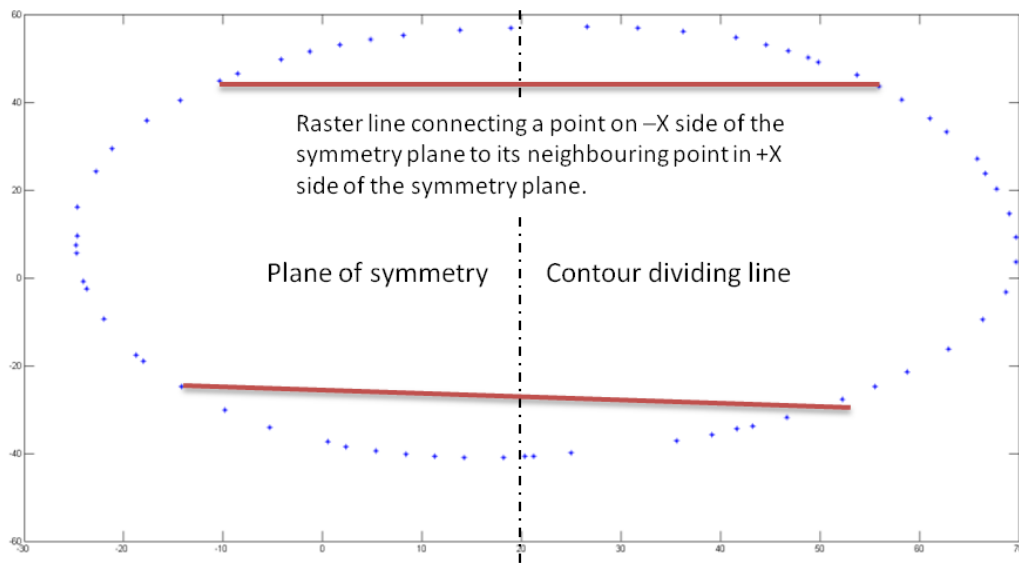


Figure 4.2.7 Matlab-based visualisation of naïve algorithm for adding raster lines

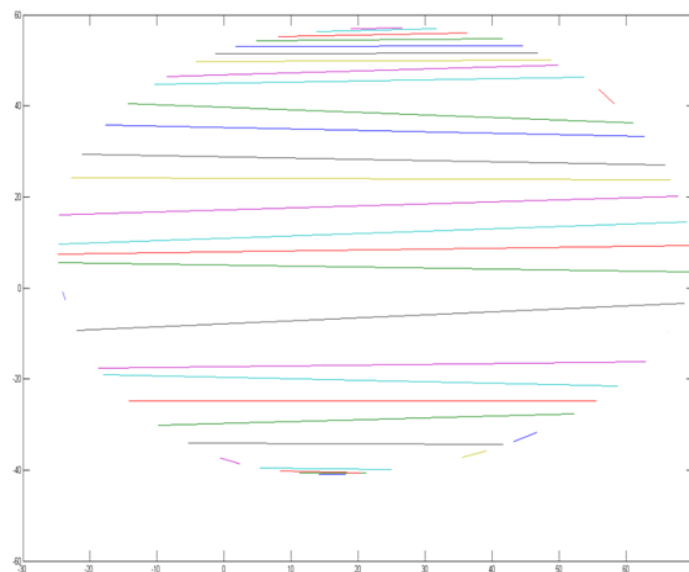


Figure 4.2.8 Matlab output of naïve algorithm showing irregularly spaced raster lines

In order to solve the problem of irregularly spaced raster lines, a novel algorithm based on the principle of plane sweep was implemented. The problem set of the sweep algorithm is given as follows:

- **Problem:**
 - Given the following sets:

a contour defined by an ordered set of points $S = \{\{X_1, Y_1, Z_1\}, \{X_2, Y_2, Z_2\}, \{X_3, Y_3, Y_3\} \dots \{X_n, Y_n, Z_n\}\}$.

- A set of $L = \{L_1, L_2, L_3 \dots L_n\}$ of n line segments in a plane separated by a distance x .
- Our task is to compute all pairs of (L_i, L_j) , $i \neq j$ of segments that intersect.
- **Solution:**
 - The main loop of our algorithm sweeps a vertical line L from $-X$ to $+X$ direction through the set S (see Fig 4.2.9 for an illustration of the sweep line algorithm).
 - The sweep increments i are defined by the filament distance provided by the user and is a major determinant of the final porosity.
 - The data structure R (which is initialised as empty) is used to store lines from S currently intersecting the vertical lines.
 - Whenever the sweep line (SL) intersects with a line defined by two adjoining points in S , the intersection points are entered into the data structure R .

In lay terms, this sweep algorithm moves a line across the 2-dimensional Euclidean plane in which the points reside to find intersection points. If the line moves from $-x$ to $+x$ direction, all the intersecting points to the $-x$ direction of the line have already been detected. As the sweep line passes through an intersecting point, it creates and updates a nested data structure consisting of the slope, XY intercept coordinates, the closest point to the $-x$ direction of the sweep line and the closest point in the $+x$ direction (Fig 4.2.9). At the end of the sweep, the Cartesian coordinates of the intersecting points are obtained from the data structure and saved as a text file. Readers are encouraged to read an excellent paper by Chazelle and Edelsbrunner

[296] explaining the variety of data structures that can be used with such sweep algorithms.

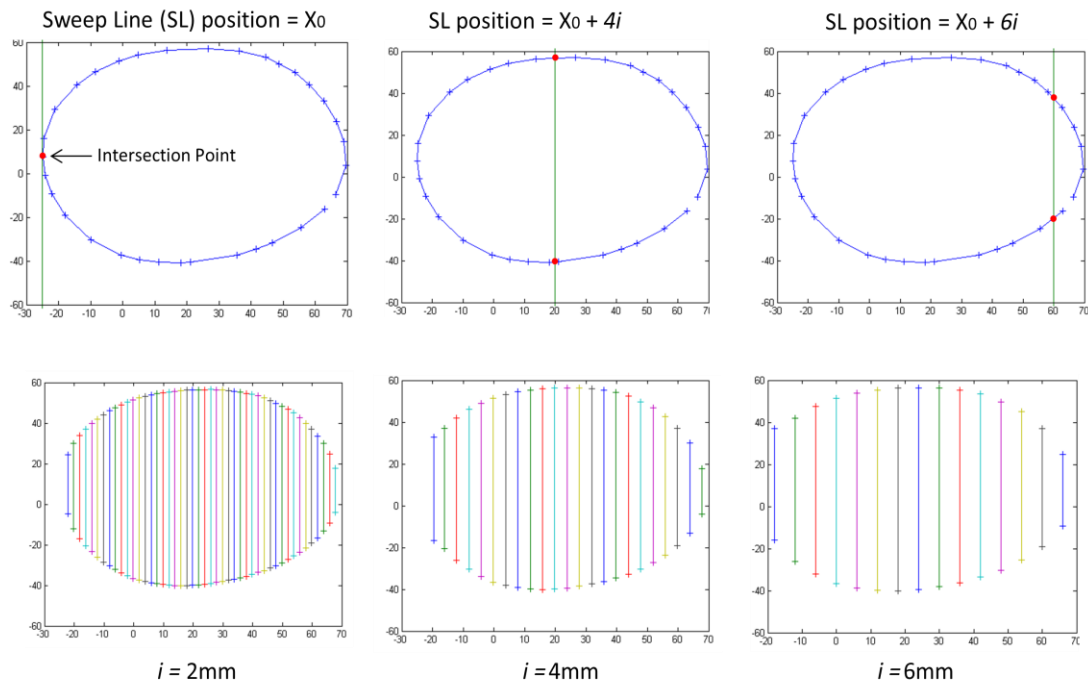


Figure 4.2.9. Results of sweep line algorithm to generate raster lines plotted in Matlab. The sweep line (SL) moves from $-X$ to $+X$ position on the layer outline. The incremental steps are determined by the user and govern the overall porosity of the scaffold. Once the SL intersects with two opposite points on the layer contour, it saves their coordinates and generates a raster line connecting the two points

3) Rotational matrices to generate pores.

Once the raster line generation process is complete, the raster lines of every layer are still aligned parallel to each other – compromising fluid flow and mechanical properties within the scaffolds. In order to generate the “criss-cross” pattern commonly used in scaffolds, a rotational matrix needs to be implemented. The algorithm shown in Fig 4.2.10 governs the rotational matrices.

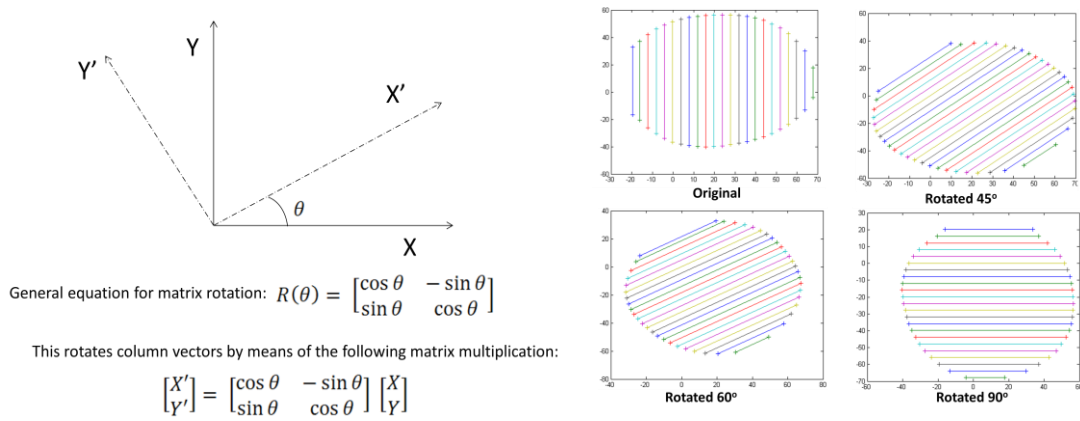


Figure 4.2.10 (LEFT) Algorithm governing rotational matrices. (RIGHT) Results from implementing the algorithm on a randomly selected layer (plotted using Matlab).

All algorithms described in this chapter were used sequentially on breast as well as hip CAD files to obtain porous models suitable for tissue engineering (Fig 4.2.11).

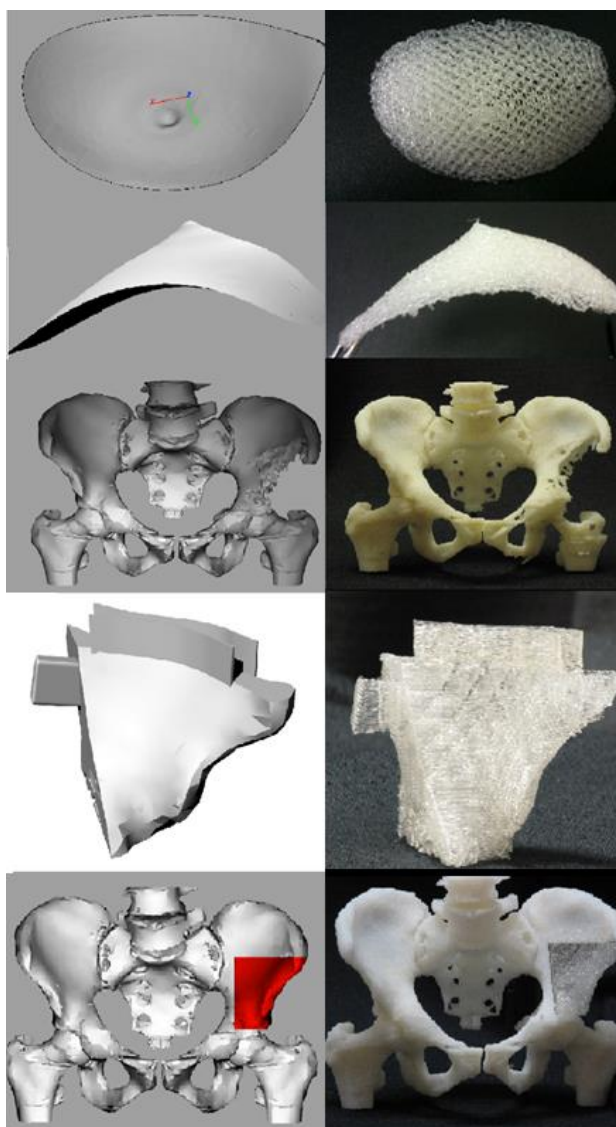


Figure 4.2.11 Results showing fabrication of different types of scaffolds using the STL-Gcode conversion algorithm as a proof-of-concept. Left panel shows the original solid CAD files generated from medical imaging scans. Right panel shows porous scaffold designs generated using software described in section 4.2.2. Complementary structures were also designed in order to temporarily support overhangs in the scaffold geometries. The supporting structures were fabricated with a water-soluble polymer polyvinyl alcohol (PVA) (diameter 1.75mm, melting point 160-170oC, density 1.25-1.35 g/cm³) (Kuraray USA, Houston, USA) and were dissolved by immersing the scaffolds in a water bath set at 37°C for 30 minutes.

4.2.3 Development of a software package for rapid generation of finite element models from numerical-code programming languages

4.2.3.1 Introduction

Tissue engineering uses scaffolds that fill the defect, stimulate new tissue growth, and become resorbed over time as they are replaced by newly formed tissue [3]. Scaffolds intended for different anatomical sites within the human body require different physical and mechanical properties to ensure optimal tissue growth. In case of breast tissue engineering, the mechanical properties and stiffness of the scaffold should match the stiffness of the tissue in the breast region to minimize patient discomfort. Moreover, research has also shown that stiffness of the tissue engineered construct affects the differentiation of progenitor cells, less stiff implants promoting the differentiation of progenitor cells into adipose cells [169, 297]. Therefore, a scaffold intended for the reconstruction of such soft tissue needs to be elastomeric in nature, with a low overall stiffness. On the other hand, bone tissue engineering requires a scaffold architecture with high bulk modulus as the scaffold should be able to bear the load imposed during the early recovery period without collapsing. In a similar manner, biomaterial-based scaffolds for cartilage tissue engineering require flexible, elastomeric materials to match the properties of native cartilagenous environment. Several methods are currently being investigated to fabricate anatomically-shaped tissue engineering scaffolds with a high degree of precision. Among such methods, additive manufacturing methods, in particular the Fused Deposition Modelling (FDM) process, garners the highest amount of attention and is arguably the most feasible method of fabricating multi-material cell-laden tissue engineering constructs [4].

Current paradigm of additive manufacturing methods relies upon a certain set of established laydown patterns and filament thicknesses to modify the mechanical properties of tissue engineering scaffolds for various applications. However, much of the development still relies upon heuristic trial-and-error methods. Although several studies exist which demonstrate *in silico* modelling of different scaffold and unit cell architectures for a wide variety of anatomical sites, to our knowledge, these methods have not been consolidated towards the design and fabrication of geometric- and anatomically-shaped scaffolds containing optimal mechanical properties for *in vitro* and *in vivo* research purposes. Adding complexity to this problem is the fact that fabrication of scaffolds by FDM process often relies upon slicing of a solid CAD model with no inherent porosity. Parameters such as laydown pattern, filament spacing and filament thickness, which primarily control the mechanical properties of the scaffold are controlled by the software controlling the FDM machine and are described within the computer-numerical-code (CNC) machining code. The movement of the FDM machine, and consequently the final architecture, entirely depends on the CNC code. Therefore, generation of a finite element mesh directly from the CNC has the potential to recapitulate the final architectural properties of the scaffold. However, most recent literature concerned with FEA analysis of scaffolds manufactured by additive manufacturing relies on designing the final architecture of the scaffold using a 3D modelling software and then meshing it [298, 299]. Not only is this process time-consuming and labour intensive, the accuracy of the model also depends greatly on the skill of the person performing the modelling steps - which makes it inherently challenging for scientists not trained in 3D modelling. Moreover, a different 3D model needs to be generated and meshed for each modification in scaffold design parameters.

Therefore, as a part of this PhD project, development of automated computer programs that can rapidly generate finite element models of a set of scaffolds varying in porosity, filament thickness, and pore interconnectivity directly from the CNC machining code was undertaken. Such a technology platform in the future could enable even the non-engineers to perform a goal-driven parametric analysis of scaffold-designs containing different filament spacings, laydown patterns, filament thickness etc from a single solid CAD model in order to determine the optimum parameters and architectures tailored for their specific tissue engineering application.

4.2.3.2 Materials and Methods

CAD/FEA interfacing algorithm

Slicing is the first step in generating nodes within a solid CAD model. The 3D solid model has to be converted into a series of two-dimensional (2D) slices (contours representing boundaries) depending on the slice thickness specified by the user as described in section 4.1.2. Data from these slices are converted in numerical-code programming language (NC G-code) and grouped into nodes. If the algorithm detects that the user has supplied a pre-generated CNC tool-path file, it parses the file to find the points used for linear interpolation of the raster toolpath and groups them into nodes. Fig 4.2.12 outlines the algorithmic steps designed to parse the nodes from a CNC tool-path file:

Algorithm 1. Generating FE nodes

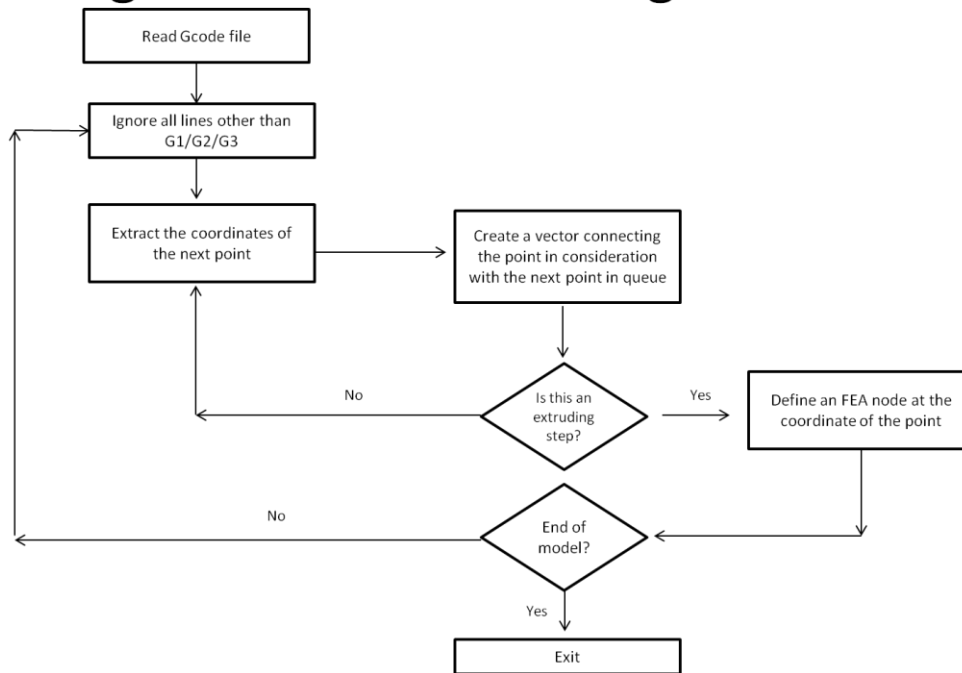


Figure 4.2.12 Algorithmic steps designed to parse the nodes from a CNC tool-path file

The algorithm then asks the user to provide the following values:

- Filament thickness
- Loading conditions in terms of force/displacement.
- Material properties (Young's modulus and Poisson ratio).

If the distance between two adjacent nodes is larger than the threshold level specified by the user, the algorithm generates additional equally-spaced nodes in-between the original adjacent pair to increase solution accuracy. Fig 4.2.13 shows a Matlab visualization of how nodes are split to increase result accuracy.

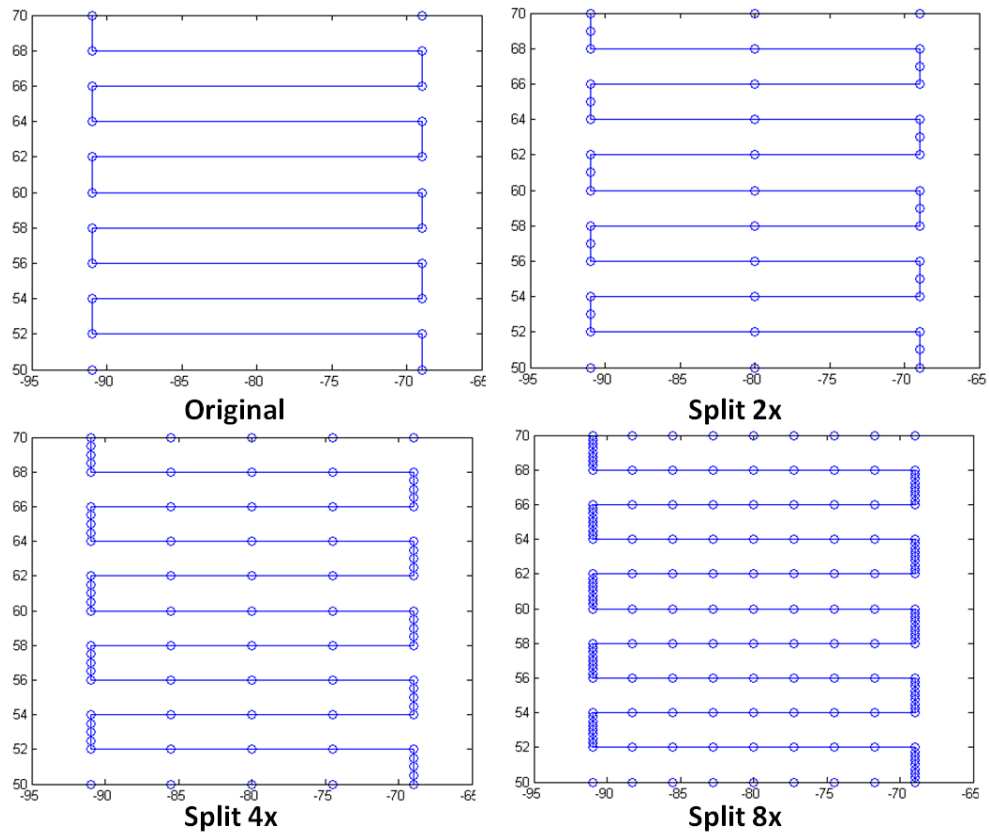


Figure 4.2.13 Matlab visualization of the node-split algorithm to increase result accuracy. Top left shows the original set of nodes parsed from the CNC output. Top Right shows an additional node generated between a pair of original nodes (2x split), Bottom Left shows a 4x split and Bottom Right shows an 8x split.

Once all nodes are identified, the algorithm iteratively cycles through the set of nodes in each layer. For each node, it finds the succeeding node based on the raster toolpath and uses their coordinates to generate a 3-dimensional cylindrical beam element (3-noded quadratic BEAM188). Previous studies undertaken within our group have shown that BEAM188, which enables shear stress calculations through the elements using the Timoshenk beam theory, is the most accurate beam element and suits the filament geometry in our model [300, 301].

A BEAM188 element is defined by nodes I and J in the coordinate system (see Fig 4.2.14) while Node K is always required to define the orientation of the element. Since the coordinates of I and J are already determined in the previous step,

coordinates of Node K are found using basic trigonometry operations. The radius of the cylinder equals the filament radius provided by the user.

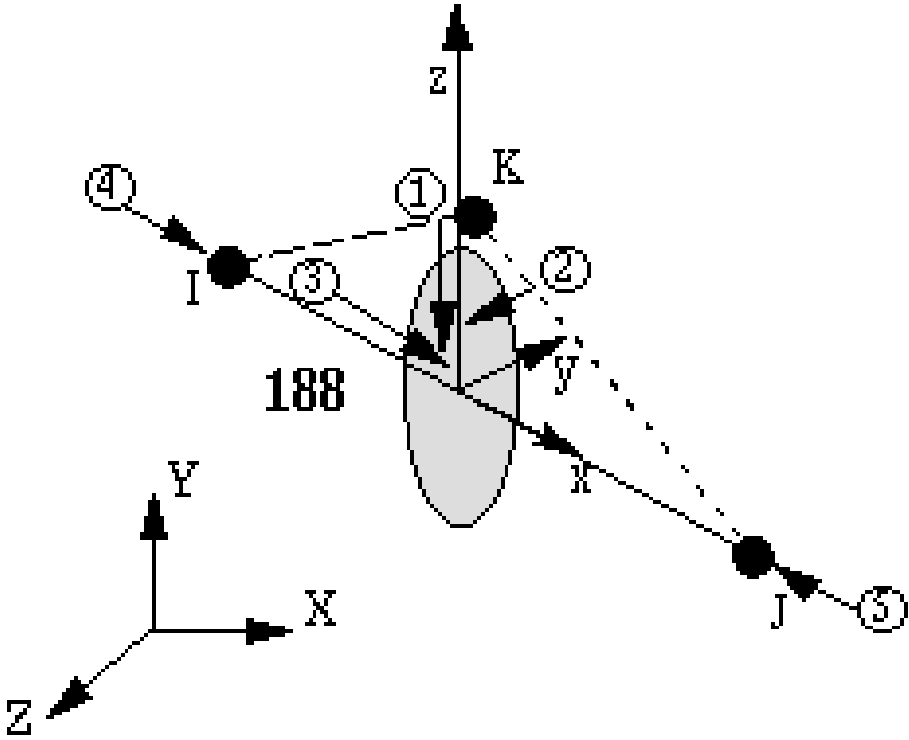


Figure 4.2.14 Geometry, node locations and the coordinate system for BEAM188 3-D Finite Strain Beam. Image adapted from [302].

This cycle repeats for all layers within the geometry and once the sets of elements belonging to different layers have been formed, connections are made automatically by the FEA software (eg Abaqus, Ansys) between successive layers to form an interconnected geometry. The cross-sectional area of the beam elements is calculated using the filament thickness value entered by the user.

Many scaffold shapes contain >1 closed contour loops separated by a non-extruding machine movement code (Fig 4.2.12) – this problem is especially exacerbated in case of Gcode flavors catering to continuous extrusion 3D printers as no distinction is made, in terms of Gcode, between extruding and non-extruding steps. In these cases, it becomes important to detect these non-extruding travelling steps and eliminate

them from further processing. An intelligent travel path sensing algorithm was therefore developed which could detect layers having >1 closed loops and subsequently separate the travelling movements from the final results (shown in Fig 4.2.15, 4.2.16, 4.2.17, 4.2.18).

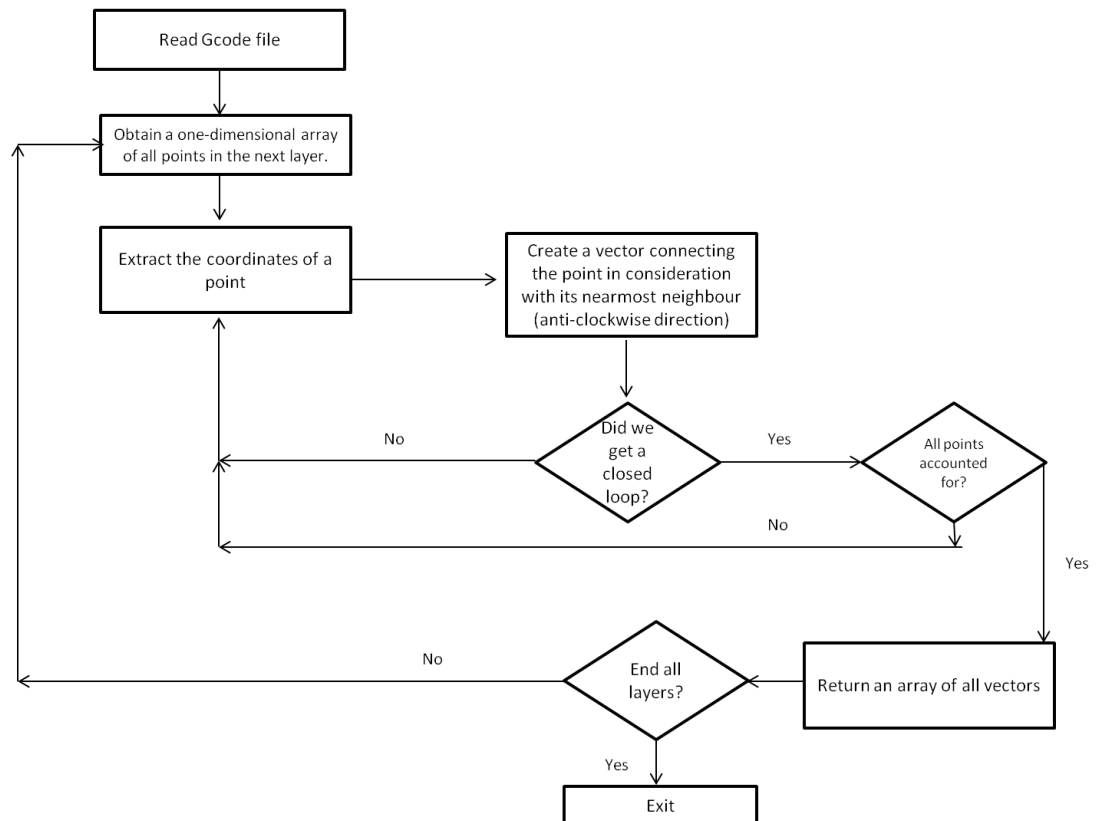


Figure 4.2.15 Intelligent travel path sensing algorithm to detect layers having multiple closed loops

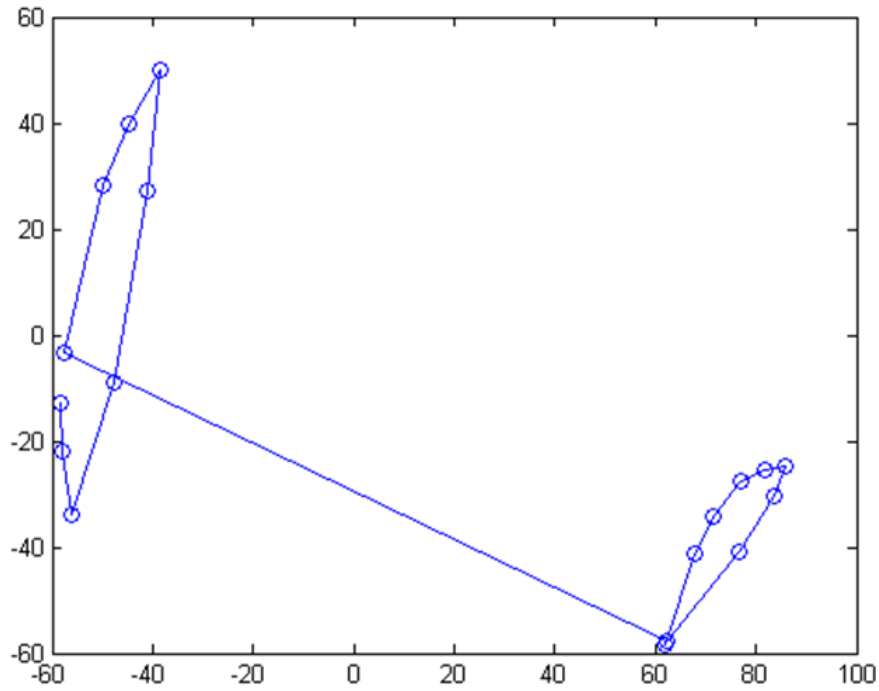
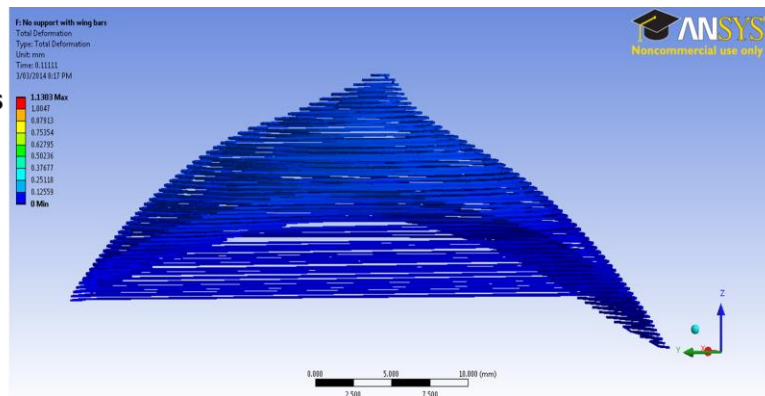


Figure 4.2.16 Matlab plot of a randomly selected layer containing two closed loops connected by a non extruding raster line

Breast scaffold with contours
Not separated



Breast scaffold with contours
separated

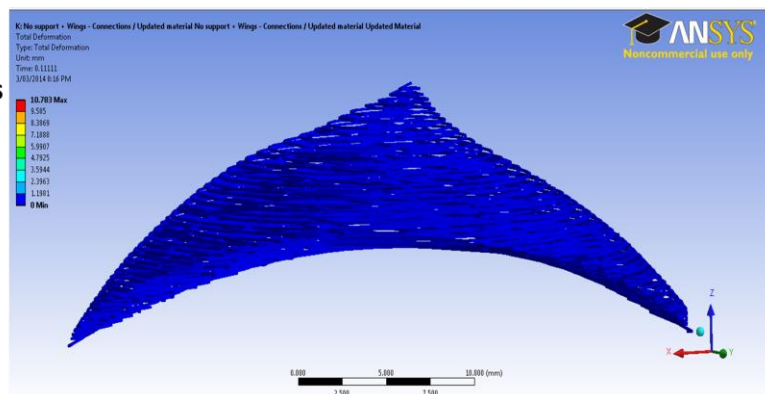


Figure 4.2.17 (TOP) FE nodes and elements of a breast scaffold with travelling paths not separated. (BOTTOM) FE nodes and elements of a breast scaffold with travelling paths separated using the intelligent travel path sensing algorithm.

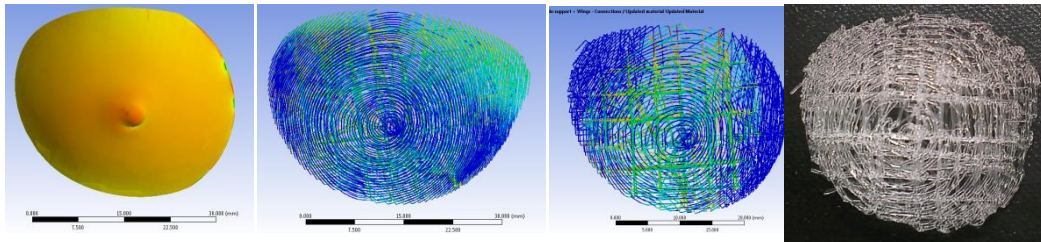


Figure 4.2.18 Differences in distribution of bending moments in FE meshes of scaffolds with different architectures. From LEFT to RIGHT: non-porous breast scaffold, porous breast scaffold with layer boundary shells, porous breast scaffold without layer boundary shells, picture of actual fabricated scaffold

In the final step, the algorithm converts the nodes, elements, material properties, loading conditions and boundary conditions into an Abaqus Input file (.inp) which has a fully self-contained finite element model of the scaffold architecture and can directly be imported into almost any FEA program to obtain the desired results.

The mesh density of an FE model must be selected to ensure a computationally efficient analysis is performed with suitable accuracy. A coarser mesh results in less precision of the results due to the reduced number of nodes at which a solution may be found and the necessity for interpolation of results across large distances between nodes. However, fine meshes significantly increase the degrees of freedom of the solution and therefore result in long computational times. Therefore, the use of an extremely fine mesh density will result in very high solution times with little benefit in terms of improved accuracy of results.

To determine a suitable mesh density for the scaffolds, various meshes were analysed using a fixed loading condition – a 50% strain was applied in the $-Z$ axis of a breast scaffold with a known young's modulus and the results for axial stress generated within the model were compared. The *in silico* model was also designed to closely mimic the experimental setup of compressing the fabricated breast scaffolds shown in Fig 4.2.19.

Test setup

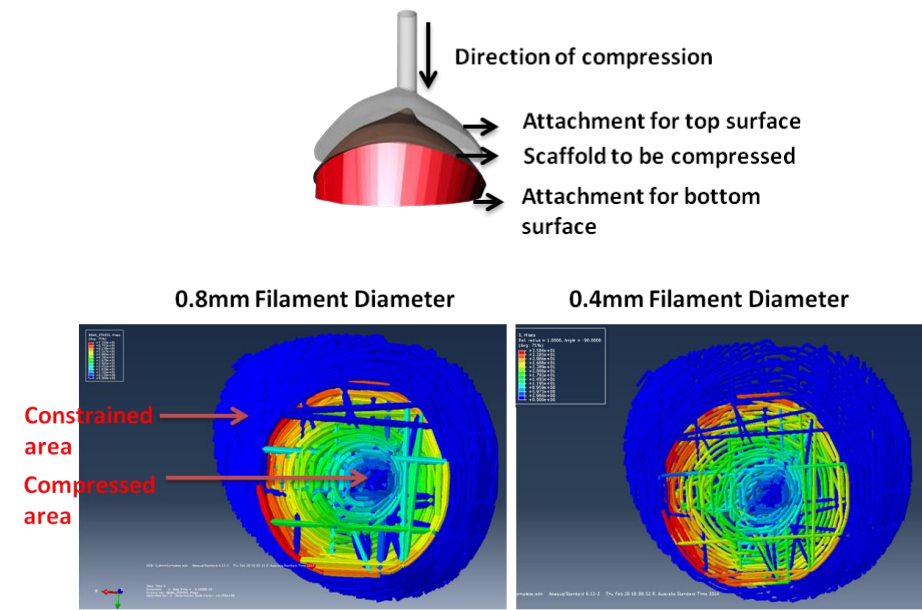


Figure 4.2.19 **TOP**: Schematic diagram of the test setup used for compression testing of scaffolds.

Due to the curved nature of the scaffold surfaces, special top and bottom surface attachments following the contours of the scaffolds were produced. The top attachment links with the Instron microtester plunger providing uniform stress across the entire scaffold. The attachments were produced with non-porous acrylonitrile butadiene styrene (ABS) with a considerable higher stiffness compared to the 90% porous PDLA scaffolds, to minimise their influence on the load readings.

BOTTOM: Distribution of von Mises stresses in scaffolds with different internal architectures and filament thicknesses.

Six different mesh densities were analysed:

- No node splitting (1x1).
- 2 extra nodes added between 2 successive nodes (4x1).
- 3 extra nodes added between 2 successive nodes (6x1).
- 4 extra nodes added between 2 successive nodes (8x1).

As expected, although with each split of the node sets, the solution accuracy increased dramatically, the computational time also increased exponentially (see Fig 4.2.20), with the 8x1 split mesh displaying the best balance between solution accuracy and computational time (analysis was performed on a desktop computer

equipped with an Intel i7-2600 CPU clocking at 3.40 GHz and 8GB of system RAM).

Mesh Optimisation

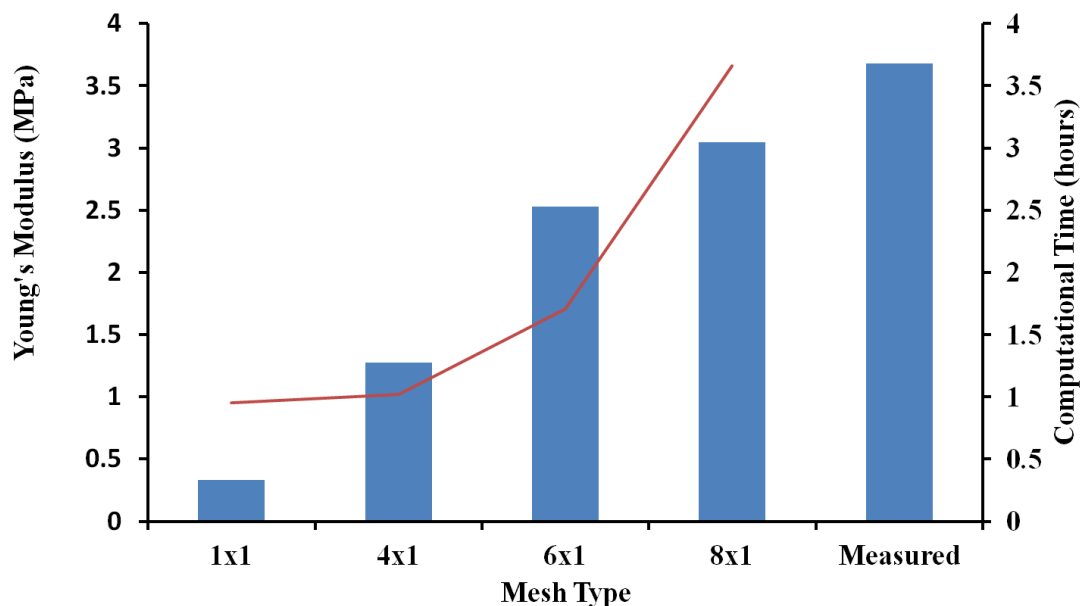


Figure 4.2.20 Mesh optimization study performed to test the accuracy of the meshes and the FEA method. Blue columns refer to the young's modulus while the red line refers to the computational time axis.

The final mechanical properties of a scaffold are a function of both the material property of the biopolymer and its architecture [3, 104]. In terms of base mechanical properties, presently there exists no suitable biodegradable polymer which can easily be processed using additive manufacturing whose mechanical property is appropriate for soft tissue engineering. Therefore, for all future studies, we selected the architecture which provided the most elasticity to the scaffold irrespective of the polymer and fabricated the scaffolds using a model biodegradable polymer (Poly-D,L Lactide). Properties of this architecture are given in Table 4.2.1. In this project, our main focus was on the design and fabrication of anatomically-shaped patient-specific scaffolds using a polymer that degrades over the time scale of 1-2 years; we did not aim to produce a scaffold whose mechanical properties matched those of

native adipose tissue. Our vision is that in the future when a suitable soft and elastomeric biopolymer has been discovered, its mechanical properties can be plugged directly into the Gcode-to-FEA software to design a scaffold optimised for breast tissue engineering.

Material	Porosity	Laydown pattern	Filament diameter	Young's Modulus
Poly-D,L Lactide	95%	0-60-120	0.4mm	3.068 MPa

Table 4.1 Scaffold properties

4.2.4 Overall Discussion

There has been a palpable trend since mid-2000's to transfer the CAD/CAM techniques from bench to bedside [303-306]. Clinicians have been employing custom-made metal prostheses for the treatment of various bone defects for over 20 years [307, 308]. Such prostheses, which are often fitted with custom-made surgical guides, are produced using high resolution MRI or CT-scan data. Although they provide clinicians with many reconstructive options, their failure rates remain high [308]. A majority of breast reconstructions are also currently being performed using implantable prostheses composed of a vulcanised silicone rubber sac filled with saline or liquid silicone solution. Such implants, as explained in a previous section, often lead to formation of rigid, fibrous scar tissue surrounding the implant – a painful condition termed as capsular contracture. Transplantation of autologous free or pedicled flaps gives a natural appearance and feel; however, they such approaches for breast reconstruction are marred with problems of tissue resorption and necrosis. Therefore, a reconstructive method is needed which does not rely on the use of permanent prosthetic implants but rather on biodegradable and biocompatible materials supporting natural healing processes.

In this study, the feasibility to employ CAD/CAM as an aid for autologous tissue regeneration has been demonstrated. A versatile approach has been developed to generate patient-specific scaffolds not only for breast reconstruction, but also for virtually any defect. This approach allows for high level of automation and requires minimal manual handling. For this, we made use of freely available open-source software to convert high resolution MRI or CT scan data into 3D CAD models using the thresholding technique. The specific advantage of the thresholding technique is that it allows for relatively easy differentiation of tissue/area of interest from its surrounding region. Using this method, porous models mimicking the overall shape of a scanned tissue region can be generated.

For most tissue engineering constructs, a suitable scaffold porosity lies between 70-90% [3, 309] to allow optimum effective and efficient nutrient transport as well as vasculogenesis. The pore sizes, on the other hand, vary depending on the application. For regenerating small volumes of tissue 400 μ m pore sizes may be adequate, whereas pore sizes >1-2mm are required for regenerating large volumes of hypoxia-sensitive tissue [310, 311].

However, such high levels of porosity and large pore sizes are likely to compromise the mechanical strength of the constructs. While the considerations for high mechanical strengths bear less importance in the case of breast reconstructions, they become important if the scaffold is intended to be used at a load-bearing site. The overall porosity and pore sizes can also be precisely controlled using the inherent porosity inducing algorithm. However, these values are limited by the resolution and accuracy of the employed CAM method. Although in the past few months, proprietary software have been developed for FDM machines specialised for scaffold fabrication [312-314], such software are closed source, do not support the fabrication

of porous models and are unavailable for use with custom-made biofabrication machines. Moreover, it was found that such software packages have not yet achieved the level of sophistication and control over extrusion parameters required in the biofabrication industry. Using the presented method for fabricating scaffolds is not only versatile across almost all FDM or CNC machines. The cross-platform nature of all the software packages used also makes this process suitable for use with experimental additive manufacturing devices being developed.

An independent method has already been developed by our research group to laser scan a breast surface, generate a 3D model and fabricate a porous prototype using non-biodegradable materials [91]. The method developed during the course of this PhD project complements this method in that it allows the fabrication of porous, biodegradable scaffolds using more ubiquitous MRI and CT scans. Combined together, these methods encompass an almost comprehensive range of avenues for generating porous patient-specific scaffolds.

In this project, we have taken the idea of designing and fabricating porous patient-specific scaffolds to the next level by incorporating *in silico* pre-testing methods into the design process. Currently, a majority of scaffold designs are generated using heuristic methods whereby scientists fabricate a range of scaffolds with different architectures in the hope that one candidate will display suitable mechanical and physical properties when subjected to compression/tensile/torsional testing. However, this approach is inherently inefficient as the time needed to fabricate a single scaffold can range from 30 minutes to >5 hours depending on the size of the scaffold and print resolution. In contrast, the Gcode-to-FEA program described in this chapter helps researchers, especially those without an engineering background, to predict the physical properties of their scaffolds before the fabrication process –

resulting in time and cost savings. The obtained results showed that the software is promising because of its efficiency and simplicity. At the same time, it is also important to be aware of some limitations of the software because biomaterial behaviour and physical properties *in vivo* are more complex than the simplified models currently being used in the software. The software designed uses BEAM188 elements to model the scaffold filaments. Such elements have been previously used in previous studies done in our group [301] and are based on the Timoshenko beam theory which is a first order shear deformation theory with the underlying assumption that transverse shear strain is constant through the cross section [302]. However one of the limitations of this approach is that only moderately thick beams can be analysed. Moreover, many FEA software packages do not provide options to calculate the torsional shear distribution on such cross sections. Other assumptions such as degradation kinetics, change in Young's modulus and the effect of tissue infiltration on the mechanical properties were also excluded. However, it is expected that the development of this software will continue beyond the duration of this PhD project and future versions will incorporate more complex models of material behaviour and form a basis for future parametric studies to be investigated.

4.2.5 Conclusion

In conclusion, the designing of a scaffold that will yield the best possible properties to facilitate tissue regeneration is a complex problem and will require a multitude of *in vitro* and *in vivo* experiments. This chapter described a holistic methodology enabling a researcher to obtain optimally designed porous constructs directly from medical imaging scans in one streamlined approach, and in turn creating synergies between disparate research fields such as medical imaging, biomaterial science, additive manufacturing and *in silico* modelling. The ultimate goal of the presented

software is to evolve into a complex system that will integrate seamlessly with high-end bioprinting hardware and enable a complete design process to facilitate fabrication of optimal scaffolds for not only the tissue engineering purposes, but also the broader advanced manufacturing and industrial design industries.

4.3 STUDY THREE (PAPER THREE)

Sustained Regeneration of High-volume Adipose Tissue for Breast Reconstruction using Computer Aided Design and Biomanufacturing

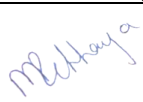
Journal: Biomaterials

Status: Accepted

Chhaya, MP, Melchels, FPW, Holzapfel, BM, Baldwin, JG, Hutmacher, DW

The authors listed below have certified* that:


1. they meet the criteria for authorship in that they have participated in the conception, execution, or interpretation, of at least that part of the publication in their field of expertise;
2. they take public responsibility for their part of the publication, except for the responsible author who accepts overall responsibility for the publication;
3. there are no other authors of the publication according to these criteria;
4. potential conflicts of interest have been disclosed to (a) granting bodies, (b) the editor or publisher of journals or other publications, and (c) the head of the responsible academic unit, and
5. they agree to the use of the publication in the student's thesis and its publication on the QUT ePrints database consistent with any limitations set by publisher requirements.

Contributor	Statement of contribution
Mohit P. Chhaya	Performed laboratory experiments, experimental design, data analysis and interpretation. Wrote the manuscript.
 Signature	
Date 30 Jan 2015	
Ferry PW Melchels	Involved in the conception and design of the project. Assisted in reviewing the manuscript.
Boris M Holzapfel	Assisted in animal surgeries and data interpretation.
Jeremy Baldwin	Assisted in cell culture experiments.
Dietmar W. Hutmacher	Involved in the conception and design of the project. Provided technical guidance and assisted in reviewing the manuscript.

Principal Supervisor Confirmation

I have sighted email or other correspondence from all Co-authors confirming their certifying authorship.

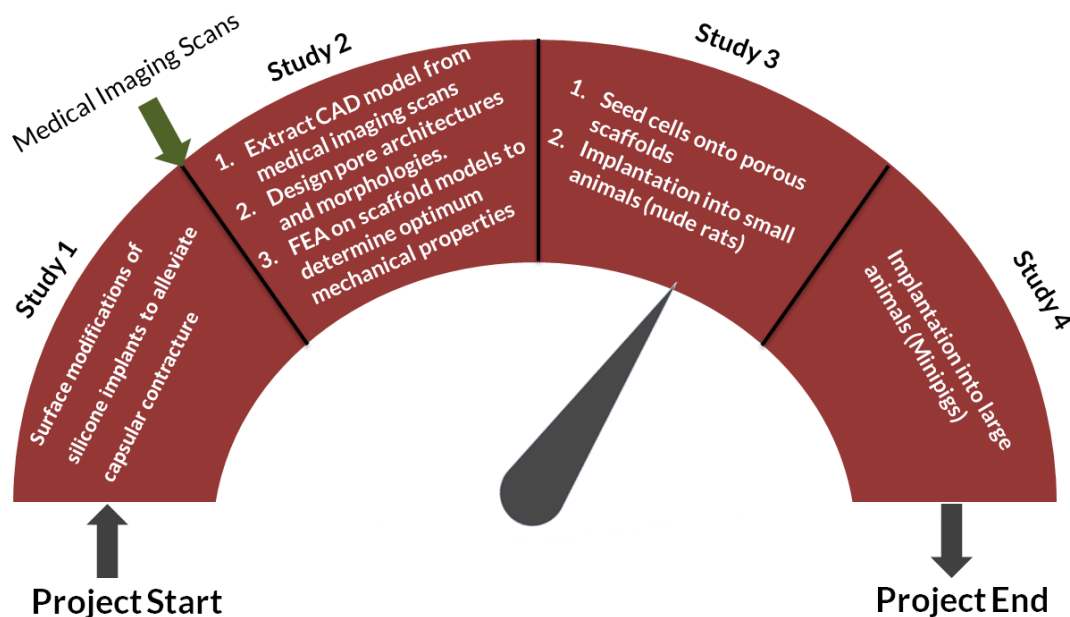
Dietmar W. Hutmacher
Name


Signature

30.01.2015
Date

Thesis Progress:

The following figure shows the flow of activities undertaken and methodologies developed as part of this PhD project. The previous study showed a versatile methodology developed to obtain patient-specific scaffolds suitable for tissue engineering purposes directly from medical imaging scans. This chapter will focus on testing the regenerative potential of the fabricated scaffolds in a small animal subcutaneous model.



4.3.1 Introduction

Breast cancer is a global problem and a major cause of morbidity, with an estimated number of approximately 300,000 new cases diagnosed in 2013 [315]. While treatment concepts have moved from radical mastectomy to lumpectomy and adjuvant therapies such as chemotherapy, radiation or hormone therapy, there is still a significant number of patients suffering from the consequences of surgical removal of breast tissue. Such procedures often have negative psychological effects on the well-being of the patients. Earlier studies by Renneker *et al.* [9] showed that mastectomy is directly related to a psychological syndrome “marked by anxiety,

insomnia, depressive attitudes, occasional ideas of suicide, and feelings of shame and worthlessness” [9]. Although several new approaches exist today in order to anatomically reconstruct the breast, some women still report the feeling of an altered body image [316]. This might partly be due to the fact that reconstructive methods available today repair, yet do not regenerate native adipose tissue, which is necessary for restoring the natural shape and feel of a breast. Prosthetic silicone-based implants are associated with a high occurrence of foreign body response altering the shape of the breast [36, 37, 40]. Autologous fat tissue transplantation and free tissue flap transfers are also a popular option among plastic surgeons. However, they are associated with a high risk of tissue shrinkage, fat necrosis and/or oil cyst formation [52, 53].

To overcome the limitations of current breast reconstructive techniques, impetus has been steadily growing towards cell-based regeneration of adipose tissue. Tissue Engineering and Regenerative Medicine (TE&RM) approaches aim to move the field away from methods to replace damaged tissue with permanent implants to more biological solutions that are able to restore structure and function of autologous tissue [311]. Since the publication of the pioneering research paper in year 1999 by Patrick *et al.* [73] who used preadipocyte-seeded polyglycolic acid (PLGA) scaffolds for regenerating small volumes of adipose tissue, many research groups around the world [16, 20-22, 317-321] have produced interesting results in the field. However, formation of sufficient volumes of mature adipose tissue remains a major problem and so far it has not been possible to maintain the structural entity of these constructs for more than 8-16 weeks [72, 322]. Current developmental efforts are therefore directed towards resolving problems that prevent the upscale of adipose tissue

engineering concepts towards clinically relevant volumes that can be maintained throughout the life of the patient.

Previous studies undertaken in our laboratory have established a clinically viable methodology to design scaffolds for breast tissue engineering from patient-specific imaging data [91]. In this project, our main focus was on the design and fabrication of anatomically-shaped patient-specific scaffolds using a polymer that degrades over the time scale of 1-2 years. Previous reports have indicated that a scaffold made out of such a slow-degrading polymer provides a long-term stable platform for the adipose tissue to regenerate and to mature, remodel its environment and stabilise [323]. We hypothesised that a slow-degrading polymer with pore sizes in the range 1-2 mm allows for efficient vascular in-growth and long-term sustained regeneration of high volume adipose tissue.

4.3.2 Methods and Materials

Image acquisition and Computer Aided Design (CAD) model generation

A 3D cad file was generated based on a 3D laser scan performed on a 46 year old female patient who suffered from an invasive ductal carcinoma from a data set previously derived [91]. Briefly, a Vivid 910 dot-laser scanner with built-in high precision camera (Konica Minolta, Marinouchi, Japan) was used to perform a 3D scan of the patient from three angles (0° frontal, and -30° and $+30^\circ$ oblique anterior). The images were imported in Rapidform2006 (Inus Technology, Seoul, South Korea) and merged into a single-shell object [81]. A custom surfacing algorithm was generated to model a virtual chest wall which was merged with the breast surface shell to obtain a watertight model of the solid breast. This watertight model was then meshed and exported as a Standard-Tessellation-Language (STL) file.

Design & Fabrication of scaffolds

The volume of the original CAD model (194 cm³) was scaled down to 3 cm³. Skeinforge-55, open-source slicing software, was used to generate machining computer-numerical-control (CNC) code from the CAD file. Custom slicing software was designed to selectively remove the perimeter shells of each layer. The resultant CNC code was then used to fabricate the scaffolds using the Replicator 3D printer (Makerbot Industries, New York, USA). During extrusion of the scaffolds, the layer thickness was set to 0.37 mm, porosity value was set to 90%, operating flow rate and feed rate were matched to 41 mm/s and extrusion temperature was set to 220°C.

MicroCT (μ CT) evaluation of scaffolds

The specimens were scanned on a Scanco μ CT40 (Scanco AG, Brüttisellen, Switzerland), employing 55 kV and 145 μ A with 250 ms exposure time. Porosity, pore-size and filament-size distributions were obtained by employing a modified trabecular bone histomorphometry algorithm.

Isolation and culturing of primary human umbilical cord perivascular cells

(HUCPVCs)

HUCPVCs represent a rich source of human mesenchymal cells found in the perivascular region of the human umbilical cord [324] and have recently gained attention in the tissue engineering field due to their short doubling time, and high occurrence of colony-forming-unit-fibroblast (CFU-F). HUCPVCs isolated from consenting full-term caesarean section patients were obtained from Tissue Regeneration Therapeutics Inc. (Toronto, Canada). The HUCPVCs were isolated as reported previously [324] and were received in passage 2. HUCPVCs were maintained in Dulbecco's Modified Eagle Medium (containing 4600 mg/L glucose) (Invitrogen, Carlsbad, USA) growth media supplemented with 10% (v/v) fetal

bovine serum (Lonza, Basel, Switzerland) and 1% (v/v) Penicillin (10,000 U/ml) – Streptomycin (10,000 µg/ml) (Invitrogen, Carlsbad, USA) in a humidified incubator at 37°C and 5% (v/v) CO₂.

Culturing of primary human umbilical vein endothelial cells (HUVECs)

HUVECs were obtained from American Type Culture Collection (Rockville, MD, USA) and maintained in F12K medium (Invitrogen, Carlsbad, USA) supplemented with 0.1 mg/ml heparin (Sigma, St Louis, USA), 0.05 mg/ml Endothelial Cell Growth Supplement (Millipore, Billerica, USA), 10% (v/v) fetal bovine serum (Lonza) and 1% (v/v) Penicillin (10,000 U/ml) – Streptomycin (10,000 µg/ml) (Invitrogen, Carlsbad, USA), in a humidified incubator at 37°C and 5% (v/v) CO₂. HUVECs were used between passages 2 and 8.

Production of GFP Lentiviruses and transduction of HUVECs

HUVECs were labelled with enhanced green fluorescent protein (eGFP) using a pLenti CMV GFP Puro (658-5) plasmid (Addgene 17448) and packaged with plasmids pRSV-Rev, pMDLg/pRRE and pMD2.G (contains VSV.G gene) (Addgene 12253, 12251 and 12259). The pLenti CMV GFP Puro plasmid were amplified in *Escherichia coli* and purified using W/Endo-free Qiagen Maxi-Prep Kit (Promega) according to the manufacturer's instructions and packaging plasmids were amplified in *Escherichia coli* and purified using Maxi-Prep Kits (Qiagen). Packaging cell line 293T cells (GenHunter Corp.) in a T75 flask were transfected with 6.6 mg pLenti CMV GFP Puro (empty) and 3.3 mg of each packaging plasmids pRSVRev, pMDLgpRRE and pMD.G in 133 µl 1.25 M CaCl₂, 0.5 ml H₂O and 0.66 ml 2 x HEPES buffered saline and the cells were incubated at 37°C/ 5% CO₂. Four hours later, the medium was removed, cells were washed twice with warm phosphate-

buffered saline (PBS) and replaced with 5 mL of complete DMEM. The cell culture supernatant was harvested 48 hr later by centrifugation at 850 g for 7 min at 4°C, followed by filtration of the supernatant through a 0.45 µm filter. The viral supernatant was concentrated 80-100 times using Amicon Ultra 15 ml centrifugal filter units (Millipore). The lentiviral stocks were stored in small aliquot at -80°C for titration and cell transfection. Titer of the concentrated lentiviral was determined by plating 4×10^5 293T cells in 6-well plate and infecting the cells with serial (10-fold) dilutions of concentrated lentivirus. After 48 hours, cells were trypsinised, washed three times with cold PBS and fixed with 1% paraformaldehyde (PFA) for 30 mins. The fixed cells were analyzed using FACSCalibur for eGFP expression and for a typical preparation, the titer was approximately 10^7 to 10^8 infectious units per ml.

GFP

HUVECs (2×10^6) in T175 flask were infected with 10 infectious units per cell in 5 ml of complete DMEM with polybrene (8 µg/ml) (Santa Cruz biotechnology) for 1 hr incubation at 37°C/ 5% CO₂ before the addition of 15 ml of complete DMEM/polybrene. Incubation was continued for 24 hrs before DMEM/polybrene media was replaced by complete DMEM. 48 hours post-transduction, the media was replaced with DMEM complete with 0.5 µg/mL of puromycin (Invitrogen), as determined previously by a puromycin kill curve (0.2-4 µg/mL) with HUVECs, in order to select for eGFP positive cells.

Preparation of cell-seeded TECs

Breast-shaped PDLLA scaffolds were first washed with sterile PBS and for sterilisation immersed in 70% ethanol overnight. Once the ethanol evaporated, the scaffolds were subjected to UV-irradiation for 30 minutes on each surface. Sterilised scaffolds were later placed in PBS overnight to pre-wet them. HUCPVC were

detached using 0.25% trypsin, washed with PBS and resuspended in culture media. 20×10^6 HUCPVC were seeded onto each scaffold within a fibrin matrix (Baxter, Toongabbie, Australia) to improve cell attachment. After trypsinisation, the cell suspension was diluted with thrombin solution at a ratio of 1:1. 600 μ L of cell/thrombin suspension was mixed with 600 μ L fibrinogen solution and seeded on each scaffold. Cell-seeded scaffolds were cultured at 37°C and 5% CO₂ in complete DMEM.

After 4 weeks of static culture, all scaffolds were subjected to a dynamic culture environment for 2 weeks utilising the TisXell biaxially rotating bioreactor (QuinXell Technologies, Singapore) for 8 hours per day at 5 rpm. The bioreactor setup has been previously described elsewhere [325, 326].

In vivo implantation into athymic nude rats

The animal experiments were approved by the Animal Ethics Committee of the Queensland University of Technology (ethics approval number: 11-147). Three 7-weeks old male athymic nude rats were purchased from the Animal Resources Centre (Perth/Australia). Rats were anaesthetized with a mixture of Ketamine (100 mg/kg) and xylazine (10 mg/kg). Surgeries were performed in a laminar hood under sterile conditions. A single 3 cm midline incision was made over the spine of the rats. Subcutaneous pockets were created on both flanks by blunt dissection and one scaffold was placed in each pocket. Before the wound was closed, scaffolds were injected with a solution of HUVEC encapsulated in Matrigel (1.3×10^6 cells per scaffold). The wound was closed with clips and swabbed with sterile iodine. At the end of the surgery, analgesic (Buprenorphine at 0.05 mg/kg s.c.) was administered subcutaneously.

Fluorescent imaging

In vivo imaging to detect the GFP signal from HUVEC was performed on the IVIS Spectrum imaging system (Caliper Life Sciences, Alameda, California) every 3 weeks. Rats were anaesthetized with 5% isoflurane and remaining fur was gently removed. Imaging was performed by setting the emission filter at 540 nm, excitation filter at 500 nm, exposure time at 0.2 seconds and luminescent exposure at 2 seconds. The images were imported into IVIS Living Image (version 4.3.1) software (Caliper Life Sciences, San Jose, USA) and native tissue autofluorescence was subtracted using a spectral unmixing algorithm. Once the autofluorescence was subtracted, all images were normalised to a minimum colour scale of 800 counts.

Mechanical Testing

Compression testing was performed on the explanted TECs using an Instron 5848 microtester fitted with a 500 N load cell (Instron, Norwood, USA). Since the top and bottom surfaces of the patient-specific scaffolds are convex in nature, a support and a loading mould (illustrated in Supplementary Fig 4.3.3) were fabricated in order to evenly distribute the forces on the TECs. The supporting structures were fabricated with Acrylonitrile butadiene styrene (ABS) polymer with a young's modulus of 3.5 GPa. In order to minimise mechanical damage to the soft tissue, the testing protocol comprised a 2 mm compression of the scaffold at a rate of 0.6 mm/min.

μCT Angiography

Scaffolds (n=3) were used for μCT angiography. All animals were euthanized by CO₂ asphyxiation 6 months post implantation. Radiopaque contrast agent-enhanced μCT angiography was performed using a protocol adapted from Duvall *et al.* [327]. Briefly, a surgical catheter was inserted into the left ventricle of the heart and

advanced into the ascending aorta. Isotonic saline was perfused into the vascular system using a peristaltic pump until the blood was washed out. Following this procedure, a polymerizable, lead chromate-based, radiopaque contrast agent (Microfil MV-122, Flow Tech, Carver, USA) prepared according to manufacturer's instructions was perfused into the vascular system. Animal carcasses were stored at 4°C for 24 hours to allow polymerisation of the contrast agent. Scaffolds were then removed from the animals and stored in 4% PFA for 24 hours until μ CT analysis.

Histological and immunohistochemical analyses

Hematoxylin & Eosin (H & E)

Tissue was harvested from the rats after 5 and 15 weeks using a 5 mm biopsy punch penetrating through the entire height of the TECs (see Supplementary Fig 4.3.5). After explantation, TECs were fixed with 4% PFA, dehydrated and embedded in paraffin using a tissue processor (Excelsior ES, Thermo Scientific, Waltham, USA). Constructs were horizontally sliced to 5 μ m, deparaffinised with Xylene, rehydrated with a decreasing series of ethanol and stained with H & E. Stained slides were scanned with the SCN400 slide scanner (Leica, Solms, Germany) at 20x magnification.

Immunohistochemical staining

Endogenous peroxidase activity was blocked by incubating the slides with 3% H₂O₂ at room temperature. Slides were washed three times with Tris-HCL (pH 7.4) for 2 minutes and placed in tri-sodium citrate buffer for 20 min at 95 °C in a decloaking chamber. The slides were incubated with 2% bovine serum albumin (BSA) for 60 minutes at room temperature and incubated with prediluted corresponding primary antibody overnight at 4°C. All the four primary antibodies used are listed in Supplementary Table 1. The slides were then incubated with immunoglobulin as

secondary antibody as part of the DAKO Envision Dual Link System-HRP (Ref: K4061, Dako, Glostrup, Denmark) for 30-45 min at room temperature. The slides were washed 3 times with Tris-HCl and colour was developed by incubating the slides with 3,3'-Diaminobenzidine (DAB) solution (1:50) [DAKO liquid DAB+ substrate Chromagen System, Ref: K3468, Dako, Glostrup, Denmark]. Finally, the slides were washed once with Tris-HCl for 2 minutes and counter-stained with Haematoxylin for 2 minutes followed by 30 second immersion in 0.1% Ammonium Hydroxide.

Histomorphometry

Histomorphometrical analyses were undertaken using two methods: a manual method and an automated approach. The manual method was undertaken using the Osteomeasure histomorphometry analysis system (Osteometrics Inc., Decatur, GA, USA). All measurements were performed blinded on 4 consecutive sections from each scaffold at each time point. To determine the average adipose tissue area, the total area of the adipose tissue was first calculated (A). Secondly, the total area occupied by the scaffold struts was measured (S). Finally, the combined area of the tissue section was measured (C). The ratio of adipose tissue area to total tissue area (R) was calculated using the following formula:

$$R = \frac{A}{(C - S)} * 100\%$$

ImageJ (National Institutes of Health, MA, USA), in conjunction with Adipocyte Tools plugin developed by Montpellier RIO Imaging (Montpellier, France), was used for all automated calculations involving cell size distribution. The field of view (FOV) from each histological section was kept uniform at 4795 x 2282 μm . Background was first removed from each histological section by the pre-processing

macro within the Adipocyte Tools plugin using the thresholding method. Minimum size of each cell was chosen to be 40 μm , maximum size as 800 μm and the number of dilates were set to be 10. The same threshold was also chosen to automatically set regions of interest (ROI) around the adipose cells. The automated method generated a small number of ROI artefacts. Artefacts that could be detected visually were manually removed. In order to remove the remaining artefacts, 10% of the smallest and 10% of the largest ROIs were excluded from any further analysis. Visualisation of both the manual as well as the automatic method can be found in Supplementary

Fig 4.3.2.

Fibrotic capsules were identified from H & E stained histological sections as a dense layer of collagen fibres aligned parallel to the implant surface with a variable presence of fibroblasts and inflammatory cells [328]. 3 images chosen randomly from each scaffold were imported in ImageJ and measurement lines, approximately 50 μm apart, were defined on the fibrotic capsule. Average thickness of the fibrotic capsule was derived from the average of such measurement lines.

Statistical analysis

All data are represented as mean \pm SD and are subjected to one-way analyses of variance (one-way ANOVA) and Tukey's post-hoc test (Sigmaplot 12.5). Significance levels were set at $p < 0.05$. All error bars represent standard deviation.

4.3.3 Results

Characterisation of scaffolds

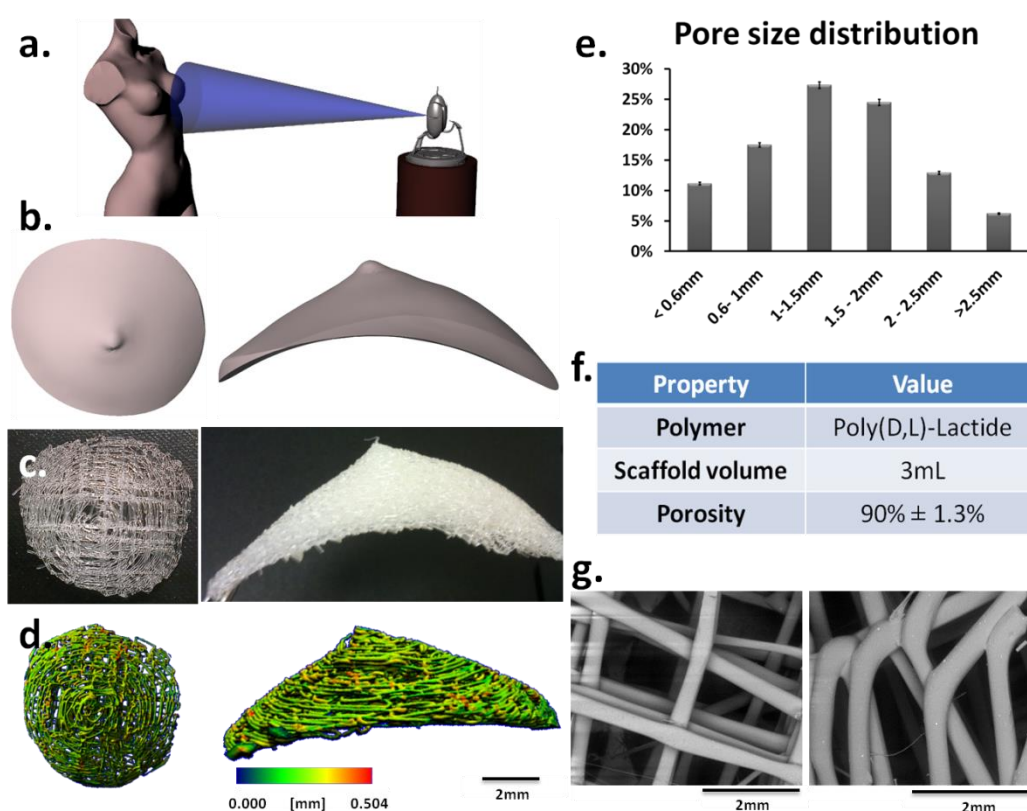


Figure 4.3.1 Scaffold fabrication and characterisation. (a) Illustration of laser scanning performed on a patient suffering from invasive ductal carcinoma. (b) The data from the laser scan was used to generate a CAD model of the patient's left breast. (c) The CAD model was used to generate porous patient-specific scaffolds (shrunk down to 25% of their original size) showing high shape fidelity to the CAD model. (d) MicroCT scans of the fabricated scaffolds showed homogeneity of filament thickness across the entire volume of the scaffold. (e) Histogram of pore size measurements showing the distribution of pore sizes in the scaffolds. (f) Scaffolds fabricated with a highly reproducible porosity of 90 %. (g) SEM images showing the surface of the scaffold bars and struts

The gross morphology of the fabricated PDLLA scaffolds was highly similar to the CAD file obtained from the laser scanning of the breast region (Fig 4.3.1. a-c) and

contained a regular array of interconnected pores. The axial pores of the scaffolds were larger than the transverse pores of the scaffolds. This observation was confirmed by μ CT measurements (Fig 4.3.1(e)), where the smaller pore sizes (200-400 microns) reflected the transverse pores of the constructed scaffolds as seen in Fig 4.3.1(d, right). The larger pore sizes (500-1000 microns) reflect the axial pores of the scaffolds as seen in Fig 4.3.1(d, left). The high porosity value of the scaffolds also implies more volume available for tissue/vascular ingrowth. From the 3D μ CT reconstructed images it was also shown that the filament thicknesses across the entire scaffolds were largely homogeneous (Fig 4.3.1d).

In vitro culture

To improve the seeding efficiency of cells onto the large volume scaffolds, a clinically approved hydrogel system, namely fibrin glue, was used. A fibrinogen/cell suspension was mixed with thrombin and immediately added to the scaffolds so that the fibrin clot was formed *in situ* within the scaffold pores. The scaffolds were also pre-wet in sterile PBS overnight prior to seeding them with cells. Initially, when the cells were encapsulated in fibrin glue, they showed a rounded morphology, however as shown in the light microscopy image in Supplementary Fig 4.3.1a, after 24 hours, filopodia began to develop. After day 28 days of static culture cells were seen to be bridging across the pores of the scaffold (Supplementary Fig 4.3.1b). The rotational motion of the TisXell bioreactor leading to increased perfusion of nutrients facilitated cell growth, as observed from the size and number of bridges across the pores, which increased significantly in 2 weeks under dynamic culture (Supplementary Fig 4.3.1b, c).

Fluorescent imaging

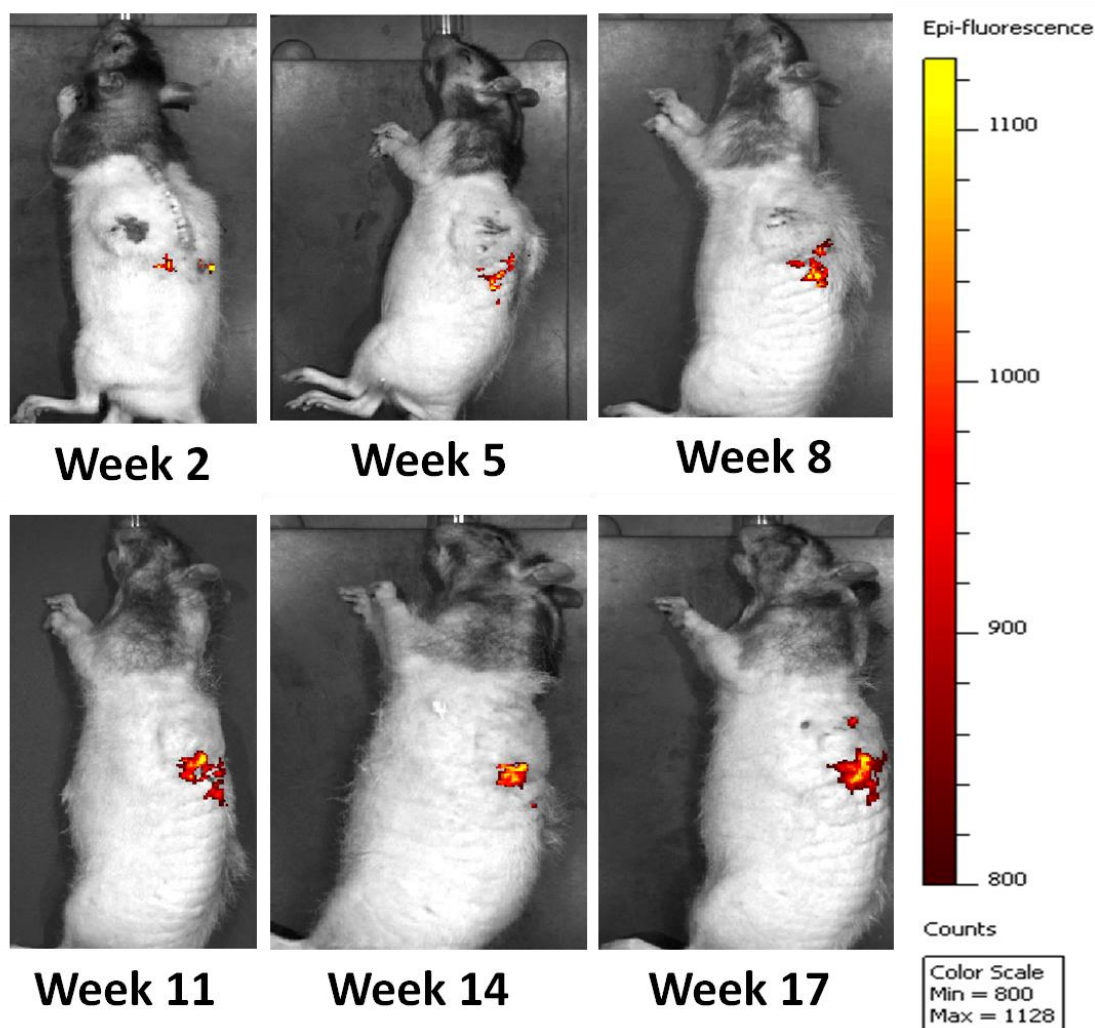


Figure 4.3.2 Fluorescence signal from the GFP-labelled HUVECs detected using an IVIS bioluminescence scanner. The signal from viable HUVECs increased steadily from week 2 until week 17.

Prior to the implantation of scaffolds into rats, the pre-cultured scaffold/cell constructs were further seeded with a suspension of GFP-labelled HUVECs in Matrigel in order to enhance the angiogenic potential of the TECs. The rats were subjected to *in vivo* fluorescence imaging every 3 weeks to detect the fluorescent signal from the implanted GFP-labelled HUVECs. The fluorescence signal could not be distinguished from the background noise on week 0. On week 2, the signal was localised at the right wing of the scaffold (Fig 4.3.2a). Over the next 15 weeks, the

signal persisted at the initial location and seemed to invade towards the central regions of the scaffold (Fig 4.3.2 b-f).

Scaffold explantation and degradation

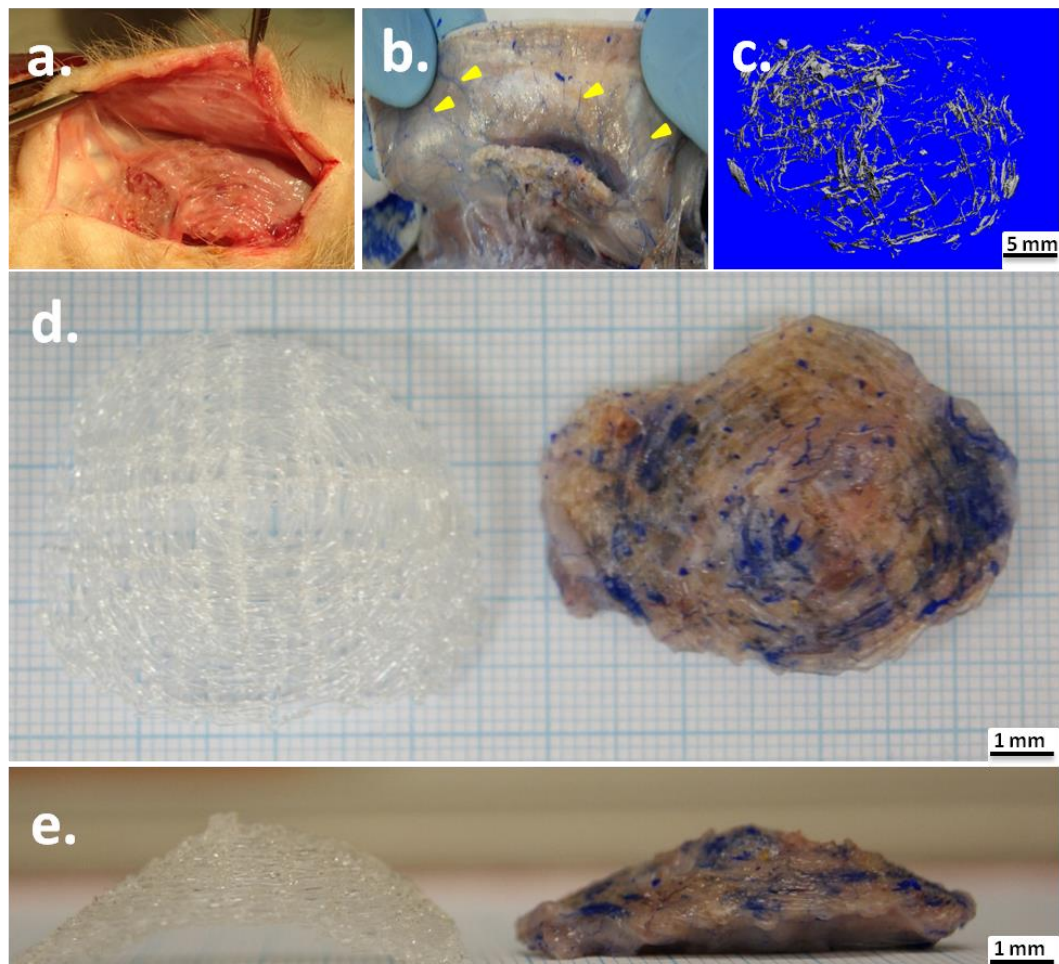


Figure 4.3.3 (a) Scaffolds explanted after 24 weeks showed good integration with the host tissue with no observable signs of inflammation and fibrotic encapsulation. (b) Perfusing the animals with Microfil allowed the visualisation of all blood vessels within the scaffold and the surrounding tissue areas. The arrows in yellow show large blood vessels supplying oxygen and nutrients to the tissue within the scaffolds. (c) 3D image obtained from microCT reconstruction of the scaffolds explanted from Microfil-perfused animals showing a well-established network of capillaries throughout the entire volume of the scaffold. (d) Top view and (e) side view of fabricated scaffold (left) and explanted tissue engineered constructs (TECs) (right) after 24 weeks. The distribution of capillaries can be qualitatively visualised on the explanted TECs.

No postoperative infections or macroscopic signs of foreign body reaction to the TECs occurred over the entire period of implantation. After 6 months of implantation, the TECs were retrieved for histological analysis. Upon visual

examination, it was shown that the scaffolds were well integrated into the host body with no apparent major inflammatory reaction (Fig 4.3.3 a). Visual examination of the Microfil perfused samples revealed a widespread invasion of host vasculature into the engineered adipose tissue (Fig 4.3.3 b, c, d). MicroCT angiography of the scaffolds revealed a high degree of vascularisation equally distributed throughout the architecture (Fig 4.3.3c). Furthermore, it was also found that the scaffolds did show, as anticipated, significant degree in weight loss (Fig 4.3.3 e). Our tissue engineering concepts [329] are based on the principle that the overall shape of the scaffold remained intact (Fig 4.3.3d).

Formation of vascularised adipose tissue

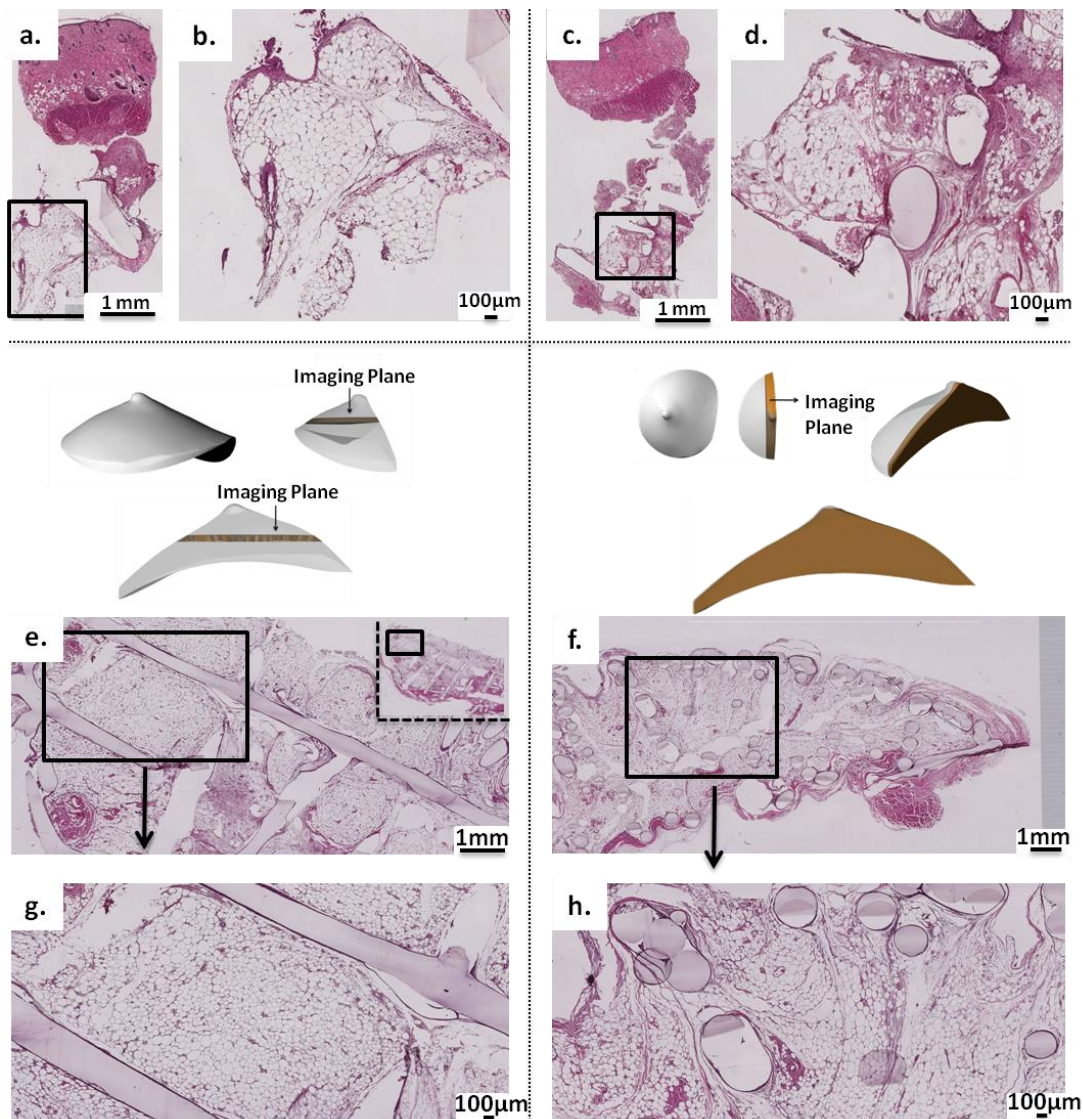


Figure 4.3.4 (a, b, c, d) Hematoxylin and Eosin (H&E) staining of tissue samples explanted at week 5 (a,b) and 15 (c,d) show a well vascularised adipose tissue and no signs of major inflammation or cyst formation. (e, f, g, h) H&E staining of samples explanted at Week 24. The scaffolds were sectioned in two orientations: transverse (e, g) and longitudinal (f, h). Representative sections are shown.

Widespread regeneration of well-vascularised adipose tissue was observed throughout the length, breadth and height of the scaffolds. No regions of necrosis, major inflammation or cysts were observed

H & E staining revealed formation of adipose tissue and blood vessels across all time points (Fig 4.3.4 a-h). H&E staining of tissue samples explanted at week 5 (Fig 4.3.4 a & b) and 15 (Fig 4.3.4 c & d) showed a well vascularised adipose tissue construct. H&E staining of tissue samples explanted at week 24 demonstrated widespread

regeneration of well-vascularised adipose tissue throughout the length, width and height of the scaffolds. No regions of necrosis, inflammation or cysts were observed. All constructs showed the formation of a thin fibrotic capsule around the constructs. Adipose cells could be identified microscopically by their typical ring-like morphology and a large vacuole in the middle of the cell. These characteristics enabled quantification of the area of fat tissue.

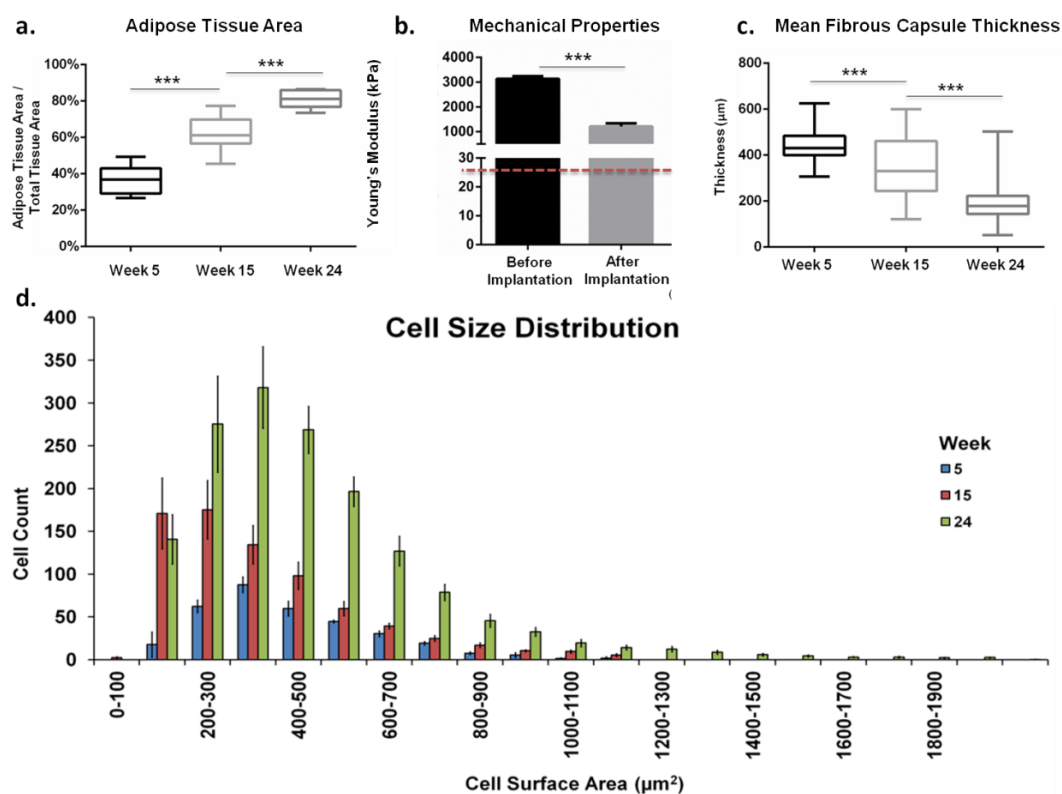


Figure 4.3.5 (a) Box and whiskers plot showing the adipose tissue area relative to total tissue area over 24 weeks. Adipose tissue area increased significant ($p < 0.01$) from approximately 40% on Week 5 to approximately 60% on Week 15 finally reaching almost 80% on week 24 ($p < 0.01$). The variability across the samples was low, especially in the Week 24 tissue extracts. (b) Graph showing the compressive Young's modulus of scaffold pre- and post-implantation. Mechanical properties of the scaffold decreased significantly ($p < 0.01$) from 3MPa to 1MPa over 24 weeks *in vivo* implantation. The stiffness of native adipose tissue is represented by the red dashed line [330]. (c) Box and whiskers plot showing mean thicknesses of the fibrous capsule surrounding the scaffold. As the scaffold degraded the thickness of the capsule decreased significantly ($p < 0.01$) from 400μm to 300 μm between weeks 5 and 15 and down to 200 μm in week 24. The variability in the samples was high on week 15. (d) Histogram showing the distribution of adipose cells according to the cell surface area. Generally, the number of adipose cells increased significantly from week 5 to 24. At week 5, a majority of the cells had a surface area between 200 and 500 μm². On week 15, the cells generally shrunk in area, with the majority of cells having an area between 150 and 350 μm². Finally on week 24, the cells once again expanded in area and the majority had surface area between 200 and 500 μm².*** statistically significant, $p < 0.01$.

The percentage of adipose tissue compared to overall tissue area increased from 37.17% to 62.30% between week 5 and week 15, and grew to 81.2% between week 15 and week 24 (Fig 4.3.5a). The stiffness of the TECs decreased significantly from 3 MPa to 1 MPa over 24 weeks of *in vivo* implantation (Fig 4.3.5b). The results from the fibrotic capsule thickness measurements are displayed in Fig 4.3.5c. The semi-quantitative analysis of the thickness revealed that the size of the capsule increased from approximately 350 μm to 450 μm between week 5 and 15. However, as the scaffold degraded over time, the size of the capsule decreased to 200 μm as observed at week 24.

Quantification of adipose cell area allowed the visualization of the distribution of different-sized cells as a histogram (Fig 4.3.5d). At week 5, the majority of the cells had a surface area between 200 and 500 μm with the histogram skewing towards the right and a small number of outliers. At week 15, the number of cells counted increased considerably, but the histogram continued to remain skewed to the right with a higher number of outliers compared to those at week 5. The majority of cells had a surface area between 100 and 300 μm at week 15. The histogram at week 24 was more balanced compared to week 5 and 15, however it had the highest spread of values, having a considerably higher number of cells with a surface area larger than 1000 μm . The cell count also increased significantly between week 5 and 15.

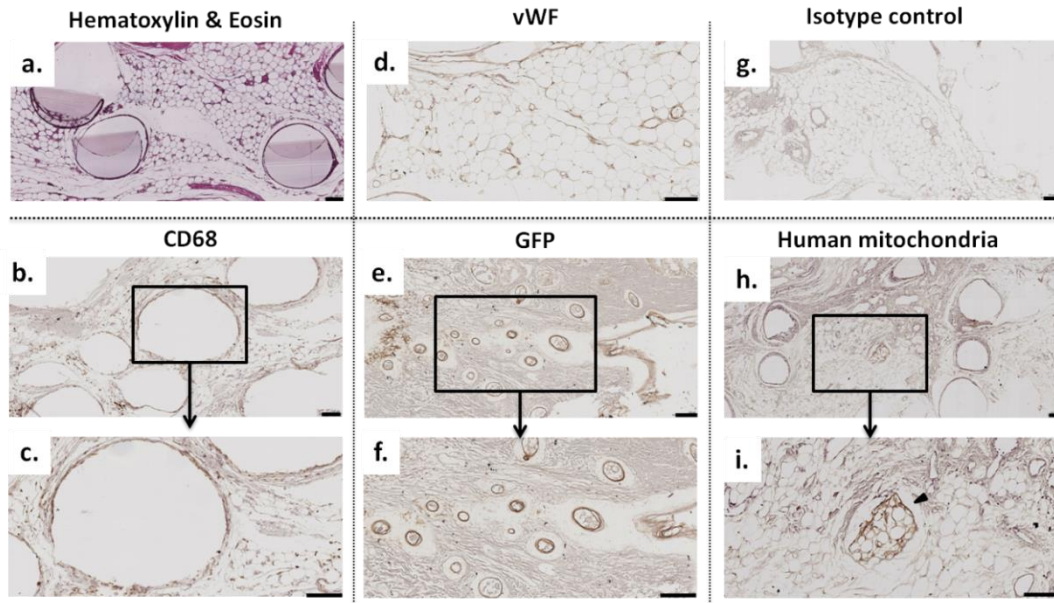


Figure 4.3.6 Histological staining of scaffolds explanted on week 24. (a) Haematoxylin and Eosin (H & E) staining of scaffolds showing overall tissue morphology. (b & c) CD68 staining showing the presence of macrophages near the scaffold strands. Density of macrophages was low in areas away from the scaffold strands. (d) Anti-vWF staining for the blood vessels showing a well vascularised tissue. (e & f) Anti-GFP staining for the presence of GFP-labelled HUVECs showing the assembly of HUVECs into functional capillaries. (g) isotype control. (h & i) Staining for human mitochondria showing the host-origin of the regenerated tissue. Human fat cells (black arrow) were localised in small islands near the scaffold strands. Scale bars = 100µm

Immunohistochemical staining for anti-human-mitochondria antibodies showed that a majority of the adipose tissue within the scaffold was of host origin, with human adipocytes aggregating into a small number of islands near the scaffold strands (Fig 4.3.6 h , i). Staining for anti-GFP showed that a significant number of HUVECs self-organised into a functional capillary network within the scaffold strands (Fig 4.3.6 e , f). A majority of the capillaries formed by HUVECs had a diameter less than 100 µm, were clustered into domains approximately 800 µm x 400 µm in size and localised on the periphery of the TECs. All such capillaries also had presence of red blood cells, indicating their functional nature. Anti-CD68 staining showed that the scaffolds invoked an unspecific inflammatory response in close proximity to the scaffold strands (Fig 4.3.6 b, c). CD68-positive macrophages were not found more than 400 µm away from the nearest scaffold strand showing that unspecific immune

reaction was not widespread and localised within a radius of approximately 400 μm of the scaffold strands.

4.3.4 Discussion

The overall goal of breast reconstruction after mastectomy is to restore the patient's breast with functional tissue interfaces, and to maintain tactile sensation. The shape and size of the breast is different for each patient, hence the scaffold supporting the regeneration of the tissue interfaces needs to be customised. Here, the translation of scaffold-based tissue engineering applying the toolbox provided by Computer-Aided-Design and Computer-Aided-Manufacturing (CAD/CAM) opens up new vistas for scaffold-based patient-specific breast reconstruction. In this article, we present an integrated strategy where images are first taken of the breast region of a mastectomy patient using medical imaging techniques. The images captured can then be processed into a patient-specific 3D computer-aided design (CAD) model which is then sent to a 3D printer to be fabricated into a highly porous biodegradable scaffold. The porosity and pore sizes can be tailored independently by changing the laydown pattern. The optimal porosity is always determined by a trade-off between mechanical properties and pore volume available for tissue ingrowth [249]. Stiffness and strength should be sufficient in the context of breast tissue engineering, as the scaffold should be sufficiently robust to not only resist changes in shape *in vitro* as a result of cell contraction forces *yet* also the wound contraction forces which will be invoked during tissue regeneration. Furthermore, the breast region is also subjected to high biomechanical loads during sleeping and sports activities, and the TECs must be able to withstand those forces over a long period of time.

Patrick *et al.* were among the first to study adipose tissue engineering *in vivo* [73]. Since then several research groups have developed different approaches to engineer

fat tissue using different types of cells and/or scaffolds. Most of these studies used small volume scaffolds and implants (Supplementary Fig 4.3.4); therefore, there is a direct need of sustained regeneration of clinically relevant high-volume adipose tissue. Furthermore, very few studies have analysed the long-term behaviour of tissue engineered breast constructs to date. To our knowledge, we present the first such study utilising a large-volume patient-specific TEC in an *in vivo* model and achieving a sustained regeneration of adipose tissue up to 24 weeks.

The volume of the originally designed patient-specific scaffold (194 cm^3) was scaled down for the rodent experiment to 3 cm^3 (Table 3); yet it is important to note that it is a considerably larger volume than reported in most previous studies (for a comparison of volumes of scaffolds used for adipose tissue engineering, please see Supplementary Fig 4.3.4) was reconstructed. Furthermore, a 3 cm^3 scaffold leads to a breast/body volume of 0.84% in a rodent, considerably larger than that of an average human female (0.63%). For a detailed comparison, see Supplementary Table 2.

It is important to note here that, based on our tissue engineering philosophy[310, 329] we did not aim to produce a scaffold whose mechanical properties matched those of native adipose tissue. PDLA has been also been used previously to engineer adipose tissue [331, 332]. PDLA is a aliphatic polyester which characterized by bulk degradation and has a modulus of 1.5 GPa [333, 334]. Our hypothesis was that the highly porous scaffold would maintain its shape and volume for at least 9-12 month without showing any signs of mass loss so that the regenerated tissue stably remodels several times in the highly porous scaffold architecture without being influenced by any degradation by products.

As the scaffolds showed qualitative signs of degradation, their mechanical properties also changed significantly over a period of 8 month (2 month *in vitro* and 6 month *in*

vivo). Measurement of the Young's modulus after explantation revealed that the TECs had 33% of the Young's modulus compared to the original scaffold values; however, the form stability and integrity and form specificity remained unchanged, with the TEC recovering shape and volume completely after being subjected to 10% compression. The stiffness of the scaffold was measured at 3 MPa in comparison to the TEC which had a stiffness of 1 MPa post-implantation (Fig 4.3.5b) which is 2 orders of magnitude stiffer compared to native adipose tissue. As PDLA degradation occurs throughout the whole via bulk degradation, the scaffolds did lose its stiffness uniformly throughout its volume [335]. However, as per our hypothesis, the biodegradable scaffold was able to withstand the contraction forces for at least 6 months *in vivo* and did not show any mass loss or volume contraction.

Scaffold architecture has a major impact on adipose tissue formation. Scaffolds morphologies formed by Fused Deposition Modelling (FDM) are homogeneously organised with precisely deposited struts and contain a highly interconnected channel network. Previous work within our group [336] and elsewhere [72] have shown that scaffolds containing small pores and pore interconnections are unsuitable for high volume adipose tissue regeneration. Diffusion of oxygen from the surrounding tissues is sufficient only over a distance up to approximately 150 μm [175]. Therefore, in tissue constructs without adequate vascularization, autologous adipose tissue loses up to 60% of its volume post-transplantation because the cells in the centre of the graft are inadequately supplied with nutrients and transport of waste is not possible [176, 177]. Pore sizes of 1.5 mm used in the presented study allowed vascular ingrowth into the scaffold during the early stages of the implantation which helped sustain the adipose volume for an extended period of time.

Our results from anti-CD68 staining show the presence of macrophages, primarily bordering the scaffold strands which can be interpreted as an unspecific immune reaction. The invasion of these macrophages may have had a large role to play in the subsequent adipogenesis and vasculogenesis. Moldovan [337] and Anghelina *et al.* [338, 339] have shown that upon implantation, monocytes and macrophages first invade the extracellular matrix around the graft and form tunnels while clearing ECM along their path. Subsequently, endothelial cells and adipocytes are visualised in these macrophage-lined tunnels, indicating their development into functional capillary-like structures and vascularised adipose tissue. However, further investigations done by Debels *et al.* [340] have found no conclusive evidence of macrophages playing a direct role in neoadipogenesis and claim that the perceived neoadipogenesis is simply a result of increased angiogenesis, without further involvement of macrophages.

Immunohistochemistry on paraffin embedded explants samples with human-specific mitochondria antibody confirmed the host derivation of the newly formed adipose tissue, indicating that the regeneration process is dependent on inductive factors embedded within Matrigel or excreted by the transplanted cells, rather than direct tissue formation by provided precursor cells. This finding complies with a study performed by Stillaert *et al.* [341] who also used Matrigel in combination with FGF2 and concluded that such an inductive graft causes the recruitment and differentiation of host-derived precursor cells into adipose cells. Previous studies [342, 343] have shown that adult adipose tissue houses a significant number of mesenchymal stem cells with pluripotential characteristics. There is a high likelihood that these cells were significantly involved in the neoadipogenesis process. Athymic nude rats are characterised by their lack of normal thymus and functionally mature T cells and are

therefore useful in xenograft models [344]. However, they still possess allo- and xeno-reactive natural killer cells that can recognise and kill major histocompatibility complex (MHC) incompatible cells through the recognition of both mismatches in the classical (RT 1.A) and non-classical (RT1.C/E) MHC class 1 regions. With increasing age, nude rats develop leukocytes, for example dendritic cells, T-like cells and T-cell receptors which may also contribute to specific innate immune responses [344]. At the time of implantation, it is reasonable to assume that the HUCPVC were mostly localised on the scaffold strands, which is also the region encapsulated by fibrous tissue and granulomatose reaction. It is therefore likely that the implanted HUCPVC were constantly triggering a response by the innate immune system of the host and did not survive long-term.

As described previously, one of the goals of this research project was to construct a human vascular bed within a nude rat model. The aims of such a pursuit are not limited to tissue engineering applications where vasculogenesis by means of precursor cell induction can provide nutrition to adipose cells, but also to basic cancer research whereby humanised vascular structures can be used as a model to study the growth and proliferation of cancer metastases [345]. *In situ* fluorescent imaging showed that on week 2, the eGFP signal from the implanted HUVECs was localised onto to the right wing of the scaffold. This observation was unexpected since the HUVECs were distributed homogeneously throughout the scaffold. One argument is that the movement of the rat and gravitational forces caused the cells to accumulate on the bottom region of the scaffold. Another possibility is that the HUVECs in the core regions of the scaffolds perished due to hypoxia, while those on the periphery survived owing to a greater nutrient exchange at these sites.

Anti-GFP staining showed that in contrast to HUCPVC, GFP-labelled HUVECs survived the 6-month implantation process all throughout the scaffolds. However, their self-assembly into capillaries of diameters less than 100 μm was observed only around the periphery of the scaffold. The clustering of cells in the posterior regions of the scaffold may have led to increased cell-to-cell contact in these regions, which is a very important factor determining the extent of capillary network formation with a minimum critical density required for optimal capillary bed formation [346, 347]. Although further investigation is needed, the maintenance of such a humanised capillary bed in a nude rat model for 24 weeks *in vivo* opens up the possibility of generating vascular networks spanning a greater area for many tissue engineering approaches.

4.3.5 Conclusion

We have demonstrated a clinically viable route to design and fabricate biodegradable patient-specific scaffolds directly from 3D imaging data sets. To our knowledge this is the first study showing a sustained regeneration of high volume adipose tissue over a long period of time using a patient-specific biodegradable scaffold. While the mechanical properties of the TECs, in particular the stiffness, remain to be desired closer to native breast tissue, the presented approach of fabricating patient-specific scaffolds using 3D patient body scans represents a facile approach towards engineering clinically relevant and stable volumes of adipose tissue for breast reconstruction. These scaffolds, that contain large pores and pore interconnections, facilitate the ingrowth of host vasculature throughout the entire scaffold architecture which is crucial for long-term sustenance and viability of adipose tissue.

4.3.6 Acknowledgements

The authors would like to acknowledge Samuel Perry for his assistance with the production and packaging of the lentiviral particles and Dr. Elizabeth Rosado Balmayor for providing critical feedback. This work was supported by the European Union (Marie Curie Fellowship PIOF-GA-2010-272286 to Ferry Melchels) and the Australian Research Council (Future Fellowship to Dietmar W. Hutmacher). The authors would also like to thank Dr. Jan-Thorsten Schantz for providing the laser scan data.

4.3.7 Supplementary Tables and Figures

<u>Primary Antibodies</u>	<u>Description</u>
Anti-Von Willebrand factor	Polyclonal Rabbit Anti-Human Von Willebrand Factor: Ref A 0082 (DAKO, Glostrup, Denmark)
Anti-CD68	Monoclonal Mouse Anti Rat CD68: Ref MCA341GA (AbD Serotec, Oxfordshire, UK)
Anti-GFP	Rabbit Polyclonal Anti-GFP antibody: Ref AB290 (Abcam, Cambridge, UK)
Anti-human mitochondria	Mouse monoclonal anti-human mitochondria antibody: Ref AB92824 (Abcam, Cambridge, UK)

Table 4.2 List of primary antibodies

Type of Tissue	Volume (cm ³)	Breast/Body Volume	Ref
Whole human body	66,400	0.63%	[348]
Human breast volume	420		[349]

Whole rat body	353	[350]
Breast scaffold volume	3	0.84%

Table 4.3 Comparison of breast/body volumes of humans and rodents



Figure 4.3.7 (a) Cell morphology on day 1 post seeding suspended in fibrin glue. Cells do not remain rounded and are seen to spread and connect with neighbouring cells. (b) 28 days post culture the cells begin to form wide bridges across the gaps of the scaffolds (dotted by yellow triangles). (c) DAPI-Phalloidin staining of cells at 28 days post-culture to visualise cells forming a continuous sheet along the scaffold strands. Blue (DAPI): cell nuclei, Red (Phalloidin): cell actin filament.

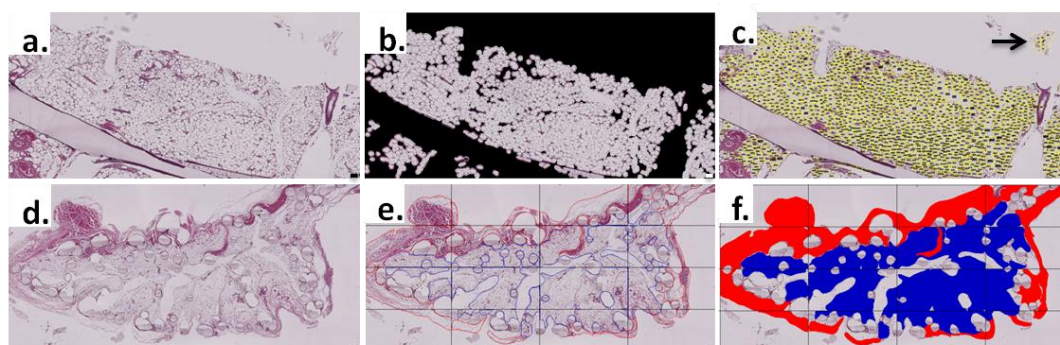


Figure 4.3.8 (a-c) Images depicting the workflow of the automated algorithm to count the number of adipose cells on a histology section and also their cell surface areas. (d-f) Images depicting the workflow showing manual demarcation of adipose tissue areas using Osteomeasure software.

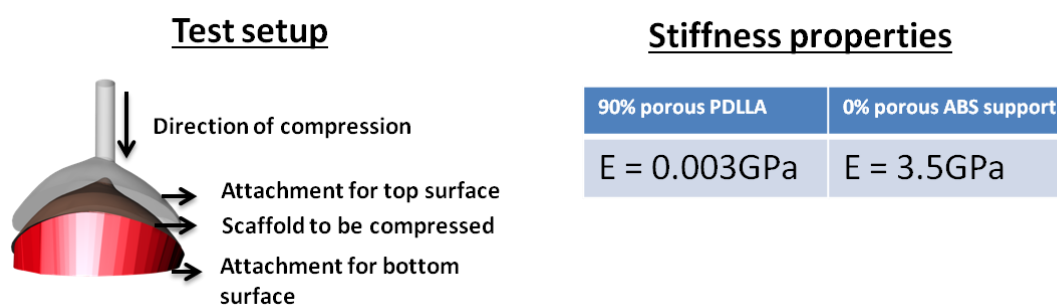


Figure 4.3.9 Schematic diagram of the test setup used for compression testing of scaffolds. Due to the curved nature of the scaffold surfaces, special top and bottom surface attachments following the

contours of the scaffolds were produced. The top attachment links with the Instron microtester plunger providing uniform stress across the entire scaffold. The attachments were produced with non-porous acrylonitrile butadiene styrene (ABS) with a considerable higher stiffness compared to the 90% porous PDLA scaffolds, to minimise their influence on the load readings

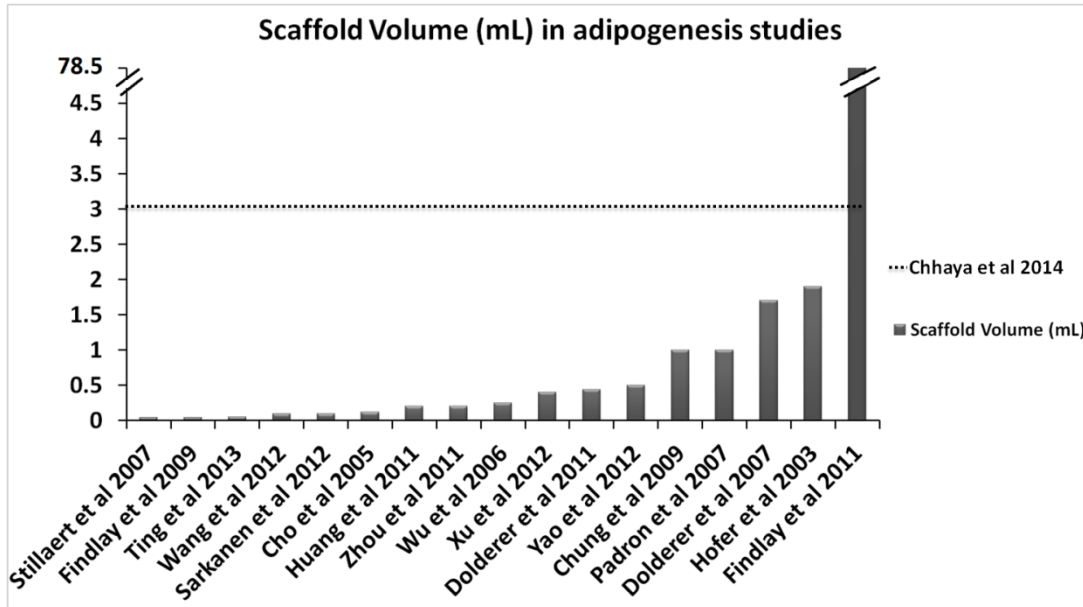


Figure 4.3.10 Graph showing comparison of volumes of scaffolds used for adipose tissue engineering research. Volume of the scaffold used in the present study is dotted by a horizontal line showing that it is considerably higher than the volumes used in most other studies

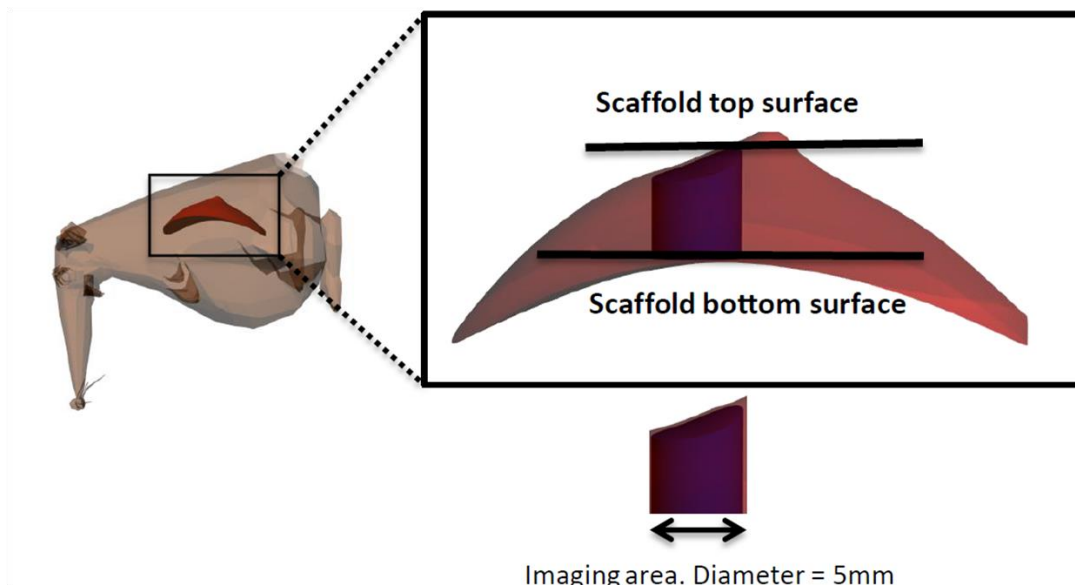


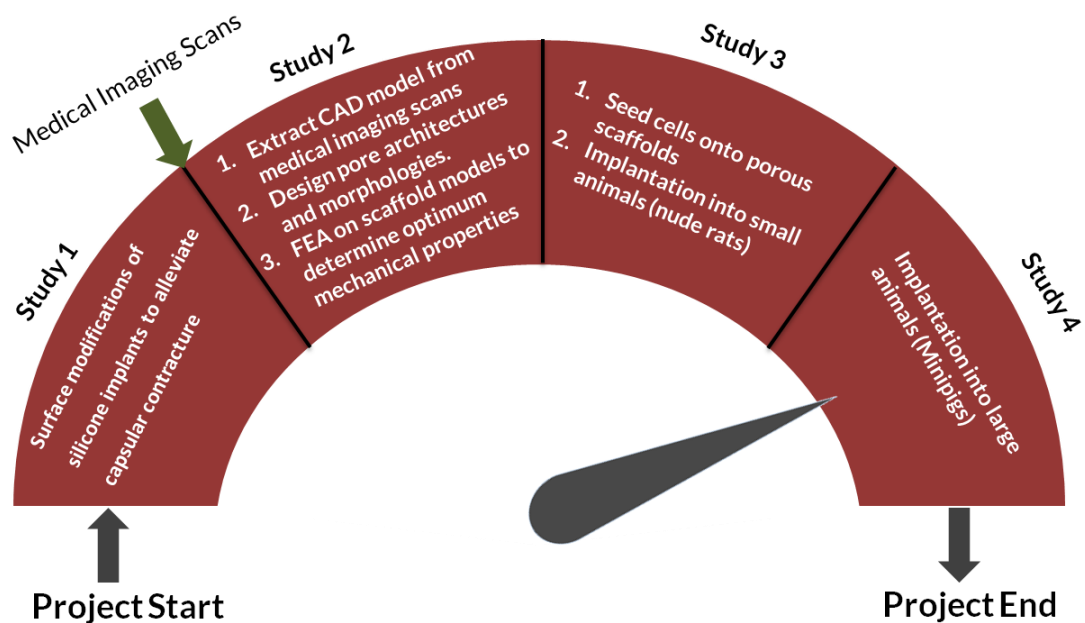
Figure 4.3.11 Illustration showing the position of the samples collected using biopsy punch outs at weeks 5 and 15. Areas shaded in dark purple represent tissue excised by the biopsy punch

4.4 STUDY FOUR (MANUSCRIPT IN PREPARATION)

Breast Reconstruction using Computer Aided Design and Biomanufacturing – towards engineering clinically relevant volumes of adipose tissue.

Thesis Progress:

The following figure shows the flow of activities undertaken and methodologies developed as part of this PhD project. The previous study showed positive adipose tissue regeneration outcome in a small animal model. This study aimed to scale up the volumes of regenerated tissue within a subglandular pig model.



4.4.1 Introduction

In recent years, there have been significant advances in medical techniques for the replacement and/or reconstruction of lost body tissues, mostly due to innovative developments in the fields of surgery, material science and bioengineering. There are various medical conditions where replacement or reconstruction of lost body tissues becomes an important treatment option. Such medical conditions include trauma, tumor removal, diverse chronic diseases and certain congenital anomalies.

A typical example of a medical condition where tissue replacement/reconstruction is often carried out is breast cancer. Breast cancer is a major cause of illness for women, with an estimated number of approximately 300,000 new cases diagnosed in 2013 [315, 351]. Unfortunately, currently available clinical treatments and filler materials for breast reconstruction or augmentation yield unsatisfying results [30, 34]. Reconstruction using silicone-based implants leads to severe medical complications such as formation of a rigid fibrous tissue surrounding the implant, causing significant soft tissue irritation via capsular contracture and giving, from a cosmetic point of view, an unnatural appearance to the breast [352]. A second reconstruction method which is popular among surgeons is lipofilling. In this case, the surgeon isolates fat from a donor site within the patient's body via liposuction and injects it back into the breast region. However, without a structural support, the newly injected fat quickly gets remodelled by the body after 2-3 months – thus requiring 3-4 additional lipofilling sessions before the tissue stabilises [353]. Therefore, impetus has been gradually growing towards cell-based regeneration of adipose tissue for breast reconstruction.

Stem cell-based approaches are very promising for complete regeneration of breast tissue; however, they also lead to several disadvantages – ranging from problems with scaling up of tissue culture to requiring complex GMP-certified laboratories for tissue culturing [250-256]. Furthermore, it is challenging to efficiently vascularise large clinically relevant scaffolds whose volumes can reach up to 150 cm³.

In order to solve the aforementioned problem of vascularization and adipose tissue remodeling, we have devised the concept of delayed fat injection combined with an acellular biodegradable scaffold. In this method of implantation, the scaffold is first implanted with no fat tissue into the implantation site. A fibrin clot is formed

immediately after implantation of the scaffold from the hematoma caused by the surgical procedure [354, 355]. The clot consists of platelets embedded in a mesh of cross-linked fibres, together with a growth-factor rich cocktail of fibronectin, vitronectin and thrombospondin. We hypothesise that the fibrin clot and the associated growth-factor cocktail would stimulate a strong angiogenic response and induce highly organized connective tissue to penetrate into the scaffold [356, 357]. After a fixed period of time, fat is isolated from a donor site within the patient's body and injected into the scaffold (see Fig 4.4.1 for a visualization of this process). The amount of fat that can be harvested from the patient without encountering donor site morbidity depends on the body composition of the patient – whereby a larger volume of fat can be extracted from patients with higher body fat percentage. In this study, based on the expertise of our surgical team, 4 cm³ of adipose tissue was considered to be the maximum amount that can be harvested from a patient with a very low body fat percentage without encountering donor-site complications. Therefore, the scaffolds were seeded with 4 cm³ of fat isolated from the donor – representing 5.23% of the total volume of the scaffolds. We further hypothesise that the presence of a pre-formed bed of connective tissue and vasculature would allow the injected fat to remain stable within the implantation site with minimal tissue necrosis and resorption.

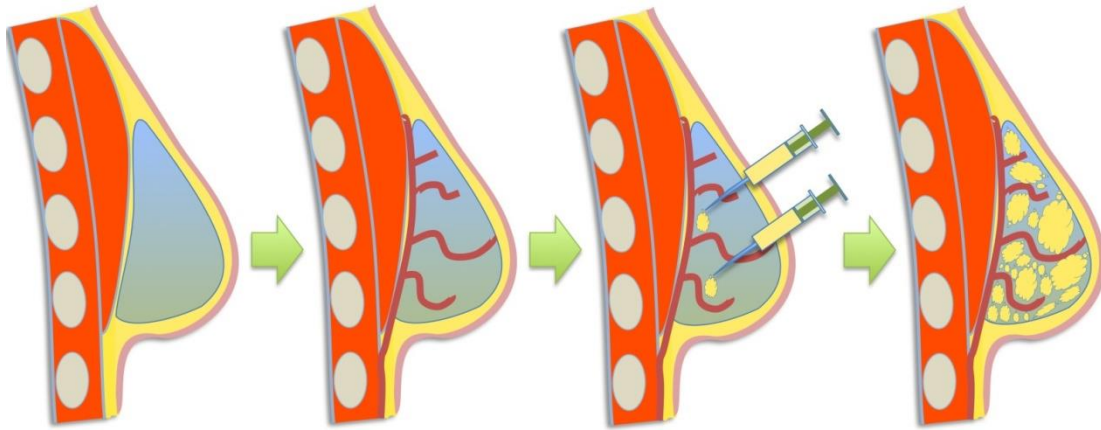


Figure 4.4.1 Overall concept of the prevascularisation and delayed fat injection. Empty scaffold is first implanted at the breast region without the addition of any cells or growth factors. Over the next 2-3 weeks, connective tissue and vasculature invades within the scaffold volume forming a bed of capillaries within the pores. Fat is then injected into the pores of the scaffold. Owing to the presence of the pre-formed vascular bed would allow the fat to remain stable at the implantation sites.

This study evaluated adipose tissue retention in large 75 cm³ acellular polycaprolactone-based scaffolds subjected to a delayed fat injection for a period of 24 weeks.

4.4.2 Materials and Methods

Design & Fabrication of scaffolds

Rapid prototyped hemisphere-shaped shell-shaped polycaprolactone-based scaffolds were designed and manufactured by Osteopore International (Singapore). All scaffolds were produced under GMP conditions.

MicroCT (μ CT) evaluation of scaffolds

Biopsy punch-outs of the scaffolds ($r=5$ mm) were taken at randomly selected spots ($n=6$ per scaffold x 3 scaffolds). The resultant specimens were scanned on a Scanco μ CT40 (Scanco AG, Brüttisellen, Switzerland) at 8 μ m resolution, employing 55 kV and 145 μ A with 250 ms exposure time. Porosity, pore-size and filament-size

distributions were obtained by employing a modified trabecular bone histomorphometry algorithm.

In vivo implantation into minipigs

The animal experiments were performed under GMP conditions at PWG Laboratories, Singapore with ethical approval from National University of Singapore. Two female adult immunocompetent minipigs were used in this study. The operation was performed under general anesthesia, following the standard protocol of sterility requirements for breast augmentation procedures. Careful homeostasis was also maintained throughout the surgical procedure. 3 separate subglandular pockets were created on each side of the mammary region via a longitudinal incision. 6 implants were placed in each animal. Prior to implantation, all scaffolds were trimmed and re-shaped at the operating table by the surgeon in a careful but non standardised manner to ease the implantation process and gain access to the inner pores by removing the outer shells of the scaffolds. To test our hypothesis, 3 study groups were included in this study:

- 1) Empty scaffold (n=4).
- 2) Scaffold containing 4 cm³ lipoaspirated adipose tissue (n=4).
- 3) Empty scaffold + 2 week prevascularisation period. After 2 weeks of prevascularisation, 4 cm³ of lipoaspirated adipose tissue was injected into scaffolds (n=4).

In groups 2 and 3, a midline incision was made and adipose tissue was obtained via the Tulip system (Tulip Medical Products, San Diego, USA). The lipoaspirated fat was injected directly into the interconnected pore architecture of the scaffolds- using a 10-cm³ Tulip cell-friendly injector.

After the placement of the implants each pocket was closed with absorbable vicryl sutures, such that the implants were fixed stably and had no contact to each other. Finally, the skin was sutured with interrupted 2.0 Ethilon sutures.

Histological and immunohistochemical analyses

Hematoxylin & Eosin (H & E)

Implants were harvested from the minipigs after 24 weeks and TECs were fixed with 4% PFA, cut into 10mm x 10mm cube sections, dehydrated and embedded in paraffin using a tissue processor (Excelsior ES, Thermo Scientific, Waltham, USA). Constructs were horizontally sliced to 5µm, deparaffinised with Xylene, rehydrated with a decreasing series of ethanol and stained with H & E. Stained slides were scanned with a BIOREVO BZ-9000 microscope (Keyence, Itasca, USA) at 5x magnification.

Massons Trichrome

The slides were deparaffinised with Xylene, rehydrated with a decreasing series of ethanol and re-fixed in Bouin's solution at room temperature overnight. After rinsing in tap water for 10 minutes, the slides were stained in Weigert's iron hematoxylin for 10 minutes, rinsed in running warm tap water, stained in Biebrich scarlet-acid fuchsin solution for 10 minutes and transferred directly into aniline blue solution and stained for 10 minutes. The slides were rinsed briefly in distilled water and differentiated into 1% acetic acid solution for 5 minutes.

Histomorphometry

Histomorphometrical analyses were undertaken the Osteomeasure histomorphometry analysis system (Osteometrics Inc., Decatur, GA, USA). All measurements were performed blinded on 4 consecutive sections from each scaffold from each group. To

determine the average adipose tissue area, the total area of the adipose tissue was first calculated (A). Secondly, the total area occupied by the scaffold struts was measured (S). Finally, the combined area of the tissue section was measured (C). The ratio of adipose tissue area to total tissue area (R) was calculated using the following formula [358]:

$$R = \frac{A}{(C - S)} * 100\%$$

ImageJ (National Institutes of Health, MA, USA), in conjunction with Adipocyte Tools plugin developed by Montpellier RIO Imaging (Montpellier, France), was used for all automated calculations involving cell size distribution. The field of view (FOV) from each histological section was kept uniform at 4795 x 2282 μm . Background was first removed from each histological section by the pre-processing macro within the Adipocyte Tools plugin using the thresholding method. Minimum size of each cell was chosen to be 80 μm , maximum size as 800 μm and the number of dilates were set to be 10. These threshold values were kept constant across all samples and groups. The same threshold was also chosen to automatically set regions of interest (ROI) around the adipose cells. The automated method generated a small number of ROI artefacts. Artefacts that could be detected visually were manually removed. In order to remove the remaining artefacts, 10% of the smallest and 10% of the largest ROIs were excluded from any further analysis.

In order to calculate the blood vessel density, all blood vessels that showed red erythrocytes within the lumen were counted. The number of blood vessels was divided by the total tissue area to get the density. Values based on 4 stitched microphotographs from each scaffold per experimental condition.

Statistical analysis

All data are represented as mean \pm SD and are subjected to one-way analyses of variance (one-way ANOVA) and Tukey's post-hoc test (Prism 6, GraphPad, San Diego, USA). Significance levels were set at $p < 0.05$. All error bars represent standard deviation.

4.4.3 Results

Clinical Observations

The surgery and implant placement were tolerated well by all animals and no apparent clinical signs of infection were apparent throughout the implantation period. 12 weeks after the initiation of the study, one scaffold was observed to have seroma accumulation in the surgically-created pocket and was therefore excluded from further analysis.

Scaffold characterization

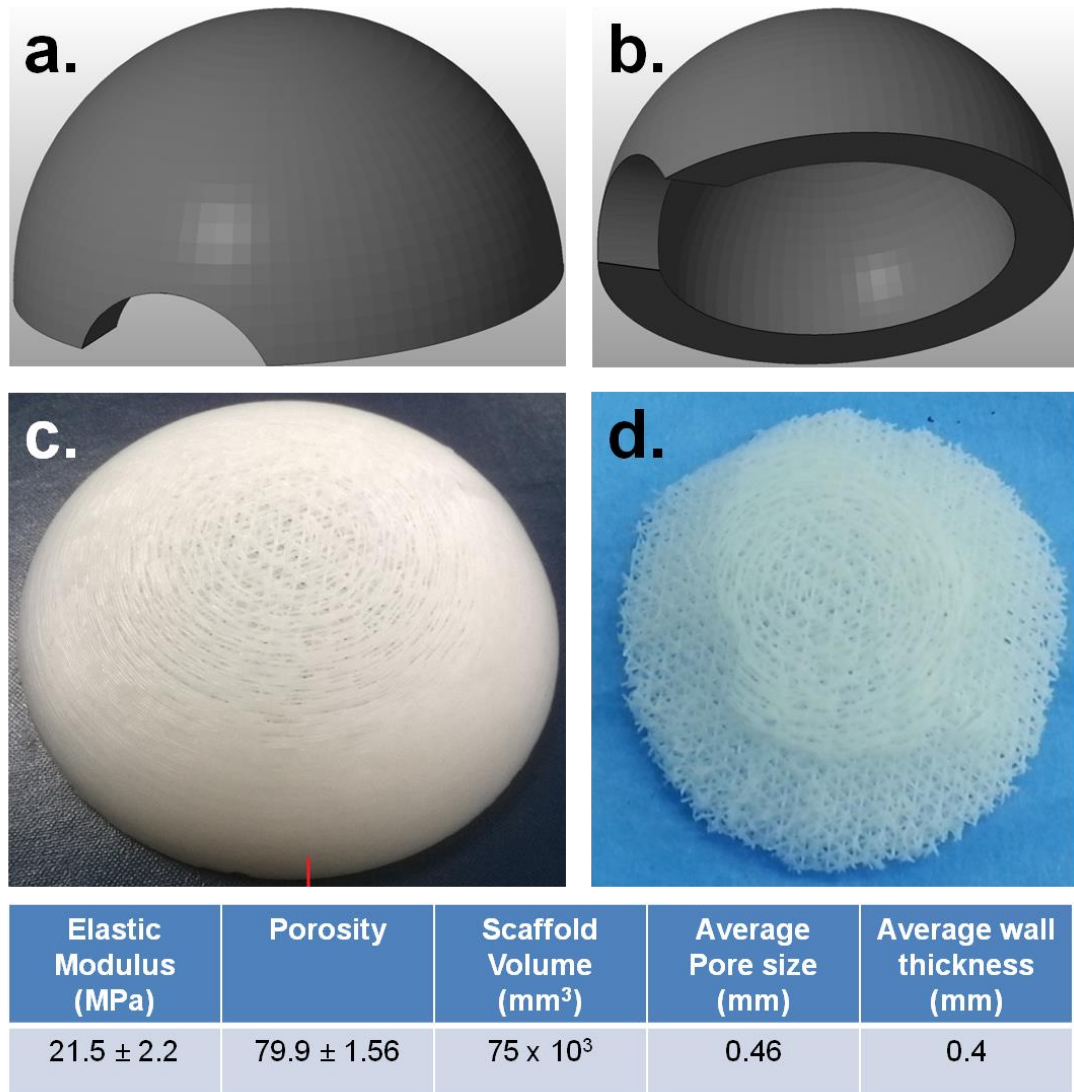


Figure 4.4.2 (a, b) Rendering of the CAD model used to fabricate the scaffold. (c) Original form of the scaffold once 3D printed. (d) Final scaffold form after being processed by the surgeon at the operating table to trim the outer boundary shells.

The shape and volume of the scaffold was similar to that of a silicone implant used for breast augmentation and its gross morphology was highly similar to the CAD file used to design it (Fig 4.4.2). Further gross morphological evaluation also showed that scaffold contained a regular array of interconnected pores, which was confirmed using microCT measurements. The high porosity value of the scaffolds implies that more volume is available for tissue ingrowth.

As described in Study 2, the fabrication of scaffolds containing overhangs requires a sacrificial support structure. Osteopore International does not have capabilities of co-extruding a sacrificial polymer which could act as such a supporting material. Therefore, the dome-shaped scaffolds were produced by placing a solid dome, whose dimensions matched those of the inner hollow lumen of the scaffolds, into the extrusion chamber and fabricating the actual scaffold around this structure. After the fabrication step, the solid dome was detached manually to obtain the final scaffold structure.

Furthermore, due to software limitations, the scaffold contained boundary shells on the exterior edges which hindered access to the pores in the interior regions of the scaffold. Therefore, the surgeon trimmed the sides of the scaffolds at the operating theatre to remove these outer shells.

The scaffold also contained an access cut-out and a hollow region to enable insertion of an arterio-venous shunt loop; however, such a loop was unnecessary for the purposes of this study and these features were not utilized.

The stiffness values of the scaffold, obtained from the manufacturer, were 3 orders of magnitude higher than those of native breast tissue (the Young's modulus of natural breast tissue is ~30kPa [330]).

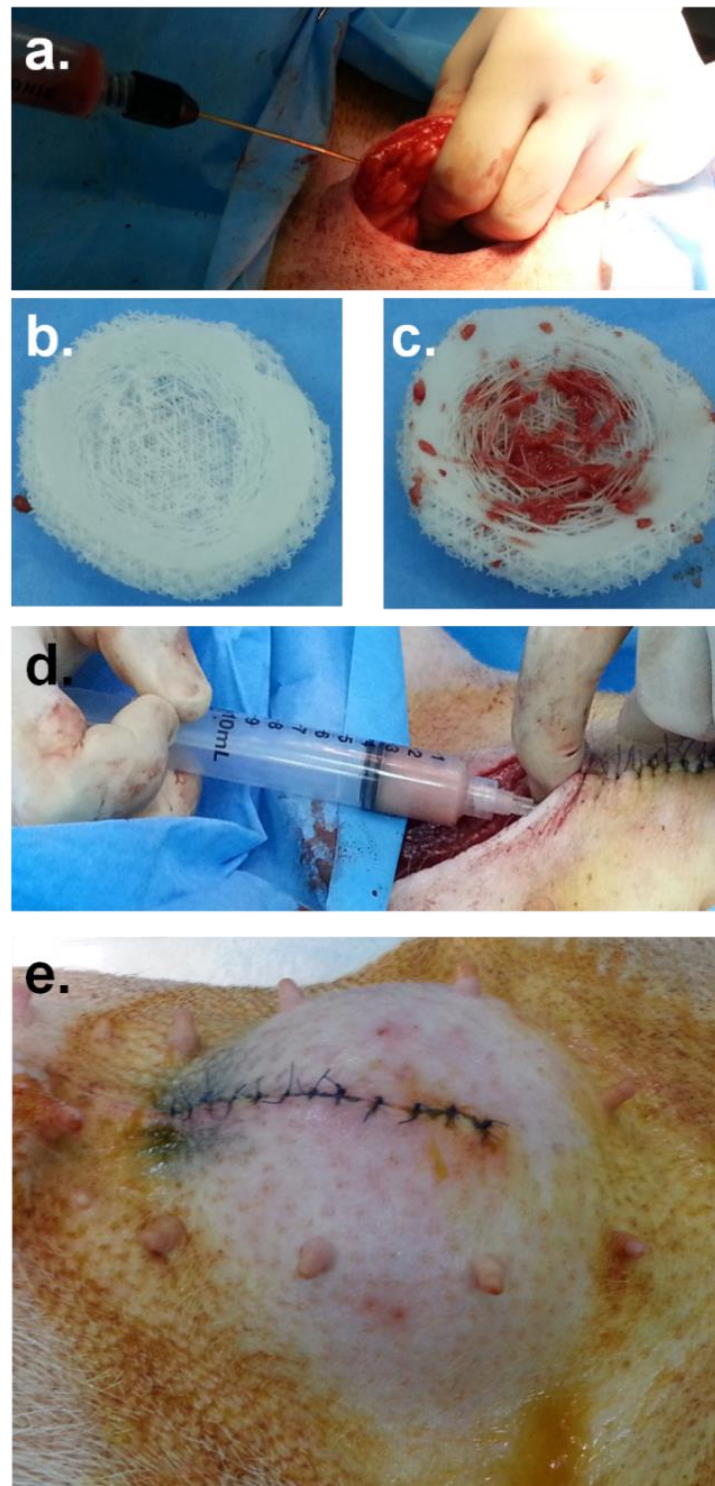


Figure 4.4.3 Implantation process of the scaffolds. (a) Liposuction procedure near the abdominal midline incision. (b, c) Process of injecting fat into the pores of the scaffold placed in the lipoaspirate only group. (b) an empty scaffold while (c) a completely filled scaffold. (d) process of injecting fat into the prevascularisation + lipoaspirate group scaffolds. The scaffolds are placed empty into the implantation site and 2 weeks later, fat is injected into the scaffold pores while the scaffold remains implanted. (e) the final form of the scaffolds conforms highly to the natural breast shape.

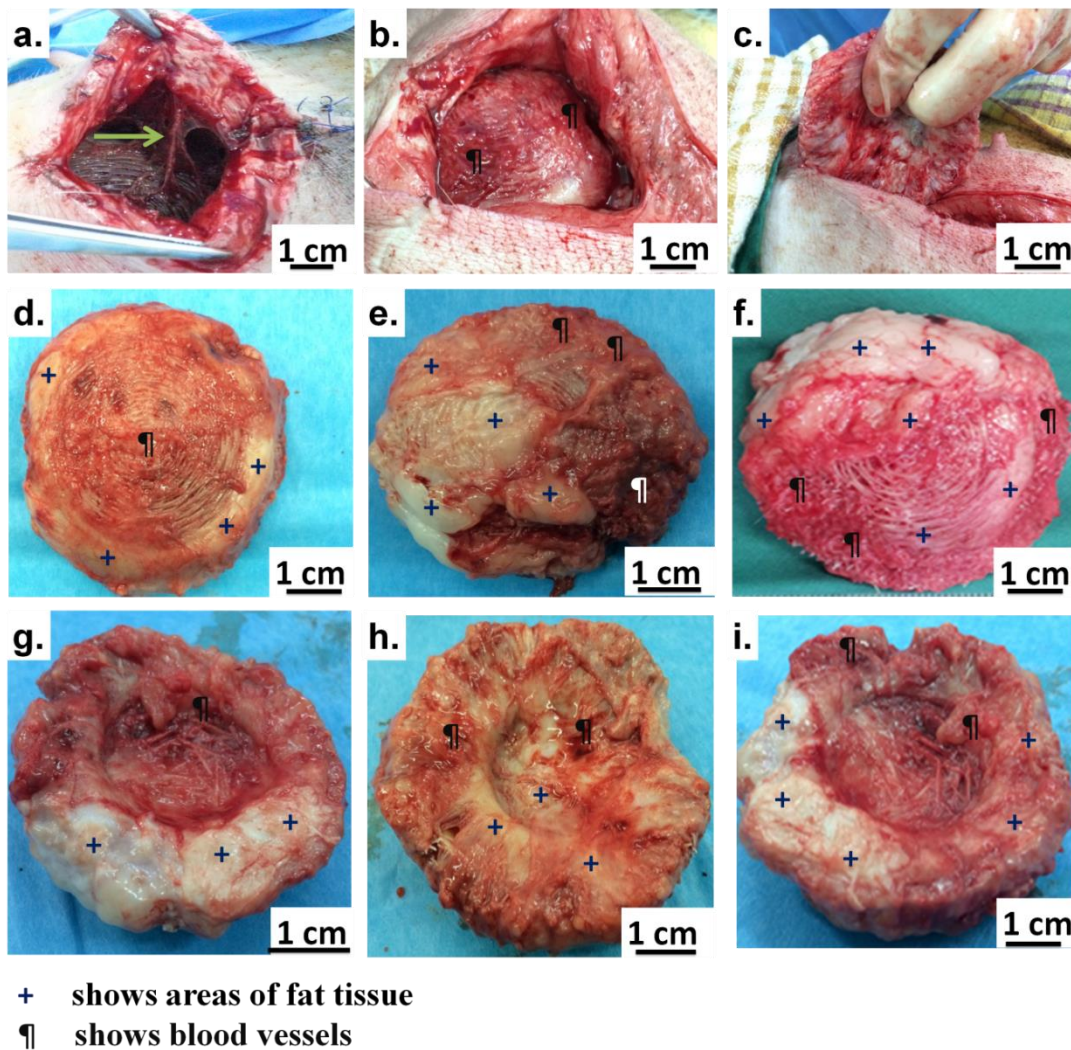


Figure 4.4.4 Explantation images showing the integration of TECs with the host tissue. Green arrow point out major blood vessels supplying blood to the TEC. (d, g) show empty scaffold-only group (e, h) show lipoaspirate-only group (f, i) show prevascularisation+lipoaspirate group. All scaffolds show good integration with the host tissues and large areas of fat (marked with +) and vascularisation (marked with ¶) were observed qualitatively on all scaffolds.

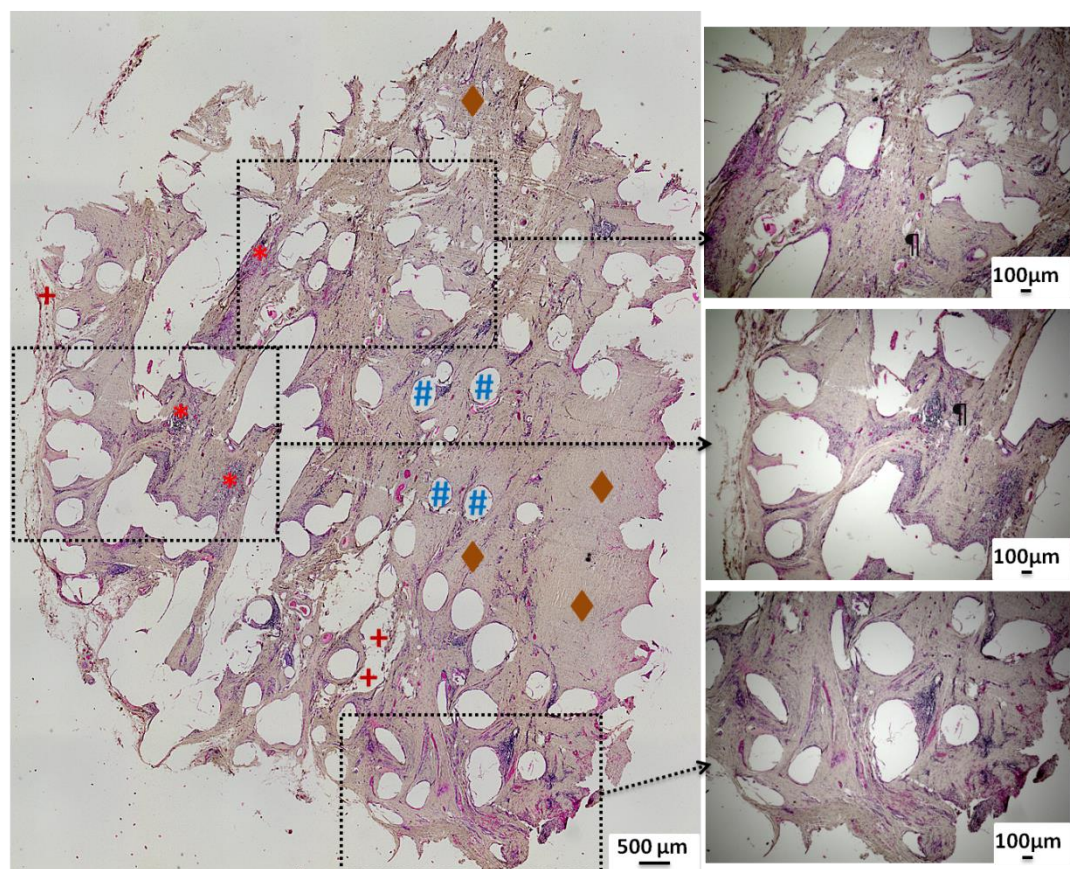
Scaffold explantation and degradation

After 6 months of implantation, the TECs were retrieved for histological analysis. The scaffolds were well integrated with the surrounding tissue and there was a widespread invasion of host vasculature into the constructs (Fig 4.4.4a-c). Visual examination revealed that the overall shape of the scaffolds did not change drastically over the implantation period. All scaffolds showed good integration with the host tissues and large areas of fat and vascularisation were observed qualitatively

on all scaffolds. Visually, it was also clear that prevascularisation+lipoaspirate group (Fig 4.4.4 f, i) had the highest degree of vascularisation and fat tissue deposits, followed by lipoaspirate-only group (Fig 4.4.4 e, h). Although empty scaffold-only group also showed deposits of adipose tissue (Fig 4.4.4 d, g) they were not as widespread as in the other groups.

Formation of vascularized adipose tissue

Negative Control Empty Scaffold group (Superficial Layers)



- +** shows areas of fat tissue
- ¶** shows blood vessels
- #** shows scaffold strands
- *** shows areas of lymphatic structures
- ◆** shows connective tissue

Figure 4.4.5 Representative images showing H&E staining of tissue explanted from the empty scaffold group (superficial layers). A majority of the tissue can be identified as being connective tissue and collagen with only very small patches of fat tissue.

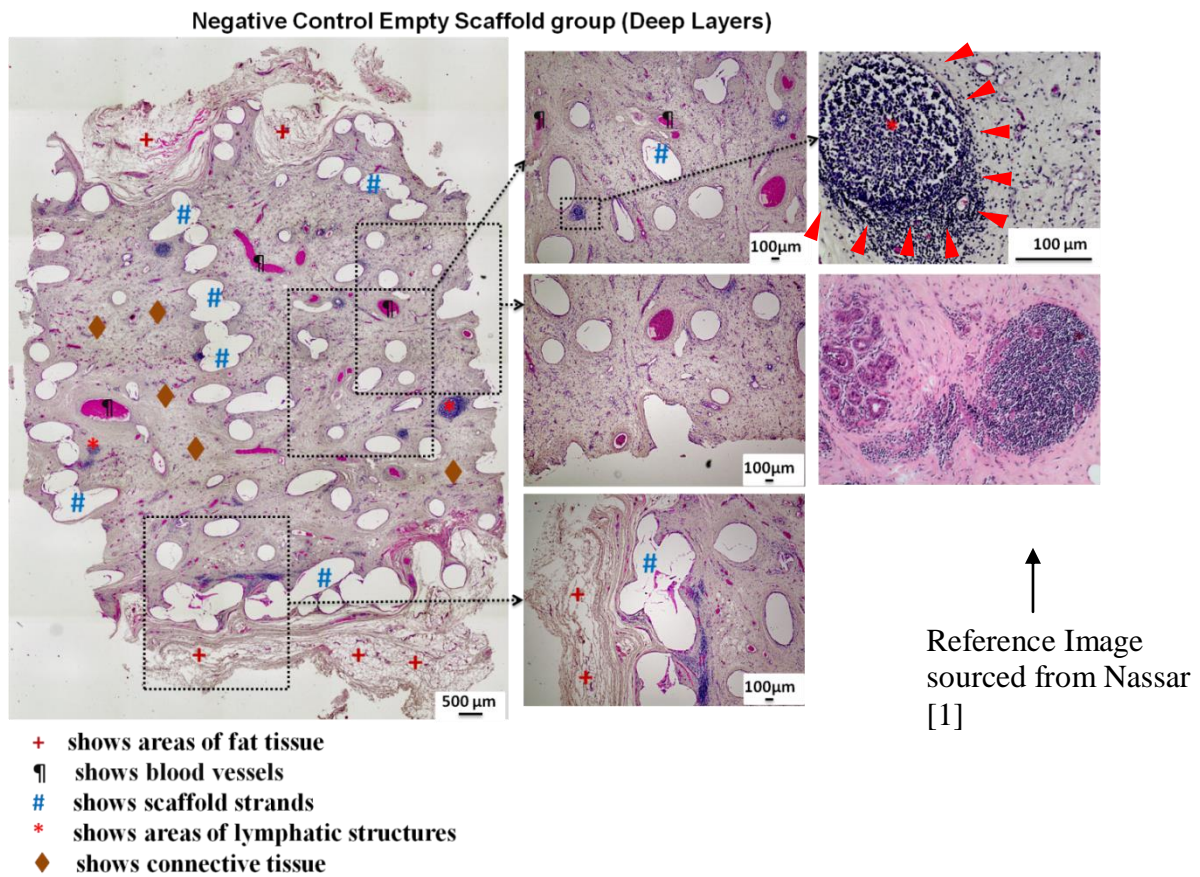
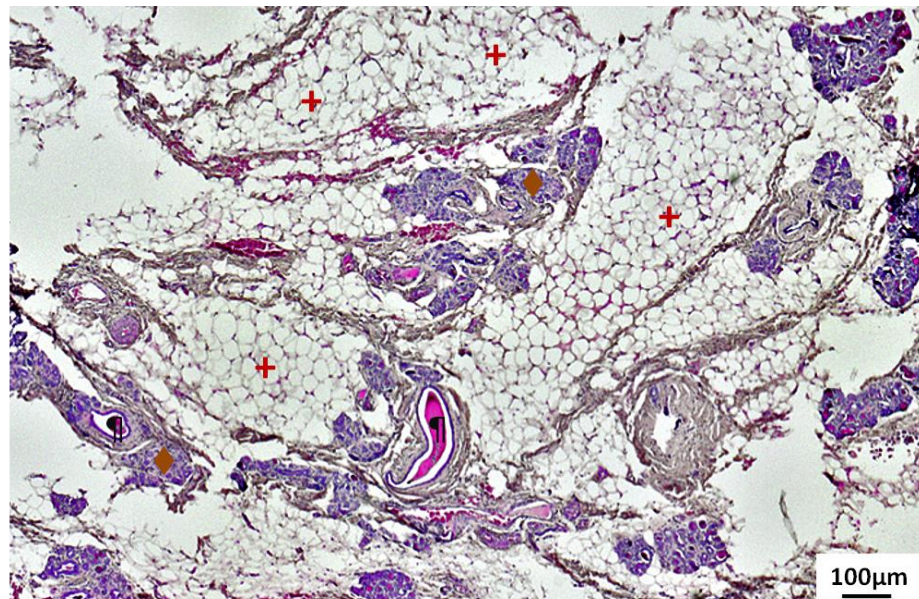


Figure 4.4.6 Representative images showing H&E staining of tissue explanted from the empty scaffold group (deep layers). Adipose tissue is only seen at the edges of the construct and not in the central regions of the scaffold. Lymphatic structures (right panel, marked by red arrows) were also observed in all groups mainly localised near scaffold strands. They were identified by comparing the micrograph to a reference image dataset obtained from Nassar [1] and using the surgical team's expertise. A representative image from the reference dataset has been shown

Figure 4.4.5-10 show representative H&E stained images of all scaffold groups after 24 weeks *in vivo*. All sections showed typical ring-like morphology of fat tissue. Overall, multiple areas of well vascularised adipose tissue were found in all groups. H&E staining of tissue explanted from the empty scaffold group showed that although the newly infiltrated tissue was highly vascular, a majority of the tissue was connective tissue and collagen with only very small patches of fat tissue (Fig 4.4.5, 6) (identified in the micrographs by their typical ring-like morphology and the empty vacuole in the middle of the cell – see Fig 4.4.7 for an H&E stained slide of native breast tissue). The deeper layers of the empty scaffolds also showed similar results.

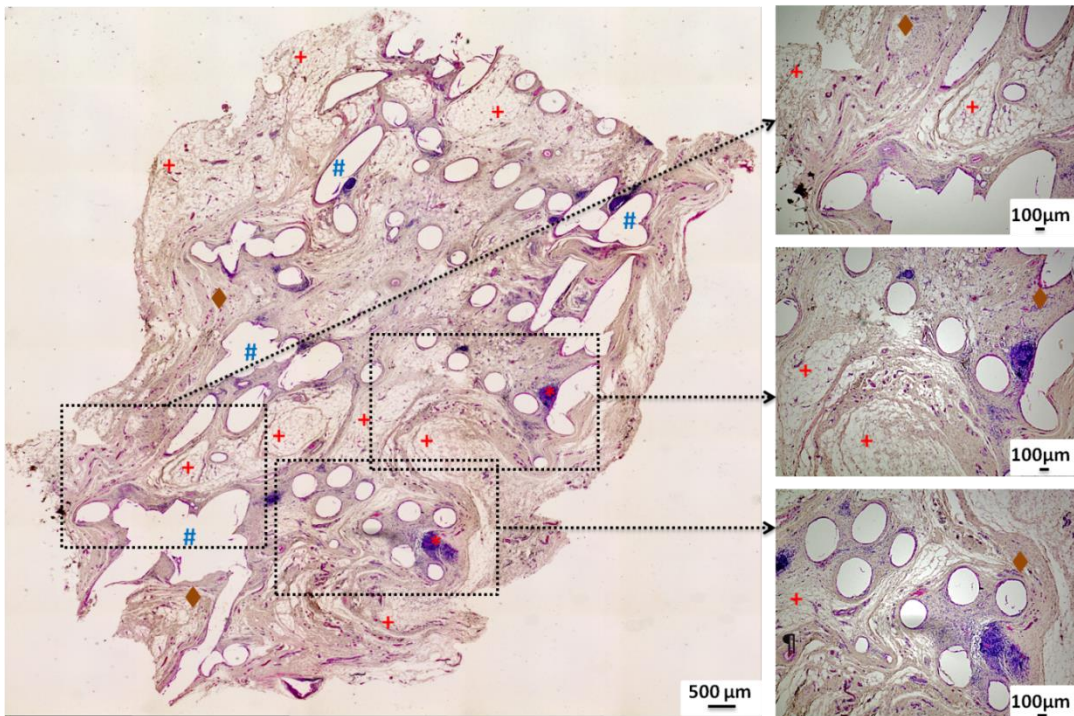
Positive Control Breast Tissue



- + shows areas of fat tissue**
- # shows blood vessels**
- # shows scaffold strands**
- * shows areas of lymphatic structures**
- ◆ shows connective tissue**

Figure 4.4.7 Representative images showing H&E staining of tissue explanted from native breast tissue. Morphology is characterised by adipose tissue regions interspersed between regions of connective tissue

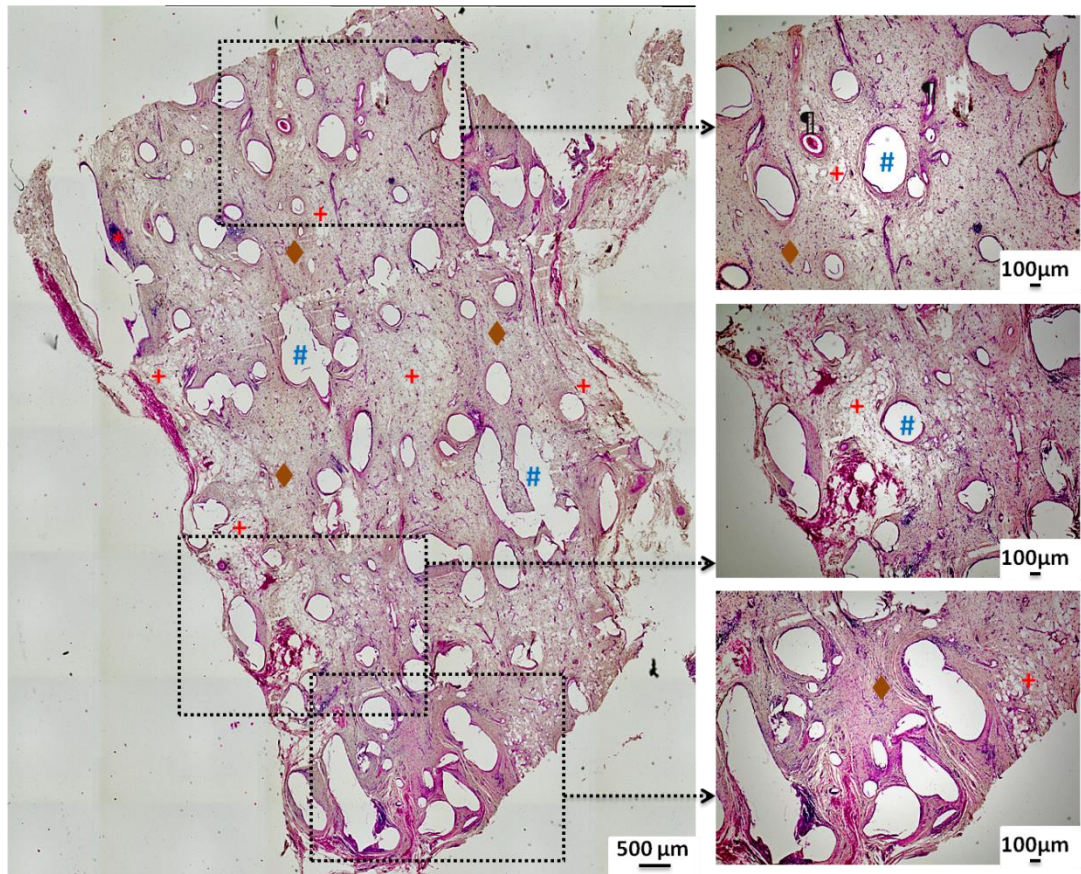
Lipoaspirate-only group – Superficial layers



- + shows areas of fat tissue**
- ¶ shows blood vessels**
- # shows scaffold strands**
- * shows areas of lymphatic structures**
- ◆ shows connective tissue**

Figure 4.4.8 H&E stained sections of lipoaspirate-only group (superficial layers). Overall, a higher percentage of fat tissue compared to overall tissue area, compared to empty scaffold group, was observed in this group.

Lipoaspirate-only group – Deep layers



- + shows areas of fat tissue**
- ¶ shows blood vessels**
- # shows scaffold strands**
- * shows areas of lymphatic structures**
- ◆ shows connective tissue**

Figure 4.4.9 H&E stained sections of lipoaspirate-only group (deep layers). Deeper layers of the scaffold showed lower relative adipose tissue areas and lower degrees of vascularisation.

Fig 4.4.8, 9 show the H&E stained sections of lipoaspirate-only group. Overall, a higher percentage of fat tissue compared to overall tissue area (referred from here on as relative tissue area) was observed in this group. The superficial layers of the scaffold especially showed widespread distribution of adipose tissue whose relative tissue area matched closely to that of native breast tissue. However, the deeper layers of the scaffold showed lower relative adipose tissue areas and lower degrees of vascularisation (Fig 4.4.9).

Prevascularisation + Lipoaspirate group – Superficial layers

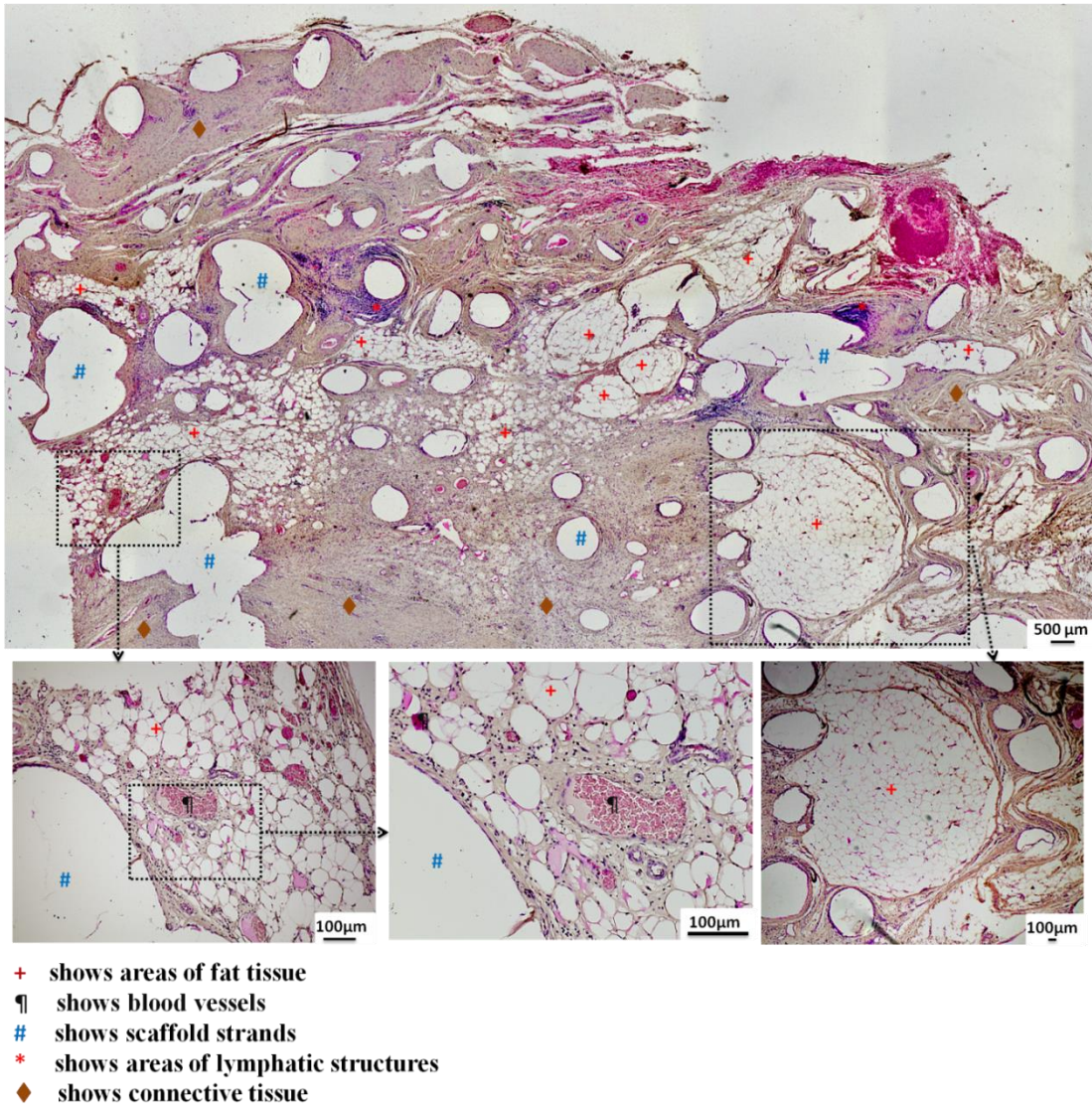


Figure 4.4.10 H&E stained sections of prevascularisation + lipoaspirate group (superficial layers). This group showed the highest accumulation of adipose tissue interspersed between connective tissue. Tissue morphology also showed similarities with native tissue.

Prevascularisation + Lipoaspirate group – Deep layers

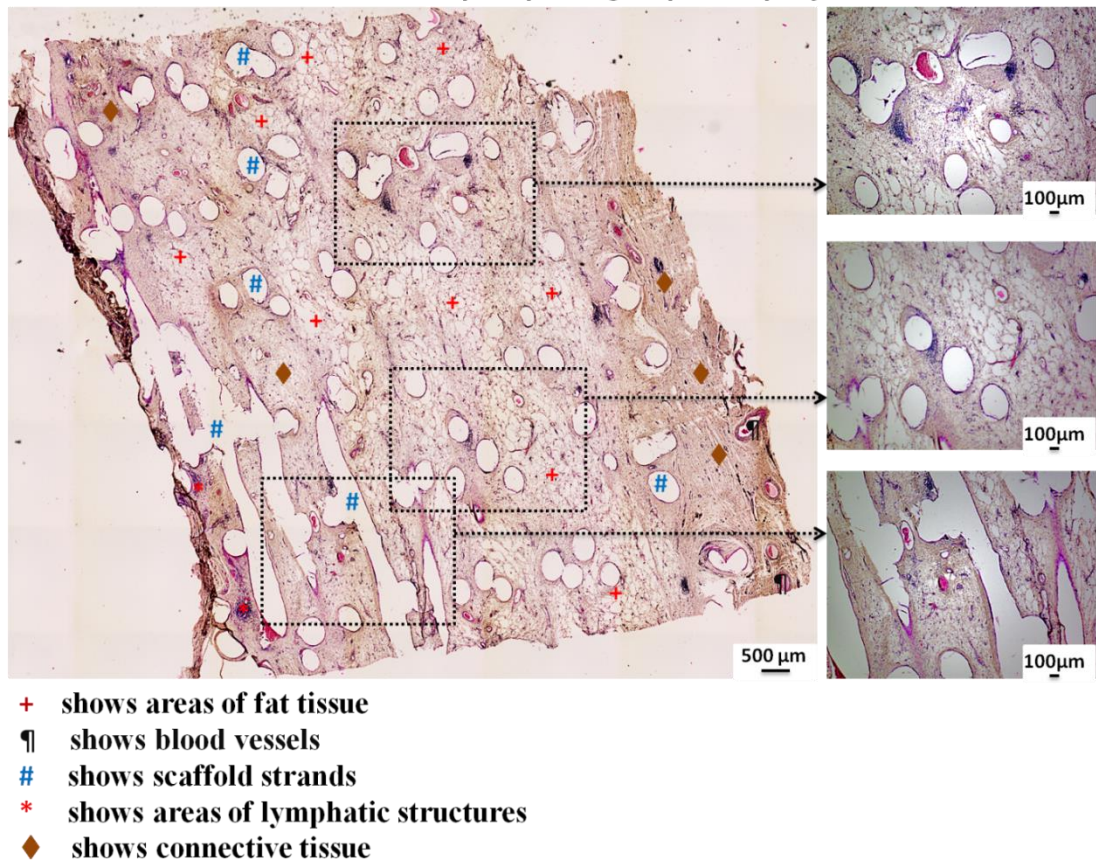


Figure 4.4.11 H&E stained sections of prevascularisation + lipoaspirate group (deep layers). Adipose tissue area was the highest among all other groups. Adipose tissue regions seemed to be better connected to each other and formed interconnected structures.

Fig 4.4.10, 11 show the H&E stained sections of prevascularisation + lipoaspirate group. This group showed the highest amount of fat tissue compared to all other groups. There were large highly vascularised regions of fat tissue interspersed between connective tissue. This tissue morphology was highly similar to that of native breast tissue. Furthermore, the relative adipose tissue area was also considerably higher in the deeper layers of this group compared to all other groups (Fig 4.4.10). Unlike the superficial layers however, the adipose tissue regions seemed to be better connected to each other and formed interconnected structures (Fig 4.4.11).

While no major signs of chronic inflammation were observed in the tissue sections or in the gross morphology of the constructs, non-specific localised low-grade

granulomatose reactions were observed in the vicinity of the localised scaffold strands (Fig 4.4.12). Lymphatic structures (Fig 4.4.6 right panel, marked by red arrows) and leucocytes were also observed in all groups localised mainly near scaffold strands. These structures were identified by comparing the micrograph to a reference image dataset obtained from Nassar [1].

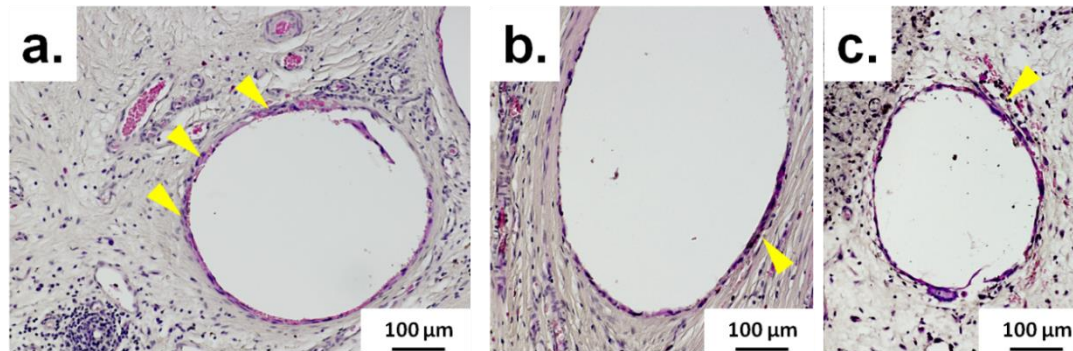


Figure 4.4.12 Representative H&E-stained micrographs of regions around the scaffold strands showing non-specific minor granulomatose reactions. (a) shows empty scaffold-only group, (b) shows lipoaspirate-only group (c) shows prevascularisation+lipoaspirate group. Yellow arrows point to macrophages

To identify the nature and composition of the connective tissue, Masson's trichrome staining was performed (Fig 4.4.13 a-c). Green colour indicates collagen fibres, red colour indicates muscle fibres and dark brown shows cell nuclei. As can be seen from the micrographs, besides the adipose tissue, a majority of the tissue filling the pores of the implant consisted of collagen fibres.

Thin layers of smooth muscle tissue were also observed, however it was only lining the boundaries of the scaffold strands. These smooth muscle layers had the highest thickness in case of the prevascularisation + lipoaspirate group (Fig 4.4.13 c).

In order to quantify adipose tissue regeneration, the total area of the adipose tissue relative to the total tissue area was counted on all slides. As expected, the negative control empty scaffold group had the lowest relative area of adipose tissue ($8.31\% \pm 8.94$) which was significantly lower than both lipoaspirate-only ($39.67\% \pm 2.04$) and

prevascularisation + lipoaspirate group ($47.32\% \pm 4.12$) and also compared to native breast tissue ($44.97\% \pm 14.12$) ($p < 0.05$, $p < 0.01$ and $p < 0.01$ respectively). However, there was no statistically significant difference in relative adipose tissue area between the native breast tissue, lipoaspirate-only and prevascularisation + lipoaspirate group.

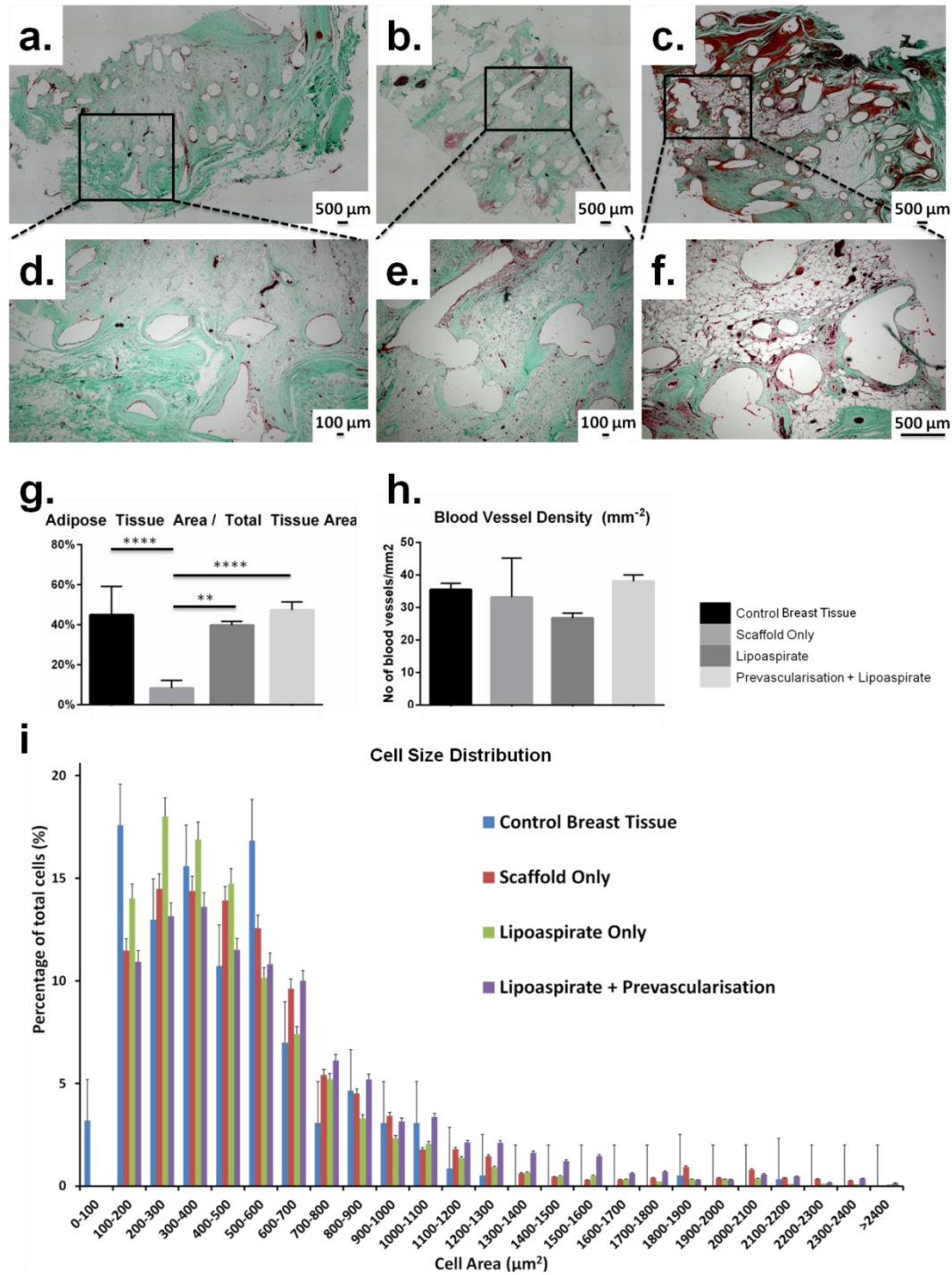


Figure 4.4.13 Representative images of Masson's Trichrome stained tissue sections. Green colour indicates collagen fibres, red colour indicates muscle fibres and dark brown shows cell nuclei (a, d)

show empty scaffold group (b, e) show prevascularisation + lipoaspirate group (c, f) shows lipoaspirate-only group. Besides the adipose tissue, a majority of the tissue filling the pores of the implant consisted of connective tissue. Smooth muscle tissue was also detected lining the strands of the scaffold. These smooth muscle layers had the highest thickness in case of the prevascularisation + lipoaspirate group. (g) Column plot showing showing the adipose tissue area relative to total tissue area over 24 weeks. Negative control scaffold-only group had the lowest relative area of adipose tissue ($8.31\% \pm 8.94$) which was significantly lower than both lipoaspirate-only ($39.67\% \pm 2.04$) and prevascularisation + lipoaspirate group ($47.32\% \pm 4.12$) and also compared to native breast tissue ($44.97\% \pm 14.12$) ($p < 0.05$, $p < 0.01$ and $p < 0.01$ respectively). No statistically significant difference in relative adipose tissue area was observed between the native breast tissue, lipoaspirate-only and prevascularisation + lipoaspirate group. (h) Graph showing blood vessel density in the tissue sections from different groups. Highest blood vessel density was observed in the prevascularisation + lipoaspirate group ($38.01/\text{mm}^2 \pm 2.02$), however the density was not statistically significantly higher than the scaffold-only ($33.13/\text{mm}^2 \pm 12.03$), lipoaspirate-only ($26.67/\text{mm}^2 \pm 1.6$) or control breast tissue ($35.45/\text{mm}^2 \pm 1.93$). (i) Histogram showing the distribution of adipose cells according to the cell surface area. In all groups, the histograms were skewed to the right suggesting that a majority of adipose cell surface areas lay in the range of $100\text{-}700 \mu\text{m}^2$. The distribution of the cell sizes in control breast tissue was considerably different compared to rest of the groups – with the highest percentage of cells in the $100\text{-}200$, $300\text{-}400$ and $500\text{-}600 \mu\text{m}^2$ range. The empty scaffold and lipoaspirate-only groups had a low number of adipose cells whose surface areas were larger than $800\mu\text{m}^2$; however, the prevascularisation + lipoaspirate group showed a more equalised distribution with a significantly large number of cells having a surface area larger than $1000\mu\text{m}^2$.

To quantify neovascularisation, blood vessels were counted on all slides. These blood vessels were identified by a ring/tubular structure, with only those lined with red blood cells included in the count as functional blood vessels. In general, all constructs, including the empty scaffold-only group, showed a substantial ingress of neovascularisation. The highest blood vessel density was observed in the prevascularisation + lipoaspirate group ($38.01/\text{mm}^2 \pm 2.02$), however the density was not statistically significantly higher than the scaffold-only ($33.13/\text{mm}^2 \pm 12.03$), lipoaspirate-only ($26.67/\text{mm}^2 \pm 1.6$) or control breast tissue ($35.45/\text{mm}^2 \pm 1.93$). H&E sections of constructs also showed blood vessel on and parallel to the surface of the constructs, suggesting that new capillaries are likely to have sprouted from these larger vessels that penetrated into the scaffolds.

Quantification of adipose cell area allowed the visualization of the distribution of different-sized cells as a histogram (Fig 4.4.13d). In all groups, the histograms were skewed to the right suggesting that a majority of adipose cell surface areas lay in the range of $100\text{-}700 \mu\text{m}^2$. The distribution of the cell sizes in control breast tissue was

considerably different compared to rest of the groups – with the highest percentage of cells in the 100-200, 300-400 and 500-600 μm^2 range. The empty scaffold and lipoaspirate-only groups had a low number of adipose cells having a surface area larger than 800 μm^2 ; whereas, the prevascularisation + lipoaspirate group showed a considerably higher number of cells having a surface area larger than 800 μm^2 .

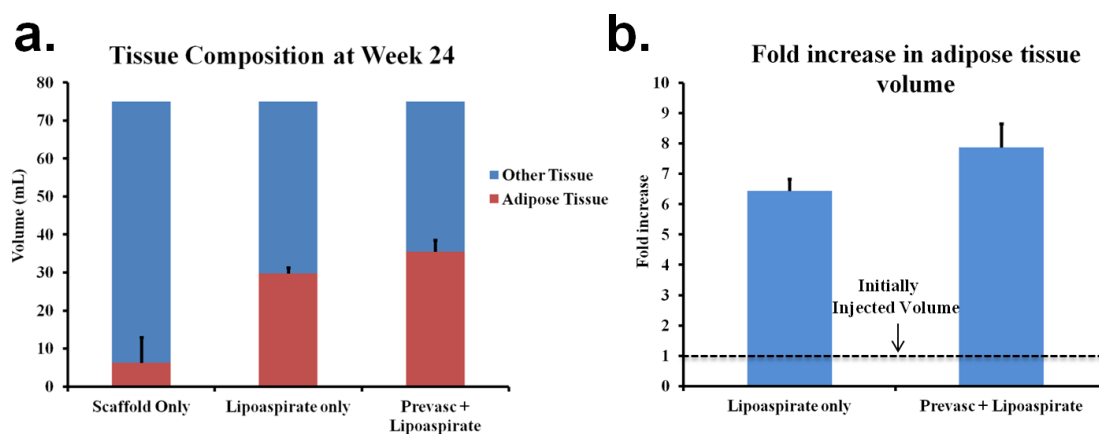


Figure 4.4.14 (a) Clustered column graph showing tissue composition at week 24 in various groups. Since the entire volume of the scaffold was filled with host tissue, it is reasonable to assume that each scaffold held 75 cm^3 of total tissue volume at the end of the implantation period. From the relative adipose tissue fraction values shown in Fig 4.4.13(g), the estimated volume fraction of adipose tissue in each was calculated. TECs from empty scaffold group contained an average of 6.23 cm^3 (\pm 2.71) of adipose tissue, TECs from lipoaspirate-only group contained an average of 29.75 cm^3 (\pm 1.53) of adipose tissue, whereas TECs from prevascularisation+lipoaspirate group contained an average of 35.49 cm^3 (\pm 3.1) of adipose tissue. (b) Column graph showing fold increase in adipose tissue volume compared to initial injected lipoaspirate volume (4 cm^3) in the lipoaspirate-only and Prevascularisation+Lipoaspirate groups. Prevascularisation+Lipoaspirate group had a higher fold increase in adipose tissue volume compared to lipoaspirate-only group; however, the difference was not statistically significant ($p=0.143$). Data for empty scaffold group has not been included because lipoaspirate was not injected into these scaffolds.

From data showing the percentage of adipose tissue area relative to total tissue area, the fold increase in adipose tissue volume was calculated (see Fig 4.4.14). Prevascularisation+Lipoaspirate group had a higher fold increase in adipose tissue volume compared to lipoaspirate-only group (6.44 \pm 0.38 vs 7.87 \pm 0.77); however, the difference was not statistically significant ($p=0.143$).

4.4.4 Discussion

The ability to generate *de novo* adipose tissue for postmastectomy breast reconstruction is widely thought to revolutionise the field of breast reconstructive surgery [27, 77, 341, 353, 359]. Previous long-term rodent studies in our laboratory have shown sustained regeneration of high volumes of fat using cell-seeded anatomically shaped scaffolds [358]. These cell-based approaches are very promising for the regeneration of complex, living tissue; however, they also lead to several disadvantages with problems ranging from scaling up of tissue culture to requiring complex GMP-approved laboratories for tissue culturing. To circumvent these problems while scaling up the volumes of adipose tissue being regenerated, here we have followed the philosophy of implanting only a breast-shaped scaffold and using the patient's body as a bioreactor. However, in the absence of a strong adipogenic stimulus, the scaffold gets filled with mostly non specific fibrovascular tissue [360, 361].

Here we have shown regeneration of *de novo* autologous adipose tissue by injecting a small volume of lipoaspirated tissue with no additional growth factors, cell transplantation or ligated vascular pedicles by introducing a completely novel prevascularisation technique that uses the patient's own body as a bioreactor and a source of blood vessels. To our knowledge, no studies exist that provide a reliable reference on the maximum amount of volume that can be extracted from patients with low body fat percentage. This aspect is routinely determined in the clinic using the plastic surgeon's experience and expertise. Based on our surgical team's expertise, it was determined that 4 cm³ of adipose tissue is close to the maximum amount of fat that can be safely harvested from patients with low body fat. In terms

of percentage, it represents 5.3% of total volume of the scaffold at the time of implantation.

The delayed lipo-injection technique allowed the formation of a bed of vascular and connective tissue within the scaffold volume. The presence of such vascular and connective tissue has previously been found to support early adipogenesis, provided sufficient mesenchymal stem cells or adipose progenitor cells have been recruited to the implantation site [361, 362]. Consequently, the adipose tissue, when injected into the already prevascularised scaffold, remained stably within the implantation sites with no tissue necrosis and resorption. Over a period of 24 weeks, this resulted into a fold increase of 6.44 (± 0.38) in case of lipoaspirate-only and 7.87 (± 0.77) in case of prevascularisation + lipoaspirate group. However, the final tissue composition requirements also depend upon the surgical procedure. If the surgery is done mainly for aesthetic breast augmentation, one of the main goals is to maintain the natural tactile sensation of the breast. For this reason, the regenerated tissue needs to consist mainly of adipose tissue with smaller amounts of organised connective tissue in order to mimic the natural tissue morphology of the breast region. In case of post-mastectomy breast reconstruction, one of the major goals is to prevent a cancer relapse. In this case, adipose progenitor cells infiltrating into the scaffold may favour breast cancer recurrence via HGF/c-Met signalling [363]. Therefore, a majority of the regenerated tissue needs to be composed of highly organised connective tissue. The results of this study have demonstrated that the morphology of the regenerated tissue can be predicted depending on initial scaffold treatment strategy (empty scaffold vs prevascularisation + lipoaspirate) – whereby empty scaffolds yield highly organised connective tissue whereas scaffolds containing lipoaspirate yield tissue

rich in adipose tissue. In this way, scaffolds can truly be tailored for either an aesthetic augmentation procedure or a total reconstruction procedure.

We believe that the stiffness of the constructs played a significant role in the neoadipogenesis process. Contrary to musculoskeletal systems, where tissue such as bone and muscle grow in response to mechanical forces [364, 365], adipogenesis seems to be inhibited by mechanical forces [366]. The scaffolds used in this study had a stiffness value that was 3 orders of magnitude higher than native breast tissue. We surmise that such mechanically robust scaffolds would exert a shielding effect on the newly formed adipose tissue and reduced the effects of the compressive, tensile and shear forces acting on the fat tissue. This decreased mechanical stimuli would have allowed the cells to maintain a round morphology which, in turn, would have promoted adipogenesis of the adipose progenitor cells [367].

From a clinical point of view, the stiffness of the scaffolds must also be made dependent upon their placement. In case of most cosmetic augmentations whereby the implants are placed in a subglandular pocket, the scaffold needs to remain elastomeric and flexible so as to not cause patient discomfort; whereas in case of most post-mastectomy breast reconstruction procedures whereby the implants are placed in a submuscular pocket and no other supporting tissue remains, stiff implants must be used in order to properly support the regeneration of the entire breast region [368]. Indeed, the role that mechanical forces play in the regeneration of high volumes of fat tissue warrants further research and it would be interesting to test scaffolds with various stiffness properties and compare their regenerative capacities.

Non-specific localised low-grade granulomatose reactions were observed in the vicinity of the localised scaffold strands, consistent with previous reports [358]. A granuloma is an organised collection of macrophages [369]. While the roles of

macrophages in angiogenesis are not yet completely understood, various research groups have shown that macrophages have the potential to contribute in angiogenesis [370-372]. More specifically, M1 macrophages secrete VEGF which initiates the process of angiogenesis, M2a macrophages secrete Platelet-Derived Growth Factor (PDGF)-BB known to be involved in later stages of angiogenesis, while M2c macrophages secrete high levels of Matrix Metallo-Proteinase (MMP)-9 known to have a role in remodelling of vasculature [373]. It has also been reported in the literature that macrophages can secrete alpha smooth muscle actin and can transdifferentiate into smooth muscle cells [374, 375]. All groups showed accumulation of smooth muscle tissue around the scaffold strands (Fig 4.4.13 a-c) which can perhaps be taken as an indirect evidence of the fact that macrophages may have played a role in angiogenesis and consequently higher adipogenesis in this group. Since the constructs were placed in PFA for an extended period of time post explantation, the proteins within the samples were denatured and immunohistology therefore could not be undertaken to provide direct evidence of this effect.

While no major outward signs of chronic inflammation were observed clinically or in the gross morphology of the constructs, lymphatic structures and leucocytes were detected in the histology of all groups – which is to be expected because the study used an immunocompetent animal model. Although polycaprolactone has met FDA approval and been proven in multiple independent studies to be cytocompatible [98, 253, 323, 376, 377], the increased leucocyte count may be explained by the fact that during the lipoaspiration process, adipose cells may have formed non-viable aggregates in the syringe which, when injected into the scaffold, triggered an auto-immune reaction from the host aiming to break them down, ultimately leading to the ingression of lymphatic vessels.

Limitations of this study include the scaffold design. As described previously, owing to hardware and software limitations, the scaffold formation was a 3-step process – the first step being fabrication of the solid supporting dome, second step being the fabrication of the scaffold main body and the final step being manual trimming of the outer boundary shells to obtain a porous structure. In the real world, such a clinical solution is clearly impractical as the scaffold morphology is ultimately fixed by the surgeon and therefore is not reproducible. To overcome this limitation, software packages described in Study 2 were developed to fabricate completely patient-specific scaffolds based on an Additive Biomanufacturing principle which can be fabricated using a support material of either a water-soluble polymer or a breakaway structure fabricated with the same material as the main structure. It is important to reiterate here that chronologically, this study, being a proof-of-principle study, was undertaken prior to the development of these software packages.

Finally, the scaffold used in this study did not imbibe adequate design principles that would allow a surgeon to efficiently and accurately deposit the fat at predetermined regions in the scaffold. Indeed, this novel approach would be rendered impractical if the host connective tissue occupies a majority of the volume of the scaffold such that no further volume remains for the secondary injection of fat tissue. In this study, adipose tissue was injected directly into the vascular bed which may have caused localised tissue disruption. While such a tissue disruption may prove to enhance vascularisation [378], this phenomenon cannot be controlled within a clinical setting. Therefore, the scaffolds were completely redesigned using the software packages described in Study 2. The next generation scaffolds contain specialised channels which can act as recipients for the lipoaspirated tissue and are described in more detail in Appendix 1.

4.4.5 Conclusion

This study, based on a foundation of previous small animal studies and clinical observations [336, 358], was used to provide proof of principle that the prevascularisation and delayed fat injection techniques can be used for efficient regeneration of large volumes of adipose tissue for long periods of time. It provides an important validation point for the regeneration of clinically relevant volumes of vascular-rich tissues in post-mastectomy breast reconstruction surgeries - paving the way for future clinical trials of scaffolds employing this principle.

Chapter 5: Discussion, Conclusions and Future Directions

Breast cancer is the second leading form of cancer in women in Australia [351], affecting one in every eight women in western countries and one in every three women with cancer. Owing to the large number of clinical occurrences, breast reconstruction following lumpectomy (partial removal of breast tissue) or radical mastectomy (total removal of the breast) has become the sixth most common reconstructive procedure performed worldwide [315]. Lumpectomy defects of less than 25% of the total breast volume can typically be corrected by rearranging the local breast tissue [77]. Larger lumpectomies and mastectomies require more drastic reconstruction modalities. Reconstruction using silicone-based implants leads to formation of a rigid fibrous tissue surrounding the implant giving it an unnatural appearance. In such cases, the implant needs to be replaced. Lipofilling is another popular reconstruction method whereby the surgeon isolates fat from another region of the patient's body via liposuction and injects it back into the breast region. However, without a structural support, the newly injected fat quickly gets remodelled by the body – requiring 3-4 additional lipofilling sessions before the tissue stabilises and the final form and volume are achieved [71]. Currently there exists no surgical platform that overcomes these problems and supports stable development of breast tissue.

Therefore, this PhD project focused on the testing of surface-modified silicone implants to assess whether they reduce the severity of capsular contracture. Subsequently, the project was focused on the fabrication of a patient-specific biodegradable scaffold using additive manufacturing technology. We hypothesized

that a slow-degrading polymer with pore sizes >1.5 mm allows for efficient vascular in-growth and long-term sustained regeneration of high volume adipose tissue, thereby potentially providing an effective treatment for bone defects circumventing the shortcomings of current breast reconstruction techniques.

5.1 Summary of Study 1

Chapter Title: Evaluation of modified breast implant surfaces in a Minipig-Model

This study aimed to establish a reproducible large animal subglandular model recapitulating the environment of a breast surgery in a healthy female patient and also, at the same time, evaluate the impact of three different surface structures on the development of fibrosis and subsequent capsular contracture. As mentioned previously, it was hypothesised that the data obtained in terms of surface roughness and its impact on tissue adhesion and fibrosis would provide unique insights which would influence the design of porous biodegradable scaffolds from a completely different point of view.

The implants were manufactured and kindly provided by Mentor LLC with 3 different surfaces: one surface with 100 pores per inch, having an average surface pore diameter of 57.71 μm (Small pores – SP); one surface with 65 pores per inch, having an average surface pore diameter of 95.52 μm (Large pores – LP) and one with a smooth surface (S). Six female adult Ellegaard Göttingen Minipigs were randomly allocated to two groups: a 10-weeks and a 20-weeks group. N=6 implants were placed in separate subglandular pockets in each animal.

It was observed that the minipigs developed Baker Grade 3 and 4 capsular contractures after 10 weeks of implantation. At the end of the 20 week implantation period, it was observed that capsules derived from LP implants had the highest stiffness, followed by SP while S implants showed the lowest stiffness.

Corresponding with capsule stiffness, LP implants also had a significantly higher stiffness compared to both SP and S implants ($p < 0.01$). In terms of tissue makeup, S group showed the least amount of collagen at 10-week time point while SP group were found to have the highest concentration. At 20-week time point, the collagen expression in S and LP group increased while it decreased in case of SP implants. Immunohistological staining performed on the tissue sections showed that at 10-week time point, S group had the highest concentration of alpha smooth muscle actin (SMA) while SP had the lowest; whereas at 20-week time point LP implants had the highest expression of alpha SMA and SP still showing the lowest expression. At 10-week time point, SP group showed the highest expression of Integrin B1 while S implant had the least expression. None of the groups showed any major expression of osteopontin at any of the time points.

On one hand, the established subglandular *in vivo* model now makes it possible to test silicone implants as well as scaffolds in an environment that is very close to the human equivalent. This will allow researchers to iteratively improve the surface microstructures designs and hopefully lead to novel approaches that can limit the incidences of capsular contracture. On the other hand, the effect of different surface topologies, at least within the experimental time period, did not improve the outcome of capsular contracture significantly when compared to smooth implants.

It was concluded that a porous biodegradable implant based on tissue engineering principles would provide an effective solution to many of the challenges posed by current generation of silicone implants. Therefore, further work undertaken as part of this PhD thesis focused on developing novel methodologies to design and fabricate such highly customised scaffolds for breast reconstruction following a tissue engineering and personalized medicine approach.

5.2 Summary of Study 2

Chapter Title: Development of a methodology to fabricate highly customised patient-specific biodegradable scaffolds

The first part of Study 2 focused on establishing a streamlined methodology to convert medical imaging data sets into high-fidelity 3D CAD models appropriate for additive manufacturing. To this end, a versatile approach was developed to generate patient-specific scaffolds not only for breast reconstruction, but also for virtually any defect site in the body. This approach allows for a high level of automation and requires minimal manual handling. For this, we made use of freely available open-source software to convert high resolution MRI or CT scan data into 3D CAD models using the thresholding technique. The specific advantage of the thresholding technique is that it allows for relatively easy differentiation of tissue/area of interest from its surrounding region. Using this method, porous models mimicking the overall shape of a scanned tissue region were generated.

Second part of Study 2 focused on converting a 3D CAD model into scaffold architectures suitable for tissue engineering purposes. Although in the past few years, proprietary software have been developed for FDM machines for fabricating solid, watertight 3D structures [312-314], such software are closed source, do not support the fabrication of porous models and are unavailable for use with custom-made bioprinters. Moreover, such software packages have not yet attained the level of sophistication and control over extrusion parameters required in the biofabrication industry. Using our method for fabricating scaffolds is not only versatile across almost all FDM or CNC machines, but the cross-platform nature of all the software packages used also makes this process suitable for use with experimental additive manufacturing devices yet to be developed. An independent method has already been

developed by our research group to laser scan a breast surface, generate a 3D model and fabricate a porous prototype using non-biodegradable materials [91]. The method developed during the course of this PhD project complements this method in that it allows the fabrication of porous, biodegradable scaffolds using more ubiquitous MRI and CT scans. Combined together, these methods encompass an almost comprehensive range of avenues for generating porous patient-specific scaffolds from medical imaging data sets.

5.3 Summary of Study 3

Chapter Title: Sustained Regeneration of High-volume Adipose Tissue for Breast Reconstruction using Computer Aided Design and Biomanufacturing

Adipose tissue engineering offers a promising alternative to the current breast reconstruction options. Our hypothesis was that a scaffold would maintain its shape and volume for at least 9-12 months post implantation without showing any signs of mass loss so that the regenerated tissue stably remodels several times in the highly scaffold architecture without being influenced by any degradation by-products.

In this work, patient-specific scaffolds with large pore sizes and pore interconnections were fabricated with a biodegradable poly(D,L)-lactide polymer. Human umbilical cord perivascular cells were isolated from human umbilical cord and seeded onto the breast-shaped scaffolds. The tissue engineered constructs (TEC) were cultured under static conditions for 4 weeks and subsequently 2 weeks under dynamic conditions in a biaxial rotating bioreactor before being combined with Human Umbilical Vein Endothelial Cells (HUVEC) and implanted subcutaneously into athymic nude rats for 6 months.

Angiogenesis and adipose tissue formation were observed throughout all constructs at all timepoints. The percentage of adipose tissue compared to overall tissue area

increased from 37.17% to 62.30% between week 5 and week 15 ($p < 0.01$), and increased to 81.2% at week 24 ($p < 0.01$). The stiffness of the constructs decreased by 66% over 24 weeks, while the seeded endothelial cells self organised to form a functional capillary network.

Adipose tissue has been reported to be highly vascular [174]. In fact, Patrick [77] reports that each adipocyte is connected to at least one capillary – with the volume of capillary beds in adipose tissue being higher than even muscular tissue. Furthermore, adipose cells die within 3 hours when deprived of oxygen [77]. This occurs because the diffusion of oxygen from the surrounding tissues is sufficient only over a distance up to $\sim 150 \mu\text{m}$ for adipose tissue [175]. Therefore, in tissue constructs without adequate vascularization, autologous adipose tissue loses up to 60% of its volume post-transplantation because the cells in the centre of the graft are inadequately supplied with oxygen [176, 177]. Hence, it becomes important to ensure that the tissue engineered constructs have access to an adequate vascular network. Since the diameters of a large number of rat blood vessels infiltrating into a tissue-engineered construct lie in the 500-1500 μm range [379], we hypothesized that a slow-degrading polymer with pore sizes in the range 1000-2000 μm mm allows for efficient vascular in-growth. However, as pore sizes increase, the overall shape fidelity of the 3D printed scaffold decreases and so do the scaffold stability and mechanical properties (see Fig 5.1). The scaffolds fabricated in this study provided the best compromise between pore sizes, shape fidelity and mechanical properties and were therefore chosen as the final design candidates.

The long term strategy of our research group with respect to the above mentioned vascularisation problem is to allow the infiltration of the host vasculature into the scaffold. We have already published a study where we fabricated polycaprolactone

and polyurethane-based scaffolds with an average pore-size of 450-560 microns [336], seeded them with adipose-derived MSCs and implanted them into nude rats. Our results showed <10% of adipose tissue survived a 4-week implantation period. Retrospectively, we surmised that one of the main causes leading to the tissue remodelling was a lack of widespread infiltration of blood vessels from the host into the scaffolds.

The presented approach of fabricating patient-specific scaffolds using 3D scans represents a facile approach towards engineering clinically relevant volumes of adipose tissue for breast reconstruction. We have demonstrated a clinically viable route to design and fabricate biodegradable patient-specific scaffolds directly from 3D imaging data sets. To our knowledge this is the first study showing a sustained regeneration of high volume adipose tissue over a long period of time using a patient-specific biodegradable scaffold. These scaffolds, which are optimised for large volume adipose tissue regeneration, contain large pores and pore interconnections, facilitate the ingrowth of host vasculature throughout the entire scaffold architecture which is crucial for long-term sustenance and viability of adipose tissue.

5.4 Summary of Study 4

Chapter Title: Breast Reconstruction using Computer Aided Design and Biomanufacturing – towards engineering clinically relevant volumes of adipose tissue.

Progenitor cell-based approaches are very promising for complete regeneration of breast tissue; however, they also lead to several disadvantages – ranging from problems with scaling up of tissue culture to requiring complex GMP-certified laboratories for tissue culturing [250-256].

To overcome these limitations, we have devised a concept of delayed fat injection combined with an empty biodegradable scaffold. According to this concept, an empty scaffold is first placed at the implantation site and allowed to remain for 2 weeks during which time connective tissue and host vasculature is expected to penetrate into the scaffold pores. After the prevascularisation time, a pre-determined volume of autologous lipoaspirated adipose tissue is injected into the pores of the scaffold. The presence of a pre-formed bed of connective tissue and vasculature would allow the injected fat to remain stable within the implantation site with minimal tissue necrosis and resorption.

To test this hypothesis, 3 study groups were included in this study:

- 1) Empty scaffold.
- 2) Scaffold containing 4 cm³ lipoaspirated adipose tissue.
- 3) Empty scaffold + 2 week prevascularisation period. After 2 weeks of prevascularisation, 4 cm³ of lipoaspirated adipose tissue was injected into scaffolds.

6 implants were placed in each animal (n = 2 per group) and the animals were sacrificed after 24 weeks. Histological evaluation showed that multiple areas of well vascularised adipose tissue were found in all groups. The negative control empty scaffold group had the lowest relative area of adipose tissue (8.31% ± 8.94) which was significantly lower than both lipoaspirate-only (39.67% ± 2.04) and prevascularisation + lipoaspirate group (47.32% ± 4.12) and also compared to native breast tissue (44.97% ± 14.12) (p<0.05, p<0.01 and p<0.01 respectively). However, there was no statistically significant difference in relative adipose tissue area between the native breast tissue, lipoaspirate-only and prevascularisation + lipoaspirate group. The highest blood vessel density was observed in the prevascularisation +

lipoaspirate group ($38.01/\text{mm}^2 \pm 2.02$), however the density was not statistically significantly higher than the scaffold-only ($33.13/\text{mm}^2 \pm 12.03$), lipoaspirate-only ($26.67/\text{mm}^2 \pm 1.6$) or control breast tissue ($35.45/\text{mm}^2 \pm 1.93$).

While no major signs of chronic inflammation were observed in the tissue sections or in the gross morphology of the constructs, non-specific localised low-grade granulomatose reactions were observed in the vicinity of the localised scaffold strands. Lymphatic structures and leucocytes were also observed in all groups localised mainly near scaffold strands.

In this study, we have shown regeneration of *de novo* autologous adipose tissue by injecting a small volume of lipoaspirated tissue with no additional growth factors, cell transplantation or ligated vascular pedicles by introducing a completely novel prevascularisation technique that uses the patient's own body as a bioreactor and a source of blood vessels.

5.5 Limitations and recommendations for future work

In this project, a foundation, in terms of methodologies, animal models and scaffold designs, has been laid which may accelerate the research into the field of breast tissue engineering. However, there remain many avenues open for further development and more work needs to be done to get a clearer understanding of how to optimise the breast scaffolds to promote vascularisation. The limitations of this PhD project along with the recommended future work are discussed hereafter:

5.5.1 Biopolymer characteristics and degradation models were simplified for the FE analysis

Establishing a comprehensive model of biomaterial behaviour, degradation and physical properties *in vivo* is a lengthy and complex exercise, perhaps requiring a

research project of its own. Therefore in this project, it was assumed that the biomaterials have a perfectly linear elasticity and that they follow Hooke's law (the linear elastic isotropic model). Other parameters such as polymer viscosity, degradation kinetics, change in Young's modulus and the effect of tissue infiltration on the mechanical properties were also excluded. The development of this software will continue beyond the duration of this PhD project and future versions will incorporate more complex models of material behaviour and form a basis for future parameteric studies to be investigated.

5.5.2 Scaffold mechanical properties

During the process of designing a scaffold for tissue engineering, a balance must be achieved between the porosity and the mechanical integrity – see Fig 5.1 for an illustration of the relationship between porosity, pore sizes, cellular response and mechanical strength.

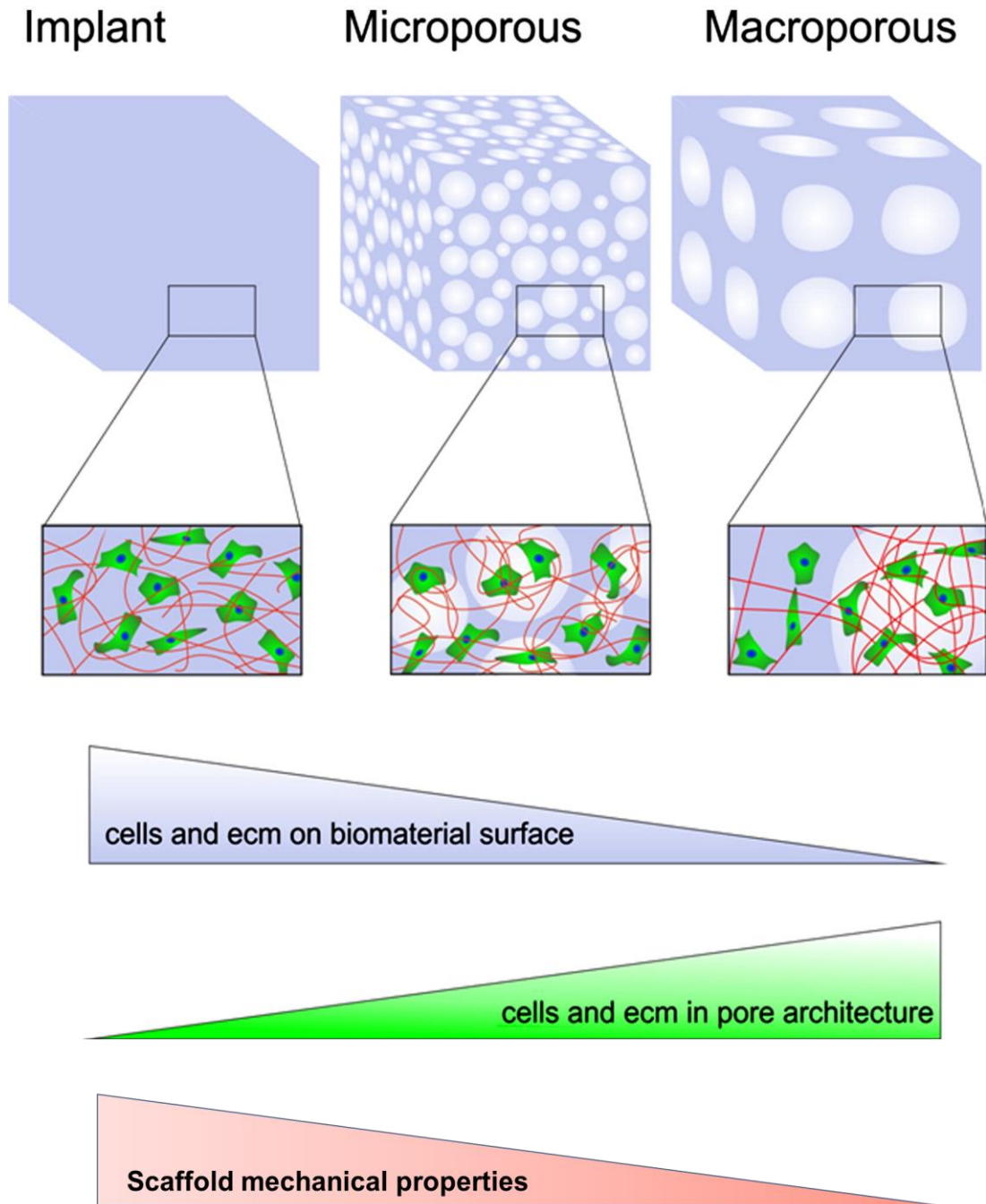


Figure 5.1 Illustration of the relationship between porosity, pore sizes, cellular response and mechanical strength. Adapted from Holzapfel et al [311]. The mechanical properties of the scaffolds can be controlled in 2 ways: by controlling the overall porosity of the scaffold and by controlling its internal architecture. Increasing the overall porosity reduces the mechanical properties, but it also increases the density of cells and ECM in pore architecture since there is less surface area available on the scaffold strands. On the other hand, a macroporous scaffold can also be made mechanically stronger/stiffer by altering its pore architecture – which fundamentally alters the stress distribution within the scaffold.

Stiffness and strength properties of the scaffold should also be optimised to allow it to resist changes in shape *in vivo* when the breast region is subjected to high biomechanical loads during sleeping and sports activities.

On the other hand, patient comfort, quality of life and tissue irritation are also three of the major concerns which are insufficiently addressed. Also, from a clinical point of view, the stiffness of the scaffolds must be tailored dependent upon their placement. In case of most cosmetic augmentations whereby the implants are placed in a subglandular pocket, the scaffold needs to remain elastomeric and flexible so as to not cause patient discomfort; whereas in case of most post-mastectomy breast reconstruction procedures whereby the implants are placed in a submuscular pocket and no other supporting tissue remains, stiff implants must be used in order to properly support the regeneration of the entire breast region [368] (see Fig 5.2).

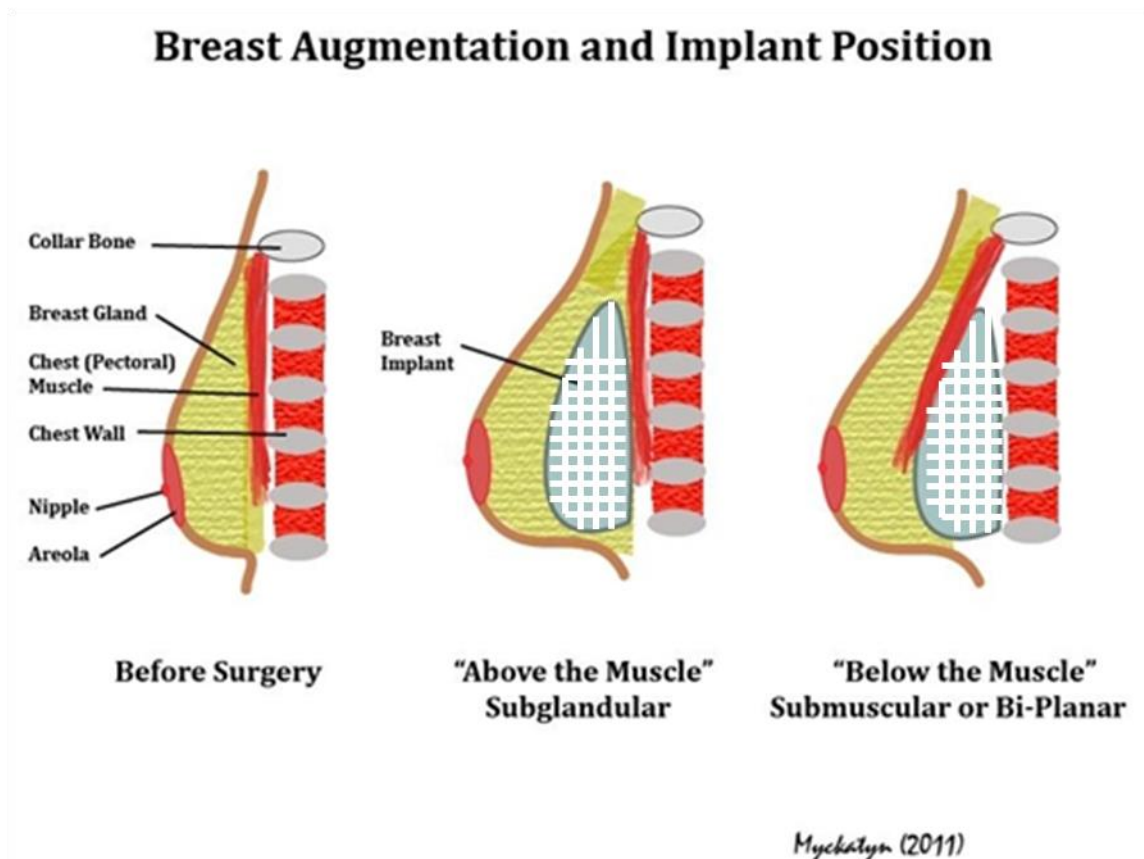


Figure 5.2 Graphic showing subglandular vs submuscular placement of implants. Figure adapted from Myckatyn [380]

PROPERTY	AESTHETIC BREAST	TOTAL BREAST
	AUGMENTATION	RECONSTRUCTION
Scaffold Placement	Scaffold normally placed above the pectoral muscles but below the mammary gland (subglandular placement). Such a placement gives the most aesthetically appealing outcome.	Scaffold normally placed below the pectoralis major muscle such that the muscle covers the upper half of the implant (submuscular placement). Such a placement shields the implant from the irradiated breast tissue and prevents it from causing capsular contracture.
Tissue constitution	One of the main goals is to maintain the natural tactile sensation of the breast. For this reason, the regenerated tissue needs to consist mainly of adipose tissue with smaller amounts of organised connective tissue.	All total breast reconstructions are undertaken after mastectomy or tumour abscission. One of the major goals is to prevent a cancer relapse. In this case, adipose progenitor cells infiltrating into the scaffold may favour breast cancer recurrence via HGF/c-Met signalling [363]. Therefore, a majority of the regenerated tissue needs to be composed of highly organised connective tissue.
Scaffold mechanical properties	Scaffold needs to be soft, elastomeric and flexible to minimise patient discomfort since there is no muscle layer shielding the scaffold from the inner layers of skin.	Following mastectomy, almost all of the breast tissue is abscised. Therefore, the scaffold needs to be mechanically stable enough to bear the biomechanical forces of the entire region. Also, the scaffold is normally placed behind the muscle, which acts as a barrier - reducing patient discomfort.
Scaffold	In case of young patients	In case of patients undergoing

Degradation	undergoing augmentation, reconstructive breast surgery post
Rate	the tissue is healthy and tumour resection, the tissue is heavily hasn't undergone radiation damaged due to radiation therapy. therapy. Therefore, the Hence the regenerative capacity of the body has a higher rate of body is compromised and the scaffold regeneration and the needs to stay intact for longer periods of scaffold needs to degrade time. Additional research is needed to faster determine optimum degradation rate.

In order to further progress such composite scaffolds into real world applications, one would need to find a balance between suitable scaffold mechanical properties, bioactivity, and porosity. One way to improve the scaffold mechanical strength while not compromising the scaffold bioactivity and porosity is to explore the different scaffold architectures by varying the scaffold lay-down pattern. Research performed previously in our lab has proven that a change in the scaffold laydown pattern can significantly alter the mechanical properties of the scaffold owing to a difference in the stress distribution[381]. Alternatively, one can produce a composite scaffold formed out a slow degrading highly porous polymer backbone acting as a skeleton for a soft degradable hydrogel-based material. Indeed, it is planned that future extensions of this PhD project would focus on addressing the problem of scaffold mechanical properties using the tools and methodologies developed in this project.

5.5.3 Scaffold *in vivo* degradation behaviour

In this PhD project, we validated the degradation rate of various scaffolds by using their mechanical properties as a benchmark. The changes in the molecular structure of the polymer chains also need to be investigated – especially in cases of novel biopolymers. Furthermore, when implanted *in vivo*, the scaffolds not only undergo

hydrolytic degradation, but also enzymatic degradation facilitated by macrophages [110]. Therefore, longer term *in vivo* studies are required to fully characterise this behaviour at the mammary sites. Such a long-term study would ideally employ methods such as evaluation of mechanical properties of the scaffold as well as the crystallinity and changes in the molecular structure of the biopolymer chains as measures of degradation.

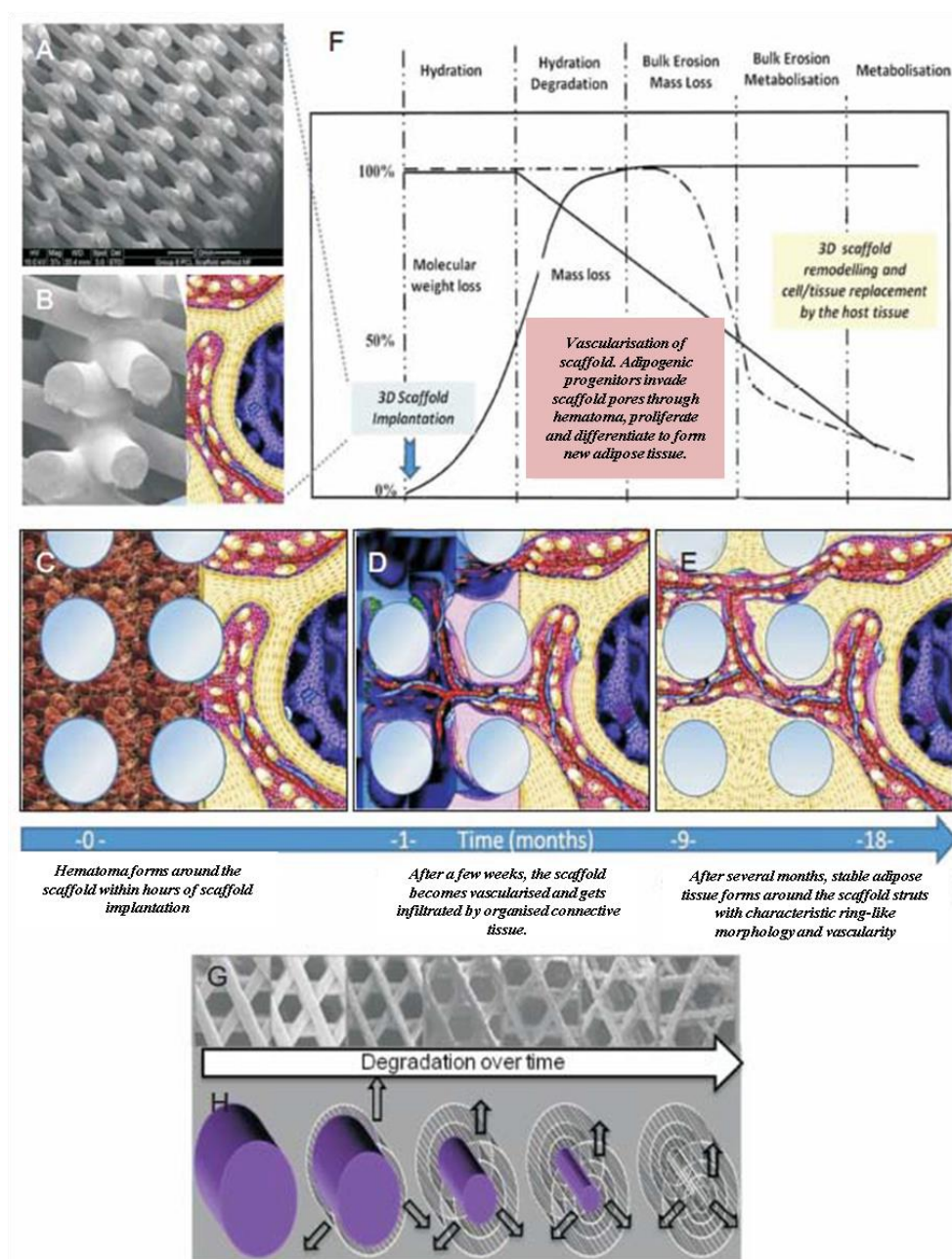


Figure 5.3 Schematic illustrating the interdependence of molecular weight loss and mass loss of a slow-degrading PCL scaffold plotted against time, which corresponds with tissue regeneration.

Scaffold, as shown by SEM (A) is implanted at $t = 0$ (B) with lower figures (C-E) showing a conceptual illustration of the biological processes of adipose tissue formation over time. The scaffold is immediately filled with a hematoma on implantation (C) followed by vascularization (D) and gradually new adipose tissue is formed within the scaffold (E). As the scaffold degrades over time there is increased tissue remodelling within the implantation site until eventually the scaffold pores are entirely filled with stable adipose tissue and vascularity. SEM of scaffold degraded over time (G) with associated schematic visualization of how PCL scaffolds degrade via long-term bioerosion process, which takes up to 36 months in vivo (h). Figure adapted from Woodruff *et al* [310].

5.5.4 Characterisation of tissue morphology and make-up

In studies 2, and 4, we primarily focused on the morphology of the adipose tissue, localised fibrotic reactions and presence of blood vessels. However, other aspects of tissue make-up such as the interactions between the macrophages and the implanted cells, changes in blood leucocyte count, intracutaneous reactivity, acute systemic toxicity and hemolysis fell out of the scope of these two studies. It is expected that once an optimum tissue engineered construct is found which could mimic the properties of native adipose tissue, all aspects of tissue morphology and immunological behaviours towards the constructs will be studied in detail.

5.5.5 Scaffold form in study 4 was not adequate for delayed fat injections

The hemispherical shell-based scaffold used in study 4 did not imbibe adequate design principles that would allow a surgeon to efficiently and accurately deposit the fat at predetermined regions in the scaffold. Indeed, this method would be rendered impractical if the host connective tissue occupies a majority of the volume of the scaffold such that no further volume remains for the secondary injection of fat tissue. Therefore, we have developed a system of removable space-occupying structures within the scaffold which can be removed prior to injection of the fat (see Appendix 1). These space-occupying structures, when removed, would create voids within the scaffold which can then be used to inject the fat.

5.5.6 Drug Delivery using biodegradable scaffolds

The applications of biodegradable breast scaffolds could also be extended to anti-cancer drug delivery applications – an application of particular interest both to breast augmentation patients and post-cancer mastectomy patients. In case of young patients choosing to undergo aesthetic breast augmentation procedures, the scaffold can be loaded with adipogenic growth factors which may stimulate a faster regenerative response from the body. One of the simplest strategies to immobilise growth factor particles onto a scaffold is through crosslinking of a biodegradable polymer coating loaded with growth factor (GF) molecules onto the scaffold surface [382]. Another approach could be a combination of GF -releasing microspheres and a macroporous scaffold [383, 384]. This approach could be useful in cases where the scaffold biomaterial is not suitable for controlled release of GF molecules. Interested readers are encouraged to read a review on these growth factor delivery applications by Mourino *et al* to obtain further information [385].

On the other hand, this strategy must be used with caution in case of post-mastectomy breast reconstruction patients. One of the major issues currently unresolved in this field is the fact that after tumour removal, cancerous cells may still remain inside the breast region. If the scaffold triggers excessive angiogenic or proliferative signals (due to presence of MSCs or GF), the remaining cancerous cells in the region may trigger a malignant tumour formation. Therefore, in such cases, the scaffold can be loaded with anti-cancer drugs to balance the proliferative effects of the growth factor molecules. This aspect of breast tissue engineering warrants further research to determine the perfect balance between GF and anti-cancer drugs.

5.6 Overall discussion and conclusion

An upcoming clinical area for the application of adipose tissue reconstruction is breast reconstruction post-mastectomy. Currently, a majority of breast reconstructions are performed with the use of non-degradable prosthetic implants or by transplantation of autologous free or pedicled tissue flaps consisting of skin, muscle and connected vasculature [51]. A different, more promising approach towards the reconstruction of breast volume has been proposed in this PhD project. This method advocates for the use of personalised biodegradable scaffolds fabricated by additive manufacturing. Since the publication of the highly cited research paper by Patrick[27, 204] that used preadipocyte-seeded polyglycolic acid (PLGA) scaffolds for regenerating small volumes of adipose tissue, many research groups around the world [3-11] have produced interesting results in respect to the regeneration of adipose tissue using cell-based approaches. These cell-based approaches are very promising for the regeneration of complex, living tissue; however, they also lead to several disadvantages – ranging from problems with scaling up of tissue culture to requiring complex GMP-approved laboratories for tissue culturing. Furthermore, it is inherently challenging to embrace the complexities and intricacies of a human body and distil them down to highly controllable experimental variables to be used in an *in vitro* culture model.

To avoid using such cells and biological factors, and alternatively to achieve an adipoconductive polymer-based scaffold, one approach is to implant the scaffold acellularly and subsequently introduce autologous tissue into the pores of the scaffold. Although not used in breast tissue engineering research, this so-called “body as a bioreactor” approach has been successfully implemented in bone and cartilage tissue regeneration [250-256]. The advantage of such an approach is its

simplicity as it does not rely on the delivery of exogenous growth factors and/or cells which is especially important in case of adipose tissue engineering whereby large volumes of adipose tissue needs to be harvested and cultured for long periods of time in order to generate cell numbers sufficient to populate the large volume scaffolds (see Table 5.1).

STRATEGY	ADVANTAGES	DISADVANTAGES
Silicone Implants	Can be manufactured in a broad range of sizes, contours, profiles and textures. Easy to handle and implant. Surgery times are lower compared to breast reconstruction surgeries using autologous tissue.	Capsular contracture. Elevated siloxanes and platinum levels are detrimental to patient's health. High likelihood of repeat surgeries being needed to replace leaking implants or remove fibrous capsule.
Cell/Growth Factor-laden scaffolds	Have the potential to regenerate complex hierarchical tissues and mimic cellular organization of natural tissues. By seeding endothelial cells, it is theoretically possible to generate a vascular bed <i>in vitro</i> within the scaffolds prior to implantation.	Manual cell seeding and culturing of cell-laden large volume scaffolds is time consuming, user-dependent, semi-efficient and, therefore, economically unviable [4]. Regulatory approvals and Quality Assurance guidelines for cell-laden constructs are complex and expensive.
Cell/Growth	Manual cell seeding not required.	As of yet, this technique is

<p>Factor-free scaffolds</p>	<p>Therefore, the production process can be upscaled in case of large volume scaffolds and be made economically viable with fewer obstacles.</p> <p>Permeable entry barriers. Quality Assurance guidelines are significantly less complex and expensive.</p> <p>Using the “body as a bioreactor” approach [256], it is possible to induce infiltration of vasculature from the host body.</p>	<p>unsuitable for use to give rise to complex hierarchical tissue organisation.</p>
-------------------------------------	---	---

Therefore, in this PhD project, and indeed for future *in vivo* studies, we ultimately aimed to pursue the cell-free scaffold concept in the field of adipose tissue engineering.

In this PhD project, patient-specific biodegradable scaffolds were fabricated using a unique computer-aided-tissue-engineering (CATE) strategy encompassing:

- Conversion of medical imaging scans into CAD models suitable for additive manufacturing.
- Conversion of solid CAD models into scaffold architectures for use in tissue engineering.
- Direct conversion of porous scaffold geometries into finite elements for *in silico* mechanical testing.

It was shown *in vitro* that the scaffolds showed good cell compatibility and aided in the proliferation of multipotent cells in 3 dimensions. Cell-seeded constructs were later implanted in nude rats for 24 weeks, after which we observed that although widespread regeneration of adipose tissue was observed throughout the spans of the

constructs, the newly regeneration fat was of host origin while a majority of the grafted cells did not survive the implantation process. We also obtained positive results in a scaled-up minipig model whereby cell-free scaffolds were implanted into the test subjects combined with lipoaspirated autologous fat tissue extracted during the surgery. Efficient and anatomically relevant regeneration of adipose tissue was once again observed within this minipig model.

Taking all this into consideration, the implications of a cell-free patient-specific biodegradable scaffold for breast tissue engineering are far-reaching. Throughout the world, academic, clinical, and industrial efforts are increasingly being directed toward the use of regenerative medicine-based therapies for the diagnosis and treatment of a range of pathologies and injuries. In a cost-controlled healthcare environment, new technologies must be assessed on the basis of their potential to improve patient quality of life relative to the additional cost burden placed on the health system. Only those technologies that demonstrate adequate cost effectiveness ratios will be driven forward to broad clinical application. Our approach of using cell-free scaffolds represents a next generational approach in the field of breast tissue engineering with the clear potential to meet this criterion – with potential to restore the natural form and feel of breast tissue without the need for ongoing treatment and support. The work presented in this thesis, when furthered in the future by world-class research teams, will enable the establishment of a world leading research program in soft tissue engineering and regenerative medicine.

Epilogue

This thesis is not only an embodiment of 3 years of work, and as much as I'd like to boast that I am a one-man-army handling all aspects of this project single-handedly, saying so would be blatantly false. Indeed, without the contribution of tens of people in Brisbane, Utrecht and Germany and their unwavering support, I would not have been able to accomplish even half the work that I've been able to show here. I will not try to mention all students, postdocs and staff members I've shared good times with by name, as I'm sure I will forget some. I thank you all! Instead, in this Epilogue, I will focus on persons who really were influential in setting the directions of this thesis.

My first thanks go to Edward Ren, for had it been some other RA on that fateful night in October 2011, perhaps you would not be reading this thesis today. I'd like to thank Ed not only for coaxing me into a PhD, but also for teaching me the necessary skills of tissue sectioning and immunohistology – without these skills the directions of this thesis would have been radically different. After initially submitting my PhD application in October 2011, there was a period of 3 months when I was effectively unemployed. During this time, I asked my future Associate Supervisor, Dr. Ferry PW Melchels, if I could come in anyway and learn some 3D printing skills. I thought even if I didn't get into the PhD programme, I would be a legend among my circle of friends if I told them I knew how to 3D print. Luckily, Ferry agreed to teach me how to 3D print over the next few months and fortunately, I was accepted into the PhD programme. Ferry, since that time, you have put a lot of work in converting me from, as you Dutchmen say, a clueless prutser to a scientist. I remember coming to your desk Friday every week with an “improved” scaffold design and a smug look on my

face – thinking I'd made some real breakthrough. You nearly always went “nah, not good enough mate” and that would give me some fuel to produce the next improvement in the coming week. When finally, in September 2012, we made the first porous breast scaffolds (used in Study 3), you went “Wow! These look awesome” and the look on your face was reward enough for all the previous work. I cannot put a count on the number of things I learnt from you, and for me you will always remain a mentor. Thank you so much for guiding me in this journey.

One of the first things I learned, apart from 3D printing, was tissue culture. Dr. Anna Taubenberger was the resident expert on cell culture and my training started with pipetting a known volume of water onto a weighing tray and matching the dispensed volume with the weight. If volume = weight, I was doing it right. I was a born natural at this – as, I suspect, is 99.99% of the population. But the lessons got more complex following that and another PhD student, Jeremy Baldwin, got involved into my training. Jeremy, I am very thankful for your fastidious cell culture training, which helped me immensely in my 2nd year, when I was juggling ~100 T75 flasks like a professional. I also thoroughly enjoyed our time as desk-neighbours. Listening to your multitude of good ideas about tissue engineering indeed fascinated me (truth) and gave me an avenue to discuss my own project with someone else. Thank you also for the miniature Jefferson, Bruce Lee and the unforgettable Pet-Rock.

Animal experiments followed cell culture. It is here that I got to collaborate with another good friend of mine, Boris Holzapfel. Boris, you really took the fear of handling those frightening rats out of my mind by bringing in the barbeque glove. I am very grateful for that. I am also thankful for showing me how important it is to think about the clinical aspects of their strategies and view things from a surgeon's point of view. This new thinking really served as a guide for the rest of my PhD

(Study 4 and beyond). I hope we can continue having these discussions even after you go back to Germany.

I would also like to thank Ingo Fehr for showing me how to put the “engineering” in Tissue Engineering. You are still the best roommate I’ve ever had and amongst the brightest engineers I’ve met. The crazy ideas about scaffold manufacturing you gave me towards the end of this project, I suspect will play a major role in the coming years. Vielen Dank for the wine tasting lessons and the great time I’ve spent with you during our shared lunch sessions and our road-trips in Australia, India and Germany.

To be able to work hard, I am really grateful for the support of Patrina Poh. From our first meeting during the shared lunch sessions, you have constantly been a source of forward momentum and fresh perspectives for me. You pushed me and enabled me to do things I often I would never accomplish. You showed me how little things, when added together, could add up to produce great effects – both good and bad. This realization shaped this PhD journey more than anything else and for this I owe an inexpressible load of gratitude to you. Finally, I apologise for making you listen to all of my sometimes crazy ideas and for making sure they were made sense before presenting them to Dietmar.

Every person mentioned in this Epilogue played a major influence on this project. But the one person without which none of this would have been possible is Dietmar. Dietmar, firstly I thank you for assuming the courage to hire such a wet-behind-the-ears student as part of such an ambitious team. Apart from all the science, I have learnt so much about being a leader and an innovator from you – knowledge that will inspire me throughout my career. You have always found the time to review texts

and presentations, coming up with innovative ideas and showing me the big picture when I was lost in details. In doing this, you have truly brought credence to the term “Doktorvater”. Thank you very much for all the interesting talks about football, cooking tips, stock market and also for opening your house to me when I was apartment-hunting. For this, I will forever be grateful.

For many, the end of their PhD is the beginning of a new era. So many things learned, so many experiences lived – bringing about a yearning to make one’s own mark in the world of science. For me it is no different, this thesis is only a milestone in the bigger picture, for I have many more promises to keep, and miles to go before I sleep.

References

- [1] Nassar H. Breast - nonmalignant Inflammatory / infectious Lymphocytic mastitis. 2014.
- [2] Vacanti JP, Langer R. Tissue engineering: the design and fabrication of living replacement devices for surgical reconstruction and transplantation. *The Lancet*. 1999;354:S32-S4.
- [3] Hutmacher DW. Scaffolds in tissue engineering bone and cartilage. *Biomaterials*. 2000;21:2529.
- [4] Melchels FPW, Domingos MAN, Klein TJ, Malda J, Bartolo PJ, Hutmacher DW. Additive Manufacturing of Tissues and Organs. *Progress in Polymer Science*. 2011.
- [5] Viola J, Lal B, Grad O. The Emergence of Tissue Engineering as a Research Field. National Science Foundation; 2003.
- [6] GLOBOCAN. All Cancers (excluding non-melanoma skin cancer) Estimated Incidence, Mortality and prevalence Worldwide in 2012. 2012.
- [7] Surgeons ASOP. Cosmetic Procedure Trends. 2011 Plastic Surgery Statistics Report: American Society of Plastic Surgeons; 2011.
- [8] Cordeiro PG. Breast reconstruction after surgery for breast cancer. *N Engl J Med*. 2008;359:1590.
- [9] Renneker R, Cutler M. Psychological problems of adjustment to cancer of the breast. *Journal of the American Medical Association*. 1952;148:833.
- [10] Asplund O. Capsular contracture in silicone gel and saline-filled breast implants after reconstruction. *Plastic and reconstructive surgery*. 1984;73:270.
- [11] Feller AM. Free TRAM. Results and abdominal wall function. *Clin Plast Surg*. 1994;21:223.
- [12] Serletti JM, Moran SL. Free versus the pedicled TRAM flap: A cost comparison and outcome analysis. *Plast Reconstr Surg*. 1997;100:1418.
- [13] Patrick Jr C, Chauvin P, Hobbey J, Reece G. Preadipocyte seeded PLGA scaffolds for adipose tissue engineering. *Tissue engineering*. 1999;5:139.
- [14] Tabata Y, Miyao M, Inamoto T, Ishii T, Hirano Y, Yamaoki Y, et al. De novo formation of adipose tissue by controlled release of basic fibroblast growth factor. *Tissue Eng*. 2000;6:279.
- [15] Mian R, Morrison WA, Hurley JV, Penington AJ, Romeo R, Tanaka Y, et al. Formation of new tissue from an arteriovenous loop in the absence of added extracellular matrix. *Tissue Eng*. 2000;6:595.
- [16] Walton RL, Beahm EK, Wu L. De novo adipose formation in a vascularized engineered construct. *Microsurgery*. 2004;24:378-84.
- [17] Fischbach C, Seufert J, Staiger H, Hacker M, Neubauer M, Göpferich A, et al. Three-dimensional in vitro model of adipogenesis: comparison of culture conditions. *Tissue Eng*. 2004;10:215.
- [18] Kang X, Xie Y, Kniss DA. Adipose tissue model using three-dimensional cultivation of preadipocytes seeded onto fibrous polymer scaffolds. *Tissue Eng*. 2005;11:458.
- [19] Masuda T, Furue M, Matsuda T. Novel strategy for soft tissue augmentation based on transplantation of fragmented omentum and preadipocytes. *Tissue Eng*. 2004;10:1672.
- [20] Cho SW, Kim SS, Won Rhie J, Mi Cho H, Yong Choi C, Kim BS. Engineering of volume-stable adipose tissues. *Biomaterials*. 2005;26:3577.

- [21] Santiago LY, Nowak RW, Peter Rubin J, Marra KG. Peptide-surface modification of poly (caprolactone) with laminin-derived sequences for adipose-derived stem cell applications. *Biomaterials*. 2006;27:2962-9.
- [22] Unger RE, Sartoris A, Peters K, Motta A, Migliaresi C, Kunkel M, et al. Tissue-like self-assembly in cocultures of endothelial cells and osteoblasts and the formation of microcapillary-like structures on three-dimensional porous biomaterials. *Biomaterials*. 2007;28:3965-76.
- [23] Jain RK, Au P, Tam J, Duda DG, Fukumura D. Engineering vascularized tissue. *Nat Biotechnol*. 2005;23:821.
- [24] Rouwkema J, Rivron NC, van Blitterswijk CA. Vascularization in tissue engineering. *Trends Biotechnol*. 2008;26:434.
- [25] Radisic M, Malda J, Epping E, Geng W, Langer R, Vunjak-Novakovic G. Oxygen gradients correlate with cell density and cell viability in engineered cardiac tissue. *Biotechnol Bioeng*. 2005;93:332.
- [26] Lovett M, Lee K, Edwards A, Kaplan DL. Vascularization strategies for tissue engineering. *Tissue Engineering Part B: Reviews*. 2009;15:353-70.
- [27] Patrick CW. Breast Tissue Engineering. *Annual Review of Biomedical Engineering*. 2004;6:109-30.
- [28] Patrick Jr C. Tissue engineering strategies for adipose tissue repair. *The Anatomical Record*. 2001;263:361-6.
- [29] Patrick CW, Mikos AG, McIntire LV. *Frontiers in tissue engineering: A Pergamon Title*; 1998.
- [30] Rozen WM, Rajkomar AKS, Anavekar NS, Ashton MW. Post-mastectomy breast reconstruction: a history in evolution. *Clinical breast cancer*. 2009;9:145-54.
- [31] Welfare AIoHa. Breast cancer in Australia: an overview, 2009. 2009.
- [32] Surgeons ASoP. Report of the 2010 Plastic Surgery Statistics. 2010.
- [33] Blondeel PN, Vanderstraeten G, Monstrey S, Van Landuyt K, Tonnard P, Lysens R, et al. The donor site morbidity of free DIEP flaps and free TRAM flaps for breast reconstruction. *British journal of plastic surgery*. 1997;50:322-30.
- [34] Robb GL. *Reconstructive Surgery*. In: Hunt K, Robb G, Strom E, editors. *Breast Cancer*. New York: Springer-Verlag; 2001. p. 223-53.
- [35] Muzaffar AR, Rohrich RJ. The silicone gel-filled breast implant controversy: An update. *Plastic and reconstructive surgery*. 2002;109:742.
- [36] Flassbeck D, Pfleiderer B, Klemens P, Heumann KG, Eltze E, Hirner AV. Determination of siloxanes, silicon, and platinum in tissues of women with silicone gel-filled implants. *Analytical and bioanalytical chemistry*. 2003;375:356-62.
- [37] Pollock H. Breast capsular contracture: A retrospective study of textured versus smooth silicone implants. *Plastic and reconstructive surgery*. 1993;91:404-.
- [38] Peters W, Pritzker K, Smith D, Fornasier V, Holmyard D, Lugowski S, et al. Capsular calcification associated with silicone breast implants: incidence, determinants, and characterization. *Annals of plastic surgery*. 1998;41:348.
- [39] Coleman DJ, Foo ITH, Sharpe DT. Textured or smooth implants for breast augmentation? A prospective controlled trial. *British journal of plastic surgery*. 1991;44:444-8.
- [40] Baran CN, Peker F, Ortak T, Sensoz O, Baran NK. A different strategy in the surgical treatment of capsular contracture: leave capsule intact. *Aesthetic plastic surgery*. 2001;25:427-31.
- [41] Gerszten PC. A formal risk assessment of silicone breast implants. *Biomaterials*. 1999;20:1063-9.

- [42] Burkhardt B, Dempsey P, Schnur P, Tofield J. Capsular contracture: a prospective study of the effect of local antibacterial agents. *Plastic and reconstructive surgery*. 1986;77:919.
- [43] Hakelius L, Ohlsén L. A clinical comparison of the tendency to capsular contracture between smooth and textured gel-filled silicone mammary implants. *Plastic and reconstructive surgery*. 1992;90:247.
- [44] Gylbert L, Asplund O, Jurell G. Capsular contracture after breast reconstruction with silicone-gel and saline-filled implants: a 6-year follow-up. *Plastic and reconstructive surgery*. 1990;85:373.
- [45] Contant CME, van Geel AN, van der Holt B, Griep C, Tjong Joe Wai R, Wiggers T. Morbidity of immediate breast reconstruction (IBR) after mastectomy by a subpectorally placed silicone prosthesis: the adverse effect of radiotherapy. *European Journal of Surgical Oncology (EJSO)*. 2000;26:344-50.
- [46] Vandeweyer E, Deraemaeker R. Radiation therapy after immediate breast reconstruction with implants. *Plastic and reconstructive surgery*. 2000;106:56.
- [47] Jacobson GM, Sause WT, Thomson JW, Plenk HP. Breast irradiation following silicone gel implants. *International Journal of Radiation Oncology* Biology* Physics*. 1986;12:835-8.
- [48] Rosato RM, Dowden RV. Radiation therapy as a cause of capsular contracture. *Annals of plastic surgery*. 1994;32:342.
- [49] Ma PX, Elisseeff J. *Scaffolding in tissue engineering*. Boca Raton, Florida, USA: CRC; 2005.
- [50] Clough KB, O'Donoghue JM, Fitoussi AD, Nos C, Falcou MC. Prospective evaluation of late cosmetic results following breast reconstruction: I. Implant reconstruction. *Plastic and reconstructive surgery*. 2001;107:1702.
- [51] Cordeiro PG. Breast reconstruction after surgery for breast cancer. *New England Journal of Medicine*. 2008;359:1590-601.
- [52] Niechajev I, Sevcuk O. Long-term results of fat transplantation: clinical and histologic studies. *Plastic and reconstructive surgery*. 1994;94:496.
- [53] Matsudo PKR, Toledo LS. Experience of injected fat grafting. *Aesthetic plastic surgery*. 1988;12:35-8.
- [54] Lee K, Halberstadt C, Holder W, Mooney D. Breast reconstruction. In: Lanza R, Vacanti J, editors. *Principle of tissue engineering*. San Diego: Academic Press; 2000.
- [55] Khouri R. *Breast Reconstruction After Mastectomy*. 2011.
- [56] Coleman SR. Facial recontouring with lipostructure. *Clinics in plastic surgery*. 1997;24:347.
- [57] Hartrampf C, Schefflan M, Black PW. Breast reconstruction with a transverse abdominal island flap. *Plastic and reconstructive surgery*. 1982;69:216.
- [58] Allen RJ, Treece P. Deep inferior epigastric perforator flap for breast reconstruction. *Annals of plastic surgery*. 1994;32:32.
- [59] Gill PS, Hunt JP, Guerra AB, Dellacroce FJ, Sullivan SK, Boraski J, et al. A 10-year retrospective review of 758 DIEP flaps for breast reconstruction. *Plastic and reconstructive surgery*. 2004;113:1153.
- [60] Blondeel PN, Arnstein M, Verstraete K, Depuydt K, Van Landuyt KH, Monstrey SJ, et al. Venous congestion and blood flow in free transverse rectus abdominis myocutaneous and deep inferior epigastric perforator flaps. *Plastic and reconstructive surgery*. 2000;106:1295.
- [61] Nahabedian MY, Momen B, Galdino G, Manson PN. Breast reconstruction with the free TRAM or DIEP flap: Patient selection, choice of flap, and outcome. *Plastic and reconstructive surgery*. 2002;110:466.

- [62] Feller AM. Free TRAM. Results and abdominal wall function. *Clinics in plastic surgery*. 1994;21:223.
- [63] Arnez Z, Khan U, Pogorelec D, Planinsek F. Rational selection of flaps from the abdomen in breast reconstruction to reduce donor site morbidity* 1,* 2,* 3,* 4,* 5,* 6. *British journal of plastic surgery*. 1999;52:351-4.
- [64] Serletti JM, Moran SL. Free versus the pedicled TRAM flap: A cost comparison and outcome analysis. *Plastic and reconstructive surgery*. 1997;100:1418.
- [65] Serletti JM, Moran SL. *Microvascular reconstruction of the breast*. Wiley Online Library; 2000. p. 264-71.
- [66] Kroll SS, Gherardini G, Martin JE, Reece GP, Miller MJ, Evans GRD, et al. Fat necrosis in free and pedicled TRAM flaps. *Plastic and reconstructive surgery*. 1998;102:1502.
- [67] Kroll SS, Schusterman MA, Reece GP, Miller MJ, Robb G, Evans G. Abdominal wall strength, bulging, and hernia after TRAM flap breast reconstruction. *Plastic and reconstructive surgery*. 1995;96:616.
- [68] Kroll SS, Marchi M. Comparison of strategies for preventing abdominal-wall weakness after TRAM flap breast reconstruction. *Plastic and reconstructive surgery*. 1992;89:1045.
- [69] Edsander-Nord Å, Jurell G, Wickman M. Donor-site morbidity after pedicled or free TRAM flap surgery: A prospective and objective study. *Plastic and reconstructive surgery*. 1998;102:1508.
- [70] Blondeel P. One hundred free DIEP flap breast reconstructions: A personal experience. *British journal of plastic surgery*. 1999;52:104-11.
- [71] Kroll SS. Fat necrosis in free transverse rectus abdominis myocutaneous and deep inferior epigastric perforator flaps. *Plastic and reconstructive surgery*. 2000;106:576.
- [72] Patrick Jr C, Zheng B, Johnston C, Reece G. Long-term implantation of preadipocyte-seeded PLGA scaffolds. *Tissue engineering*. 2002;8:283-93.
- [73] Patrick Jr C, Chauvin P, Hobley J, Reece G. Preadipocyte seeded PLGA scaffolds for adipose tissue engineering. *Tissue engineering*. 1999;5:139-51.
- [74] Entenmann G, Hauner H. Relationship between replication and differentiation in cultured human adipocyte precursor cells. *American Journal of Physiology-Cell Physiology*. 1996;270:C1011-C6.
- [75] Hausman G, Richardson R. Newly recruited and pre-existing preadipocytes in cultures of porcine stromal-vascular cells: morphology, expression of extracellular matrix components, and lipid accretion. *Journal of animal science*. 1998;76:48.
- [76] Shillabeer G, Forden J, Lau D. Induction of preadipocyte differentiation by mature fat cells in the rat. *Journal of Clinical Investigation*. 1989;84:381.
- [77] Patrick Jr CW. Adipose tissue engineering: the future of breast and soft tissue reconstruction following tumor resection. Wiley Online Library; 2000. p. 302-11.
- [78] Moore K. *Clinically Oriented Anatomy*. Baltimore: Williams & Wilkins; 1992.
- [79] Park J, DeSouza GN, Kak AC. Dual-beam structured-light scanning for 3-D object modeling. *IEEE*; 2001. p. 65-72.
- [80] Kovacs L, Eder M, Hollweck R, Zimmermann A, Settles M, Schneider A, et al. New aspects of breast volume measurement using 3-dimensional surface imaging. *Annals of plastic surgery*. 2006;57:602.
- [81] Kovacs L, Eder M, Hollweck R, Zimmermann A, Settles M, Schneider A, et al. Comparison between breast volume measurement using 3D surface imaging and classical techniques. *The Breast*. 2007;16:137-45.

- [82] Eder M, Schneider A, Feussner H, Zimmermann A, Höhnke C, Papadopoulos N, et al. [Breast volume assessment based on 3D surface geometry: verification of the method using MR imaging]. *Biomedizinische Technik Biomedical engineering*. 2008;53:112.
- [83] Beekman FJ, McElroy DP, Berger F, Gambhir SS, Hoffman EJ, Cherry SR. Towards in vivo nuclear microscopy: iodine-125 imaging in mice using micro-pinholes. *European journal of nuclear medicine and molecular imaging*. 2002;29:933-8.
- [84] Frankle WG, Slifstein M, Talbot PS, Laruelle M. Neuroreceptor imaging in psychiatry: theory and applications. *International Review of Neurobiology*. 2005;67:385-440.
- [85] Herman GT. *Fundamentals of Computerized Tomography: Image Reconstruction from Projections*: Springer Verlag; 2009.
- [86] Weber DA, Ivanovic M. Ultra-high-resolution imaging of small animals: implications for preclinical and research studies. *Journal of Nuclear Cardiology*. 1999;6:332-44.
- [87] Hendee WR, Morgan CJ. *Magnetic Resonance Imaging Part I—Physical Principles*. *Western Journal of Medicine*. 1984;141:491.
- [88] Hohe J, Ateshian G, Reiser M, Englmeier KH, Eckstein F. Surface size, curvature analysis, and assessment of knee joint incongruity with MRI in vivo. *Magnetic Resonance in Medicine*. 2002;47:554-61.
- [89] Smith-Bindman R, Lipson J, Marcus R, Kim KP, Mahesh M, Gould R, et al. Radiation dose associated with common computed tomography examinations and the associated lifetime attributable risk of cancer. *Archives of Internal Medicine*. 2009;169:2078.
- [90] Berrington de Gonzalez A, Mahesh M, Kim KP, Bhargavan M, Lewis R, Mettler F, et al. Projected cancer risks from computed tomographic scans performed in the United States in 2007. *Archives of Internal Medicine*. 2009;169:2071.
- [91] Melchels F, Wigganhauser PS, Warne D, Barry M, Ong FR, Chong WS, et al. CAD/CAM-assisted breast reconstruction. *Biofabrication*. 2011;3:034114.
- [92] Chua C, Chou S, Ng W, Chow K, Lee S, Aung S, et al. An integrated experimental approach to link a laser digitiser, a CAD/CAM system and a rapid prototyping system for biomedical applications. *The International Journal of Advanced Manufacturing Technology*. 1998;14:110-5.
- [93] Sachlos E, Czernuszka J. Making tissue engineering scaffolds work. Review: the application of solid freeform fabrication technology to the production of tissue engineering scaffolds. *Eur Cell Mater*. 2003;5:39-40.
- [94] Tan Q, Li S, Ren J, Chen C. Fabrication of porous scaffolds with a controllable microstructure and mechanical properties by porogen fusion technique. *International journal of molecular sciences*. 2011;12:890-904.
- [95] Hutmacher DW. Scaffold design and fabrication technologies for engineering tissues state of the art and future perspectives. *Journal of Biomaterials Science, Polymer Edition*. 2001;12:107-24.
- [96] Zein I, Hutmacher DW, Tan KC, Teoh SH. Fused deposition modeling of novel scaffold architectures for tissue engineering applications. *Biomaterials*. 2002;23:1169-85.
- [97] Hutmacher DW, Sittinger M, Risbud MV. Scaffold-based tissue engineering: rationale for computer-aided design and solid free-form fabrication systems. *TRENDS in Biotechnology*. 2004;22:354-62.

- [98] Hutmacher DW, Schantz T, Zein I, Ng KW, Teoh SH, Tan KC. Mechanical properties and cell cultural response of polycaprolactone scaffolds designed and fabricated via fused deposition modeling. *Journal of biomedical materials research*. 2001;55:203-16.
- [99] Domingos M, Dinucci D, Cometa S, Alderighi M, Chiellini F. Polycaprolactone scaffolds fabricated via bioextrusion for tissue engineering applications. *International journal of biomaterials*. 2009;2009.
- [100] Melchels FPW. Preparation of advanced porous structures by stereolithography for application in tissue engineering: University of Twente; 2010.
- [101] Xu T, Jin J, Gregory C, Hickman JJ, Boland T. Inkjet printing of viable mammalian cells. *Biomaterials*. 2005;26:93-9.
- [102] Mironov V, Boland T, Trusk T, Forgacs G, Markwald RR. Organ printing: computer-aided jet-based 3D tissue engineering. *TRENDS in Biotechnology*. 2003;21:157-61.
- [103] Williams JM, Adewunmi A, Schek RM, Flanagan CL, Krebsbach PH, Feinberg SE, et al. Bone tissue engineering using polycaprolactone scaffolds fabricated via selective laser sintering. *Biomaterials*. 2005;26:4817-27.
- [104] Holzapfel BM, Reichert JC, Schantz JT, Gbureck U, Rackwitz L, Noth U, et al. How smart do biomaterials need to be? A translational science and clinical point of view. *Advanced drug delivery reviews*. 2013;65:581.
- [105] Heiny M, Wurth JJ, Shastri VP. Chapter 9 - Progress in Functionalized Biodegradable Polyesters. In: Kumbar SG, Laurencin CT, Deng M, editors. *Natural and Synthetic Biomedical Polymers*. Oxford: Elsevier; 2014. p. 167-80.
- [106] Patrick CW, Jr., Chauvin PB, Hobley J, Reece GP. Preadipocyte seeded PLGA scaffolds for adipose tissue engineering. *Tissue Eng*. 1999;5:139.
- [107] Shanti RM, Janjanin S, Li WJ, Nesti LJ, Mueller MB, Tzeng MB, et al. In vitro adipose tissue engineering using an electrospun nanofibrous scaffold. *Ann Plast Surg*. 2008;61:566.
- [108] Neubauer M, Hacker M, Bauer-Kreisel P, Weiser B, Fischbach C, Schulz MB, et al. Adipose tissue engineering based on mesenchymal stem cells and basic fibroblast growth factor in vitro. *Tissue Eng*. 2005;11:1840-51.
- [109] Chhaya MP, Melchels FPW, Wigganhauser PS, Schantz JT, Hutmacher DW. Breast reconstruction using biofabrication-based tissue engineering strategies. In: Forgacs G, Sun W, editors. *Biofabrication: Micro- and Nano-fabrication, Printing, Patterning and Assemblies*. Oxford, UK: Elsevier Inc.; 2013. p. 183-207.
- [110] Woodruff MA, Hutmacher DW. The return of a forgotten polymer— Polycaprolactone in the 21st century. *Prog Polym Sci*. 2010;35:1217.
- [111] Wigganhauser PS, Muller DF, Melchels FP, Egana JT, Storck K, Mayer H, et al. Engineering of vascularized adipose constructs. *Cell and tissue research*. 2012;347:747.
- [112] Gefen A, Dilmoney B. Mechanics of the normal woman's breast. *Technology and health care : official journal of the European Society for Engineering and Medicine*. 2007;15:259.
- [113] Melchels F, Wigganhauser PS, Warne D, Barry M, Ong FR, Chong WS, et al. CAD/CAM-assisted breast reconstruction. *Biofabrication*. 2011;3:034114.
- [114] Guelcher SA. Biodegradable polyurethanes: synthesis and applications in regenerative medicine. *Tissue engineering Part B, Reviews*. 2008;14:3.
- [115] Gunatillake PA, Adhikari R. Biodegradable synthetic polymers for tissue engineering. *Eur Cell Mater*. 2003;5:1.

- [116] Gugerell A, Kober J, Laube T, Walter T, Nurnberger S, Gronniger E, et al. Electrospun poly(ester-Urethane)- and poly(ester-Urethane-Urea) fleeces as promising tissue engineering scaffolds for adipose-derived stem cells. *PloS one*. 2014;9:e90676.
- [117] Cowie JMG, Arrighi V. *Polymers: Chemistry and physics of modern materials*. *Journal of Polymer Science Part A: Polymer Chemistry*. 1992;30:1777-.
- [118] Amsden B. Curable, biodegradable elastomers: emerging biomaterials for drug delivery and tissue engineering. *Soft Matter*. 2007;3:1335-48.
- [119] Serrano MC, Chung EJ, Ameer GA. Advances and applications of biodegradable elastomers in regenerative medicine. *Advanced Functional Materials*. 2010;20:192-208.
- [120] Shi R, Chen D, Liu Q, Wu Y, Xu X, Zhang L, et al. Recent advances in synthetic bioelastomers. *International journal of molecular sciences*. 2009;10:4223-56.
- [121] Whatley BR, Kuo J, Shuai C, Damon BJ, Wen X. Fabrication of a biomimetic elastic intervertebral disk scaffold using additive manufacturing. *Biofabrication*. 2011;3:015004.
- [122] Agrawal CM, Parr JE, Lin ST. *Synthetic bioabsorbable polymers for implants: Astm Intl*; 2000.
- [123] Tatai L, Moore TG, Adhikari R, Malherbe F, Jayasekara R, Griffiths I, et al. Thermoplastic biodegradable polyurethanes: the effect of chain extender structure on properties and in-vitro degradation. *Biomaterials*. 2007;28:5407-17.
- [124] Bhattacharyya S, Nair LS, Singh A, Krogman NR, Bender J, Greish YE, et al. Development of biodegradable polyphosphazene-nanohydroxyapatite composite nanofibers via electrospinning. *Cambridge Univ Press*; 2004.
- [125] Schacht E, Vandorpe J, De Jardin S, Lemmouchi Y, Seymour L. Biomedical applications of degradable polyphosphazenes. *Biotechnology and bioengineering*. 1996;52:102-8.
- [126] Honarkar H, Rahimi A. Applications of Inorganic Polymeric Materials, III: Polyphosphazenes. *Monatshefte für Chemie/Chemical Monthly*. 2007;138:923-33.
- [127] Yi F, LaVan DA. Poly (glycerol sebacate) nanofiber scaffolds by core/shell electrospinning. *Macromolecular bioscience*. 2008;8:803-6.
- [128] Wang Y, Ameer GA, Sheppard BJ, Langer R. A tough biodegradable elastomer. *Nature biotechnology*. 2002;20:602-6.
- [129] Wang Y, Kim YM, Langer R. In vivo degradation characteristics of poly (glycerol sebacate). *Journal of Biomedical Materials Research Part A*. 2003;66:192-7.
- [130] Jeong CG, Hollister SJ. Mechanical, permeability, and degradation properties of 3D designed poly (1, 8 octanediol-co-citrate) scaffolds for soft tissue engineering. *Journal of Biomedical Materials Research Part B: Applied Biomaterials*. 2010;93:141-9.
- [131] Yang J, Webb AR, Ameer GA. Novel Citric Acid-Based Biodegradable Elastomers for Tissue Engineering. *Advanced Materials*. 2004;16:511-6.
- [132] Yang J, Webb AR, Pickerill SJ, Hageman G, Ameer GA. Synthesis and evaluation of poly (diol citrate) biodegradable elastomers. *Biomaterials*. 2006;27:1889-98.
- [133] Moroni L, Licht R, De Boer J, De Wijn JR, Van Blitterswijk CA. Fiber diameter and texture of electrospun PEOT/PBT scaffolds influence human mesenchymal stem cell proliferation and morphology, and the release of incorporated compounds. *Biomaterials*. 2006;27:4911-22.

- [134] Catalani LH, Collins G, Jaffe M. Evidence for molecular orientation and residual charge in the electrospinning of poly (butylene terephthalate) nanofibers. *Macromolecules*. 2007;40:1693-7.
- [135] Mathew G, Hong J, Rhee J, Lee H, Nah C. Preparation and characterization of properties of electrospun poly (butylene terephthalate) nanofibers filled with carbon nanotubes. *Polymer testing*. 2005;24:712-7.
- [136] Deschamps AA, Claase MB, Sleijster WJ, de Bruijn JD, Grijpma DW, Feijen J. Design of segmented poly (ether ester) materials and structures for the tissue engineering of bone. *Journal of controlled release*. 2002;78:175-86.
- [137] Webb AR, Yang J, Ameer GA. Biodegradable polyester elastomers in tissue engineering. *Expert opinion on biological therapy*. 2004;4:801-12.
- [138] Lee SH, Kim BS, Kim SH, Choi SW, Jeong SI, Kwon IK, et al. Elastic biodegradable poly (glycolide-co-caprolactone) scaffold for tissue engineering. *Journal of Biomedical Materials Research Part A*. 2003;66:29-37.
- [139] Pego AP, Poot AA, Grijpma DW, Feijen J. In vitro degradation of trimethylene carbonate based (co) polymers. *Macromolecular bioscience*. 2002;2:411-9.
- [140] Zhang Z, Kuijter R, Bulstra SK, Grijpma DW, Feijen J. The in vivo and in vitro degradation behavior of poly (trimethylene carbonate). *Biomaterials*. 2006;27:1741-8.
- [141] Bat E, Kothman BHM, Higuera GA, van Blitterswijk CA, Feijen J, Grijpma DW. Ultraviolet light crosslinking of poly (trimethylene carbonate) for elastomeric tissue engineering scaffolds. *Biomaterials*. 2010;31:8696-705.
- [142] Bat E, van Kooten TG, Feijen J, Grijpma DW. Crosslinking of Trimethylene Carbonate and D, L-Lactide (Co-) Polymers by Gamma Irradiation in the Presence of Pentaerythritol Triacrylate. *Macromolecular bioscience*. 2011.
- [143] Pêgo AP, Poot AA, Grijpma DW, Feijen J. Biodegradable elastomeric scaffolds for soft tissue engineering. *Journal of controlled release*. 2003;87:69-79.
- [144] Pego A, Van Luyn M, Brouwer L, Van Wachem P, Poot A, Grijpma D, et al. In vivo behavior of poly (1, 3-trimethylene carbonate) and copolymers of 1, 3-trimethylene carbonate with D, L-lactide or ϵ -caprolactone: Degradation and tissue response. *Journal of Biomedical Materials Research Part A*. 2003;67:1044-54.
- [145] Pego AP, Poot AA, Grijpma DW, Feijen J. Physical properties of high molecular weight 1, 3-trimethylene carbonate and D, L-lactide copolymers. *Journal of Materials Science: Materials in Medicine*. 2003;14:767-73.
- [146] Dong Y, Liao S, Ngiam M, Chan CK, Ramakrishna S. Degradation behaviors of electrospun resorbable polyester nanofibers. *Tissue Engineering Part B: Reviews*. 2009;15:333-51.
- [147] Li L, Chu CC. Nitroxyl radical incorporated electrospun biodegradable poly (ester amide) nanofiber membranes. *Journal of Biomaterials Science, Polymer Edition*. 2009;20:341-61.
- [148] Garg P, Klee D, Keul H, Möller M. Electrospinning of Novel Poly (ester amide) s. *Macromolecular Materials and Engineering*. 2009;294:679-90.
- [149] Tsitlanadze G, Kviria T, Katsarava R, Chu C. In vitro enzymatic biodegradation of amino acid based poly (ester amide) s biomaterials. *Journal of Materials Science: Materials in Medicine*. 2004;15:185-90.
- [150] Young DA, Christman KL. Injectable biomaterials for adipose tissue engineering. *Biomedical materials*. 2012;7:024104.
- [151] Ducheyne P, Healy K, Huttmacher DE, Grainger DW, Kirkpatrick CJ. *Comprehensive Biomaterials: Online Version: Newnes*; 2011.

- [152] Chandler EM, Berglund CM, Lee JS, Polacheck WJ, Gleghorn JP, Kirby BJ, et al. Stiffness of photocrosslinked RGD-alginate gels regulates adipose progenitor cell behavior. *Biotechnol Bioeng.* 2011;108:1683.
- [153] Borzacchiello A, Mayol L, Ramires PA, Pastorello A, Di Bartolo C, Ambrosio L, et al. Structural and rheological characterization of hyaluronic acid-based scaffolds for adipose tissue engineering. *Biomaterials.* 2007;28:4399.
- [154] Wu X, Black L, Santacana-Laffitte G, Patrick CW, Jr. Preparation and assessment of glutaraldehyde-crosslinked collagen-chitosan hydrogels for adipose tissue engineering. *Journal of biomedical materials research Part A.* 2007;81:59.
- [155] Casadei A, Epis R, Ferroni L, Tocco I, Gardin C, Bressan E, et al. Adipose tissue regeneration: a state of the art. *Journal of biomedicine & biotechnology.* 2012;2012:462543.
- [156] Butler MJ, Sefton MV. Cotransplantation of adipose-derived mesenchymal stromal cells and endothelial cells in a modular construct drives vascularization in SCID/bg mice. *Tissue engineering Part A.* 2012;18:1628.
- [157] Verseijden F, Posthumus-van Sluijs SJ, van Neck JW, Hofer SO, Hovius SE, van Osch GJ. Comparing scaffold-free and fibrin-based adipose-derived stromal cell constructs for adipose tissue engineering: an in vitro and in vivo study. *Cell transplantation.* 2012;21:2283.
- [158] Ahmed TA, Dare EV, Hincke M. Fibrin: a versatile scaffold for tissue engineering applications. *Tissue engineering Part B, Reviews.* 2008;14:199.
- [159] Alhadlaq A, Tang M, Mao JJ. Engineered adipose tissue from human mesenchymal stem cells maintains predefined shape and dimension: implications in soft tissue augmentation and reconstruction. *Tissue Eng.* 2005;11:556.
- [160] Brandl FP, Seitz AK, Tessmar JK, Blunk T, Gopferich AM. Enzymatically degradable poly(ethylene glycol) based hydrogels for adipose tissue engineering. *Biomaterials.* 2010;31:3957.
- [161] Vashi AV, Keramidaris E, Abberton KM, Morrison WA, Wilson JL, O'Connor AJ, et al. Adipose differentiation of bone marrow-derived mesenchymal stem cells using Pluronic F-127 hydrogel in vitro. *Biomaterials.* 2008;29:573.
- [162] Benton JA, DeForest CA, Vivekanandan V, Anseth KS. Photocrosslinking of gelatin macromers to synthesize porous hydrogels that promote valvular interstitial cell function. *Tissue engineering Part A.* 2009;15:3221.
- [163] Song S-J, Choi J, Park Y-D, Hong S, Lee JJ, Ahn CB, et al. Sodium Alginate Hydrogel-Based Bioprinting Using a Novel Multinozzle Bioprinting System. *Artificial Organs.* 2011;35:1132-6.
- [164] Pescosolido L, Schuurman W, Malda J, Matricardi P, Alhaique F, Coviello T, et al. Hyaluronic acid and Dextran based Semi-IPN Hydrogels as Biomaterials for Bioprinting. *Biomacromolecules.* 2011.
- [165] Chang R, Nam J, Sun W. Computer-Aided Design, Modeling, and Freeform Fabrication of 3D Tissue Constructs for Drug Metabolism Studies. *Computer-Aided Design and Application.* 2008;5:21-9.
- [166] Khalil S, Sun W. Biopolymer deposition for freeform fabrication of hydrogel tissue constructs. *Materials Science and Engineering: C.* 2007;27:469-78.
- [167] Bat E. Elastomeric networks based on trimethylene carbonate polymers for biomedical applications: physical properties and degradation behaviour: University of Twente; 2010.
- [168] Hudalla GA, Eng TS, Murphy WL. An approach to modulate degradation and mesenchymal stem cell behavior in poly (ethylene glycol) networks. *Biomacromolecules.* 2008;9:842-9.

- [169] Boontheekul T, Hill EE, Kong HJ, Mooney DJ. Regulating myoblast phenotype through controlled gel stiffness and degradation. *Tissue engineering*. 2007;13:1431-42.
- [170] Bryant SJ, Anseth KS. Hydrogel properties influence ECM production by chondrocytes photoencapsulated in poly (ethylene glycol) hydrogels. *Journal of biomedical materials research*. 2002;59:63-72.
- [171] Hou Q, Grijpma DW, Feijen J. Preparation of interconnected highly porous polymeric structures by a replication and freeze-drying process. *Journal of Biomedical Materials Research Part B: Applied Biomaterials*. 2003;67:732-40.
- [172] Schugens C, Maquet V, Grandfils C, Jérôme R, Teyssie P. Biodegradable and macroporous polylactide implants for cell transplantation: 1. Preparation of macroporous polylactide supports by solid-liquid phase separation. *Polymer*. 1996;37:1027-38.
- [173] Zhang R, Ma PX. Synthetic nano-fibrillar extracellular matrices with predesigned macroporous architectures. 2000.
- [174] Crandall DL, Hausman GJ, Kral JG. A review of the microcirculation of adipose tissue: anatomic, metabolic, and angiogenic perspectives. *Microcirculation*. 1997;4:211-32.
- [175] Awwad HK, Aggar ME, Mocktar N, Barsoum M. Intercapillary distance measurement as an indicator of hypoxia in carcinoma of the cervix uteri. *International Journal of Radiation Oncology* Biology* Physics*. 1986;12:1329-33.
- [176] S'mahel J. Experimental implantation of adipose tissue fragments. *British journal of plastic surgery*. 1989;42:207-11.
- [177] Czerny M. Reconstruction of the breast with a lipoma. *Chir Kongr Verh*. 1895;2:216.
- [178] Patrick CW. Breast tissue engineering. *Annu Rev Biomed Eng*. 2004;6:109-30.
- [179] Rouwkema J, Rivron NC, van Blitterswijk CA. Vascularization in tissue engineering. *Trends Biotechnol*. 2008;26:434-41.
- [180] Bauer-Kreisel P, Goepferich A, Blunk T. Cell-delivery therapeutics for adipose tissue regeneration. *Advanced drug delivery reviews*. 2010;62:798.
- [181] Lovett M, Lee K, Edwards A, Kaplan DL. Vascularization strategies for tissue engineering. *Tissue engineering Part B, Reviews*. 2009;15:353-70.
- [182] Christiaens V, Lijnen HR. Angiogenesis and development of adipose tissue. *Molecular and cellular endocrinology*. 2010;318:2.
- [183] Findlay MW, Dolderer JH, Trost N, Craft RO, Cao Y, Cooper-White J, et al. Tissue-engineered breast reconstruction: bridging the gap toward large-volume tissue engineering in humans. *Plast Reconstr Surg*. 2011;128:1206-15.
- [184] Hadjipanayi E, Schilling AF. Hypoxia-based strategies for angiogenic induction: the dawn of a new era for ischemia therapy and tissue regeneration. *Organogenesis*. 2013;9:261.
- [185] Hoshiba T, Lu H, Kawazoe N, Chen G. Decellularized matrices for tissue engineering. *Expert Opin Biol Ther*. 2010;10:1717.
- [186] Young DA, Ibrahim DO, Hu D, Christman KL. Injectable hydrogel scaffold from decellularized human lipoaspirate. *Acta biomaterialia*. 2011;7:1040.
- [187] Choi JS, Yang HJ, Kim BS, Kim JD, Lee SH, Lee EK, et al. Fabrication of porous extracellular matrix scaffolds from human adipose tissue. *Tissue engineering Part C, Methods*. 2010;16:387.
- [188] Poon CJ, Pereira ECMV, Sinha S, Palmer JA, Woods AA, Morrison WA, et al. Preparation of an adipogenic hydrogel from subcutaneous adipose tissue. *Acta biomaterialia*. 2013;9:5609.

- [189] Cheung HK, Han TT, Marecak DM, Watkins JF, Amsden BG, Flynn LE. Composite hydrogel scaffolds incorporating decellularized adipose tissue for soft tissue engineering with adipose-derived stem cells. *Biomaterials*. 2014;35:1914.
- [190] Richardson TP, Peters MC, Ennett AB, Mooney DJ. Polymeric system for dual growth factor delivery. *Nat Biotechnol*. 2001;19:1029.
- [191] Vashi AV, Abberton KM, Thomas GP, Morrison WA, O'Connor AJ, Cooper-White JJ, et al. Adipose tissue engineering based on the controlled release of fibroblast growth factor-2 in a collagen matrix. *Tissue Eng*. 2006;12:3035.
- [192] Ehrbar M, Metters A, Zammaretti P, Hubbell JA, Zisch AH. Endothelial cell proliferation and progenitor maturation by fibrin-bound VEGF variants with differential susceptibilities to local cellular activity. *Journal of controlled release : official journal of the Controlled Release Society*. 2005;101:93.
- [193] Marra KG, Defail AJ, Clavijo-Alvarez JA, Badylak SF, Taieb A, Schipper B, et al. FGF-2 enhances vascularization for adipose tissue engineering. *Plast Reconstr Surg*. 2008;121:1153.
- [194] Moya ML, Cheng MH, Huang JJ, Francis-Sedlak ME, Kao SW, Opara EC, et al. The effect of FGF-1 loaded alginate microbeads on neovascularization and adipogenesis in a vascular pedicle model of adipose tissue engineering. *Biomaterials*. 2010;31:2816.
- [195] Yang F, Cho SW, Son SM, Bogatyrev SR, Singh D, Green JJ, et al. Genetic engineering of human stem cells for enhanced angiogenesis using biodegradable polymeric nanoparticles. *Proceedings of the National Academy of Sciences of the United States of America*. 2010;107:3317.
- [196] Hollenbeck ST, Senghaas A, Komatsu I, Zhang Y, Erdmann D, Klitzman B. Tissue engraftment of hypoxic-preconditioned adipose-derived stem cells improves flap viability. *Wound repair and regeneration : official publication of the Wound Healing Society [and] the European Tissue Repair Society*. 2012;20:872.
- [197] Dolderer JH, Abberton KM, Thompson EW, Slavin JL, Stevens GW, Penington AJ, et al. Spontaneous large volume adipose tissue generation from a vascularized pedicled fat flap inside a chamber space. *Tissue Eng*. 2007;13:673.
- [198] Patrick CW. Breast Tissue Engineering. *Annu Rev Biomed Eng*. 2004;6:109.
- [199] Flynn L, Woodhouse KA. Adipose tissue engineering with cells in engineered matrices. *Organogenesis*. 2008;4:228.
- [200] Cawthorn WP, Scheller EL, MacDougald OA. Adipose tissue stem cells meet preadipocyte commitment: going back to the future. *J Lipid Res*. 2012;53:227.
- [201] Rodeheffer MS, Birsoy K, Friedman JM. Identification of White Adipocyte Progenitor Cells In Vivo. *Cell*. 2008;135:240.
- [202] Stacey DH, Hanson SE, Lahvis G, Gutowski KA, Masters KS. In vitro adipogenic differentiation of preadipocytes varies with differentiation stimulus, culture dimensionality, and scaffold composition. *Tissue engineering Part A*. 2009;15:3389.
- [203] Lilja HE, Morrison WA, Han XL, Palmer J, Taylor C, Tee R, et al. An adipoinductive role of inflammation in adipose tissue engineering: key factors in the early development of engineered soft tissues. *Stem cells and development*. 2013;22:1602.
- [204] Patrick CW, Jr., Zheng B, Johnston C, Reece GP. Long-term implantation of preadipocyte-seeded PLGA scaffolds. *Tissue Eng*. 2002;8:283.
- [205] Wechselberger G, Russell RC, Neumeister MW, Schoeller T, Piza-Katzer H, Rainer C. Successful transplantation of three tissue-engineered cell types using

- capsule induction technique and fibrin glue as a delivery vehicle. *Plast Reconstr Surg.* 2002;110:123.
- [206] Schoeller T, Lille S, Wechselberger G, Otto A, Mowlavi A, Piza-Katzer H. Histomorphologic and volumetric analysis of implanted autologous preadipocyte cultures suspended in fibrin glue: a potential new source for tissue augmentation. *Aesthetic Plast Surg.* 2001;25:57.
- [207] Gimble JM, Bunnell BA, Frazier T, Rowan B, Shah F, Thomas-Porch C, et al. Adipose-derived stromal/stem cells: a primer. *Organogenesis.* 2013;9:3.
- [208] Dominici M, Le Blanc K, Mueller I, Slaper-Cortenbach I, Marini F, Krause D, et al. Minimal criteria for defining multipotent mesenchymal stromal cells. The International Society for Cellular Therapy position statement. *Cytotherapy.* 2006;8:315.
- [209] Secunda R, Vennila R, Mohanashankar AM, Rajasundari M, Jeswanth S, Surendran R. Isolation, expansion and characterisation of mesenchymal stem cells from human bone marrow, adipose tissue, umbilical cord blood and matrix: a comparative study. *Cytotechnology.* 2014. Epub ahead of print.
- [210] Neubauer M, Hacker M, Bauer-Kreisel P, Weiser B, Fischbach C, Schulz MB, et al. Adipose tissue engineering based on mesenchymal stem cells and basic fibroblast growth factor in vitro. *Tissue engineering.* 2005;11:1840.
- [211] Choi JH, Gimble JM, Lee K, Marra KG, Rubin JP, Yoo JJ, et al. Adipose tissue engineering for soft tissue regeneration. *Tissue engineering Part B, Reviews.* 2010;16:413.
- [212] Barry FP, Murphy JM. Mesenchymal stem cells: clinical applications and biological characterization. *The international journal of biochemistry & cell biology.* 2004;36:568.
- [213] Meyerrose TE, De Ugarte DA, Hofling AA, Herrbrich PE, Cordonnier TD, Shultz LD, et al. In vivo distribution of human adipose-derived mesenchymal stem cells in novel xenotransplantation models. *Stem cells.* 2007;25:220.
- [214] Ogawa R. The importance of adipose-derived stem cells and vascularized tissue regeneration in the field of tissue transplantation. *Current stem cell research & therapy.* 2006;1:13.
- [215] Fanza DO. Tissue engineering and transplantation in the fetus. In: Lanza R, Langer R, Vacanti J, editors. *Principles of tissue engineering.* San Diego, CA, USA: Academic Press, Elsevier Inc., 2014. p. 511-25.
- [216] Puissant B, Barreau C, Bourin P, Clavel C, Corre J, Bousquet C, et al. Immunomodulatory effect of human adipose tissue-derived adult stem cells: comparison with bone marrow mesenchymal stem cells. *Br J Haematol.* 2005;129:118.
- [217] Keyser KA, Beagles KE, Kiem HP. Comparison of mesenchymal stem cells from different tissues to suppress T-cell activation. *Cell transplantation.* 2007;16:555.
- [218] Yanez R, Lamana ML, Garcia-Castro J, Colmenero I, Ramirez M, Bueren JA. Adipose tissue-derived mesenchymal stem cells have in vivo immunosuppressive properties applicable for the control of the graft-versus-host disease. *Stem cells.* 2006;24:2582.
- [219] Yoo KH, Jang IK, Lee MW, Kim HE, Yang MS, Eom Y, et al. Comparison of immunomodulatory properties of mesenchymal stem cells derived from adult human tissues. *Cellular immunology.* 2009;259:150.
- [220] Niechajev I, Sevcuk O. Long-term results of fat transplantation: clinical and histologic studies. *Plast Reconstr Surg.* 1994;94:496.

- [221] Strassburg S, Nienhueser H, Bjorn Stark G, Finkenzeller G, Torio-Padron N. Co-culture of adipose-derived stem cells and endothelial cells in fibrin induces angiogenesis and vasculogenesis in a chorioallantoic membrane model. *Journal of tissue engineering and regenerative medicine*. 2013.
- [222] Borges J, Mueller MC, Padron NT, Tegtmeier F, Lang EM, Stark GB. Engineered adipose tissue supplied by functional microvessels. *Tissue Eng*. 2003;9:1263.
- [223] Strassburg S, Nienhueser H, Bjorn Stark G, Finkenzeller G, Torio-Padron N. Co-culture of adipose-derived stem cells and endothelial cells in fibrin induces angiogenesis and vasculogenesis in a chorioallantoic membrane model. *Journal of tissue engineering and regenerative medicine*. 2013. Epub ahead of print.
- [224] Grainger SJ, Carrion B, Ceccarelli J, Putnam AJ. Stromal cell identity influences the in vivo functionality of engineered capillary networks formed by co-delivery of endothelial cells and stromal cells. *Tissue engineering Part A*. 2013;19:1209.
- [225] Traktuev DO, Prater DN, Merfeld-Clauss S, Sanjeevaiah AR, Saadatzadeh MR, Murphy M, et al. Robust functional vascular network formation in vivo by cooperation of adipose progenitor and endothelial cells. *Circulation research*. 2009;104:1410.
- [226] Yao R, Zhang R, Lin F, Luan J. Biomimetic injectable HUVEC-adipocytes/collagen/alginate microsphere co-cultures for adipose tissue engineering. *Biotechnol Bioeng*. 2013;110:1430.
- [227] Devor DE, Waalkes MP, Goering P, Rehm S. Development of an animal model for testing human breast implantation materials. *Toxicol Pathol*. 1993;21:261.
- [228] Womac DJ, Palanisamy AP, Eslick R, Schimpf DK, Chavin KD. Development of a mouse model of abdominal cutaneous flaps for breast reconstruction. *PloS one*. 2013;8:e52829.
- [229] Kuperwasser C, Chavarria T, Wu M, Magrane G, Gray JW, Carey L, et al. Reconstruction of functionally normal and malignant human breast tissues in mice. *Proceedings of the National Academy of Sciences of the United States of America*. 2004;101:4966.
- [230] Proia DA, Kuperwasser C. Reconstruction of human mammary tissues in a mouse model. *Nat Protoc*. 2006;1:206.
- [231] Holzapfel BM, Thibaudeau L, Hesami P, Taubenberger A, Holzapfel NP, Mayer-Wagner S, et al. Humanised xenograft models of bone metastasis revisited: novel insights into species-specific mechanisms of cancer cell osteotropism. *Cancer Metastasis Rev*. 2013;32:129.
- [232] Gupta V, Mun G-H, Choi B, Aseh A, Mildred L, Patel A, et al. Repair and reconstruction of a resected tumor defect using a composite of tissue flap-nanotherapeutic-silk fibroin and chitosan scaffold. *Ann Biomed Eng*. 2011;39:2374.
- [233] Eltze E, Schafer U, Bettendorf O, Rody A, Herchenroder F, Chiwritsch T, et al. Radiation-induced capsule tissue reactions around textured breast implants in a rat model. *Breast*. 2006;15:331.
- [234] Kim HK. The Effect of Anti-Adhesive Agent on Capsular Formation of Breast Implant in Rabbit. *The Aesthetic Meeting 2012: ASAPS*; 2012.
- [235] Lavker RM, Dong G, Zheng P, Murphy GF. Hairless micropig skin. A novel model for studies of cutaneous biology. *The American journal of pathology*. 1991;138:687.
- [236] Gokoo C, Burhop K. A comparative study of wound dressings on full-thickness wounds in micropigs. *Decubitus*. 1993;6:42.

- [237] Riley KN, Herman IM. Collagenase promotes the cellular responses to injury and wound healing in vivo. *Journal of burns and wounds*. 2005;4:e8.
- [238] Takeuchi H, Ishida M, Furuya A, Todo H, Urano H, Sugibayashi K. Influence of skin thickness on the in vitro permeabilities of drugs through Sprague-Dawley rat or Yucatan micropig skin. *Biological & pharmaceutical bulletin*. 2012;35:192.
- [239] Minqiang X, Jie L, Dali M, Lanhua M. Hemodynamic effect of different kinds of venous augmentation in a pig transmidline flap model of DIEP flap. *J Reconstr Microsurg*. 2013;29:379.
- [240] Minqiang X, Jie L, Dali M, Lanhua M. Transmidline abdominal skin flap model in pig: refinements and advancements. *J Reconstr Microsurg*. 2012;28:111.
- [241] Hemmrich K, Van de Sijpe K, Rhodes NP, Hunt JA, Di Bartolo C, Pallua N, et al. Autologous in vivo adipose tissue engineering in hyaluronan-based gels--a pilot study. *The Journal of surgical research*. 2008;144:82.
- [242] Findlay MW, Dolderer JH, Trost N, Craft RO, Cao Y, Cooper-White J, et al. Tissue-engineered breast reconstruction: bridging the gap toward large-volume tissue engineering in humans. *Plast Reconstr Surg*. 2011;128:1206.
- [243] Bucky LP, Ehrlich HP, Sohoni S, May Jr JW. The capsule quality of saline-filled smooth silicone, textured silicone, and polyurethane implants in rabbits: A long-term study. *Plastic and reconstructive surgery*. 1994;93:1123-31.
- [244] Capozzi A, Pennisi VR. Clinical experience with polyurethane-covered gel-filled mammary prostheses. *Plastic and reconstructive surgery*. 1981;68:512-8.
- [245] Melmed EP. Polyurethane implants: A 6-year review of 416 patients. *Plastic and reconstructive surgery*. 1988;82:285-90.
- [246] Pennisi VR. Long-term use of polyurethane breast prostheses: A 14-year experience. *Plastic and reconstructive surgery*. 1990;86:368-71.
- [247] Buie HR, Campbell GM, Klinck RJ, MacNeil JA, Boyd SK. Automatic segmentation of cortical and trabecular compartments based on a dual threshold technique for in vivo micro-CT bone analysis. *Bone*. 2007;41:505-15.
- [248] Garland M, Heckbert PS. Surface simplification using quadric error metrics. *Proceedings of the 24th annual conference on Computer graphics and interactive techniques: ACM Press/Addison-Wesley Publishing Co.*; 1997. p. 209-16.
- [249] Hollister SJ. Porous scaffold design for tissue engineering. *Nature Materials*. 2005;4:518-24.
- [250] Reichert JC, Cipitria A, Epari DR, Saifzadeh S, Krishnakanth P, Berner A, et al. A tissue engineering solution for segmental defect regeneration in load-bearing long bones. *Science Translational Medicine*. 2012;4:141ra93-ra93.
- [251] Rohner D, Hutmacher DW, Cheng TK, Oberholzer M, Hammer B. In vivo efficacy of bone-marrow-coated polycaprolactone scaffolds for the reconstruction of orbital defects in the pig. *Journal of Biomedical Materials Research Part B: Applied Biomaterials*. 2003;66:574-80.
- [252] Rohner D, Hutmacher D, See P, Tan K, Yeow V, Tan S, et al. [Individually CAD-CAM technique designed, bioresorbable 3-dimensional polycaprolactone framework for experimental reconstruction of craniofacial defects in the pig]. *Mund-, Kiefer-und Gesichtschirurgie: MKG*. 2002;6:162-7.
- [253] Schantz J-T, Lim T-C, Ning C, Teoh SH, Tan KC, Wang SC, et al. Cranioplasty after trephination using a novel biodegradable burr hole cover: technical case report. *Neurosurgery*. 2006;58:ONS-E176.
- [254] Rai B, Oest ME, Dupont KM, Ho KH, Teoh SH, Guldborg RE. Combination of platelet-rich plasma with polycaprolactone-tricalcium phosphate scaffolds for

- segmental bone defect repair. *Journal of Biomedical Materials Research Part A*. 2007;81:888-99.
- [255] Stevens MM, Marini RP, Schaefer D, Aronson J, Langer R, Shastri VP. In vivo engineering of organs: the bone bioreactor. *Proceedings of the National Academy of Sciences of the United States of America*. 2005;102:11450-5.
- [256] Stevens MM, Marini RP, Schaefer D, Aronson J, Langer R, Shastri VP. In vivo engineering of organs: the bone bioreactor. *Proceedings of the National Academy of Sciences of the United States of America*. 2005;102:11450-5.
- [257] DeSantis C, Siegel R, Jemal A. *Breast Cancer Facts and Figures 2011-2012*. Atlanta: American Cancer Society, Inc.; 2012.
- [258] Chhaya MP, Melchels FP, Wiggenhauser PS, Schantz JT, Hutmacher DW. Breast Reconstruction Using Biofabrication-Based Tissue Engineering Strategies. In: Forgacs G, Sun W, editors. *Biofabrication: Micro- and Nano-fabrication, Patterning and Assembling*. Burlington: Elsevier Science; 2013.
- [259] Asplund O. Capsular contracture in silicone gel and saline-filled breast implants after reconstruction. *Plastic and reconstructive surgery*. 1984;73:270-5.
- [260] Spear SL, Baker Jr JL. Classification of capsular contracture after prosthetic breast reconstruction. *Plastic and reconstructive surgery*. 1995;96:1119-23.
- [261] Del Pozo JL, Tran NV, Petty PM, Johnson CH, Walsh MF, Bite U, et al. Pilot study of association of bacteria on breast implants with capsular contracture. *Journal of clinical microbiology*. 2009;47:1333-7.
- [262] Pajkos A, Deva AK, Vickery K, Cope C. Detection of subclinical infection in significant breast implant capsules. *Plast Reconstr Surg*. 2003;111:1605-11.
- [263] Dobke MK, Svahn JK, Vastine VL, Landon BN, Stein PC, Parsons CL. Characterization of microbial presence at the surface of silicone mammary implants. *Annals of plastic surgery*. 1995;34:563-71.
- [264] Netscher D, Walker L, Weizer G, Thornby J, Wigoda P, Bowen D. A review of 198 patients (389 implants) who had breast implants removed. *Journal of long-term effects of medical implants*. 1994;5:11-8.
- [265] Virden CP, Dobke MK, Stein P, Parsons CL, Frank DH. Subclinical infection of the silicone breast implant surface as a possible cause of capsular contracture. *Aesthetic plastic surgery*. 1992;16:173-9.
- [266] Netscher DT. Subclinical infection in breast capsules. *Plastic and reconstructive surgery*. 2004;114:818-20.
- [267] Dobke MK, Grzybowski J, Stein P, Landon BN, Dobak J, Parsons CL. Fibroblast behavior in vitro is unaltered by products of staphylococci cultured from silicone implants. *Annals of plastic surgery*. 1994;32:118-25.
- [268] Herman S, Herman S. The meme implant. *Plastic and reconstructive surgery*. 1984;73:411-4.
- [269] Pennisi V. Polyurethane-covered silicone gel mammary prosthesis for successful breast reconstruction. *Aesthetic plastic surgery*. 1985;9:73-7.
- [270] Barone FE, Perry L, Keller T, Maxwell GP. The biomechanical and histopathologic effects of surface texturing with silicone and polyurethane in tissue implantation and expansion. *Plastic and reconstructive surgery*. 1992;90:77-86.
- [271] Bern S, Burd A, May Jr JW. The biophysical and histologic properties of capsules formed by smooth and textured silicone implants in the rabbit. *Plastic and reconstructive surgery*. 1992;89:1037-42.
- [272] Brohim RM, Foresman PA, Grant GM, Merickel MB, Rodeheaver GT. Quantitative monitoring of capsular contraction around smooth and textured implants. *Annals of plastic surgery*. 1993;30:424-34.

- [273] Clugston PA, Perry LC, Hammond DC, Maxwell GP. A rat model for capsular contracture: The effects of surface texturing. *Annals of plastic surgery*. 1994;33:595-9.
- [274] Levy L, Broad S, Diekmann D, Evans RD, Watt FM. β 1 integrins regulate keratinocyte adhesion and differentiation by distinct mechanisms. *Molecular biology of the cell*. 2000;11:453-66.
- [275] Teixido J, Hemler M, Greenberger J, Anklesaria P. Role of beta 1 and beta 2 integrins in the adhesion of human CD34hi stem cells to bone marrow stroma. *Journal of Clinical Investigation*. 1992;90:358.
- [276] Docheva D, Popov C, Mutschler W, Schieker M. Human mesenchymal stem cells in contact with their environment: surface characteristics and the integrin system. *Journal of cellular and molecular medicine*. 2007;11:21-38.
- [277] Tate MC, García AJ, Keselowsky BG, Schumm MA, Archer DR, LaPlaca MC. Specific β 1 integrins mediate adhesion, migration, and differentiation of neural progenitors derived from the embryonic striatum. *Molecular and Cellular Neuroscience*. 2004;27:22-31.
- [278] Mazzali M, Kipari T, Ophascharoensuk V, Wesson J, Johnson R, Hughes J. Osteopontin—a molecule for all seasons. *Qjm*. 2002;95:3-13.
- [279] Von Recum A, Van Kooten T. The influence of micro-topography on cellular response and the implications for silicone implants. *Journal of Biomaterials Science, Polymer Edition*. 1996;7:181-98.
- [280] Ratner BD. New ideas in biomaterials science—a path to engineered biomaterials. *Journal of biomedical materials research*. 1993;27:837-50.
- [281] Johnson PE, Kernahan DA, Bauer BS. Dermal and epidermal response to soft-tissue expansion in the pig. *Plastic and reconstructive surgery*. 1988;81:390-5.
- [282] Montagna W, Yun JS. The Skin of the Domestic Pig1. *Journal of investigative dermatology*. 1964;43:11-21.
- [283] Brohim RM, Foresman PA, Hildebrandt PK, Rodeheaver GT. Early tissue reaction to textured breast implant surfaces. *Annals of plastic surgery*. 1992;28:354-62.
- [284] Joseph J, Variathu KT, Mohanty M. Mediatory role of interleukin-6 in α smooth muscle actin induction and myofibroblast formation around silicone tissue expander. *Journal of Biomedical Materials Research Part A*. 2013;101:2967-73.
- [285] RUDOLPH R, ABRAHAM J, VECCHIONE T, GUBER S, WOODWARD M. Myofibroblasts and free silicon around breast implants. *Plastic and reconstructive surgery*. 1978;62:185-96.
- [286] Joseph J, Mohanty M, Mohanan P. Investigative study of myofibroblasts and cytokines in peri-implant tissue of silicone breast expander by RT-PCR in a rat model. *Journal of Biomaterials Science, Polymer Edition*. 2010;21:1389-402.
- [287] Hinz B, Celetta G, Tomasek JJ, Gabbiani G, Chaponnier C. Alpha-smooth muscle actin expression upregulates fibroblast contractile activity. *Molecular biology of the cell*. 2001;12:2730-41.
- [288] Adams Jr WP, Haydon MS, Raniere Jr J, Trott S, Marques M, Feliciano M, et al. A rabbit model for capsular contracture: development and clinical implications. *Plastic and reconstructive surgery*. 2006;117:1214-9.
- [289] Minami E, Koh IHJ, Ferreira JCR, Waitzberg AFL, Chifferi V, Rosewick TF, et al. The composition and behavior of capsules around smooth and textured breast implants in pigs. *Plastic and reconstructive surgery*. 2006;118:874-84.

- [290] Lossing C, Hansson H-A. Peptide growth factors and myofibroblasts in capsules around human breast implants. *Plastic and reconstructive surgery*. 1993;91:1277-86.
- [291] Stump A, Holton III LH, Connor J, Harper JR, Slezak S, Silverman RP. The use of acellular dermal matrix to prevent capsule formation around implants in a primate model. *Plastic and reconstructive surgery*. 2009;124:82-91.
- [292] Hwang K, Sim HB, Huan F, Kim DJ. Myofibroblasts and capsular tissue tension in breast capsular contracture. *Aesthetic plastic surgery*. 2010;34:716-21.
- [293] Ko CY, Ahn CY, Ko J, Chopra W, Shaw WW. Capsular synovial metaplasia as a common response to both textured and smooth implants. *Plastic and reconstructive surgery*. 1996;97:1427-33.
- [294] Tuan HS, Hutmacher DW. Application of micro CT and computation modeling in bone tissue engineering. *Computer-aided design*. 2005;37:1151-61.
- [295] Hangartner T. Thresholding technique for accurate analysis of density and geometry in QCT, pQCT and İCT images. *J Musculoskelet Neuronal Interact*. 2007;7:9-16.
- [296] Chazelle B, Edelsbrunner H. An optimal algorithm for intersecting line segments in the plane. *Journal of the ACM (JACM)*. 1992;39:1-54.
- [297] Discher DE, Janmey P, Wang Y. Tissue cells feel and respond to the stiffness of their substrate. *Science*. 2005;310:1139-43.
- [298] Fang Z, Starly B, Sun W. Computer-aided characterization for effective mechanical properties of porous tissue scaffolds. *Computer-aided design*. 2005;37:65-72.
- [299] Lal P, Sun W. Computer modeling approach for microsphere-packed bone scaffold. *Computer-aided design*. 2004;36:487-97.
- [300] Wang E, Nelson T, Rauch R. Back to elements-tetrahedra vs. hexahedra. *Proceedings of the 2004 International ANSYS Conference 2004*.
- [301] Brown TD, Slotosch A, Thibaudeau L, Taubenberger A, Loessner D, Vaquette C, et al. Design and fabrication of tubular scaffolds via direct writing in a melt electrospinning mode. *Biointerphases*. 2012;7:13.
- [302] STU_Bratislava. BEAM188 3-D Linear Finite Strain Beam. 2010.
- [303] Ciocca L, De Crescenzo F, Fantini M, Scotti R. CAD/CAM and rapid prototyped scaffold construction for bone regenerative medicine and surgical transfer of virtual planning: a pilot study. *Computerized Medical Imaging and Graphics*. 2009;33:58-62.
- [304] Cooke MN, Fisher JP, Dean D, Rimnac C, Mikos AG. Use of stereolithography to manufacture critical-sized 3D biodegradable scaffolds for bone ingrowth. *Journal of Biomedical Materials Research Part B: Applied Biomaterials*. 2002;64:65-9.
- [305] Rohner D, Hutmacher D, See P, Tan K, Yeow V, Tan S, et al. [Individually CAD-CAM technique designed, bioresorbable 3-dimensional polycaprolactone framework for experimental reconstruction of craniofacial defects in the pig]. *Mund-, Kiefer-und Gesichtschirurgie: MKG*. 2002;6:162.
- [306] Liu Y, Zhang L, Zhou G, Li Q, Liu W, Yu Z, et al. < i> In vitro</i> engineering of human ear-shaped cartilage assisted with CAD/CAM technology. *Biomaterials*. 2010;31:2176-83.
- [307] Gradinger R, Hipp E. A custom-made adaptable pelvic prosthesis. *New developments for limb salvage in musculoskeletal tumors* Springer, Berlin Heidelberg New York. 1989.

- [308] Grading R, Rechl H, Hipp E. Pelvic osteosarcoma. Resection, reconstruction, local control, and survival statistics. *Clin Orthop Relat Res*. 1991;270:149-58.
- [309] Karageorgiou V, Kaplan D. Porosity of 3D biomaterial scaffolds and osteogenesis. *Biomaterials*. 2005;26:5474-91.
- [310] Woodruff MA, Lange C, Reichert J, Berner A, Chen F, Fratzl P, et al. Bone tissue engineering: from bench to bedside. *Materials Today*. 2012;15:430-5.
- [311] Holzappel BM, Reichert JC, Schantz J-T, Gbureck U, Rackwitz L, Noeth U, et al. How smart do biomaterials need to be? A translational science and clinical point of view. *Advanced drug delivery reviews*. 2013;65:581-603.
- [312] Slic3r. Slic3r: Gcode generator for 3D printers. 2012.
- [313] Systems D. CATIA V5-6R2012 drives higher Design excellence. 2013.
- [314] Gmbh N. netfabb Studio Professional. 2012.
- [315] Department-of-Defense. Department of Defense Breast Cancer Research Program, May 2013. Department of Defense; 2013.
- [316] Harcourt DM, Rumsey NJ, Ambler NR, Cawthorn SJ, Reid CD, Maddox PR, et al. The psychological effect of mastectomy with or without breast reconstruction: a prospective, multicenter study. *Plastic and reconstructive surgery*. 2003;111:1060-8.
- [317] Tabata Y, Miyao M, Inamoto T, Ishii T, Hirano Y, Yamaoki Y, et al. De novo formation of adipose tissue by controlled release of basic fibroblast growth factor. *Tissue engineering*. 2000;6:279-89.
- [318] Mian R, Morrison WA, Hurley JV, Penington AJ, Romeo R, Tanaka Y, et al. Formation of new tissue from an arteriovenous loop in the absence of added extracellular matrix. *Tissue engineering*. 2000;6:595-603.
- [319] Fischbach C, Seufert J, Staiger H, Hacker M, Neubauer M, Göpferich A, et al. Three-dimensional in vitro model of adipogenesis: comparison of culture conditions. *Tissue engineering*. 2004;10:215-29.
- [320] Kang X, Xie Y, Kniss DA. Adipose tissue model using three-dimensional cultivation of preadipocytes seeded onto fibrous polymer scaffolds. *Tissue engineering*. 2005;11:458-68.
- [321] Masuda T, Furue M, Matsuda T. Novel strategy for soft tissue augmentation based on transplantation of fragmented omentum and preadipocytes. *Tissue engineering*. 2004;10:1672-83.
- [322] Hemmrich K, von Heimburg D, Rendchen R, Di Bartolo C, Milella E, Pallua N. Implantation of preadipocyte-loaded hyaluronic acid-based scaffolds into nude mice to evaluate potential for soft tissue engineering. *Biomaterials*. 2005;26:7025-37.
- [323] Woodruff MA, Huttmacher DW. The return of a forgotten polymer—polycaprolactone in the 21st century. *Progress in Polymer Science*. 2010;35:1217-56.
- [324] Sarugaser R, Lickorish D, Baksh D, Hosseini MM, Davies JE. Human umbilical cord perivascular (HUCPV) cells: a source of mesenchymal progenitors. *Stem cells*. 2005;23:220-9.
- [325] Zhang Z-Y, Teoh SH, Chong W-S, Foo T-T, Chng Y-C, Choolani M, et al. A biaxial rotating bioreactor for the culture of fetal mesenchymal stem cells for bone tissue engineering. *Biomaterials*. 2009;30:2694-704.
- [326] Zhang Z-Y, Teoh SH, Teo EY, Khoon Chong MS, Shin CW, Tien FT, et al. A comparison of bioreactors for culture of fetal mesenchymal stem cells for bone tissue engineering. *Biomaterials*. 2010;31:8684-95.
- [327] Duvall CL, Taylor WR, Weiss D, Guldberg RE. Quantitative microcomputed tomography analysis of collateral vessel development after ischemic injury. *American Journal of Physiology-Heart and Circulatory Physiology*. 2004;287:H302-H10.

- [328] Jensen C, Gurevich L, Patriciu A, Struijk J, Zachar V, Pennisi CP. Increased connective tissue attachment to silicone implants by a water vapor plasma treatment. *Journal of Biomedical Materials Research Part A*. 2012;100:3400-7.
- [329] Hutmacher DW. Scaffolds in tissue engineering bone and cartilage. *Biomaterials*. 2000;21:2529-43.
- [330] Gefen A, Dilmoney B. Mechanics of the normal woman's breast. *Technology and Health Care*. 2007;15:259-71.
- [331] Neuss S, Apel C, Buttler P, Denecke B, Dhanasingh A, Ding X, et al. Assessment of stem cell/biomaterial combinations for stem cell-based tissue engineering. *Biomaterials*. 2008;29:302-13.
- [332] Sollazzo V, Lucchese A, Palmieri A, Zollino I, Iaccarino C, Carnevali G, et al. Polylactide-polyglycolide resorbable plates stimulates adipose tissue-derived stem cells towards osteoblasts differentiation. *International journal of immunopathology and pharmacology*. 2010;24:59-64.
- [333] Grijpma DW, Altpeter H, Bevis MJ, Feijen J. Improvement of the mechanical properties of poly (D, L-lactide) by orientation. *Polymer international*. 2002;51:845-51.
- [334] Hiljanen-Vainio M, Karjalainen T, Seppälä J. Biodegradable lactone copolymers. I. Characterization and mechanical behavior of ϵ -caprolactone and lactide copolymers. *Journal of applied polymer science*. 1996;59:1281-8.
- [335] Makadia HK, Siegel SJ. Poly lactic-co-glycolic acid (PLGA) as biodegradable controlled drug delivery carrier. *Polymers*. 2011;3:1377-97.
- [336] Wiggenhauser PS, Müller DF, Melchels FPW, Egaña JT, Storck K, Mayer H, et al. Engineering of vascularized adipose constructs. *Cell and tissue research*. 2011;1-11.
- [337] Moldovan NI. Role of monocytes and macrophages in adult angiogenesis: a light at the tunnel's end. *Journal of hematotherapy & stem cell research*. 2002;11:179-94.
- [338] Anghelina M, Krishnan P, Moldovan L, Moldovan NI. Monocytes and macrophages form branched cell columns in matrigel: implications for a role in neovascularization. *Stem cells and development*. 2004;13:665-76.
- [339] Anghelina M, Krishnan P, Moldovan L, Moldovan NI. Monocytes/macrophages cooperate with progenitor cells during neovascularization and tissue repair: conversion of cell columns into fibrovascular bundles. *The American journal of pathology*. 2006;168:529-41.
- [340] Debels H, Galea L, Han X-L, Palmer J, Van Rooijen N, Morrison W, et al. Macrophages Play a Key Role in Angiogenesis and Adipogenesis in a Mouse Tissue Engineering Model. *Tissue Engineering Part A*. 2013;19:2615-25.
- [341] Stillaert F, Findlay M, Palmer J, Idrizi R, Cheang S, Messina A, et al. Host rather than graft origin of Matrigel-induced adipose tissue in the murine tissue-engineering chamber. *Tissue engineering*. 2007;13:2291-300.
- [342] Zuk PA, Zhu M, Mizuno H, Huang J, Futrell JW, Katz AJ, et al. Multilineage cells from human adipose tissue: implications for cell-based therapies. *Tissue engineering*. 2001;7:211-28.
- [343] Zuk PA, Zhu M, Ashjian P, De Ugarte DA, Huang JI, Mizuno H, et al. Human adipose tissue is a source of multipotent stem cells. *Molecular biology of the cell*. 2002;13:4279-95.
- [344] Rolstad B. The athymic nude rat: an animal experimental model to reveal novel aspects of innate immune responses? *Immunological reviews*. 2001;184:136-44.

- [345] Holzapfel BM, Thibaudeau L, Hesami P, Taubenberger A, Holzapfel NP, Mayer-Wagner S, et al. Humanised xenograft models of bone metastasis revisited: novel insights into species-specific mechanisms of cancer cell osteotropism. *Cancer and Metastasis Reviews*. 2013;32:129-45.
- [346] Saunders RL, Hammer DA. Assembly of human umbilical vein endothelial cells on compliant hydrogels. *Cellular and molecular bioengineering*. 2010;3:60-7.
- [347] Baldwin J, Antille M, Bonda U, De-Juan-Pardo EM, Khosrotehrani K, Ivanovski S, et al. In vitro pre-vascularisation of tissue-engineered constructs A co-culture perspective. *Vascular Cell*. 2014;6:1-16.
- [348] Wolfram|Alpha. Volume human breast. <http://www.wolframalpha.com/input/?i=volume+human+body>. 2013;Access date: 19 December 2013.
- [349] Bayer CM, Bani MR, Schneider M, Dammer U, Raabe E, Haeberle L, et al. Assessment of breast volume changes during human pregnancy using a three-dimensional surface assessment technique in the prospective CGATE study. *European journal of cancer prevention: the official journal of the European Cancer Prevention Organisation (ECP)*. 2013.
- [350] Hohl R, de Oliveira RB, de Macedo DV, Brenzikofer R. Apparatus for measuring rat body volume: a methodological proposition. *Journal of Applied Physiology*. 2007;102:1229-34.
- [351] Cancer IAfRo. World Cancer Report. International Agency for Research on Cancer; 2008.
- [352] FDA. FDA Update on the Safety of Silicone Gel-Filled Breast Implants 2011.
- [353] Patel P, Robb GL, Patrick Jr CW. Soft tissue restoration using tissue engineering. *Semin Plast Surg*. 2003;17:99-106.
- [354] Henkel J, Woodruff MA, Epari DR, Steck R, Glatt V, Dickinson IC, et al. Bone Regeneration Based on Tissue Engineering Conceptions-A 21st Century Perspective. *骨研究 (英文版)*. 2013.
- [355] Salgado AJ, Coutinho OP, Reis RL. Bone tissue engineering: state of the art and future trends. *Macromolecular bioscience*. 2004;4:743-65.
- [356] Martin P. Wound healing--aiming for perfect skin regeneration. *Science*. 1997;276:75-81.
- [357] Clark RA. Fibrin and wound healing. *Annals of the New York Academy of Sciences*. 2001;936:355-67.
- [358] Chhaya MP, Melchels F, Holzapfel BM, Baldwin J, Huttmacher DW. Sustained Regeneration of High-volume Adipose Tissue for Breast Reconstruction using Computer Aided Design and Biomanufacturing Biomaterials [Accepted]. 2015.
- [359] Beahm EK, Walton RL, Patrick Jr CW. Progress in adipose tissue construct development. *Clinics in plastic surgery*. 2003;30:547.
- [360] Lokmic Z, Thomas JL, Morrison WA, Thompson EW, Mitchell GM. An endogenously deposited fibrin scaffold determines construct size in the surgically created arteriovenous loop chamber model of tissue engineering. *Journal of vascular surgery*. 2008;48:974-85.
- [361] Findlay MW, Dolderer JH, Trost N, Craft RO, Cao Y, Cooper-White J, et al. Tissue-engineered breast reconstruction: bridging the gap toward large-volume tissue engineering in humans. *Plastic and reconstructive surgery*. 2011;128:1206-15.
- [362] Messina A, Bortolotto SK, Cassell OC, Kelly J, Abberton KM, Morrison WA. Generation of a vascularized organoid using skeletal muscle as the inductive source. *The FASEB Journal*. 2005;19:1570-2.

- [363] Eterno V, Zambelli A, Pavesi L, Villani L, Zanini V, Petrolo G, et al. Adipose-derived Mesenchymal Stem Cells (ASCs) may favour breast cancer recurrence via HGF/c-Met signaling. *Oncotarget*. 2014;5:613.
- [364] Huang C, Holfeld J, Schaden W, Orgill D, Ogawa R. Mechanotherapy: revisiting physical therapy and recruiting mechanobiology for a new era in medicine. *Trends in molecular medicine*. 2013;19:555-64.
- [365] Yuan Y, Ogawa R. Tissue-Engineered Breast Reconstruction: Bridging the Gap toward Large-Volume Tissue Engineering in Humans. *Plastic and reconstructive surgery*. 2015;135:236e-7e.
- [366] Yang X, Cai X, Wang J, Tang H, Yuan Q, Gong P, et al. Mechanical stretch inhibits adipogenesis and stimulates osteogenesis of adipose stem cells. *Cell proliferation*. 2012;45:158-66.
- [367] Nava MM, Raimondi MT, Pietrabissa R. Controlling self-renewal and differentiation of stem cells via mechanical cues. *BioMed Research International*. 2012;2012.
- [368] Vazquez B, Given KS, Houston GC. Breast augmentation: a review of subglandular and submuscular implantation. *Aesthetic plastic surgery*. 1987;11:101-5.
- [369] Mukhopadhyay S, Farver CF, Vaszar LT, Dempsey OJ, Popper HH, Mani H, et al. Causes of pulmonary granulomas: a retrospective study of 500 cases from seven countries. *Journal of clinical pathology*. 2012;65:51-7.
- [370] Baer C, Squadrito ML, Iruela-Arispe ML, De Palma M. Reciprocal interactions between endothelial cells and macrophages in angiogenic vascular niches. *Experimental cell research*. 2013;319:1626-34.
- [371] Eirin A, Zhu X-Y, Li Z, Ebrahimi B, Zhang X, Tang H, et al. Endothelial outgrowth cells shift macrophage phenotype and improve kidney viability in swine renal artery stenosis. *Arteriosclerosis, thrombosis, and vascular biology*. 2013;33:1006-13.
- [372] He H, Xu J, Warren CM, Duan D, Li X, Wu L, et al. Endothelial cells provide an instructive niche for the differentiation and functional polarization of M2-like macrophages. *Blood*. 2012;120:3152-62.
- [373] Spiller KL, Anfang RR, Spiller KJ, Ng J, Nakazawa KR, Daulton JW, et al. The role of macrophage phenotype in vascularization of tissue engineering scaffolds. *Biomaterials*. 2014;35:4477-88.
- [374] Ludin A, Itkin T, Gur-Cohen S, Mildner A, Shezen E, Golan K, et al. Monocytes-macrophages that express α -smooth muscle actin preserve primitive hematopoietic cells in the bone marrow. *Nature immunology*. 2012;13:1072-82.
- [375] Feil S, Fehrenbacher B, Lukowski R, Essmann F, Schulze-Osthoff K, Schaller M, et al. Transdifferentiation of vascular smooth muscle cells to macrophage-like cells during atherogenesis. *Circulation research*. 2014;115:662-7.
- [376] Duan H-Y, Ye L, Wu X, Guan Q, Yang X-F, Han F, et al. The in vivo characterization of electrospun heparin-bonded polycaprolactone in small-diameter vascular reconstruction. *Vascular*. 2014;1708538114550737.
- [377] Byun J-H, Lee HA, Kim TH, Lee JH, Oh SH. Effect of porous polycaprolactone beads on bone regeneration: preliminary in vitro and in vivo studies. *Biomaterials Research*. 2014;18:18.
- [378] Berner A. Quantitative and qualitative assessment of the regenerative potential of osteoblasts versus bone marrow derived mesenchymal stem cells in the reconstruction of critical sized segmental tibial bone defects in a large animal model. 2013.

- [379] Uhrig BA, Boerckel JD, Willett NJ, Li M-TA, Huebsch N, Guldberg RE. Recovery from hind limb ischemia enhances rhBMP-2-mediated segmental bone defect repair in a rat composite injury model. *Bone*. 2013;55:410-7.
- [380] Myckatyn T. *Breast Augmentation and Implant Position*. 2011.
- [381] Brown TD, Dalton PD, Hutmacher DW. Direct writing by way of melt electrospinning. *Advanced Materials*. 2011;23:5651-7.
- [382] Kim HW, Knowles JC, Kim HE. Hydroxyapatite and gelatin composite foams processed via novel freeze-drying and crosslinking for use as temporary hard tissue scaffolds. *Journal of Biomedical Materials Research Part A*. 2005;72:136-45.
- [383] Vallet-Regí M, Balas F, Colilla M, Manzano M. Bone-regenerative bioceramic implants with drug and protein controlled delivery capability. *Progress in Solid State Chemistry*. 2008;36:163-91.
- [384] Jin Q, Anusaksathien O, Webb S, Rutherford R, Giannobile W. Gene therapy of bone morphogenetic protein for periodontal tissue engineering. *Journal of periodontology*. 2003;74:202-13.
- [385] Mouriño V, Boccaccini AR. Bone tissue engineering therapeutics: controlled drug delivery in three-dimensional scaffolds. *Journal of the Royal Society Interface*. 2010;7:209-27.

Chapter 6: Appendix

Void-System for generation of void spaces within prevascularised implant for efficient transfer of free fat grafts including lipofilling

The prevascularisation method described in Study 4 would be rendered impractical if the host connective tissue occupies a majority of the volume of the scaffold such that no further volume remains for the secondary injection of fat tissue. Therefore, we have developed a system of removable space-occupying structures within the scaffold which can be removed prior to injection of the fat. These space-occupying structures, when removed, would create voids within the scaffold which can then be used to inject the fat.

a) The geometric orientation of the void spaces:

- **Non-convergent:** parallel orientated voids along one axes of the scaffold (as seen in Fig1 red). This method needs multiple access tunnels for fat transfer.
- **Convergent:** radiating from one origin to enable minimally invasive procedures by fat transfer using one central tunnel for access to all voids.

b) The technology used for space occupation:

- **Liquid/gel-like**
 - hydrogel can be aspirated by a syringe, which would help in its removal in a minimally invasive way.
- **Solid**
 - **Collapsible:**
 - biocompatible polymer material filled with saline. When the saline is removed, the polymeric tube network would collapse which aids in its explantation in a minimally invasive way.
 - **Rigid:**

- implants (e.g. made out of metal) which are placed in previously drilled wholes within the scaffold structure and removed manually before fat transfer

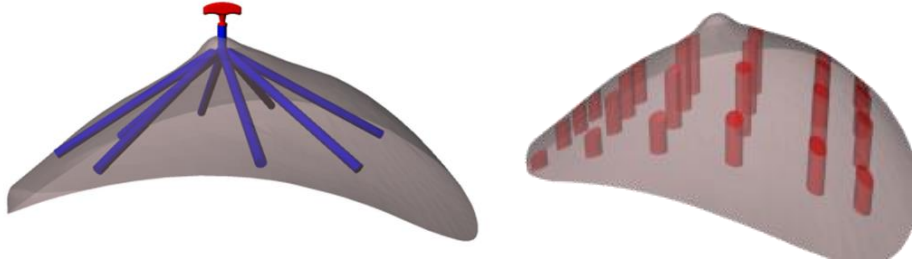


Figure 5.6.1: Rendering of a breast-shaped scaffold containing a collapsible network of interconnected tubes filled with a fluid (blue) or hydrogel (red)

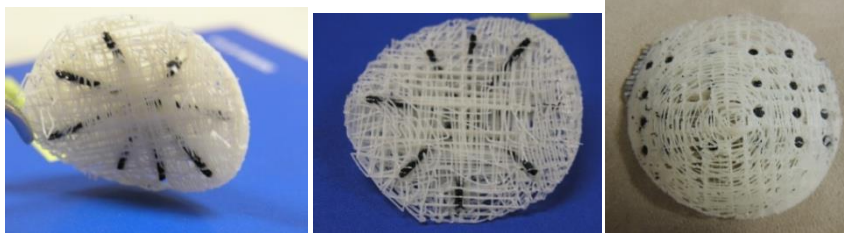


Figure 5.6.2. Prototype of a breast-shaped porous tissue engineering scaffold (white) containing templates for spacers (black). Photos with blue background show a convergent design of spacers, while photos with off-white backgrounds show a non-convergent design.

Methods for removing spacers:

Spacers fabricated with low porosity:

We propose a scaffold design containing precisely defined regions of **low porosity and low mechanical integrity** which can be subsequently removed from the scaffold by means of a specialized surgical tool. The low porosity ensures that there is no tissue ingrowth within such regions and the low mechanical integrity (created by a system similar to that of a perforated paper) will aid in their easy removal. The voids created by the removal of these regions will be filled with fat by the surgeon.

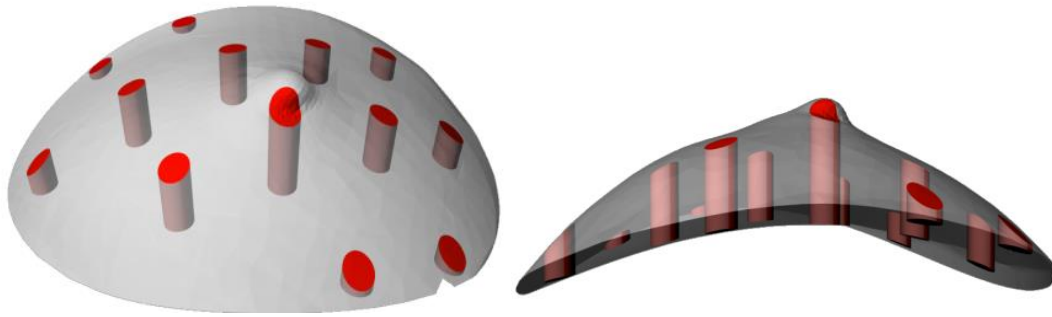


Figure 5.6.3: Rendering of a breast shaped scaffold containing regions of low porosity and low mechanical integrity (regions are shown in red).

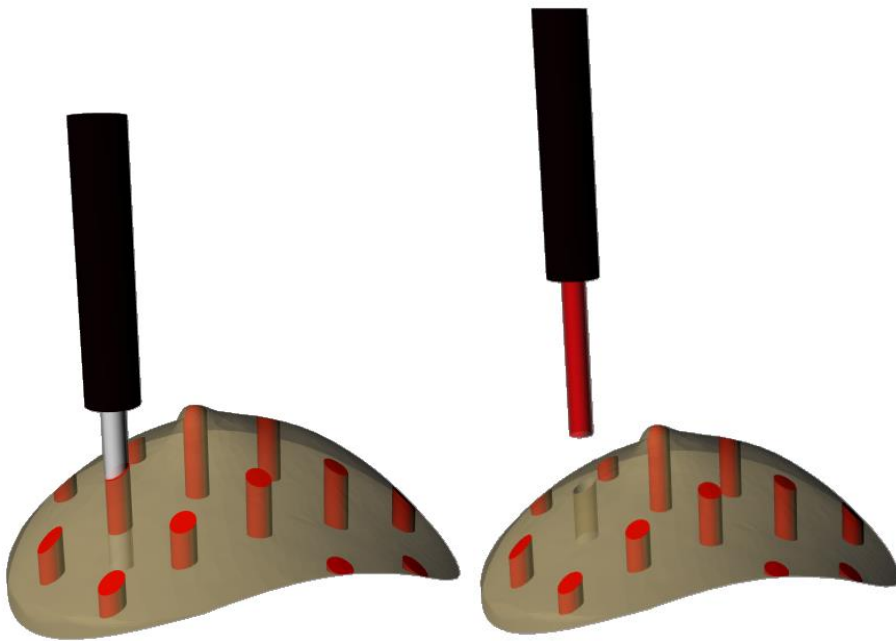


Figure 5.6.4: A specialised surgical cutting tool will be designed to remove such regions.

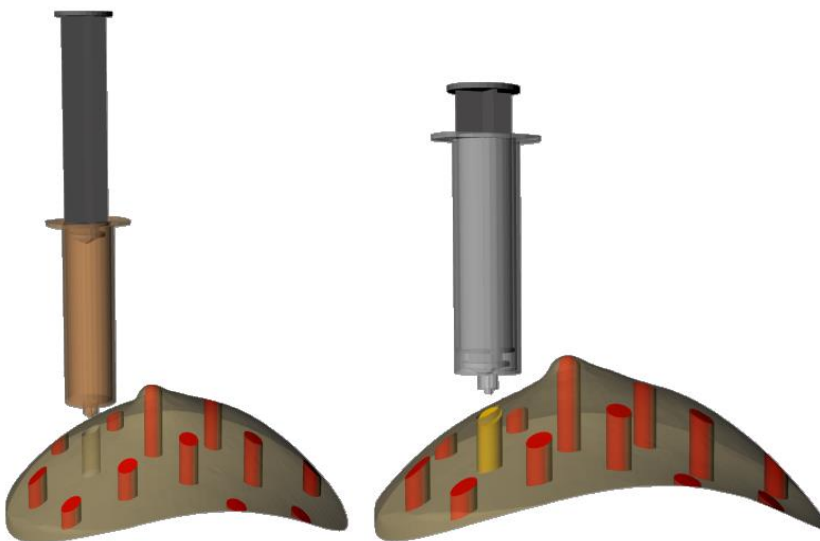


Figure 5.6.5: The void left behind by removal of the low porosity regions will be used for lipofilling (fat tissue shown in yellow)

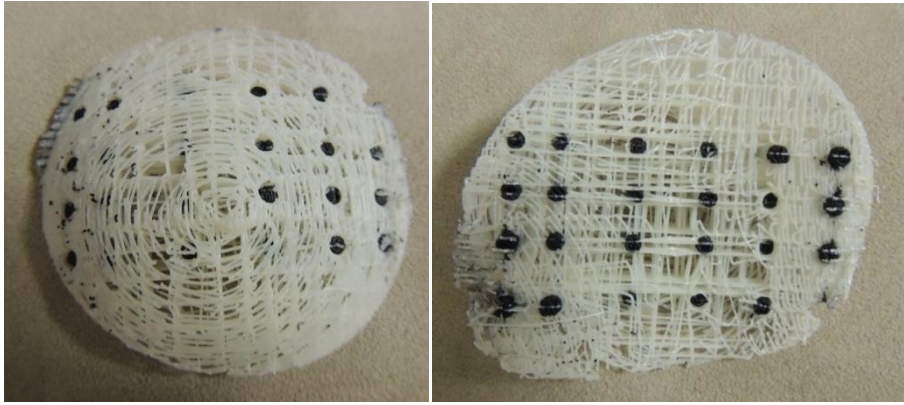


Figure 5.6.6. Fabricated breast shaped scaffold (white) containing regions of low porosity and low mechanical integrity (black).

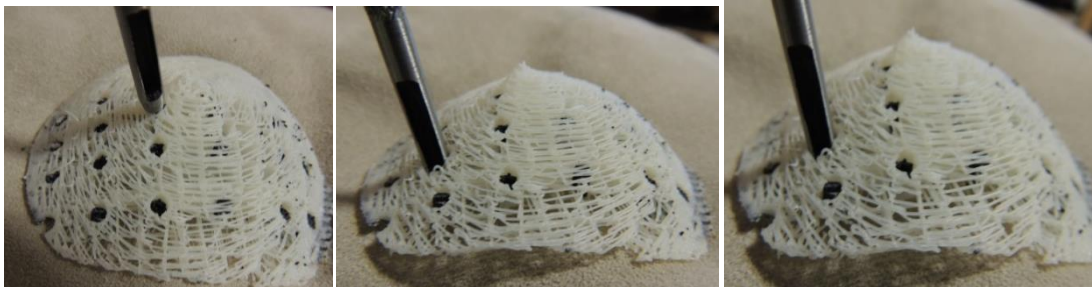


Figure 5.6.7. A cutting tool used to punch out the regions of low porosity and mechanical integrity.

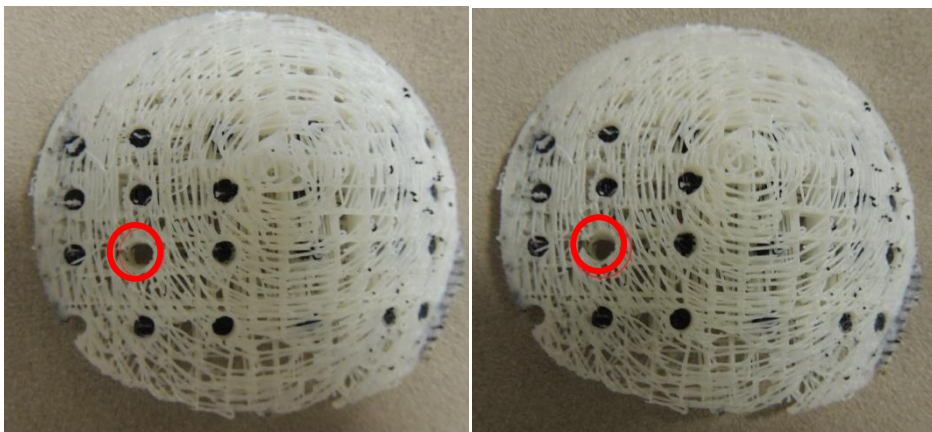


Figure 5.6.8. The void left behind by removal of the low porosity regions (highlighted with red circle) can be used for lipofilling

A pilot study was undertaken whereby $n=6$ scaffolds (volume = 125cm^3) based on Design #1 were fabricated using Poly(D,L)-Lactide polymer and implanted in immunocompetent minipigs for a period of 24 weeks. Upon explantation, the scaffolds were well integrated with the surrounding tissue and there was a widespread invasion of host vasculature into the constructs. Visual examination revealed that the overall shape of the scaffolds did not change drastically over the

implantation period. Histological evaluation showed large areas of fat and vascularisation around the injection sites on all scaffolds (Fig 5.6.9)

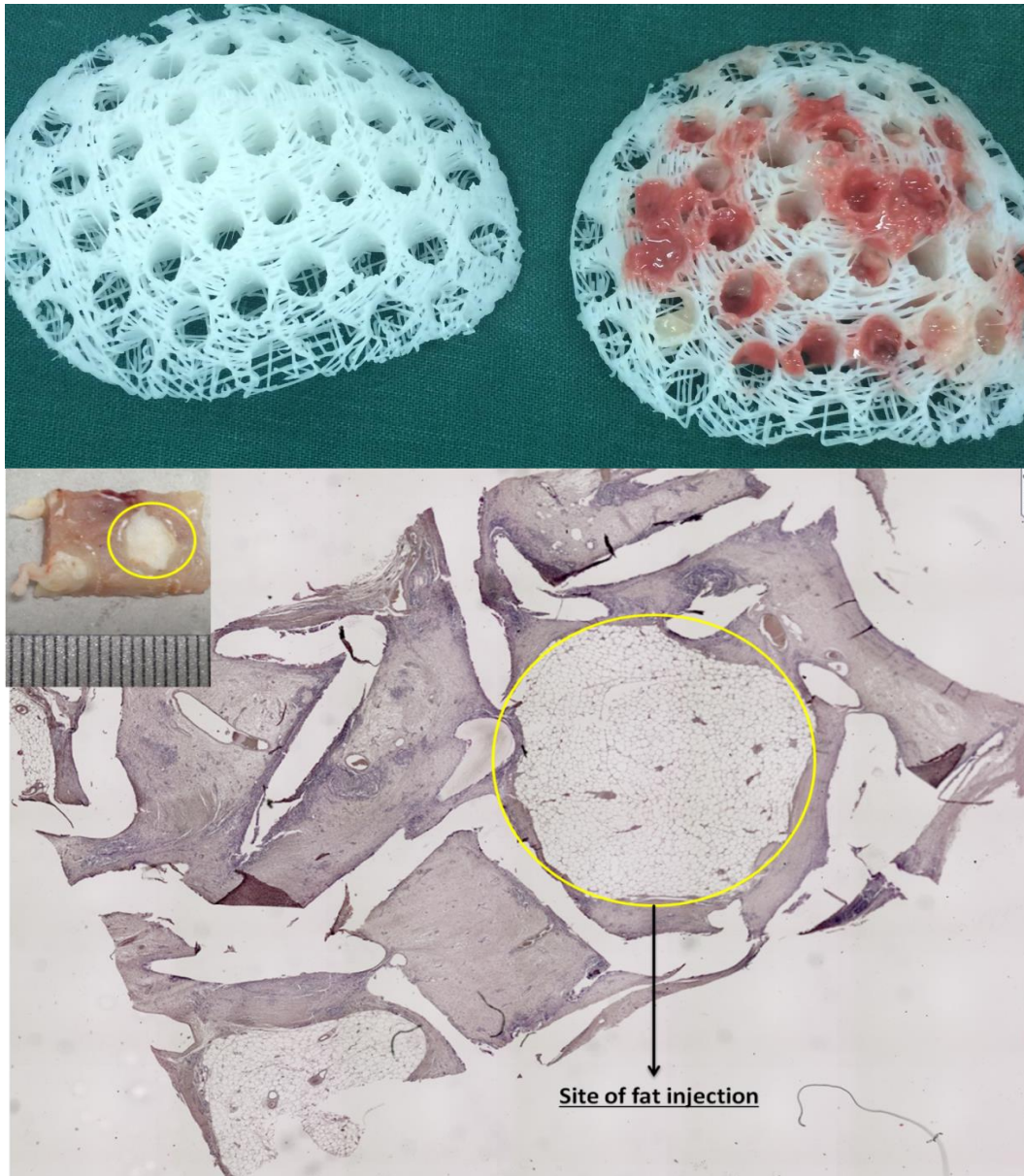


Figure 5.6.9 (TOP) Gross morphological images of scaffold containing void structures with and without the fat injected into the voids. (BOTTOM) Hematoxylin and Eosin stained section of a scaffold explanted after 6 months implantation into minipigs. Photograph on top left shows a cut out of the area surrounding a randomly selected void filled with adipose tissue (adipose tissue encircled in yellow). The corresponding area in the histological section, also encircled in yellow, shows healthy well vascularised adipose tissue at the injection site with no signs of necrosis.

1c Biodegradable implant generating prevascularized connective tissue to resemble organic stromal tissue to be in situ carrier of functional cell colonies

The impact of our technology goes beyond the reach of adipose tissue transfer. Every tissue engineering approach needs a functional vascular system within it. There are several ideas described in literature: e.g. vessel loop, printed tubular systems or coprogs. Our system is based on a rapid prototyping made scaffold that serves as organic stromal tissue. By that means our implant plays the role of the supporting connective tissue within any possible organ. Therefore our system can be used for different engineering purposes: e.g. salivary gland or pancreatic islet function.

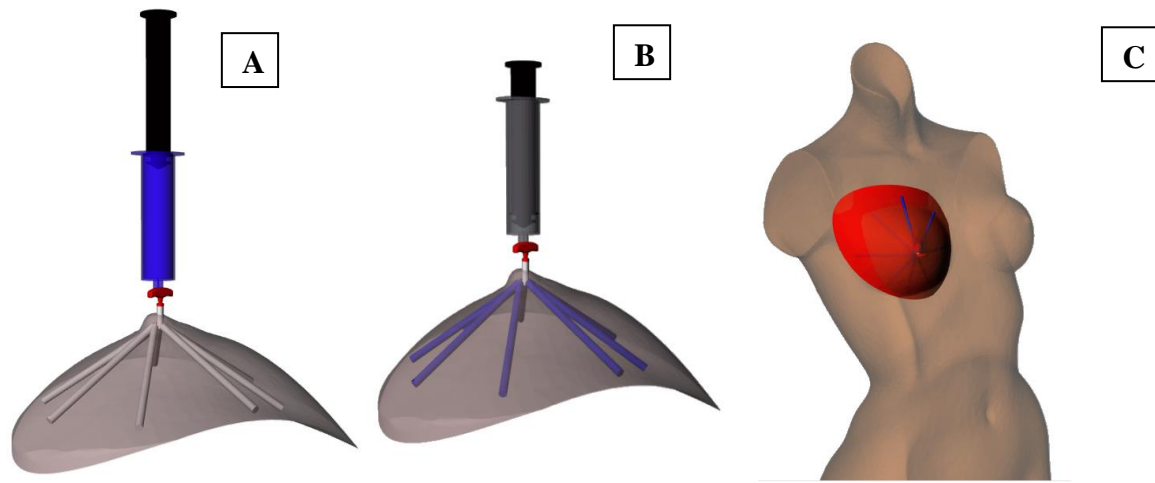
The technical idea hereby is based on the procedure using an implant that serves as connective tissue carrier in combination with our void-system: The invention of the void-system enables us to use our implant for every kind of tissue engineering approach, because after the removal of the occupying space holder, the void-system is filled with the organ specific functional cells, e.g. glandular epithelial cells or pancreatic islet cells. That leads to an universal applicability of our system in every kind of tissue engineering approach.

Design #2

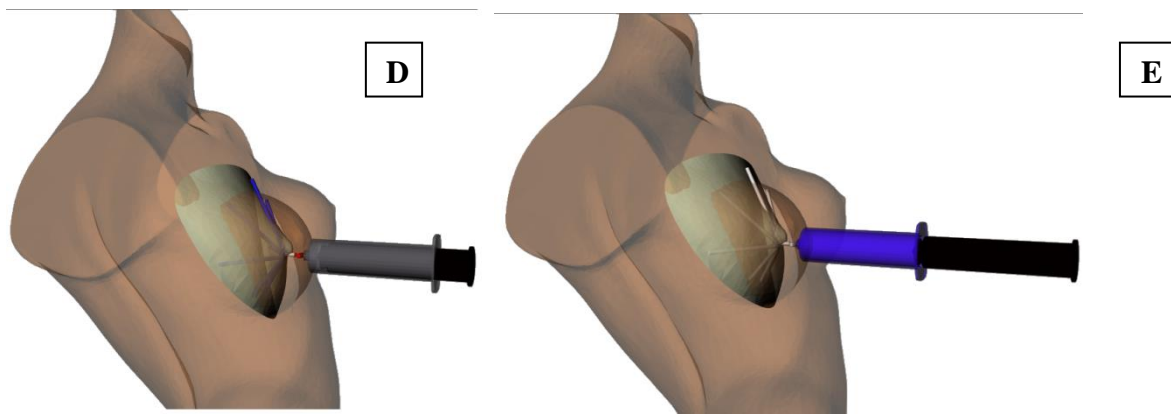
Design #2 improves Design #1 by the introduction of a minimal invasive surgical access technology consisting of scaffold design, minimal-invasive removable void-system and surgical assistance tool.

The following illustrations demonstrate the conceptual approach of the regenerative implant with a void-system.

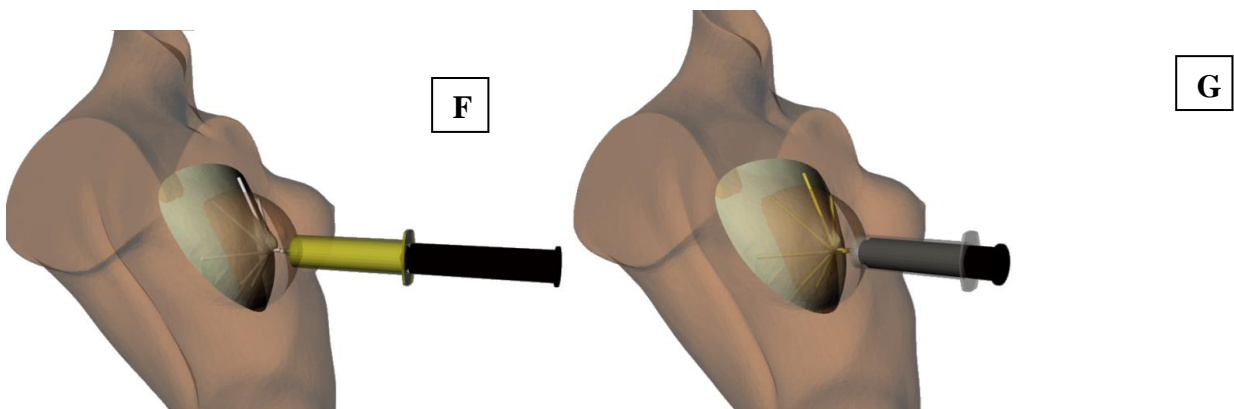
Step 1. The scaffold is fabricated along with space-occupying structures. These space-occupying structures are then filled with a saline solution or a hydrogel (A, B) and then implanted into the patient (C).



Step 2. After a period of 6-8 weeks, the fluid within the space occupying structures is removed by means of a minimally invasive procedure. This causes the structures to collapse and then they can be easily removed, leaving behind void spaces within the scaffold (D,E).



Step 3. Fat is isolated from a donor site within the patient and is then injected into the void space left by removal of the structures (F, G).



During the removal of the space-occupying structure, it would be highly beneficial to follow a minimally invasive surgical procedure. Removal of the space occupying

structures during a minimally invasive procedure would be significantly simplified if the structures do not adhere strongly to the host tissue. To achieve this, we will coat the structures with a solution of the drug Tacrolimus. Tacrolimus, an FDA approved drug, works by proliferation control and prevents a fast ingrowth of host tissue. By that means we plan to reduce the attachment of tissue to the implant and thus to reduce the adherence of the space-occupying system within the scaffold. All in all this idea facilitates the removal of the space-occupying system and minimizes complication risk due to the removal procedure like bleeding from attached tissue.

Design #3

Design #3 improves current fused deposition modeling technologies by introducing a new lay-down pattern leading to highly improved control over scaffold mechanical properties especially elasticity and compressibility.

For breast tissue engineering applications, it is important to have flexibility and compressibility in the implanted scaffold. Currently, the only way to engineer such flexibility within tissue engineering scaffolds is to use an elastomeric biomaterial. Our novel approach aims at designing flexible implants made from semi-stiff biomaterials such as Polycaprolactone.

The conventional laydown pattern for FDM-manufactured tissue engineering scaffolds is to use continuous bars and struts. Such a laydown pattern restricts lateral compressibility. Our first design modification is to use a non-continuous strut to better distribute the forces along the lateral axis.

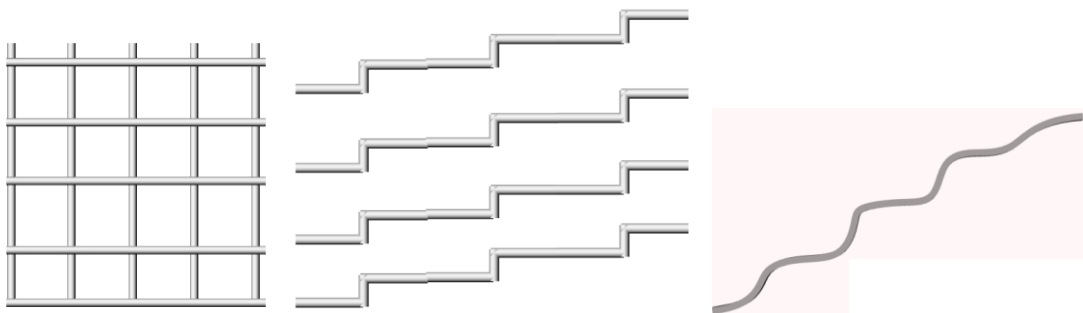
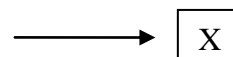


Figure 5.6.10: Left: Conventional laydown pattern consisting of continuous struts. Centre, Right: Our novel laydown patterns consisting of discontinuous struts

The second design modification we propose, is to introduce an offset between vertically stacked struts.



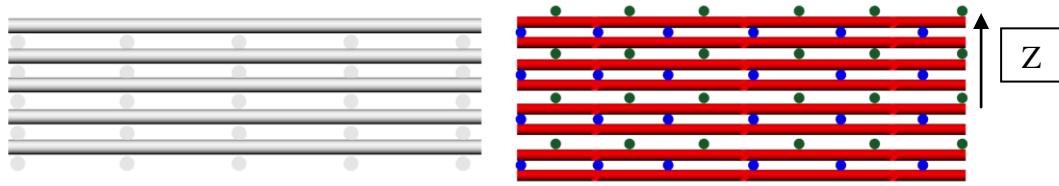


Figure 5.6.11: On the left, conventional laydown pattern. On the right: Modified laydown pattern consisting of offset struts. Note that the struts in Y axis are not laid directly on top of each other. We not only can lay down the struts differently in every second layer but also create a repetition after every n th layer.

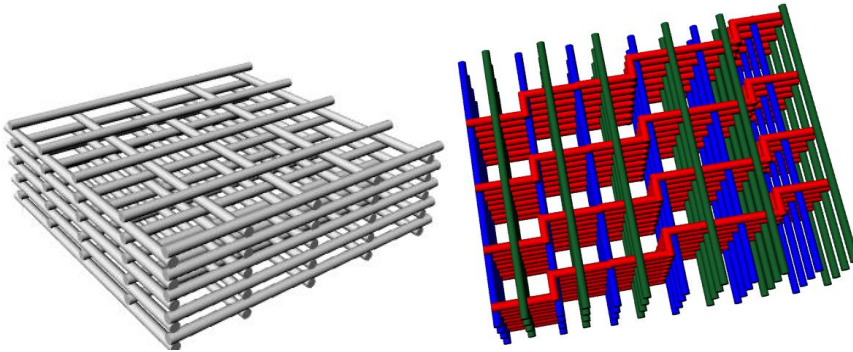


Figure 5.6.12: Left: Conventional laydown pattern. Right: Modified laydown pattern

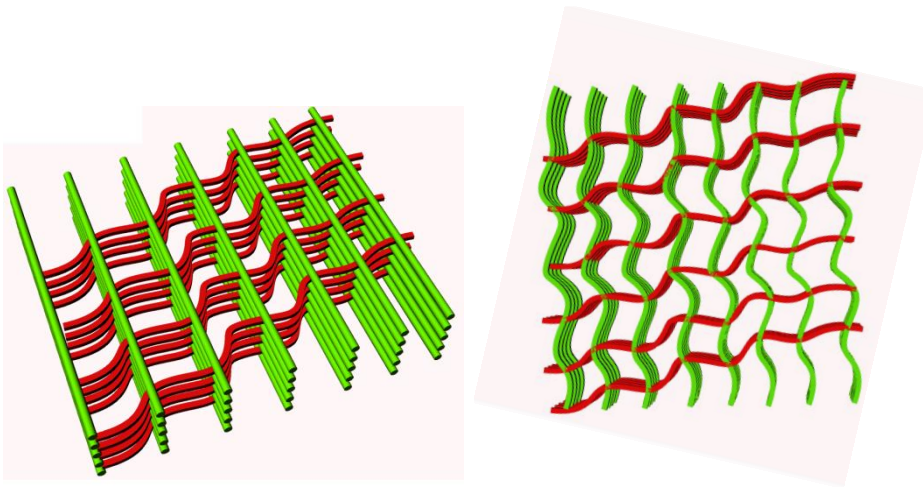


Figure 5.6.13: Other examples of novel laydown patterns.

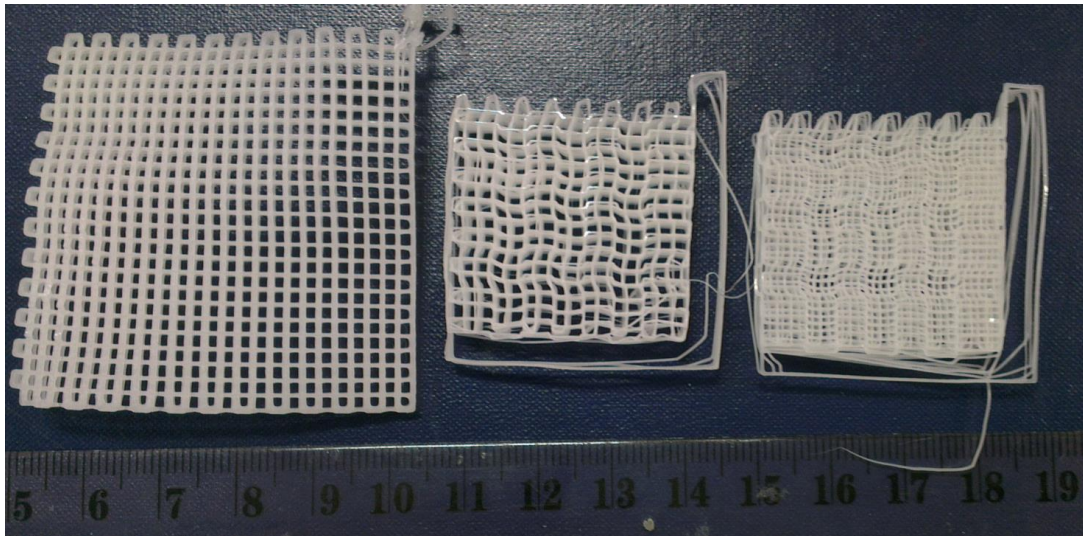
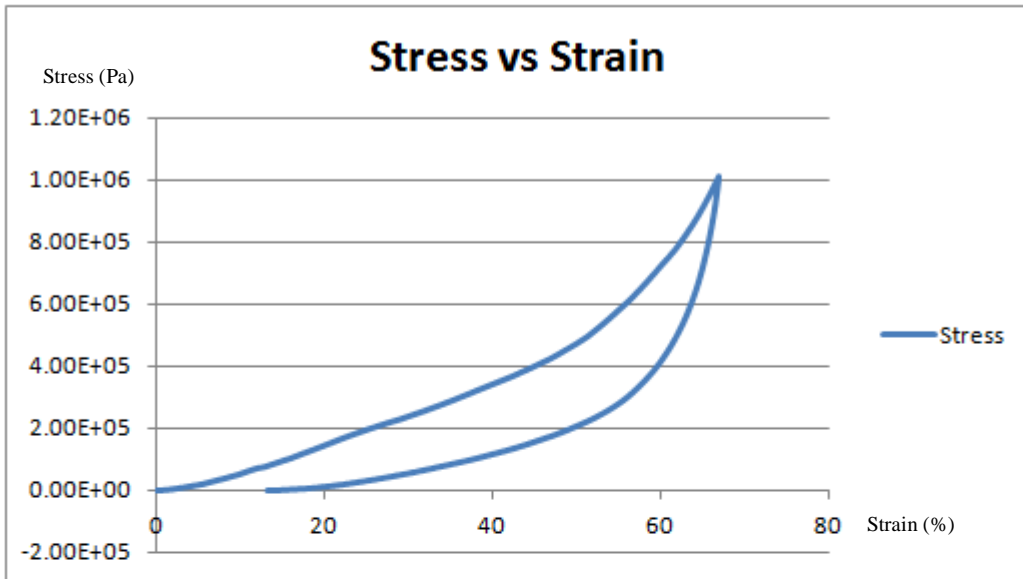


Figure 5.6.14. Left: Control polycaprolactone scaffold containing straight struts. Centre: Scaffold with zigzag laydown pattern. Right: Scaffold with zigzag laydown pattern AND offset between layers.

These modifications allow us to control the flexibility of the scaffold to adjust the PCL scaffold to specific tissue needs: from stiff bones, to elastic cartilage to compressible connective tissue. Preliminary compression testing performed on scaffolds containing such modified laydown patterns indicates that such scaffolds are more flexible, can take the same stress as the control scaffolds and display a higher range of elastic deformation as compared to control scaffolds fabricated with the same parameters.

Zigzag laydown pattern



Control laydown pattern (straight lines)

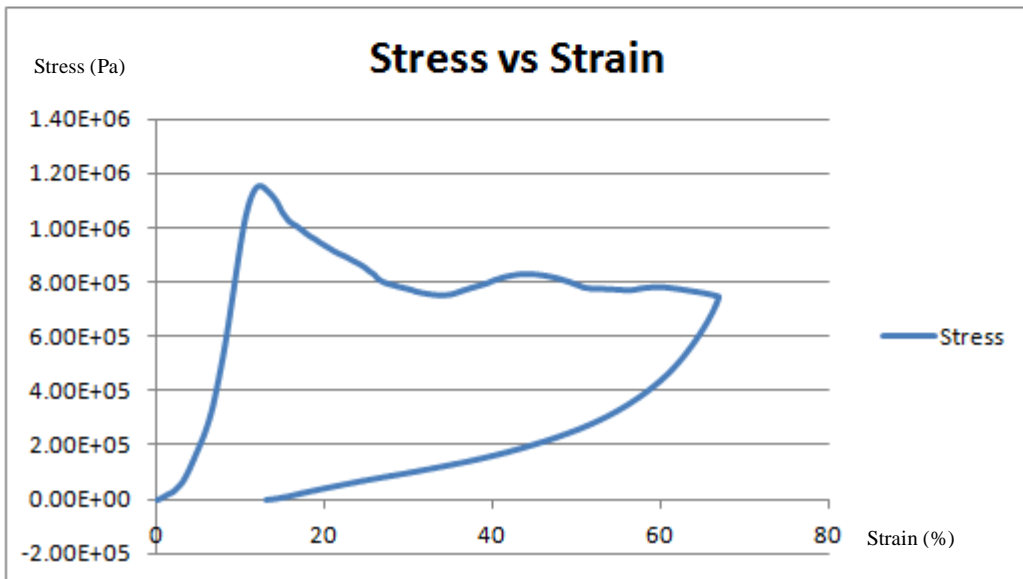


Figure 5.6.15. Stress vs Strain curves of scaffolds with either straight struts or a zigzag pattern of struts.

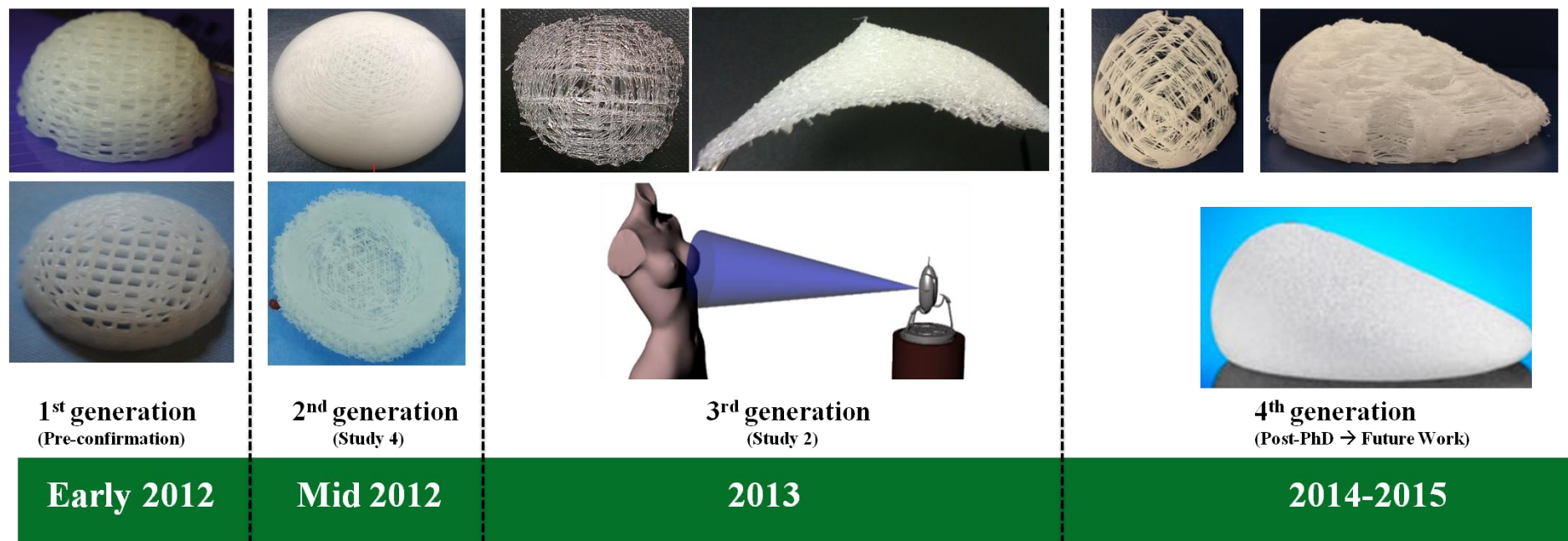


Figure 5.6.16. Timeline showing the evolution of the overall scaffold shape throughout the PhD project. Due to software limitations, scaffolds produced in 2012 were of geometrical shapes (dome-shaped). In 2013, Study 2 saw the development of computer software and algorithms which allowed fabrication of patient-specific scaffolds from medical imaging scans. However, the concave shape of the scaffolds does not permit easy and stable implantation into subglandular/submuscular pockets and, following a consultation with leading plastic surgeons, the scaffold shape was modified to match that of currently available anatomically-shaped silicone implants. The next generation implants imbibe all design principles described in the Appendix and have drastically reduced stiffness.